National Technical University of Athens
School of Civil Engineering
Institute of Structural Analysis and Antiseismic Research

Advanced computational methods for seismic design and assessment of reinforced concrete structures

PhD Dissertation

Charikleia Ch. Mitropoulou

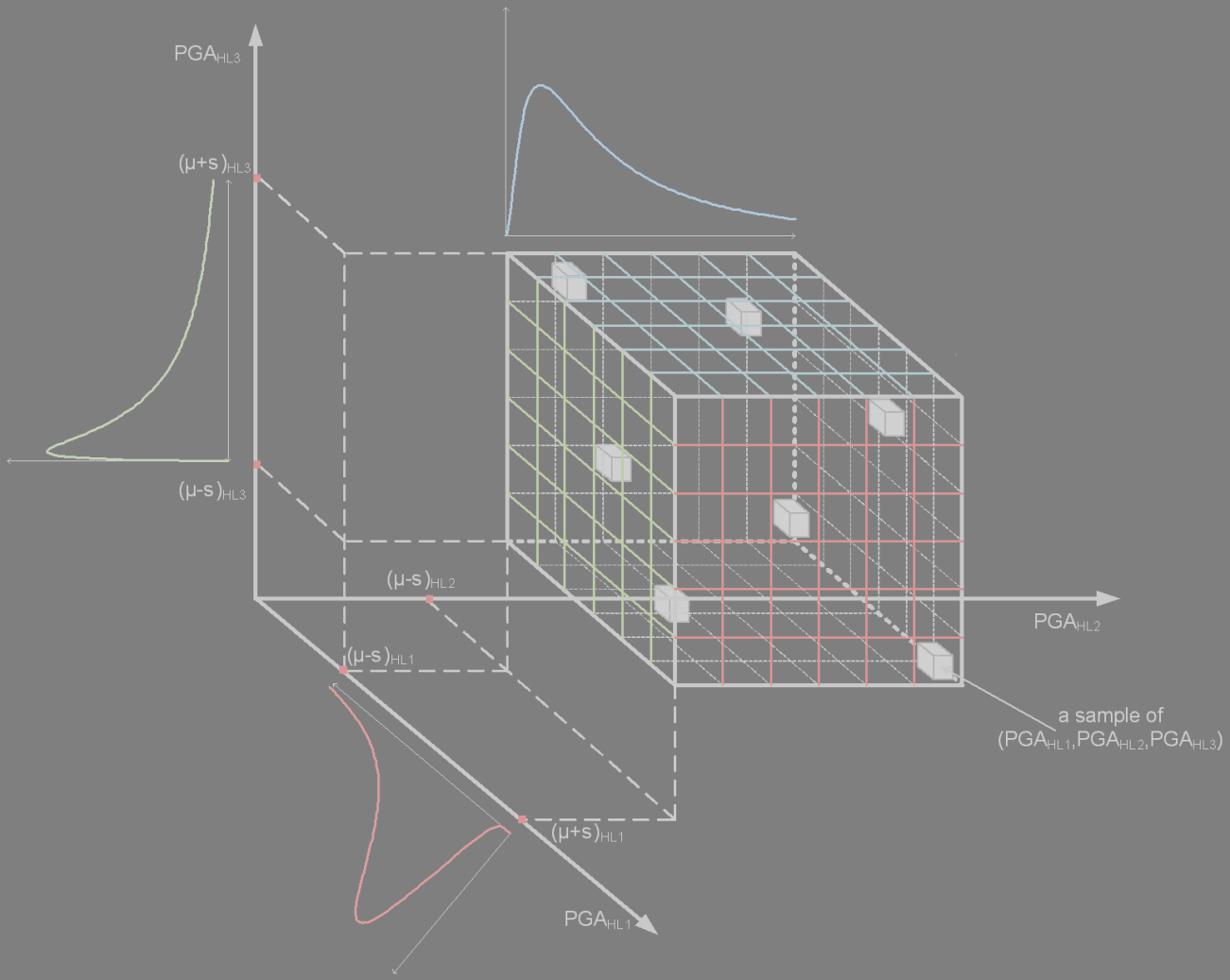

Advisor:
Professor Manolis Papadrakakis

Athens, May 2011

Εθνικό Μετσόβιο Πολυτεχνείο
Σχολή Πολιτικών Μηχανικών
Εργαστήριο Στατικής και Αντισεισμικών Ερευνών

Προηγμένες υπολογιστικές μέθοδοι αντισεισμικού σχεδιασμού και αποτίμησης κατασκευών από οπλισμένο σκυρόδεμα

Διδακτορική Διατριβή

Χαρίκλεια Χ. Μητροπούλου

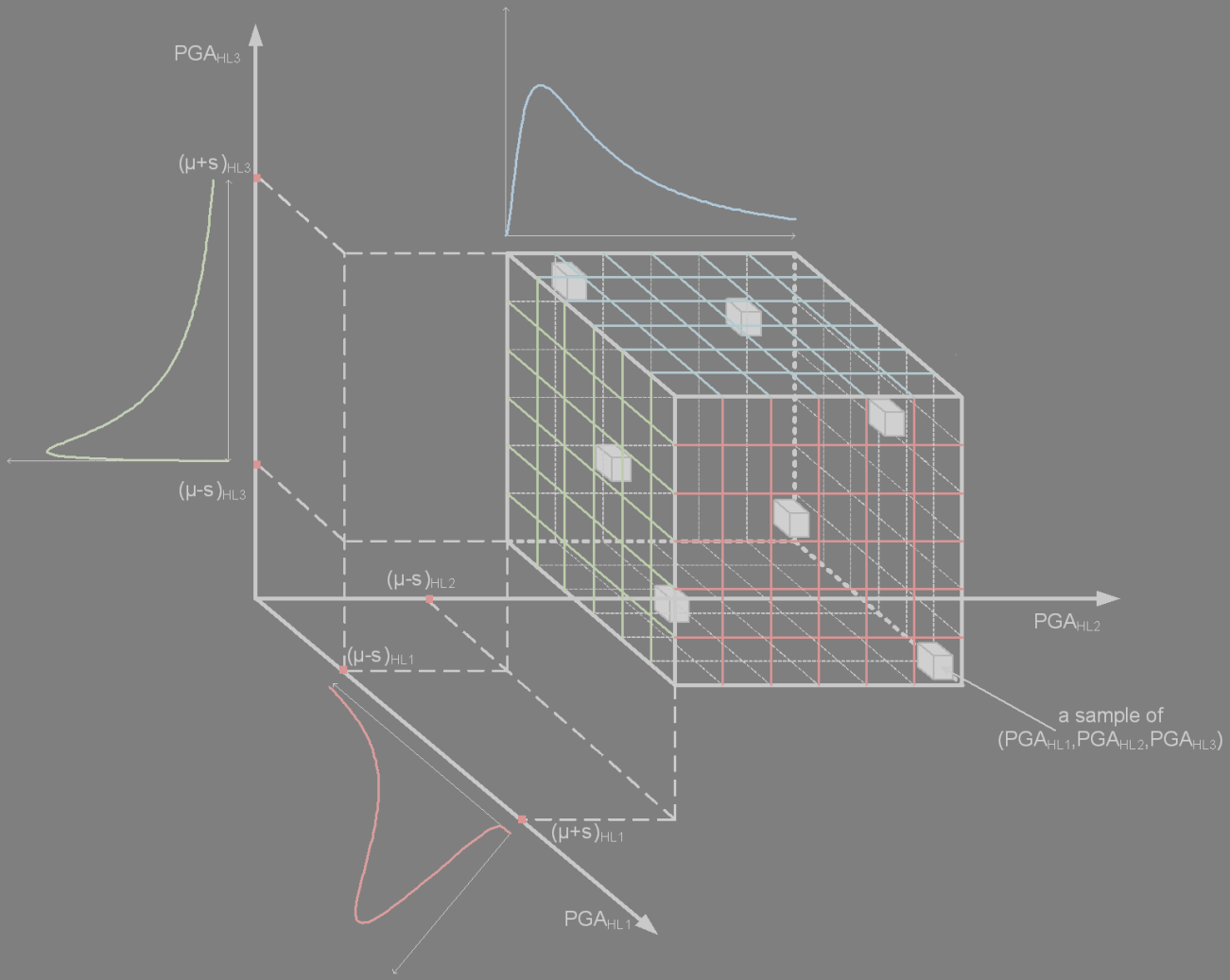

Επιβλέπων:
Καθηγητής Μανόλης Παπαδρακάκης

Αθήνα, Μάιος 2011

Dedicated to
my family

PhD Examination Committee

I certify that I have read this dissertation and that in my opinion it is fully adequate, in scope and quality, as a dissertation for the degree of Doctor of Philosophy.

Manolis Papadrakakis
Professor
(Principal Advisor)
School of Civil Engineering
National Technical University of Athens

I certify that I have read this dissertation and that in my opinion it is fully adequate, in scope and quality, as a dissertation for the degree of Doctor of Philosophy.

Christos A. Zeris
Assistant Professor
(Member of the advisory committee)
School of Civil Engineering
National Technical University of Athens

I certify that I have read this dissertation and that in my opinion it is fully adequate, in scope and quality, as a dissertation for the degree of Doctor of Philosophy.

Nikos D. Lagaros
Lecturer
(Member of the advisory committee)
School of Civil Engineering
National Technical University of Athens

I certify that I have read this dissertation and that in my opinion it is fully adequate, in scope and quality, as a dissertation for the degree of Doctor of Philosophy.

Costas A. Syrmakezis
Professor
School of Civil Engineering
National Technical University of Athens

I certify that I have read this dissertation and that in my opinion it is fully adequate, in scope and quality, as a dissertation for the degree of Doctor of Philosophy.

Costas C. Spyrakos
Professor
School of Civil Engineering
National Technical University of Athens

I certify that I have read this dissertation and that in my opinion it is fully adequate, in scope and quality, as a dissertation for the degree of Doctor of Philosophy.

Elisabeth N. Vintzileou
Professor
School of Civil Engineering
National Technical University of Athens

I certify that I have read this dissertation and that in my opinion it is fully adequate, in scope and quality, as a dissertation for the degree of Doctor of Philosophy.

Matthew G. Karlaftis
Associate Professor
School of Civil Engineering
National Technical University of Athens

Abstract

The major objective of this Dissertation is to develop an integrated framework for the economical and safe antiseismic design and assessment of new reinforced concrete (RC) structures by means of life-cycle cost and fragility analysis. This objective of the dissertation is achieved through the accomplishment of the following tasks: (i) At the first part of the Dissertation numerical calibration for some of the most popular damage indices (DIs) that have been proposed by many researchers was performed, in order to quantify the extent of damage in reinforced concrete structures. In particular, the Park and Ang local damage index, its modified variant proposed by Kunnath, Reinhorn and Lobo; the Chung, Meyer and Shinozuka local damage index; along with the maximum softening and final softening DIs proposed by Di Pasquale and Çakmak, were calibrated numerically based on a crack width list that corresponds to specific damage states. (ii) A critical assessment of prescriptive design procedures was performed with reference to their ability to lead to safe and economical designs. Furthermore, a comparison between prescriptive and performance-based seismic design (PBD) procedures was carried out. For this purpose a number of structural seismic design optimisation problems have been formulated. On the other hand, based on the calibrated DIs, structural optimization problems were formulated aiming at identifying the DI, or the combination of Dis that will provide reliable information on damage so that they can be incorporated into a Performance-Based Design framework. The ultimate objective of this task is to compare lower-bound designs that satisfy the design code requirements in the most cost-effective way using a Life-Cycle Cost Analysis (LCCA) methodology. The solution of the structural optimization problem is dealt with the most advanced metaheuristic optimization algorithms, namely the Evolution Strategies (ES) method, the Differential Evolution (DE) method, the Particle Swarm Optimization (PSO)

method as well as the Harmony Search (HS) method. (iii) The next step is to improve the LCCA procedure with reference to both its robustness and efficiency. The robustness was achieved by improving the formulation of the LCCA procedure by incorporating the maximum floor acceleration and by identifying the factors that affect the accuracy of the procedure. In order to combine robustness and computational efficiency, a procedure for selecting the most representative artificial seismic excitations at each hazard level is proposed leading to a reduction of the required computational effort for performing LCCA of structures. (iv) The last objective of the dissertation is to improve the fragility analysis procedure with reference to both robustness and efficiency. The robustness is achieved by an improved procedure for calculating the two parameters of the lognormal distribution obtained by means of the Harmony Search optimization algorithm and the maximum likelihood method. The efficiency is achieved by introducing a neural network-based incremental dynamic analysis (IDA) procedure that reduces the computational effort by one order of magnitude.

The dissertation consists of eight chapters in total, plus two appendices at the end. Its structure is organized as follows: *Chapter 1* contains the introduction of the dissertation, *Chapter 2* describes the indices that are used to quantify structural damage and their values related to particular damage states. For this purpose, five damage indices are calibrated into a number of limit states for reinforced concrete structures using solid 3D and beam-column finite element modelling. *Chapter 3* discusses the problem of deterministic single objective optimization, while various methods for solving the structural optimization problem are presented, with a particular emphasis in the metaheuristic optimization methods that have been implemented in this dissertation are discussed in more detail. *Chapter 4* presents the basic principles of the prescriptive and the PBD procedures for buildings. *Chapter 5* presents the basic principles of the probabilistic seismic hazard analysis. In order to examine the influence of the seismic records selected on an LCCA framework, three different classes of seismic records are considered in Chapter 5 and their influence on the outcome sensitivity of LCCA is examined. *Chapter 6* provides the LCCA framework which is based on economic theories and has been used as the decision-support tool. *Chapter 7* describes the fragility analysis framework along with the methods for dealing with the problem of reliability analysis. Furthermore, a methodology incorporating soft computing techniques, like neural networks and metaheuristics, for reducing the computational effort is also presented in *Chapter 7*. In *Chapter 8* the conclusions of the research work are presented. Finally, two Appendices are included: *Appendix A* contains the list and characteristic parameters of the seismic records used in the dissertation; and *Appendix B* gives details on the modelling and

the material constitutive laws that have been used in the dissertation.

Περίληψη

Ο κύριος στόχος της διατριβής είναι η ανάπτυξη ενός ολοκληρωμένου πλαισίου για την αξιολόγηση και τον οικονομικό-ασφαλή αντισεισμικό σχεδιασμό κατασκευών. Αυτός ο καθολικός στόχος της διατριβής επετεύχθη μέσω των ακόλουθων βημάτων: (i) Στο πρώτο μέρος της διατριβής πραγματοποιήθηκε αριθμητική βαθμονόμηση ορισμένων από τους πιο δημοφιλείς δείκτες βλάβης (DI) που έχουν προταθεί και υιοθετηθεί από πολλούς ερευνητές προκειμένου να προσδιορίσουν το επίπεδο ζημίας κατασκευών από οπλισμένο σκυρόδεμα. Ειδικότερα βαθμονομήθηκαν, ο τοπικός δείκτης των Park και Ang, η τροποποιημένη εκδοχή του όπως προτάθηκε από τους Kunnath, Reinhorn και Lobo, ο τοπικός δείκτης των Chung, Meyer και Shinozuka, καθώς και οι λόγοι της μέγιστης χαλάρωσης (maximum softening) και της τελικής χαλάρωσης (final softening) που προτάθηκαν από τους DiPasquale και Cakmak. (ii) Στο δεύτερο στάδιο της διατριβής πραγματοποιήθηκε αξιολόγηση των περιγραφικών διαδικασιών αντισεισμικού σχεδιασμού σε σχέση με τον συντελεστή συμπεριφοράς που υιοθετείται από τους Ευρωκώδικες και διερευνήθηκε η βέλτιστη επιλογή που οδηγεί στον οικονομικότερο και ασφαλέστερο σχεδιασμό. Επιπροσθέτως έγινε σύγκριση των μεθόδων σχεδιασμού με βάση την επίδοση σε σχέση με τις περιγραφικές μεθόδους σχεδιασμού. Και οι δύο αξιολογήσεις επετεύχθησαν μέσω της διατύπωσης προβλημάτων βέλτιστου αντισεισμικού σχεδιασμού. Στη συνέχεια, με βάση τους βαθμονομημένους δείκτες βλάβης, διατυπώθηκαν προβλήματα βελτιστοποίησης με στόχο να προσδιοριστεί ο δείκτης βλάβης ή ο συνδυασμός δεικτών βλάβης που αποτελούν την σωστότερη επιλογή προκειμένου να ενσωματωθεί στο πλαίσιο σχεδιασμού που βασίζεται στην επιτελεστικότητα (PBD). Οι βέλτιστοι σχεδιασμοί που προκύπτουν αξιολογούνται με βάση το αρχικό και το κόστος κύκλου ζωής (LCCA) . Η επίλυση του προβλήματος βελτιστοποίησης πραγματοποιήθηκε με τους πιο προηγμένους μεταευριστικούς αλγόριθμους βελτιστοποίησης, όπως είναι η

μέθοδος evolution strategies (ES), η μέθοδος deferential evolution (DE), η μέθοδος particle swarm optimization (PSO) καθώς η μέθοδος harmony search (HS). (iii) Ως επόμενο βήμα της διατριβής ήταν η βελτίωση της διαδικασίας LCCA όσον αφορά την αξιοπιστία και την υπολογιστική αποδοτικότητά της. Η αξιοπιστία επετεύχθη με τη βελτίωση της διατύπωσης της διαδικασίας LCCA μέσω της ενσωμάτωσης της μέγιστης επιτάχυνσης των ορόφων στη διαδικασία υπολογισμού και του εντοπισμού των παραγόντων που επηρεάζουν την ακρίβεια της εν λόγω διαδικασίας. Για τον συνδυασμό αξιοπιστίας και υπολογιστικής αποδοτικότητας, προτάθηκε μια διαδικασία για την επιλογή των πλέον αντιπροσωπευτικών τεχνητών σεισμικών διεγέρσεων σε κάθε επίπεδο σεισμικής επικινδυνότητας, η οποία οδηγεί στη μείωση του απαιτούμενου υπολογιστικού φόρτου για την εκτέλεση της ανάλυσης LCCA. (iv) Ο τελευταίος στόχος της διατριβής ήταν η βελτίωση της διαδικασίας ανάλυσης τρωτότητας σε σχέση με την αξιοπιστία και την υπολογιστική αποδοτικότητα. Η αξιοπιστία επιτυγχάνεται μέσω βελτίωσης της διαδικασίας υπολογισμού των δύο παραμέτρων της λογαριθμικής κατανομής, που προκύπτουν με τη βοήθεια του αλγορίθμου βελτιστοποίησης Harmony Search (HS) και της μεθόδου της μέγιστης πιθανοφάνειας. Η υπολογιστική αποδοτικότητα επετεύχθη μέσω της προτεινόμενης στο πλαίσιο της παρούσης διατριβής προσαυξητικής δυναμικής ανάλυσης με βάση πρόβλεψης νευρωνικών δικτύων η οποία μειώνει τις υπολογιστικές απαιτήσεις κατά μία τάξη μεγέθους.

Η διατριβή αποτελείται από οκτώ κεφάλαια και δύο παραρτήματα. Η δομή της είναι οργανωμένη ως εξής: Το *Κεφάλαιο 1* αποτελεί την εισαγωγή της διατριβής, στο *Κεφάλαιο 2* περιγράφονται οι δείκτες που χρησιμοποιούνται για την ποσοτικοποίηση ζημιών. Επιπλέον, βαθμονομήθηκαν πέντε δείκτες ζημίας για κατασκευές από οπλισμένο σκυρόδεμα με χρήση προσομοιωμάτων με τριδιάστατα και ραβδόμορφα πεπερασμένα στοιχεία. Στο *Κεφάλαιο 3* παρουσιάζεται το θέμα του προσδιοριστικού προβλήματος βελτιστοποίησης, επίσης παρουσιάζονται οι πιο δημοφιλείς μεταευριστικές μέθοδοι βελτιστοποίησης οι οποίες έχουν εφαρμοστεί στο πλαίσιο της διατριβής. Στο *Κεφάλαιο 4* παρουσιάζονται οι βασικές αρχές των περιγραφικών διαδικασιών σχεδιασμού καθώς και εκείνων με βάση την επιτελεστικότητα. Στο *Κεφάλαιο 5* παρουσιάζονται οι βασικές αρχές της πιθανοτικής ανάλυσης σεισμικής επικινδυνότητας. Προκειμένου να μελετηθεί η επίδραση των σεισμικών καταγραφών στο πλαίσιο LCCA, επιλέγονται τρεις διαφορετικές κατηγορίες σεισμικών καταγραφών και εξετάζεται η επιρροή τους στην ανάλυση LCCA. Στο *Κεφάλαιο 6* παρουσιάζεται το πλαίσιο LCCA το οποίο βασίζεται σε θεωρίες οικονομικής ανάλυσης και έχει χρησιμοποιηθεί ως εργαλείο υποστήριξης λήψης αποφάσεων. Το *Κεφάλαιο 7* περιγράφει το πλαίσιο ανάλυσης τρωτότητας, μαζί με τις μεθόδους που χρησιμοποιούνται

για την αντιμετώπιση του προβλήματος της ανάλυσης αξιοπιστίας. Επιπλέον, παρουσιάζεται μια μέθοδος βασισμένη σε νευρωνικά δίκτυα και μεταευριστικής βελτιστοποίησης για τη βελτίωση της υπολογιστικής αποδοτικότητας. Στο *Κεφάλαιο 8* παρουσιάζονται τα συμπεράσματα της ερευνητικής αυτής εργασίας. Τέλος, το *Παράρτημα Α* περιέχει τον κατάλογο των σεισμικών καταγραφών που χρησιμοποιούνται στη διατριβή, ενώ το *Παράρτημα Β* παρέχει λεπτομέρειες για την προσομοίωση και τους καταστατικούς νόμους των υλικών που έχουν χρησιμοποιηθεί στη διατριβή.

Acknowledgements

I would like to express my deepest gratitude to Professor Manolis Papadrakakis who was the supervisor of this research study, for giving me the opportunity to do my doctoral study at the Institute of Structural Analysis and Antiseismic Research, for his inestimable support and guidance throughout this research and for creating a friendly and collaborative working environment. His knowledge has been very instructive during this first step of my academic career.

Furthermore, I would also like to thank the two members of the advisory committee Assistant Professor Christos A. Zeris and Lecturer Nikos D. Lagaros, for their invaluable assistance and their advices during the time of my research work and the preparation of this dissertation.

I would also like to thank my family, who has been very supportive. Their encouragement and their moral support throughout the academic years have been invaluable. Also I would like to express my gratitude to my friend Maria for her encouragement during the preparation of my PhD dissertation.

Finally, I would like to express my gratitude to John Argyris Foundation, created in memory of the great Greek scientist and engineer, John Argyris, who invented the "Finite Element Method" (http://www.argyrisfoundation.org) and the Research Funding Department of the National Technical University of Athens for the financial support during the four years of the doctoral studies.

Table of Contents

Abstract i

Περίληψη v

Acknowledgements ix

Chapter 1-Introduction 1

1.1. Background & Motivation 1

1.2. Objectives-Research Framework 4

1.3. Analysis of the Contents 6

1.4. References 9

Chapter 2-Calibration of Damage Indices for RC Structures 11

2.1. Introduction 11

2.2. Damage indices based on maximum deformation 12

2.2.1. Ductility ratio 12

2.2.2. Interstorey drift 12

2.2.3. Slope ratio 13

2.2.4. Flexural damage ratio 13

2.2.5. Maximum permanent drift 13

2.3. Damage indices based on cumulative damage 13

2.3.1. Normalized cumulative rotation 13

2.3.2. Low-cycle fatigue 14

2.4. Damage indices accounting for both maximum deformation and cumulative damage 14

2.4.1. Park and Ang local damage index 14

2.4.2. Modified Park and Ang global and local damage indices 17

2.4.3. Chung, Meyer and Shinozuka's local damage index 18
2.4.4. Maximum softening and final softening 20
2.4.5. Banon and Veneziano Damage Index 24
2.5. Global damage indices 24
2.6. A Unified Procedure for Calibrating the Damage Indices 25
2.6.1. Calibration procedure 25
2.6.2. 2D test example 27
2.6.3. 3D test example 32
2.7. Discussion 36
2.8. References 38

Chapter 3-Structural Design Optimization: Formulations & Methods ... 41
3.1. Introduction 41
3.2. History of optimization 43
3.3. Formulation of the structural optimization problem 44
3.3.1. Design Variables 45
3.3.2. Objective Function 46
3.3.3. Constraint Functions 47
3.3.4. Global and local minimum 49
3.4. Classes of Optimization 50
3.4.1. Sizing Optimization 50
3.4.2. Shape Optimization 52
3.4.3. Topology Optimization 53
3.5. Evolutionary Algorithms 55
3.5.1. Recombination 56
3.5.2. Mutation 57
3.5.3. Selection 58
3.5.4. The ES algorithm 58
3.5.5. ES for structural optimization problems 59
3.6. Differential Evolution 60
3.6.1. Scheme DE1 62
3.6.2. Scheme DE2 63
3.7. Particle Swarm Optimization algorithm 64
3.7.1. Relationship of PSO with Evolutionary Algorithms 65
3.7.2. Mathematical formulation of PSO 66
3.7.3. Convergence criteria 68
3.7.4. PSO for integer optimization 69

3.8. Harmony Search ... 70
3.8.1. Algorithm Parameter Setting ... 71
3.8.2. Harmony memory initialization ... 73
3.8.3. Harmony Improvisation ... 73
3.8.4. Memory Update ... 74
3.9. References ... 75

Chapter 4-Seismic Design Procedures: Prescriptive vs Performance-Based Design ... 79
4.1. Introduction ... 79
4.2. Seismic Design Procedures ... 80
4.2.1. Prescriptive design procedures ... 81
4.2.2. Response modification factors (q or R) ... 82
4.2.3. Performance-based design procedure ... 84
4.3. Analysis procedures ... 88
4.3.1. Nonlinear Static Procedures-Pushover ... 89
4.3.2. Nonlinear Dynamic Procedures ... 92
4.4. Assessment of seismic design procedures ... 100
4.4.1. Definition of Seismic Response Spectra ... 100
4.4.2. Case study ... 103
4.4.3. Design with Greek national design codes and PBD ... 104
4.4.4. Comparison with respect to the total cost ... 107
4.4.5. Discussion ... 108
4.5. Structural Optimization: An assessment approach of design procedures against earthquake hazard ... 109
4.5.1. Formulation of the optimization problem ... 110
4.5.2. Five storey non-symmetrical test example ... 112
4.5.3. Eight storey symmetrical test example ... 113
4.5.4. Discussion ... 115
4.6. A new performance-based seismic design framework based on damage indices and structural optimization ... 115
4.6.1. Formulation of the optimization problem ... 115
4.6.2. Optimum design results ... 118
4.6.3. Assessment of the optimum design ... 119
4.6.4. Discussion ... 121
4.7. References ... 123

Chapter 5-Seismic Hazard Analysis: ground excitation for design and assessment....127
5.1. Introduction....127
5.2. Deterministic Seismic Hazard Analysis....129
5.3. Probabilistic Seismic Hazard Analysis....130
5.3.1. Seismic Source Model....132
5.3.2. Earthquake recurrence frequency....133
5.3.3. Ground Motion Model (Attenuation Relationship)....133
5.3.4. Handling Uncertainties....135
5.4. Ground Motion Excitation....136
5.4.1. Natural records....137
5.4.2. Generation of artificial accelerograms....137
5.4.3. Probabilistic definition of the artificial ground motion characteristics....139
5.5. Structural Models and Numerical Simulation....144
5.6. Intensity Measures....144
5.7. Numerical Tests....147
5.8. Implementation of the LCCA....147
5.9. Uncertainty on the seismic excitation....149
5.10. Discussion....152
5.11. References....153

Chapter 6-Life-Cycle Cost Assessment of Structures....157
6.1. Introduction....157
6.2. Literature Survey....158
6.3. Life-cycle Cost Analysis....160
6.3.1. Calculation of the life-cycle cost....161
6.3.2. Implementation of the analysis procedures in the LCCA framework....165
6.4. Illustrative example....169
6.5. LCCA of buildings designed based on energy dissipation....173
6.5.1. Five storey non-symmetrical test example....173
6.5.2. Eight storey symmetrical test example....177
6.6. Factors affecting the life-cycle cost analysis of reinforced concrete buildings....179
6.6.1. Structural Models and Numerical Simulation....180
6.6.2. Ground motion selection....181
6.6.3. Multiple Stripe Analysis Results....183
6.6.4. Sensitivity Analysis of LCCA....186

6.6.5. Nonlinear Static Analysis vs Nonlinear Dynamic Analysis 190
6.7. Discussion 192
6.8. References 193

Chapter 7-Fragility Assessment of Structural Systems 197
7.1. Introduction 197
7.2. Risk Definition 199
7.3. Risk Assessment 200
7.4. Fragility Analysis 203
7.4.1. Damage Limit States 206
7.4.2. Calculation of Damage-State Probability 209
7.4.3. Factors influence the shape of fragility curves 210
7.5. Artificial neural networks 211
7.5.1. Regularization 213
7.5.2. Learning Algorithms 214
7.6. Calculating the Probabilities - Solving the Reliability Analysis Problem 216
7.6.1. Monte Carlo simulation 216
7.6.2. First-Order Reliability method 219
7.7. Vertical & Horizontal Statistics - Incremental Dynamic Analysis 223
7.8. Seismic demand evaluations using neural networks 225
7.8.1. Selection of intensity measures 225
7.8.2. Prediction scheme 226
7.9. Structural models and Numerical simulation 228
7.10. Numerical tests 230
7.10.1. ANN predictions 231
7.10.2. Fragility analysis 233
7.10.3. Computational cost 236
7.11. Discussion 237
7.12. References 239

Chapter 8-Conclusions & Recommendations for Further Study 243
8.1. Contributions of the Study 243
8.1.1. Calibration of the damage indices 243
8.1.2. Antiseismic design procedures 243
8.1.3. Life cycle cost analysis procedure 245
8.1.4. Fragility analysis procedure 246

8.2. Software development 246
8.3. General Conclusions 247
8.4. Recommendation for Further Research 248
8.5. Publications 248

Appendix A-Seismic Records 251
A.1. Introduction 251
A.2. Seismic Records 251
A.3. References 259

Appendix B-Modelling & Constitutive Laws 261
B.1. Introduction 261
B.2. Numerical Modelling 261
B.2.1. Three-Dimensional Finite Element - Embedded Reinforcement Simulation 261
B.2.2. Formulation of Beam-Column Element 262
B.2.3. Modelling of Infill Walls 263
B.2.4. Modelling of shear reinforcement 267
B.3. Constitutive Models 267
B.3.1. Constitutive law for 3D solid elements 267
B.3.2 Constitutive law for fibre beam-column elements 268
B.4. References 273

List of Figures

Figure 1.1. Research framework of the Dissertation. 5

Figure 2.1. Damage modifier α (Chung et al., 1987). 20
Figure 2.2. IDA-based calibration procedure. 26
Figure 2.3. 2D test example – (a) front and plan views and (b) roof displacement-base shear curve. 27
Figure 2.4. 2D test example – cross sections. 28
Figure 2.5. 2D test example (a) FE mesh and (b) steel reinforcement. 28
Figure 2.6. 2D test example-cracked structure. 29
Figure 2.7. 2D test example-IDA curves. 30
Figure 2.8. 3D test example – (a) front, (b) side views and (c) roof displacement-base shear curve.. 32
Figure 2.9. 3D test example – cross sections. 33
Figure 2.10. 3D test example-(a) FE mesh and (b) steel reinforcement. 34
Figure 2.11. 3D test example-cracked structure. 34
Figure 2.12. 3D test example-IDA curves. 35

Figure 3.1. The structural optimization procedure. 42
Figure 3.2. Sizing optimization problem (a) Components of an overhead travelling crane, design variables in the (b) bridge girder and (c) runway beam. 51
Figure 3.3. Shape optimization problem (a) engine block-initial shape and (b) engine block-final shape. 52
Figure 3.4. Topology optimization for a single loading. 54
Figure 3.5. Pseudo-code of the ES algorithm. 59
Figure 3.6. Flowchart of the differential evolution algorithm. 61
Figure 3.7. Two dimensional example of an objective function showing its contour lines and the process for generating v in scheme DE1. 61
Figure 3.8. Illustration of the crossover process for n=7. 62
Figure 3.9. Two dimensional example of an objective function showing its contour lines and the process for generating v in scheme DE2. 63
Figure 3.10. Visualization of the particle's movement in a two-dimensional design space. 67
Figure 3.11. Flowchart of the particle swarm optimization algorithm. 70
Figure 3.12. Analogy between improvisation and optimization. 71
Figure 3.13. Flowchart of the harmony search algorithm. 72

Figure 4.1. Flowchart of the employed PBD design procedure. 86
Figure 4.2. The design performances objectives for different importance classes. 88

Figure 4.3. Median IDA curve of IDA curves for ten different earthquake records. 93
Figure 4.4. IDA curves for different records of seismic hazards. 94
Figure 4.5. Median IDA curve and HAZUS (2003) recommended limit states. 95
Figure 4.6. Definition of the incident angle α (Lagaros, 2010). 96
Figure 4.7. The MIDA procedure (Lagaros, 2010). 97
Figure 4.8. Latin hypercube sampling of record-incident angle pairs. 98
Figure 4.9. Multi-stripe dynamic analysis. 99
Figure 4.10. Response spectra and median (a) component X, (b) component Y for the records of Table 4.3. 103
Figure 4.11. Geometry of the three storey 3D building (a) layout, (b) front view. 104
Figure 4.12. Design $D_{q=3.5}$, beam-column reinforcement of a typical frame. 106
Figure 4.13. Design D_{PBD}, beam-column reinforcement of a typical frame. 106
Figure 4.14. Comparison of the designs with respect to (a) the normalized initial, (b) the normalized limit state and total cost. 107
Figure 4.15. Five storey test example - (a) plan view, (b) front view. 113
Figure 4.16. Eight storey test example - (a) plan view, (b) front view. 114
Figure 4.17. Test example - (a) three-storey, (b) six-storey. 117
Figure 4.18. Three-storey test example – comparison with reference to (a) maximum drift, (b) maximum floor acceleration, (c) maximum softening, (d) final softening, (e) Park & Ang damage index, (f) Kunnath, Reinhorn & Lobo damage index and (g) Chung, Meyer & Shinozuka damage index. 120
Figure 4.19. Six-storey test example – comparison with reference to (a) maximum drift, (b) maximum floor acceleration, (c) maximum softening, (d) final softening, (e) Park & Ang damage index, (f) Kunnath, Reinhorn & Lobo damage index and (g) Chung, Meyer & Shinozuka damage index. 121

Figure 5.1. Steps in deterministic seismic hazard analysis (Kramer, 1996). 130
Figure 5.2. Example of deterministic seismic hazard analysis (Kramer, 1996). 131
Figure 5.3. Steps in probabilistic seismic hazard analysis. 132
Figure 5.4. Median value and 95% confidence region predicted by the Boore, Joyner, and Fumal (1997) attenuation relationship for strike slip earthquakes and soil site conditions (taken from Field, 2010). 135
Figure 5.5. Hazard curves for the two scenarios treated as epistemic uncertainties (Field, 2010). 136
Figure 5.6. (a) Target (elastic design) response spectrum and response spectrum of the artificial accelerogram and (b) artificial accelerogram. 138
Figure 5.7. Mean response spectra of the 60 records for the class of (a) Artificial accelerograms and (b) Natural records (The dotted lines represent the μ+σ and μ-σ response spectra). 139
Figure 5.8. Mean and dispersion hazard curves of the city of San Diego, California (Latitude (N) 32.7°, Longitude (W) -117.2°). 140
Figure 5.9. Partial logic tree for the 2002 update of the California seismic hazard model (Cao et. al, 2002). 141
Figure 5.10. The UART procedure for generating artificial accelerograms based on LHS (M=3). 142
Figure 5.11. Artificial accelerograms with uncertainty (The dotted lines represent the μ+σ and μ-σ response spectra). 143
Figure 5.12. Mean and 25%, 75% confidence bounds for the values of I_A, I_C and CAV obtained for the classes of records considered. 146
Figure 5.13. Eight storey test example: (a) frequency of occurrence for the case of MSDA(60) and (b) cumulative density function. 148
Figure 5.14. Five storey test example: (a) frequency of occurrence for the case of MSDA(60) and (b) cumulative density function. 150

Figure 5.15. Variation with reference to the number of records (103 MU): (a) eight storey test example (b) five storey test example 152

Figure 6.1. Flowchart of the life-cycle cost analysis framework. 161
Figure 6.2. Hazard curve of the city of San Diego, California (Latitude (N) 32.7°, Longitude (W) -117.2°). 166
Figure 6.3. Implementation of nonlinear static analysis procedure in LCCA framework. 167
Figure 6.4. Implementation of nonlinear dynamic analysis procedure in LCCA framework. 168
Figure 6.5. The model for the C7-B5-C8-B6-C9 (a) fully infilled frame and (b) layout. 171
Figure 6.6. $(\overline{P}_i - \theta_{max,i})$ pairs and fitted curve. 172
Figure 6.7. Examples of fitted curves. 172
Figure 6.8. Five storey test example - front view. 174
Figure 6.9. Five storey test example – 50% median values of the maximum (a) interstorey drift values and (b) floor accelerations for the four designs. 175
Figure 6.10. Five storey test example - Initial (CIN), expected (CLC) and total expected (TOT) life-cycle costs for different values of the behaviour factor q (t=50 years, λ=5%). 175
Figure 6.11. Five storey test example - Contribution of the initial cost and limit state cost components to the total expected life-cycle cost for different values of the behaviour factor q. 176
Figure 6.12. Eight storey test example - front view. 176
Figure 6.13. Eight storey test example – 50% median values of the maximum (a) interstorey drift values and (b) floor accelerations for the four designs. 177
Figure 6.14. Eight storey test example - Initial (CIN), expected (CLC) and total expected (TOT) life-cycle costs for different values of the behaviour factor q (t=50 years, λ=5%). 178
Figure 6.15. Eight storey test example - Contribution of the initial cost and limit state cost components to the total expected life-cycle cost for different values of the behaviour factor q. 179
Figure 6.16. Response spectra of the group of 60 records scaled to the 10/50 hazard level, of the city of San Diego, according to the $S_A(T_1,5\%)$ (a) longitudinal and (b) transverse direction. 183
Figure 6.17. Eight storey test example: Medians and 16,84% fractiles of maximum drifts for (a) MSDA(10), (b) MSDA(20), (c) MSDA(40) and (d) MSDA(40). 184
Figure 6.18. Eight storey test example: Medians and 16,84% fractiles of maximum floor acceleration for (a) MSDA(10), (b) MSDA(20), (c) MSDA(40) and (d) MSDA(40). 185
Figure 6.19. Five storey test example: Medians and 16,84% fractiles of maximum drifts for (a) MSDA(10), (b) MSDA(20), (c) MSDA(40) and (d) MSDA(40). 186
Figure 6.20. Five storey test example: Medians and 16,84% fractiles of maximum floor acceleration for (a) MSDA(10), (b) MSDA(20), (c) MSDA(40) and (d) MSDA(40). 187
Figure 6.21. Eight storey test case: Frequency of occurrence for the case of (a) MSDA(10), (b) MSDA(20), (c) MSDA(40), (d) MSDA(60). 188
Figure 6.22. Five storey test example: Frequency of occurrence for the case of (a) MSDA(10), (b) MSDA(20), (c) MSDA(40), (d) MSDA(60). 189
Figure 6.23. Eight storey test example – Cumulative Density Function: (a) drift plus floor acceleration, (b) drift. 189
Figure 6.24. Five storey test example - Cumulative Density Function: (a) drift plus floor acceleration, (b) drift. 190
Figure 6.25. Eight storey test example: Total life-cycle cost (10^3 MU). 191
Figure 6.26. Five storey test example: Total life-cycle cost (10^3 MU). 191

Figure 7.1. PEER analysis framework. Adapted from Porter (2003). 202
Figure 7.2. Typical fragility curves versus the intensity of the seismic ground motion (F_R) 204
Figure 7.3 Multi-stripe analysis for calculating the probability of exceedance of a limit state 205
Figure 7.4. Example of fragility curves - Calculation of damage-state probability 210
Figure 7.5. A typical artificial neural network 212

Figure 7.6. MCS-NN - (a) Methodology 1, (b) Methodology 2. 218
Figure 7.7. Standard sampling method (Bucher and Bourgund, 1990) (a) before and (b) after correction. 221
Figure 7.8. The FORM-NN methodology. 222
Figure 7.9. LHS technique (a) before and (b) after correction. 223
Figure 7.10. IDA curve-"vertical" and "horizontal" statistics. 224
Figure 7.11. Latin hypercube sampling in the two-dimensional space. 226
Figure 7.12. Eight storey test example-front view. 227
Figure 7.13. Five storey test example-front view. 228
Figure 7.14. ANN-based incremental dynamic analysis. 230
Figure 7.15. Eight storey test example-ANN prediction capability over the testing set: (a) Slight damage limit state (0.25%), (b) Moderate damage limit state (0.50%), (c) Extensive damage limit state (1.50%) and (b) Collapse limit state (4.00%). 231
Figure 7.16. Five storey test example-ANN prediction capability over the testing set: (a) Slight damage limit state (0.30%), (b) Moderate damage limit state (0.70%), (c) Extensive damage limit state (2.00%) and (b) Collapse limit state (5.33%). 233
Figure 7.17. Eight storey test example-Fragility curves for four limit-states using alternative number of records. 234
Figure 7.18. Five storey test example-Fragility curves for four limit-states using alternative number of records. 235
Figure 7.19. Hazard curve for $S_A(T_1=1.0\ sec,5\%)$. 236

Figure B.1. Modelling of the inelastic behaviour-the fibre approach 263
Figure B.2. The equivalent diagonal struts. 264
Figure B.3. Strength envelope for conventional masonry infill walls. 265
Figure B.4. Shear law. 267
Figure B.5. Modified Kent-Park model, stress-strain relation for confined and unconfined concrete 270
Figure B.6. Hysteric concrete stress-strain relation 271
Figure B.7. The multi-linear stress-strain law for reinforcement. 272

List of Tables

Table 2.1. Interpretation of overall damage index (Park et al., 1986). 17
Table 2.2. Interpretation of overall damage index (Chung et al., 1993) 20
Table 2.3. Damage indices based on equivalent linear models. 23
Table 2.4. Damage state with reference to crack width (Toussi & Yao, 1983) 26
Table 2.5. 2D test example - number of elements, nodes, degrees of freedom. 28
Table 2.6. 2D test example-Damage state with reference to crack width. 31
Table 2.7. 2D test example- Coefficient of variation of the damage indices in percentages. 31
Table 2.8. 3D test example - number of elements, nodes, degrees of freedom. 33
Table 2.9. 3D test example-Damage state with reference to crack width. 36
Table 2.10. 3D test example-Coefficient of variation of the damage indices in percentages. 36

Table 3.1. Main PSO parameters. 68
Table 3.2. PSO convergence parameters. 69

Table 4.1. Limit states values defined by HAZUS (2003). 95
Table 4.2. Natural records representing the 50% in 50 year hazard level (Somerville and Collins, 2002) 100
Table 4.3. Natural records representing the 10% in 50 year hazard level (Somerville and Collins, 2002) 101
Table 4.4. Natural records representing the 2% in 50 year hazard level (Somerville and Collins, 2002) 101
Table 4.5. Seismic hazard levels (Papazachos et al., 1993). 101
Table 4.6. Comparison of steel and concrete quantities in the twelve designs. 105
Table 4.7. Detailed breakdown comparison of steel quantity (kg) in the four selected designs. 105
Table 4.8. Five storey test example - Optimum designs obtained for different values of behaviour factor q. 110
Table 4.9. Eight storey test example - Optimum designs obtained for different values of behaviour factor q. 113
Table 4.10. Definition of the limit states. 116
Table 4.11. Three-storey test example: Comparison of steel and concrete quantities in the twelve designs. 118
Table 4.12. Six-storey test example: Comparison of steel and concrete quantities in the twelve designs. 118
Table 4.13. Three-storey test example – comparison with reference to the damage indices. 121

Table 4.14. Six-storey test example – comparison with reference to the damage indices. 122

Table 6.1. Damage indices limits for bare moment resisting frames. 163
Table 6.2. Limit state cost - calculation formulas (Wen & Kang, 2001a, and 2001b). 163
Table 6.3. Limit state parameters for cost evaluation. 164
Table 6.4. Damage state drift ratio limits for ductile RC moment resisting frames with infills. 170
Table 6.5. Limit state dependent cost calculations for the fully infilled design (in 1,000 MU). 170
Table 6.6. Calculation of the limit state dependent cost for the fully infilled design. 173
Table 6.7. Five storey test example - Limit state cost components (1,000 MU). 173
Table 6.8. Eight storey test example – Cross sections of the beams and the columns 180
Table 6.9. Five storey test example - Cross sections of the beams and the columns 181

Table 7.1. The HRC-Scale: Typical damage expected in ductile, non-ductile and infilled RC moment resisting frames and in RC shear-wall structures (Rossetto & Elnasai, 2003). 207
Table 7.2 An approximate equivalence between existing damage scales and the HRC-Scale (Rossetto & Elnasai, 2003). 208
Table 7.3. Eight storey test example – Cross sections of the beams and the columns 228
Table 7.4. Five storey test example - Cross sections of the beams and the columns 229
Table 7.5. Eight storey test example-Mean annual frequencies of limit-state exceedance. 235
Table 7.6. Five storey test example-Mean annual frequencies of limit-state exceedance. 236
Table 7.7. Eight storey test example-Computational time in days. 237
Table 7.8. Five storey test example-Computational time in days. 237

Table A.1. Characteristics of the first group of 20 records 252
Table A.2. Characteristics of the second group of 20 records 253
Table A.3. Characteristics of the third group of 20 records 254
Table A.4. Characteristics of the fourth set of 22 natural records 255
Table A.5. Characteristics of the fifth set of 30 natural records 256
Table A.6. Characteristics of the sixth set of 23 natural records 257
Table A.7. Characteristics of the seventh set of 25 natural records 258

List of Acronyms

AD	Acceleration-Displacement
ANN	Artificial Neural Networks
ART	Artificial accelerograms
BW	Bandwidth
CDF	Cumulative Density Function
COV	Coefficient of Variation
CSM	Capacity Spectrum Method
DE	Differential Evolution
DI	Damage Index
DSHA	Deterministic Seismic Hazard Analysis
EA	Evolutionary Algorithms
EAK	National seismic code of Hellas
EC2	Eurocode 2
EC8	Eurocode 8
EDP	Engineering Demand Parameter
EDRs	Elastic Design Response spectrum
EKOS	National code for concrete building structures of Hellas
EP	Evolutionary Programming
ES	Evolutionary Strategies
ESDOF	Equivalent Single Degree of Freedom
FE	Finite Element
FORM	First-Order Reliability-Method

FSD	Fully Stressed Design
FW	Fret Width
GA	Genetic Algorithms
GNDC	Greek National Design Code
HL	Hazard Level
HMCR	Harmony Memory Considering Rate
HMS	Harmony Memory Size
HS	Harmony Search
IDA	Incremental Dynamic Analyses
IM	Intensity Measure
LCCA	Life Cycle Cost Analysis
LDP	Linear Dynamic Procedure
LHS	Latin Hypercube Sampling
LS	Limit States
LSP	Linear Static Procedure
MAF	Mean Annual Frequency
MCEs	Maximum Credible Earthquakes
MCS	Monte Carlo Simulation
MHC	Mean Hazard Curve
MI	Maximum Improvisation
MIDA	Multicomponent Incremental Dynamic Analysis
MmRS	Multi-modal Response Spectrum
MP	Mathematical Programming
MRF	Moment Resisting Frame
MSDA	Multiple-Stripe Dynamic Analysis
MU	Monetary Units
NAT	Natural seismic records
NDA	Nonlinear Dynamic Analysis
NDP	Nonlinear Dynamic Procedure
NSA	Nonlinear Static Analysis
NSP	Nonlinear Static Procedure
PAR	Pitch Adjusting Rate
PBEE	Performance-Based Earthquake Engineering
PGA	Peak Ground Acceleration

PGV	Peak Ground Velocity
PSHA	Probabilistic Seismic Hazard Analysis
PSO	Particle Swarm Optimization
RBO	Reliability Based Optimization
RC	Reinforced Concrete
Rprop	Resilient backpropagation
RS	Response Surface
SA	Simulated Annealing
$S_A(T_1,5\%)$	Structure's first-mode period
SC	Soft Computing
SOO	Single Objective Optimization
SORM	Second-Order Reliability-Method
SQP	Sequential Quadratic Programming
UART	Artificial accelerograms with stochastic characteristics
USGS	United States Geological Survey

Chapter 1

Introduction

1.1. Background & Motivation

The exploitation of computer technology, which is the most important technological development of the 20th century, impelled Computational Mechanics to emerge, leading to revolutionary changes in the theoretical background as well as to the engineering seismic design practice through the introduction of innovative design methodologies. These significant changes had a profound impact in the field of computational earthquake engineering. In addition to these changes that have taken place, engineers always strive to design efficient structural systems which must be as light and economic as possible, yet strong enough to withstand all possible loads arising during the building service life without catastrophic failures, and to absorb the induced base excitation energy under different levels of intensity in a controlled and predictable fashion. This effort, which is inherent in human nature, necessitates the use of advanced computational techniques and reliable numerical simulation approaches for a more accurate prediction of the nonlinear system behaviour under seismic events in order to improve the design and assessment procedures of structural steel or reinforced concrete systems under earthquake. In this Dissertation reinforced concrete buildings designed to the current seismic provisions for ductility are studied.

The design and assessment procedures of engineering structures under seismic loading are computationally intensive tasks, since in order to assess the structural performance or different hazard levels, an accurate and reliable prediction of the nonlinear dynamic response is required. Furthermore, in order to account for the handling of data on the actual geometry, the properties of the materials, the numerical modelling as well as the intensity and characteristics of the input seismic loading, life-cycle cost and fragility analyses together

with design procedures that include both aleatory and epistemic uncertainties should be considered. The computational effort required for solving different types of structural problems increases drastically, starting from the linear elastic time history dynamic analysis to the most demanding, but very essential in reaching a safe and economic design, nonlinear dynamic time history analysis performed in multiple hazard levels. Even with today's reduction in the cost of computational resources and the increasing availability of powerful processors, the cost of design of complex large-scale engineering systems and structures can become excessive. The realization, therefore, of such demanding designs could only be achieved with orders of magnitude reduction of the required computational effort. Such a reduction can be achieved by a synergy of the following actions: using cost-efficient and accurate-enough reduced numerical models for the simulation of the actual response of the physical problem. Therefore, developing an economic and safe design requires the implementation of optimization algorithms for achieving the best possible design. For this purpose the design requirements imposed by the current seismic provisions for ductile reinforced concrete buildings and the performance objectives are introduced as constraints into the formulation of the optimization problems.

Nevertheless, despite all the aforementioned computational advances, until recently the provisions of seismic design codes for buildings were based on experience that was periodically improved following damaging earthquakes. As a result, most of the current seismic design norms adopt many simplifying assumptions regarding the behaviour of the structures under seismic actions. However, recent earthquakes caused severe damages and forced the engineering community to question the effectiveness of the seismic design codes in effect. Given that the primary goal of contemporary seismic design is the protection of human life in connection to the restriction of repairing cost, it is evident that additional performance targets and earthquake intensities should be considered to assess structural performance for multiple hazard levels.

Most of the current seismic design codes belong to the category of prescriptive design procedures (or limit-state design procedures), where by a number of checks, expressed in terms of force (most frequently) and deformation limits, are satisfied in order for the structure to be considered safe since it fulfils the safety criterion against collapse. A typical limit-state based design can be viewed as one (i.e., ultimate strength) or two limit-state approach (i.e., serviceability and ultimate strength). Existing seismic design procedures are based on the principle that a structure will avoid collapse if it is designed to absorb and dissipate the kinetic energy that is induced in it during a seismic excitation. Most modern seismic norms express the ability of the structure to absorb energy through inelastic

deformation by using a reduction or behaviour factor, that depends on the material and the structural system used.

The concept of PBD was introduced a few decades ago, for designing structures subjected to seismic loading conditions. In PBD more accurate and time-consuming analysis procedures are employed in order to estimate the entire non-linear structural response. The progress that takes place in the field of computational mechanics, as well as in computer technology, continuously expands the capabilities and the scope of applicability of PBD procedures. The main objective of this kind of design procedures is to achieve more predictable and reliable levels of safety and operability against natural hazards. According to PBD procedures, the structures should be able to resist earthquakes in a quantifiable manner and to attain specific target performance levels of possible damages. PBD procedures are multi-level design approaches, in which various levels of structural performance are simultaneously considered. PBD design criteria try to define certain levels of structural performance for various levels of seismic hazard.

In construction industry decision making for structural systems situated in seismically active regions, requires consideration of damage cost and other losses resulting from earthquakes occurring during the lifespan of a structure. Thus, nowadays LCCA becomes an essential component of the design process used to control the initial and the future cost of building ownership. In early 1960s LCCA was applied in the commercial area and in particular in the design of products considering the total cost of developing, producing, using and retiring. The introduction of LCCA in construction industry was made in the field of infrastructures as an investment assessment tool. In particular, in early 1980s it was used in USA as an appraisal tool for the total cost of ownership over the lifespan of an asset. Later, in view of large losses due to extreme hazards, like earthquakes and hurricanes, there was a need for new design procedures of facilities that could lead to life protection and reduction of damage and economical impact of such hazards to an acceptable level. In this context LCCA was introduced in the field of constructions as a complex investment appraisal tool incorporating a structural performance criterion.

Over the last decades risk management of structural systems has gained the attention of various economic and technical decision centres in modern society. The optimal allocation of the public resources for a sustainable economy requires proper tools for estimating the consequences of natural hazardous events on the built environment. The risk management addresses this claim indicating the way for implementing optimal choices. Thus, the main purpose of the risk management process is to choose among different options relying on technical and economical considerations. Risk assessment and decision analysis are the

main steps of the risk management concept. It is therefore essential to establish a reliable procedure for assessing the seismic risk of structural systems. Seismic fragility analysis, which provides a measure of the safety margin for the structural system, is considered as the core of the risk assessment framework.

1.2. Objectives-Research Framework

Taking into account all the aforementioned aspects of the state of the art in computational earthquake engineering, the major objective of this dissertation is to develop an integrated framework for economical and safe antiseismic design and the assessment by means of life-cycle cost and fragility analysis of reinforced concrete structures. This goal and the steps that have been followed in order to achieve this objective are presented in Figure 1.1. The global scope of the dissertation was achieved through the accomplishment of the following tasks:

- Calibration of some of the most popular DIs that have been proposed by many researchers to identify the state of local damage, in the case of reinforced concrete members. In particular the Park and Ang (1985) local damage index, its modified variant proposed by Kunnath, Reinhorn and Lobo (1992), the Chung, Meyer and Shinozuka (1987, 1989) local damage index, along with the maximum softening and final softening proposed by DiPasquale and Çakmak (1987, 1988) were calibrated. (This task is part of the Objective 1).
- Critical assessment of prescriptive design procedures with reference to their ability to lead to safe and economical designs. Furthermore a comparison between prescriptive and performance based design procedures was carried out. For both assessments a number of structural seismic design optimisation problems have been formulated. The main task of the Objective 2 was to identify the DI or the combination of DIs that will provide reliable information on damage so that they can be incorporated into a PBD framework. The ultimate objective of this task was to compare alternative designs that still satisfy code requirements in the most cost-effective way, i.e. those with minimum cross section dimensions and amount of reinforcement. For this reason, a structural optimization problem was formulated and the designs obtained were subsequently assessed. The structural optimization problem formulated was evaluated using the most advanced metaheuristic optimization algorithms, namely (i) the Evolution Strategies method, (ii) the Differential Evolution method, (iii) the Particle Swarm Optimization method as well as (iv) the Harmony Search method. (This task is part of the Objective 2).

- Improvement of the LCCA procedure with reference to both robustness and efficiency. Improvement in the robustness of the method was achieved by improving the formulation of the LCCA tool through the incorporation of the maximum floor acceleration into the analysis and by identifying the factors that affect the accuracy of the procedure. In order to combine robustness and computational efficiency, a procedure for selecting the artificial seismic excitations at each hazard level was proposed, leading to reduction on the computational effort required to perform the LCCA. (This task is part of the Objective 3).

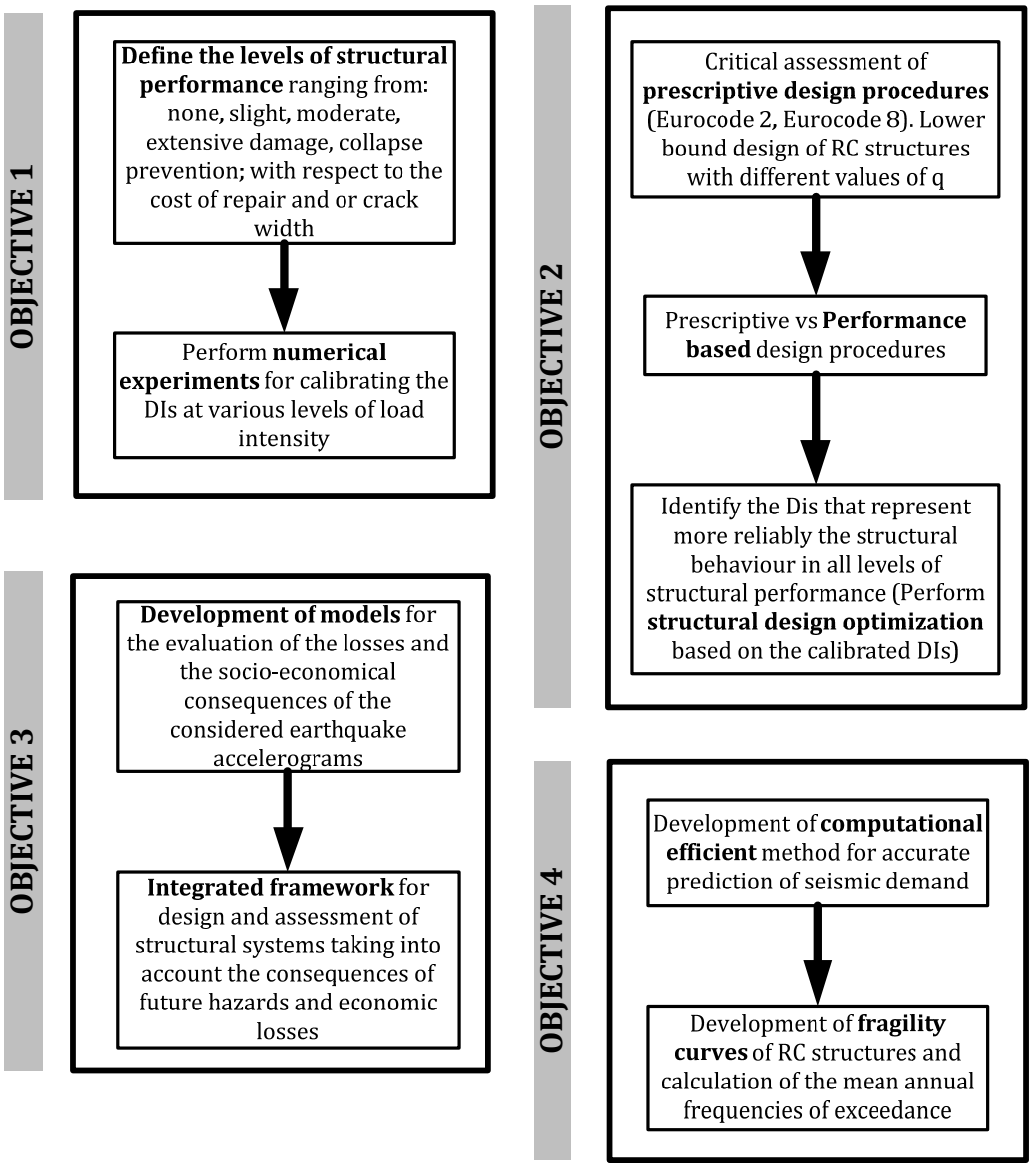

Figure 1.1. Research framework of the Dissertation.

- Elaboration on the fragility analysis procedure with reference to both robustness and efficiency. The robustness was achieved through an improvement of the procedure for the calculation the two defining parameters of the lognormal distribution (mean and standard deviation of the demand), using the Harmony

Search optimization algorithm and the maximum likelihood method. Improvement in the efficiency of the method was achieved by introducing a neural network based Incremental Dynamic Analysis procedure that result in reduction of the computational effort by one order of magnitude.

1.3. Analysis of the Contents

The dissertation consists of eight chapters and two appendices at the end. The structure of the thesis is organized as follows:

Chapter 1 is the introduction of the dissertation. In this Chapter, a general description of the background and the motivations, the objectives pursued is provided, as well as a brief description of the contents of each chapter.

In *Chapter 2* a description of the DIs that are used to quantify damage and whose values can be related to particular structural damage states is presented. The analytical damage models to compute these DIs may involve various degrees of complexity, as they account for the characteristics of the structure and its seismic response. In general, they can be broadly divided into two classes: (a) strength-based DIs; and (b) response-based Dis (which are used in this study. Strength-based DIs are simple and do not require response analysis. However, they must be calibrated against observed damage using a large experimental database. In Chapter 2 a number of DIs are calibrated into a number of limit states for reinforced concrete structures using 3D and beam finite element modelling of actual framed buildings failed in earthquake. In order to achieve this goal IDA for both types of models is performed, correlating the size of the concrete cracks (assumed to represent the state of the damage) with the DIs under investigation.

In *Chapter 3* the subject of the deterministic SOO is discussed. At the beginning of the chapter, the concept of optimum structural design is presented, followed by the definition and subsequently formulation of the deterministic SOO problem and some necessary definitions. Various methods for solving the structural optimization problem are presented, including the most important metaheuristic optimization methods that have been implemented in this dissertation later on. In particular the ES method, the DE method, the PSO method as well as the HS method are presented in detail at this part.

In *Chapter 4* is presented the basic principles of the conventional prescriptive and the Performance-Based Design procedures. Furthermore, the most widely adopted NSP and NDP procedures are presented. In particular the Displacement Coefficient Method of ASCE-

41 (2006), the Capacity Spectrum Method of ATC-40 (1996), the N2 method of Eurocode 8 (2004), the IDA, the MIDA and the MSDA methods are presented. Furthermore, in Chapter 4 a parametric study, performed in order to assess the designs obtained using either the Greek National Design Codes (GNDC, 2000) or a PBD procedure is presented. In the case of the GNDC (2000) code a linear static analysis method has been used, while in the PBD procedure the nonlinear static analysis method has been performed in order to determine the damage levels at different earthquake intensities. Additionally, a parametric investigation was performed in order to examine the influence of the behaviour factor q (EC8, 2004) on the final design of reinforced concrete buildings under earthquake loading, in terms of performance and economy. The numerical tests were performed on two multi-storey reinforced concrete buildings having symmetrical and non-symmetrical plan views which were optimally designed according to the Eurocodes EC2 (2004) and EC8 (2004).

In *Chapter 5* is presented the basic principles of the probabilistic seismic hazard analysis. The generation of the artificial accelerograms is presented by producing stationary signals that are subsequently enveloped in the time domain by a trapezoidal shape to roughly simulate the non-stationary characteristics of ground motion considering uncertainties. The artificial accelerograms are generated through the code EDRs (FEMA-356, 2000) based on the mean hazard curve of the region. The mean hazard curve is derived by taking into consideration important ground motion characterization uncertainties, such as maximum earthquake magnitude (M_0, M_{max}), earthquake recurrence rate, distribution of seismicity between faults, attenuation relationships, etc. In order to examine the influence of the seismic records selected on the LCCA framework three different classes of seismic records are considered in Chapter 5 and their influence on the LCCA outcome is examined for the two typical 3D reinforced concrete buildings previously designed. The first class of ground motion excitations is composed by a number of natural records associated to the region of interest. The second class comprises a number of artificial accelerograms, generated according to the corresponding EDRs. In order to combine robustness and computational efficiency, a procedure for a priori selection of the most representative artificial seismic excitations at each hazard level is proposed, leading to reduction on the required computational effort for performing the LCCA.

In *Chapter 6* is described the LCCA framework which is based on economic theories and has been used as a decision-support tool in design of structural systems. A detailed literature survey on LCCA dealing with loss estimation due to earthquakes is provided at the beginning of Chapter 6. It is assumed that for the problem at hand the total cost of a

structure, refers to either the design-life period of a new design or to the remaining life period of an existing or retrofitted structure. This cost, as it was implemented in this dissertation, can be expressed as a function the design vector and time. The implementation of the LCCA framework in terms of NSP and nonlinear dynamic analysis procedures is presented, while a new test example implementing the NSP is considered in order to describe the basic steps of the LCCA. Furthermore, the influence of the behaviour factor q on the design of RC buildings based on LCCA is demonstrated. In particular, NSP and MSDA were performed for the two typical 3D reinforced concrete buildings previously designed for four sample sets of seismic events, each comprising of 10, 20, 40 and 60 base excitation records, respectively. In order to study the influence of the response quantity considered, for the case of MSDA in particular, the performance of the two buildings was assessed with reference to the maximum interstorey drift and floor acceleration induced by eight hazard levels for each sample group of ground motions.

In *Chapter 7* is provided the general description of the fragility analysis framework along with the methods for dealing with the problem of reliability analysis. Furthermore, a methodology incorporating soft computing techniques, such as ANN and metaheuristics, for reducing the computational effort is presented in Chapter 7. In particular, fragility analysis of 3D reinforced concrete buildings is performed following the lognormal assumption based approach, similar to that proposed in HAZUS (2003). This approach is based on the assumption that the demand values follow the lognormal distribution, thus the fragility curves are expressed in the form of a two-parameter lognormal distribution. In this work, the Harmony Search algorithm is implemented for calculating these two parameters for each limit state considered. Furthermore, since the IDA methodology which is usually implemented for developing fragility curves requires an excessive computational effort, a NN approximation of the structural response is proposed, resulting into a reduction of one order of magnitude of the computational time. In the proposed NN-based methodology, uncertainty in the demand is treated in a straightforward manner by way of which large bins of records can be considered with little additional computational effort.

In *Chapter 8* the conclusions of the research work are presented. The original contributions of the dissertation are clearly stated, while the extensions of this work proposed future research on the subject of the dissertation are provided in Chapter 8.

Two appendices are included ate the end: Appendix A, contains the list of seismic records used in the dissertation; and Appendix B that gives details on the modelling formulations and the corresponding material constitutive laws for the definition of the building models

that have been used.

1.4. References

ASCE/SEI Standard 41-06, 2006. Seismic Rehabilitation of Existing Buildings, prepublication edition, Structural Engineering Institute, American Society of Civil Engineers.

ATC-40, Seismic evaluation and retrofit of concrete buildings, Applied Technology Council, Redwood City, 1996.

Chung Y.S., Meyer C., Shinozuka M. Seismic damage assessment of reinforced concrete members, Report NCEER-87-0022, National Center for Earthquake Engineering Research, State University of New York at Buffalo, Buffalo, NY, 1987.

Chung, Y.S., Meyer, C. and Shinozuka, M. Modelling of concrete damage. ACI Struct. J., 1989, 86(3).

DiPasquale E., Cakmak A.S. Identification of the serviceability limit state and detection of seismic structural damage, Report NCEER-88-0022, National Center for Earthquake Engineering Research, State University of New York at Buffalo, NY, 1988.

DiPasquale, E. and Cakmak, A.S. Detection and assessment of seismic structural damage, Report NCCER-87-O015, National Center for Earthquake Engineering Research, State University of New York at Buffalo, August 1987.

EC2. Eurocode 2. Design of Concrete Structures—Part 1: General Rules and Rules for Buildings. European Committee for Standardisation: Brussels, Belgium, The European Standard EN 1992-1-1: 2004.

EC8. Eurocode 8: Design of Structures for Earthquake Resistance. European Committee for Standardisation: Brussels, Belgium, The European Standard EN 1998-1: 2004.

EKOS 2000, National code for concrete building structures of Hellas, 2000.

FEMA-356, Prestandard and Commentary for the Seismic Rehabilitation of Buildings, Federal Emergency Management Agency, Washington, DC, 2000.

FEMA-356, Prestandard and Commentary for the Seismic Rehabilitation of Buildings, Federal Emergency Management Agency, Washington, DC, 2000.

FEMA-National Institute of Building Sciences. HAZUS-MH MR1, Multi-hazard Loss Estimation Methodology Earthquake Model, Washington, DC, 2003.

Kunnath S.K., Reinhorn A.M., Lobo R.F. IDARC Version 3.0: a program for the inelastic damage analysis of reinforced concrete structures, Technical Report NCEER-92-0022, National Center for Earthquake Engineering Research, Buffalo, NY, 1992.

Park Y.J., Ang A.H.-S. (1985) A Mechanistic seismic damage model for reinforced concrete, J. Struct. Div. ASCE 111(4), 722-739.

Chapter 2

Calibration of Damage Indices for RC Structures

2.1. Introduction

The emerging PBD framework requires the idealization of more clearly defined levels of inelastic response, or damage, to be targeted at different earthquake hazard levels. While there are a range of factors that could influence the level of damage and hence the performance, the design strength remains a fundamental design parameter inherently related to the structural performance. In order to implement this design framework, models for assessing structural damage within the context of a random earthquake environment are required. The idea of describing the state of damage of the structure by one number on a defined scale in the form of a DI is attractive because of its simplicity. Damage may be quantified by using several DIs whose values can be related to particular structural damage states. So far a significant number of researchers have studied various DIs for reinforced concrete or steel structures (Ghobarah et al., 1999; Estekanchi and Arjomandi, 2007).

The analytical damage models to compute these DIs may involve various degrees of complexity, as they account for the characteristics of the structure and its seismic response. In general, they can be broadly divided into two classes (Grigoriu, 1987): (a) strength-based DIs; and (b) response-based Dis (which are used in this study. Strength-based DIs are simple and do not require response analysis. However, they must be calibrated against observed damage using a large experimental database. The seismic performance of structures is commonly related to the capacity to undergo inelastic deformations. Experimental studies have shown that ductility as well as alternative measures of seismic structural performance based solely on the low-cycle fatigue theory do not seem to provide a satisfactory index for seismic damage (Banon and Veneziano, 1982). These test results are consistent with the

notion that failure of brittle systems is caused by excessive deformation while failure of ideal ductile systems is initiated by repeated inelastic deformations. Structural damage indices that are neither ideal brittle nor ideal ductile, should account for the damage effects of both excessive and repeated inelastic deformations (Park and Ang, 1985). Thus there is a need for more general and reliable indices to characterize the performance of structures. The response-based damage indices can be divided into three groups according to what the index accounts for (Ghobarah et al., 1999): (a) maximum deformation; (b) cumulative damage; and (c) maximum deformation and cumulative damage. In this work damage indices accounting for both maximum deformation and cumulative damage are implemented and in particular the Park and Ang (1985) local damage index, its modified variant proposed by Kunnath, Reinhorn and Lobo (1992), the Chung, Meyer and Shinozuka (1987, 1989) local damage index, along with the maximum softening and final softening proposed by DiPasquale and Çakmak (1987, 1988) are studied.

2.2. Damage indices based on maximum deformation

2.2.1. Ductility ratio

The ductility ratio is defined as the ratio of the maximum deformation to the yield deformation (Mahin and Bertero, 1974; Powell and Allahabadi, 1988). It has been used extensively in seismic analysis to evaluate the capacity of structures undergoing inelastic deformation and develop inelastic response spectra (Newmark and Rosenblueth, 1971). As a damage index, the ductility ratio may be unsatisfactory (Ayala and Xianguo, 1995), especially when shear distortion in joints and pull out of bottom bars are anticipated. As demonstrated by experimental studies, the ductility ratio does not account for the effect of the duration and frequency content of the ground motion.

2.2.2. Interstorey drift

The interstorey drift is the maximum relative displacement between two storeys normalized to the storey height (Sozen, 1981). Deformations characterized by drift ratio or plastic rotation at the member-ends are widely used by some guidelines given for seismic evaluation of buildings (ATC-40, 1996; FEMA-273, 1997) and in earthquake assessment procedures (Shahrooz and Moehle, 1990; Lynn, et. al., 1996; Hassan and Sozen, 1997; Mitropoulou et al., 2010; Mitropoulou and Papadrakakis, 2011). The interstorey drift does not account for effects of cumulative damage due to repeated inelastic deformation; furthermore the relationship between damage and interstorey drift varies depending on the maximum deformation at collapse which depends on the ductility class of the structure.

2.2.3. Slope ratio

The slope ratio is a measure of damage due to stiffness degradation during seismic loading. It is defined as the ratio of the secant slope (Saiidi and Sozen, 1981) of the loading branch of the force-displacement diagram to the slope of the unloading branch.

2.2.4. Flexural damage ratio

Roufaiel and Meyer (1981) suggested that the ratio of initial stiffness to the reduced secant stiffness at the maximum displacement can be used as a measure of damage. Damage indices based on extreme inelastic deformations seem to be strongly correlated so that their predictions are usually similar. The flexural damage ratio index does not account for effects of cumulative damage caused by repeated load reversals. Critical values of the *ductility ratio*, the *slope ratio* and the *flexural damage ratio* damage indices are determined from laboratory tests and field observations.

2.2.5. Maximum permanent drift

Residual drift is closely related to the plastic deformations in a structural system. Toussi and Yao (1982) and Stephens and Yao (1987) introduced a qualitative classification of damage, which, among others, included the residual drift. The shortcoming of the maximum residual drift as a measure of damage is that light damage implies a maximum residual drift of 0.5 per cent or less. Moreover, a residual drift of 0.5 per cent does not necessarily indicate light damage.

2.3. Damage indices based on cumulative damage

2.3.1. Normalized cumulative rotation

A simple measure of structural deterioration during a seismic event is the sum of all inelastic excursions experienced by the structure. The value of this measure depends on the duration and intensity of the earthquake. The normalized cumulative rotation is defined as the ratio of the sum of the inelastic rotations during half cycles to the yield rotation (Allahabadi and Powell, 1988; Banon and Veneziano, 1982). Statistical analysis of data on beam-column elements subjected to cyclic loads shows that damage indices based only on cumulative inelastic deformation or dissipated energy may be inadequate to characterize the complex process of damage propagation and subsequent failure in concrete members (Ayala and Xianguo, 1995).

2.3.2. Low-cycle fatigue

The theory of low-cycle fatigue has been applied to the seismic analysis of structures subjected to strong ground motion to estimate the state of damage (Stephens, 1985). The determination of the damage index is somewhat complex and involves the entire response history. Moreover, the index does not account for the effect of maximum inelastic deformation.

2.4. Damage indices accounting for both maximum deformation and cumulative damage

2.4.1. Park and Ang local damage index

According to Park and Ang (1985) the index is the sum of two indices, namely scaled values of ductility and dissipated energy of the local structural element during the seismic ground shaking (Park and Ang, 1985), modified later by Park et al. (1987) and Kunnath et al. (1992). Scaled ductility, defined as the ratio of the maximum experienced deformation demand δ_M, to the yield deformation, is scaled by the ratio of the ultimate deformation δ_u, under a monotonic static load, up to the yield deformation. The dissipated energy is scaled by $\beta/(Q_y\delta_u)$, where Q_y is the yield force and β is a constant calibrated from experiments. The ultimate deformation is determined when the concrete reaches a specified ultimate strain. Although the value of the index may exceed unity, failure of the structure is assumed to occur when the damage index ranges from 0.8 to 1.0. The behaviour of this index is strongly dependent on the hysteretic model of the structural elements.

Damage Model

Consistent with the dynamic behaviour of reinforced concrete structures, seismic structural damage is expressed as a linear combination of the damage caused by excessive deformation and the damage attributed to the repeated cyclic loading effect. This may be represented in terms of a DI by

$$DI_{PA} = \frac{\delta_M}{\delta_u} + \frac{\beta}{Q_y \delta_u} \int dE \qquad (2.1)$$

in which δ_M is the maximum deformation under earthquake; δ_u is the ultimate deformation under monotonic loading; Q_y is the calculated yield strength (if the maximum strength, Q_u, is smaller than Q_y, then Q_y is replaced by Q_u); dE is the incremental absorbed hysteretic energy; β is a non-negative parameter. Under elastic response, the value of DI_{PA} should theoretically be zero, although in practice the values of DI_{PA} in the elastic range are almost non-zero. Values of the damage index $DI_{PA} \geq 1.0$ signifies complete collapse or total damage.

Structural damage, therefore, is a function of the response parameters δ_M and $\int dE$ that are dependent on the loading history, whereas parameters β, δ_u and Q_y are independent of the loading history.

The Park and Ang (1985) damage model accounts for damage due to maximum inelastic deformation, as well as damage due to the cyclic history of deformations. Both components of damage are linearly combined. Three damage indices can be computed using this damage model: (i) Structural element damage index: column, beams or shear wall elements. (ii) Story damage index: vertical and horizontal components and total story damage. (iii) Overall building damage. Equation (2.1) is the basis for the DI computation in this Dissertation, although some further considerations need to be taken into account as discussed below.

Determination of Model Parameters

The three parameters δ_u, Q_y and β of the damage model proposed in Eq. (2.1) are discussed below:

Determination of ultimate deformation δ_u. When brittle shear failure is of no concern, such as for very slender beams and columns, the ultimate deformation can be evaluated from the stress-strain relationship of the materials, namely steel and concrete. However, components may fail in shear under repeated cyclic loadings even though a flexural failure is expected under monotonic loadings. All possible failure modes should be taken into account in evaluating δ_u when repeated cyclic loadings are involved. In this context, a simple empirical relation is used for determining δ_u using available monotonically loaded test data. Because the yield deformation, δ_y, can be predicted with good accuracy, a practical means to determine the ultimate deformation may be to amplify this with the ductility factor, μ_u namely:

$$\delta_u = \mu_u \cdot \delta_y \tag{2.2a}$$

Determination of the ultimate ductility factor μ_u. For the estimation of the ultimate ductility factor, μ_u, calculated according to Eq. 2.2b, 2.2c and 2.2d, are used, from Park and Ang (1985), obtained from calibration of 142 monotonically loaded beams and columns.

$$\mu_u = \left(\frac{\varepsilon_p}{\varepsilon_{cl}}\right)^{0.218\rho_w - 2.15} \exp[0.654 \cdot \rho_w + 0.38] \tag{2.2b}$$

$$\varepsilon_p = 0.5 \cdot \varepsilon_{s2} + 0.5\sqrt{\varepsilon_{s2}{}^2 + \theta_V^2} \tag{2.2c}$$

$$\theta_V = \frac{0.002}{\frac{l}{d} - 0.5}, \; l = 0.5L \tag{2.2d}$$

Where the volumetric ρ_w is the ratio of confinement reinforcement, ε_{cl} is the concrete strain at maximum stresses greater than 0.002, ε_{s2} is the concrete strain at the location of the compression reinforcement at yield and, θ_V is the contribution of shear deformations in the yield rotation θ_y. For a brittle failure, in which a member loses its strength continuously, the failure point is identified on the load-deformation curve when the strength drop exceeds a certain percentage of its previously attained maximum strength. Analyses of the ultimate ductility factors for the test specimens in the database used, a strong correlation with the flexural and shear deformations was observed. The values μ_u and δ_y may be determined independently. Yielding of a reinforced concrete component may be defined as the onset yielding in the tension reinforcement, or when the extreme fibre compressive strain in the concrete exceeds 1.5 times the crushing strain, ε_0 =2‰, whichever is less.

Determination of the parameter β. The effect of cyclic loading on the quantification of structural damage is represented by the parameter β in Eq. (2.1). The absorbed hysteretic energy up to the failure point is measured for a large set of cyclic tests of beams and columns over the entire cyclic test history. These experimental data were carefully selected from a larger set of test specimens; only those in which either an abrupt failure was clearly observed or a gradual type failure could be identified on the envelope curve were considered. Using Eq. (2.1) the load-deformation curve for each test was traced up to the failure point. Then, at the point of failure (DI_{PA} = 1.0), the corresponding value of β was evaluated. Based on the calculated β values, a negative correlation was observed between β and the confinement ratio, ρ_w, while weak positive correlations were observed between β and the shear span ratio, l/d, the longitudinal steel ratio, p_t, and the axial stress, n_0. Through a trial and error procedure, the minimum-variance values of β for Eq. (2.1) were determined in such a way that the standard deviation of D_{PA} is minimized and the mean value of DI_{PA} is close to unity, yielding the following equation:

$$\beta = \left(-0.447 + 0.073\frac{l}{d} + 0.24 n_0 + 0.314 \rho_t \right) \cdot 0.7^{\rho_w} \tag{2.3}$$

where l/d is the shear span ratio (set equal to 1.7 if l/d < 1.7); n_0 is the normalized axial stress (set equal to 0.2 if n_0 < 0.2); ρ_t is the longitudinal steel ratio as a percentage (set equal to 0.75% if ρ_t < 0.75%); and ρ_w is the confinement ratio.

Determination of the yield strength Q_y. The method for evaluating the yield strength, Q_y, may be found in standard textbooks for RC elements.

Calibration of the damage index. The Park and Ang damage model has been calibrated with observed structural damage on nine RC buildings (Park et al., 1986). Table 2.1 presents the calibrated damage index with the degree of observed damage in the structure.

Table 2.1. Interpretation of overall damage index (Park et al., 1986).

DI_{PA} value	**Degree of Damage**	**Usability**	**Physical Appearance**
0.00	None	Loss of building	Undeformed/ uncracked
0.20 - 0.30	Slight	Beyond repair	Moderate to severe cracking
0.50 – 0.60	Minor	Temporarily unusable	Spalling concrete cover
	Moderate		
	Severe	Unusable	Buckled bars, exposed core
> 1.00	Collapse		Loss of shear/axial capacity

2.4.2. Modified Park and Ang global and local damage indices

As it was mentioned in the previous section DI_{PA} was modified later by Park et al. (1987) and Kunnath et al. (1992). Direct application of the damage model to a structural element, a frame story, or to the overall building requires the determination of the corresponding overall element, storey, or building ultimate deformations. Since the inelastic behaviour is confined to plastic zones near the ends of some members, the relation between element, story or top storey building deformations, with the local plastic zone rotations is difficult to establish. For the element end-section damage the following modification to the original model was introduced by Kunnath et al. (1992):

$$\mathrm{DI}_{PAm} = \frac{\theta_m - \theta_r}{\theta_u - \theta_r} + \frac{\beta}{M_y \theta_u} \int \mathrm{dE} \tag{2.4}$$

where θ_m is the maximum rotation attained during the loading history; θ_u is the ultimate rotation capacity of the critical region; θ_r is the recoverable rotation after unloading; M_y is the yield moment; and E is the dissipated energy in the critical region. The element damage is then selected as the largest damage index of the end critical region.

Two additional story and overall damage indices were proposed, which are computed using weighting factors based on dissipated hysteretic energy at component and storey levels respectively:

$$DI_{storey} = \sum_{i=1}^{n_{el}} (\lambda_i)_{element} (DI_i)_{element} \tag{2.5a}$$

$$(\lambda_i)_{element} = \frac{E_i}{\sum_{i=1}^{n_{el}} E_i} \quad i = 1,\ldots,n_{el}(\text{number of elements}) \tag{2.5b}$$

and

$$DI_{overall} = \sum_{i=1}^{n_{st}} (\lambda_i)_{storey} (DI_i)_{storey} \tag{2.6a}$$

$$(\lambda_i)_{storey} = \frac{E_i}{\sum_{i=1}^{n_{st}} E_i} \quad i = 1,\ldots,n_{st}(\text{number of storeys}) \tag{2.6b}$$

where λ_i are energy weighting factors; E_i is the total absorbed energy by the i^{th} component or storey while n_{el} is the total number of elements and n_{st} is the total number of storeys.

2.4.3. Chung, Meyer and Shinozuka's local damage index

Chung et al. (1987) proposed a damage index which contains damage modifiers that reflect the effect of the loading history. This index considers the difference of the flexural response of members to positive and negative moments. The effect of the loading history is taken into account by a damage modifier parameter which includes the change in stiffness and sustained bending moment up to the calculation cycle. The damage index definition does not explicitly account for the damage caused by the maximum deformation experienced by the structural element.

Damage model

Many researchers express seismic damage of RC members in terms of a damage index, DI_e, which remains zero as long as the response remains in the elastic zone and indicates the failure when it reaches 1.0 (Park and Ang, 1985). The damage index is evaluated at the section level and relates to flexural response, therefore is based on curvature φ evaluation. It is expressed in the form of a modified Miner's Rule, Eq. (2.7) and it contains damage modifiers, which reflect the effect of the loading history. This type of damage index formulation takes into account the fact that reinforced concrete members typically respond differently to positive and negative loadings:

$$DI_e = \sum_{i=1}^{n_{st}} \left(\alpha_i^+ \frac{n_i^+}{N_i^+} + \alpha_i^- \frac{n_i^-}{N_i^-} \right) \tag{2.7}$$

where N_i is the number of cycles to cause failure at curvature φ_i, n_i is the number of actually applied loading cycles at curvature φ_i, α_i is the damage modifier and +/- depicts the loading direction.

The damage modifier α is defined as a function of the number of loading cycles and the previous loading history (Figure 2.1) according to the following expression:

$$\alpha_i^+ = \frac{\sum_{i=1}^{n_i^+} k_{ij}^+}{n_i^+ \cdot \bar{k}_i^+} \cdot \frac{\varphi_i^+ + \varphi_{i-1}^+}{2\varphi_i^+}$$
$$k_{ij}^+ = \frac{M_{ij}^+}{\varphi_i^+}, \quad \bar{k}_i^+ = \frac{1}{N_i^+} \sum_{i=1}^{N_i^+} k_{ij}^+ \tag{2.8a}$$

$$\alpha_i^- = \frac{\sum_{i=1}^{n_i^-} k_{ij}^-}{n_i^- \cdot \bar{k}_i^-} \cdot \frac{\varphi_i^- + \varphi_{i-1}^-}{2\varphi_i^-}$$
$$k_{ij}^- = \frac{M_{ij}^-}{\varphi_i^-}, \quad \bar{k}_i^- = \frac{1}{N_i^-} \sum_{i=1}^{N_i^-} k_{ij}^- \tag{2.8b}$$

This damage modifier is introduced to take into account that: (i) the damage increment in the first cycle is larger than that of successive cycles under constant amplitude loadings, and (ii) the damage caused by the cycle which follows a larger amplitude loading is larger than that which follows a smaller amplitude loading.

Calibration of damage model

In order to verify the accuracy of the damage models, Chung et al., (1993) used experimental load-deformation curves of one-bay one-storey RC frames that were performed by Fujikake et al. (1988). To relate the DI_e values with physical damage of RC members, a numerical calibration was made by comparing the visible damage of one-bay one storey frames and the computed DI_e values at the same loading step. The result of this calibration is summarized in Table 2.2. It was concluded that, from the engineering point of view, to prevent a total collapse, the DI_e in all members should be limited to a maximum value of 0.5. Furthermore, for an earthquake, which is expected to strike the structure several times in its service life, DI_e is equal to 0.2 which is the maximum acceptable damage to maintain the structure's serviceability with only minor repair.

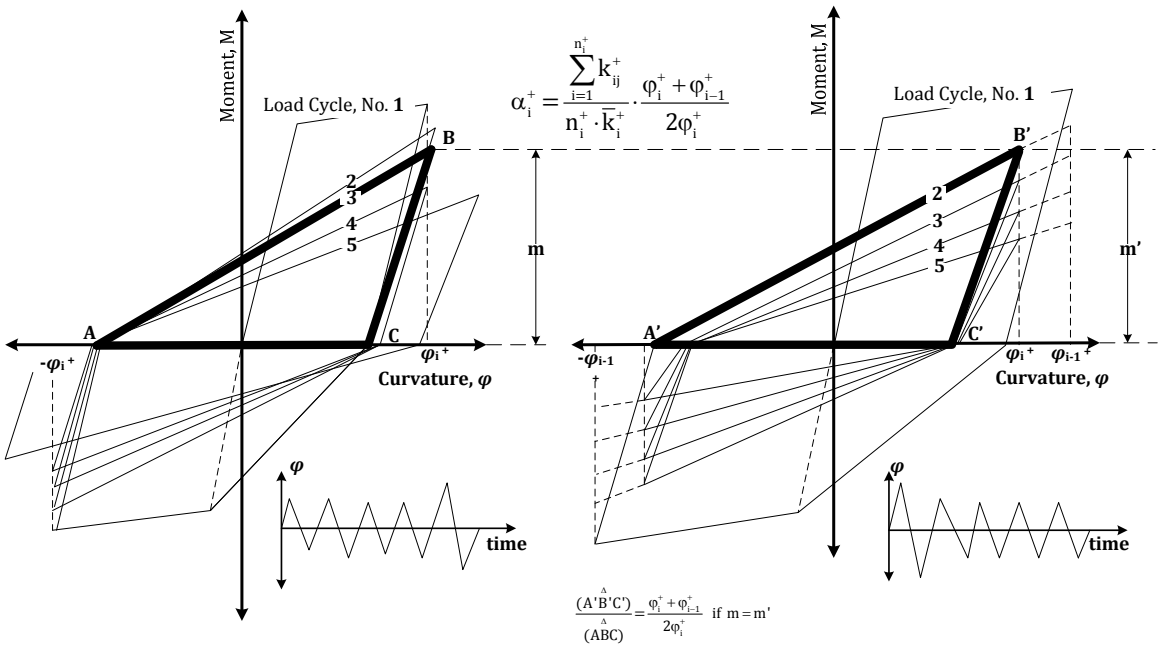

Figure 2.1. Damage modifier α (Chung et al., 1987).

Table 2.2. Interpretation of overall damage index (Chung et al., 1993).

DI_e	Physical damage	Hysteresis	State of Building
0.0-0.2	Invisible cracking	Stable hysteresis	Minor damage
0.2-0.5	Visible cracking	Small strength drop	Repairable
0.5-1.0	Concrete spalling	Progressive strength drop	Irreparable
>1.0	Concrete crushing	Significant strength drop	Structure unsafe

2.4.4. Maximum softening and final softening

DiPasquale and Çakmak (1988) developed two damage indices based on (i) the evolution of the natural period of a time-varying linear system equivalent to the actual non-linear system for a series of non-overlapping time windows (maximum softening) and (ii) the final (post earthquake) state of the building (final softening). These global damage indices depend on a combined effect of stiffness degradation and plastic deformation. However, to compute the maximum softening it is necessary to have the input ground acceleration and the acceleration at another location such as at the top of the structure. The maximum softening, index does not explicitly account for the dissipated hysteretic energy and strength deterioration and does not provide information concerning the extent of local damage sustained by the members. DiPasquale and Çakmak (1988) used the change in the fundamental period of the structure as a measure of the change in the stiffness caused by

the earthquake. However, the instantaneous fundamental period includes the effect of the inertia and damping forces. The advantage of the final softening is that it can be evaluated from the initial natural period and the final period determined from field vibration tests after the earthquake. A shortcoming of damage measurements based on the final softening is that local element and storey damage as well as the information contained in the response to the earthquake are not available. A recognized difficulty in the calculation of the post-earthquake period is due to the idealization used in the analytical procedure.

Optimal parameter estimation through system identification of the response

A linear structural system described in terms of its modal parameters has been proved to be identifiable by Beck (1978). Such modal parameters are the percent of critical damping, natural frequency and effective participation factor for each natural mode, as considered in an approximate description of the structural motion based on modal decomposition. When the structural behaviour is nonlinear, the system identification algorithm based on linear models will yield estimates of equivalent linear parameters. The nature of such an equivalence will depend on the criteria that the analyst has chosen for the purpose of the identification. Typical equivalent linearization techniques seek equivalent linear models using analytical methods such as the error-in-the-equation criterion (Caughey, 1963; Valdimarsson et al., 1981). Beck and Jennings (1980) introduced error in the output criteria in structural analysis and DiPasquale and Çakmak (1987) used maximum likelihood criteria.

The equivalent linear model that fits strong motion response histories coincides with the actual structure as long as the structure's behaviour is linear. When the structure enters a nonlinear phase, the equivalent linear model will change, reflecting the nonlinearities that take place during the strong motion. In particular, the structure will experience an apparent softening as the amplitude of the oscillation increases, and the equivalent natural frequencies will decrease. By fitting a time variant linear model to the records, a history of the equivalent linear parameters is obtained. The goal is to extract information concerning damage from the history of the modal parameters. It is clear from the start that only the natural frequencies will provide valuable information. Damping factors are entities of uncertain physical meaning, and their estimation, when the structure is in the nonlinear phase, yields results of questionable reliability. Furthermore, as has been noted by Beck (1987), the estimates of effective damping factors and effective participation factors are statistically correlated. This correlation is reduced but not eliminated when constraints are imposed on the effective participation factors (DiPasquale and Çakmak, 1987).

According to DiPasquale and Çakmak (1987) only the first (fundamental) natural frequency is considered. All computations are actually carried out based on the inverse of the fundamental period of vibration because it is the quantity most commonly considered in engineering practice. The identification problem formulated in this Dissertation is described from the following system of dynamic equations of an N degree of freedom linear structural system:

$$\mathbf{M}\ddot{u}(t)+\mathbf{C}\dot{u}(t)+\mathbf{K}u(t)=-\mathbf{M}r\ddot{u}_g(t)=P_0 \tag{2.9}$$

where u(t) is the response vector (while the dot represents time derivatives), $\ddot{u}_g(t)$ is the ground acceleration while **M**, **C** and **K** are the mass, damping and stiffness matrices, respectively. This system of dynamic equations represents a set of N coupled equations that can be uncoupled with the mode superposition method by assuming damping proportional to the mass and stiffness matrices of the system, e.g. the Rayleigh assumption, **C** = a**M** + b**K**:

$$m_i\ddot{Y}_i(t)+c_i\dot{Y}_i(t)+k_iY_i(t)=p_i \tag{2.10}$$

In this way, the solution of equation (2.9) gives the displacement of any dynamic coordinate of the system by combining all modal contributions i:

$$\ddot{u}(t)=\sum_{i=1}^{N}\Phi_i\ddot{Y}_i(t) \tag{2.11a}$$

$$\dot{u}(t)=\sum_{i=1}^{N}\Phi_i\dot{Y}_i(t) \tag{2.11b}$$

$$u(t)=\sum_{i=1}^{N}\Phi_iY_i(t) \tag{2.11c}$$

where

$$Y_i(t)=\left[\frac{\dot{Y}_i(0)+Y_i(0)\xi_i\omega_i}{\omega_{D,i}}\sin\omega_{D,i}t+Y_i(0)\cdot\cos\omega_{D,i}t\right]\cdot e^{-\xi_i\omega_i t}- \\ -\frac{1}{\omega_{D,i}}\int_0^t\ddot{u}_g(\tau)\cdot e^{-\xi_i\omega_i(t-\tau)}\cdot\sin[\omega_{D,i}(t-\tau)]d\tau \tag{2.12}$$

In order to identify the first eigenperiod of the structural system the value of ω_1 has to be identified. Therefore, an optimization problem is formulated as follows:

$$\min\left\{RMS=\sqrt{\sum_{j=1}^{N_p}\left(u_{r,j}(t)-u_{m,j}(t)\right)}\right\} \tag{2.13}$$

where $u_{r,j}(t)$ and $u_{m,j}(t)$ are the real and the model response for the i^{th} degree of freedom, while the parameters that influence the model responses are:

$\dot{Y}_i(0)$, $Y_i(0)$, ξ_i, ω_i, $P_i(\tau)$, m_i and Φ_{ij}
$i = 1,2,\ldots,N$ (the number of modes considered) (2.14)
$j = 1,2,\ldots,N_p$ (the number of dofs)

For a four degree of freedom problem (N_p=4) and in the case that two modes are to be superimposed (N=2) the total number of system parameters to be identified are 16. The aforementioned optimization problem is dealt in this Dissertation with an optimization algorithm. In particular the Differential Evolution method described in detail in Chapter 3 is used.

Damage index calculation

The interval (0, s) of the earthquake duration is divided into *n* non-overlapping time steps of width s_n sec, therefore the problem of Eqs. (2.13) and (2.14) is solved for each time step, and an equivalent fundamental period $(T_0)_n$ is computed. The first time step can be made small enough, so that it can be assumed that the structure is still vibrating in the linear regime and that $(T_0)_1$ is equal to the fundamental period of the linear oscillation of the building before the earthquake, $(T_0)_{initial}$. When the record is sufficiently long, so that the vibrations due to the strong motion have abated, and the behaviour of the structure can again be considered linear at the end of the record, the estimate of (T_0) corresponding to the last step, $(T_0)_n$, can be assumed to be equal to the fundamental period of the linear oscillation after the earthquake, namely $(T_0)_{final}$. When the final portion of the record still presents apparent nonlinearities, $(T_0)_{final}$ can sometimes be obtained from post-earthquake tests.

Table 2.3. Damage indices based on equivalent linear models.

Local phenomenon	Macroscopic feature	Global Damage Index
Stiffness degradation	Cracks	Final softening DI_F $1-\frac{(T_0)_{initial}}{(T_0)_{final}}$
Plastic deformation	Yielding of reinforcement bars	Plastic softening DI_P $1-\frac{(T_0)_{initial}}{(T_0)_{max}}$
Combined effect of plastic deformation and stiffness degradation	Onset of structural damage (serviceability limit state)	Maximum softening DI_M $1-\frac{(T_0)_{initial}}{(T_0)_{max}}$

Table 2.3 describes some parameter-based global damage indices that have been proposed by DiPasquale and Çakmak (1987) and their correlation with local damage variables and with macroscopic features of damage for RC structures. Analysis of empirical results shows that there exists a correlation between the damage state of a reinforced

concrete structure that has experienced an earthquake and the maximum softening DI_M, defined as:

$$DI_M = 1 - \frac{(T_0)_{initial}}{(T_0)_{max}} \tag{2.15}$$

It is commonly believed (Sozen, 1981) that seismic damage to reinforced concrete structures depends mostly on the maximum strain that is observed during an earthquake, while the particular sequence (or path) of loading is not very important in determining damage. It is therefore intuitive that the maximum softening DI_M, which depends on the combined effects of stiffness degradation and local nonlinearities, be used as damage index for reinforced concrete structures.

2.4.5. Banon and Veneziano Damage Index

The assumptions used in the development of the Park and Ang DI are: (a) the contributions to damage of the extreme deformation and dissipated energy can be superimposed linearly, and (b) the related evolution in time of these components can be disregarded. The results obtained by Banon and Veneziano (1982) do not support these assumptions. In addition, the value of the constant β is not specified and has to be obtained by calibration using laboratory or field data. Based on cyclic load tests of large-scale reinforced concrete elements and assemblages, a probabilistic model of member failure has been developed. The model gives the probability of safety at time t as a functional of damage ratio and dissipated energy up to t. After extension to multivariate safety of several members with correlated resistance, the model is used to calculate the safety of reinforced concrete frames subjected to given base excitation.

2.5. Global damage indices

Several of the damage indices discussed such as the local ductility ratio, the normalized cumulative rotation, the low cycle fatigue, the Park and Ang damage index and the Chung, Meyer and Shinozuka damage index, represent the local damage sustained by the individual structural elements. The analysis of local damage indices identifies the weak or vulnerable elements that should be rehabilitated. However, it is difficult to get a clear idea of a structural system's response to a given input ground motion from a long list of element damage indices. Important decisions concerning the residual strength and safety of a damaged structure are currently based on a single overall or global damage index. Global indices are required for post-earthquake evaluation of structures, reliability studies and applications in the Performance-Based Design approach. The global damage index is

obtained from special combinations of local damage measures. The simplest technique for combining local damage indices is to use a weighting scheme (Kunnath et al., 1992). The weighting factor can reflect the replacement cost and/or the relative importance of the member or substructure in maintaining the integrity of the entire structure. The use of weighted average procedures to calculate global damage index does not properly account for the local concentration of damage, does not distinguish between a column and a beam, and may lead to misleading results. It is possible for a few structural members of the building to have undergone severe damage without this being reflected in by a global index.

2.6. A Unified Procedure for Calibrating the Damage Indices

In this work five damage indices, belonging to the group of maximum deformation and cumulative damage, have been considered in order to be calibrated numerically with reference to the level of local structural damage as described by the crack width. In particular the Park and Ang damage index and its modified version as proposed by Kunnath et al. (1992); the Chung, Meyer and Shinozuka damage index, along with the maximum softening and final softening proposed by DiPasquale and Çakmak (1988) have been considered for the parametric study performed in the framework of this dissertation in an effort to propose a unified procedure for calibrating the damage indices with reference to the crack width.

2.6.1. Calibration procedure

The procedure proposed for the numerical calibration of the above mentioned five damage indices is based on the IDA procedure where “n” multiple nonlinear dynamic analyses are performed in earthquake hazard levels of increased intensity (more details on this analysis procedure can be found in Chapter 4 of this dissertation). Figure 2.2 depicts the calibration procedure, where the seismic demand used for calibrating the damage indices DI_i (i=1,2,...,n) is defined with reference to the characterization of the damage state defined with respect to the flexural crack openings as defined in Table 2.4.

In particular 60 records are scaled in multiple hazard levels and the 16%, 50% and 84% fractile curves are defined. Subsequently, the calibrated values of the DIs are computed based on the 50% fractile and are correlated with the seismic demand. The seismic demand is obtained by means of a single IDA curve defined by a solid finite element discretization of the structure while the IDA study is performed over a single artificial accelerogram generated on the basis of the mean response spectrum of the 60 natural records, while the

60 IDA curves are obtained by IDA study performed with a beam element discretization (see Figure 2.2).

Table 2.4. Damage state with reference to crack width (Toussi & Yao, 1983)

Damage state	Crack width (mm)
No damage	0.05
Slight	0.1
Moderate	0.3
Extensive	0.4

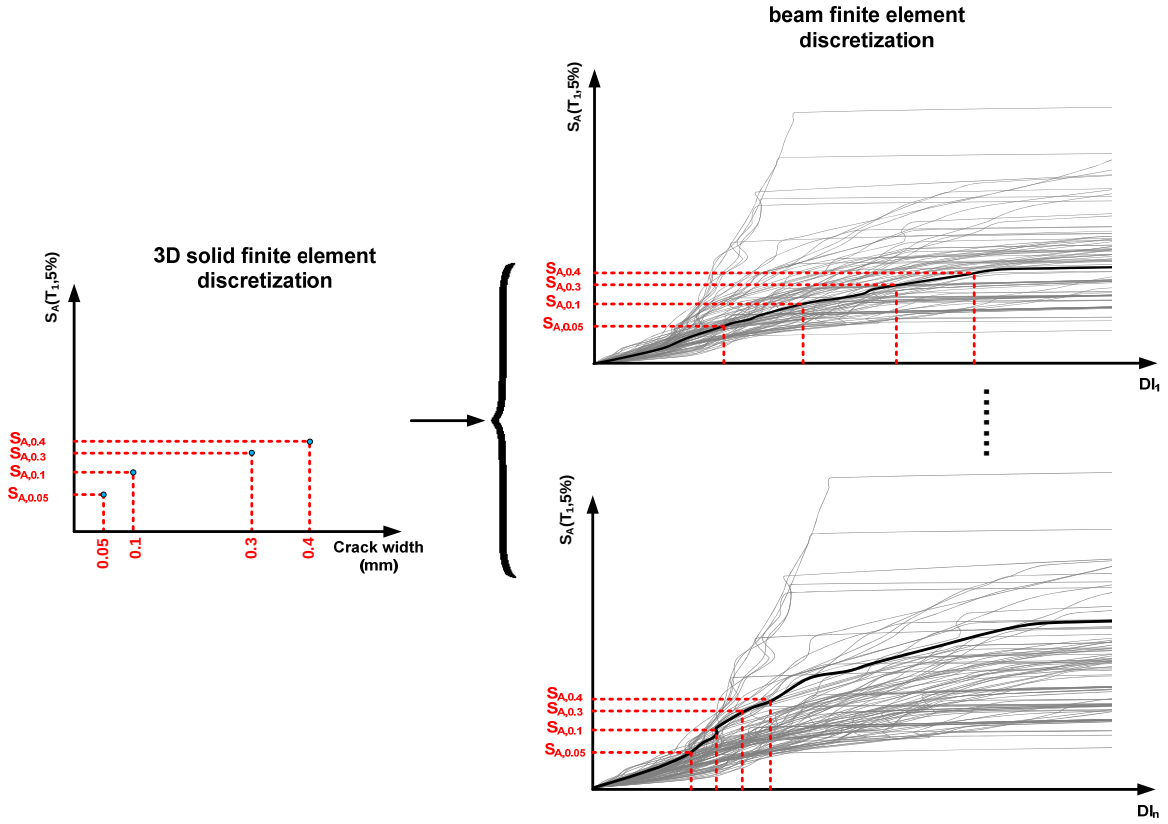

Figure 2.2. IDA-based calibration procedure.

For the purpose of the parametric study two test examples have been considered, one 2D and one 3D model. Both models have been simulated with three-dimensional solid finite elements (Hexahedral Elements) with embedded reinforcement and analysed with the finite element method using GiD and Atena3D Software (Červenka et al. 2009). The IDA-based parametric study was conducted for both models, examining the effect of seismic records of increased intensity on the structural damage. For both test examples the following material properties of concrete are considered: modulus of elasticity E_c = 30.0 GPa and characteristic

compressive strength at 28 days f_{ck}=25.0 MPa (C25/30) the mean compressive strength was used for the calculations, while the material properties of the reinforcing steel were: yield stress f_{yk}=500 MPa (S500) having a 200 GPa modulus of elasticity, while steel hardening was taken into account. The slab thickness for both test examples is equal to 18cm. In addition to the self-weight of the beams and the slab (24 kN/m^3), a distributed dead load of 2kN/m^2 due to floor finishing and partition walls are considered. The live load is assumed equal to 1.5kN/m^2. For the load combination, the dead and live loads are multiplied by 1.0 and 0.3, respectively.

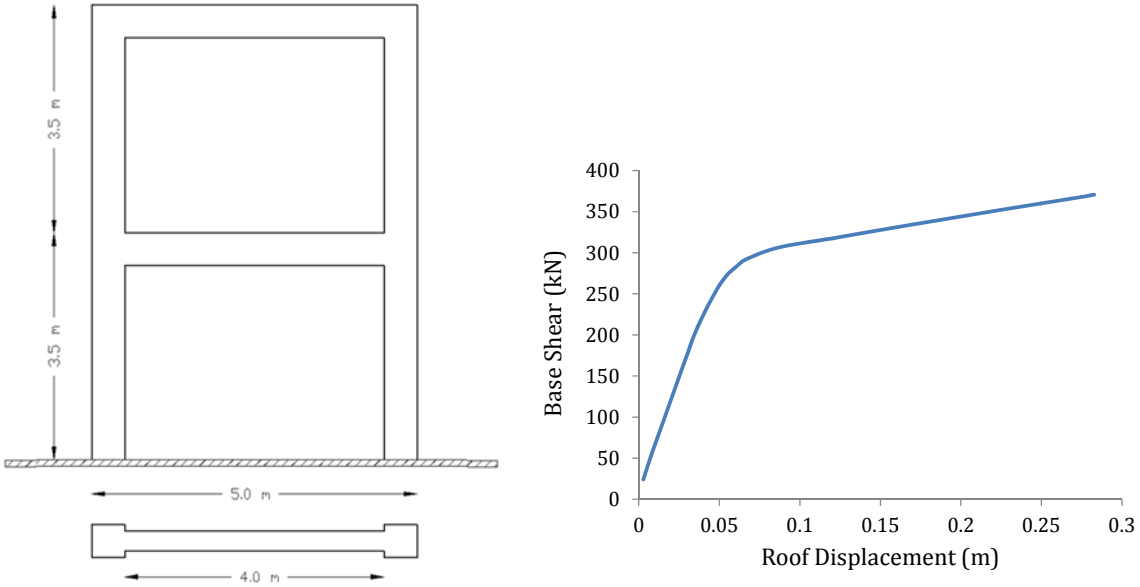

Figure 2.3. 2D test example – (a) front and plan views and (b) roof displacement-base shear curve.

2.6.2. 2D test example

The first test example considered in order to calibrate the five damage indices by means of the IDA procedure described in the previous section is a two storey 2D RC plane frame. The front and layout views of the test example are shown in Figure 2.3(a) while the roof displacement-base shear curve is shown in Figure 2.3(b). An effective area of 5×5 m^2 was considered for the calculation of loads and masses on each floor. Furthermore, rayleigh damping is used for the first and the second mode (T_1=0.448 sec, T_2= 0.313 sec and $\xi_1=\xi_2$=5.0%).

The number of the hexaedral finite elements for the analyses performed is provided in Table 2.5 below. In particular, Table 2.5 shows the number of elements (hexahedral and steel reinforcement), the number of nodes and the number of degrees of freedom. Additionally, it should be mentioned that the dimensions of the solid finite elements are 10×10×10 cm^3. The cross sections of the beams and the columns along with the longitudinal

and transverse reinforcement of the 2D test example are shown in Figure 2.4. The dimensions of the beams are 30×50cm², with longitudinal reinforcement LR: 3Ø18 top and bottom, and transverse reinforcement TR: (2)Ø8/10cm. The dimensions of the columns are 50×50cm² with longitudinal reinforcement LR: 8Ø22 and transverse reinforcement TR: (2)Ø8/20cm.

Table 2.5. 2D test example - number of elements, nodes, degrees of freedom.

Element	No of elements	Nodes	DOFs
Embedded	4,984	4,952	29,712
Hexahedral	4,850	7,320	21,960

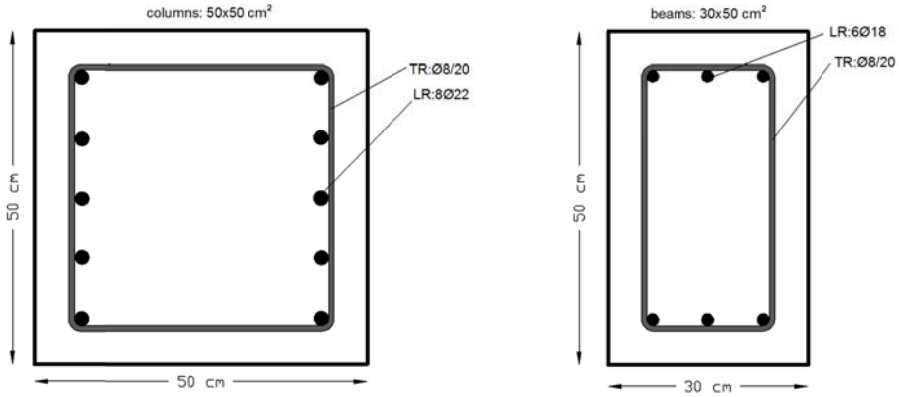

Figure 2.4. 2D test example – cross sections.

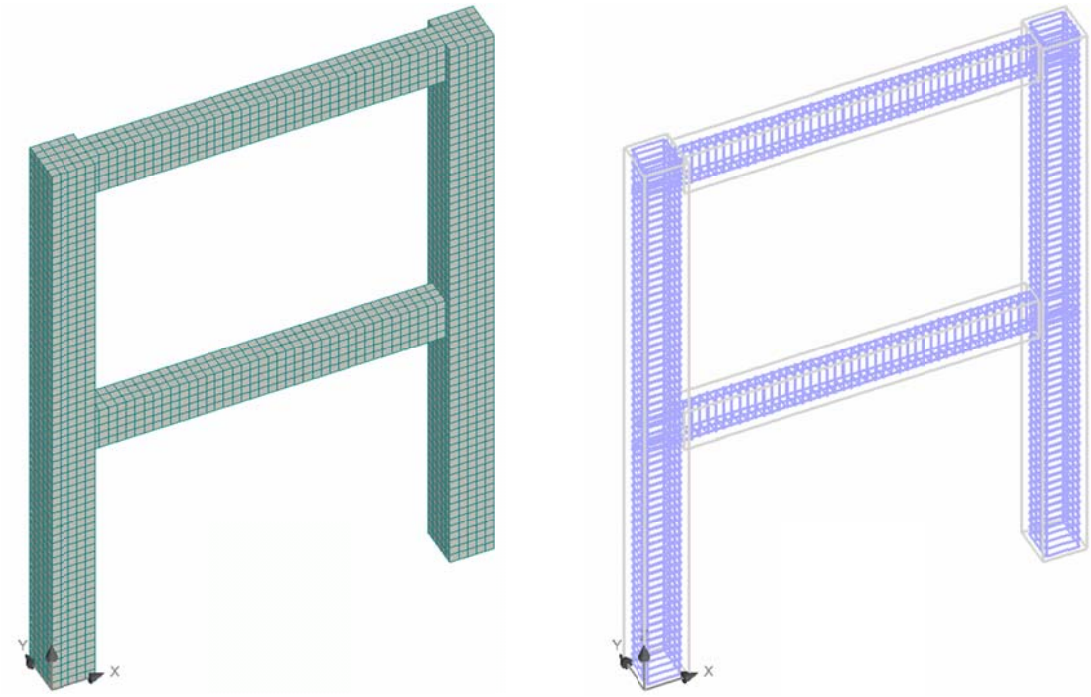

(a) (b)

Figure 2.5. 2D test example (a) FE mesh and (b) steel reinforcement.

The solid finite element discretization along with the longitudinal and transverse reinforcement for the 2D test example are shown in Figures 2.5(a) and 2.5(b), respectively. In order to calibrate the five damage indices the Incremental Dynamic Analysis procedure has been performed over the bin of sixty records (see Tables A.1 to A.3 of Appendix A for details regarding the bin of records). Based on these analyses the crack openings given in Table 2.4 have been correlated with the various damage indices and thus their median limits have been obtained (Figure 2.6 depicts a cracked structure for the 3D test example).

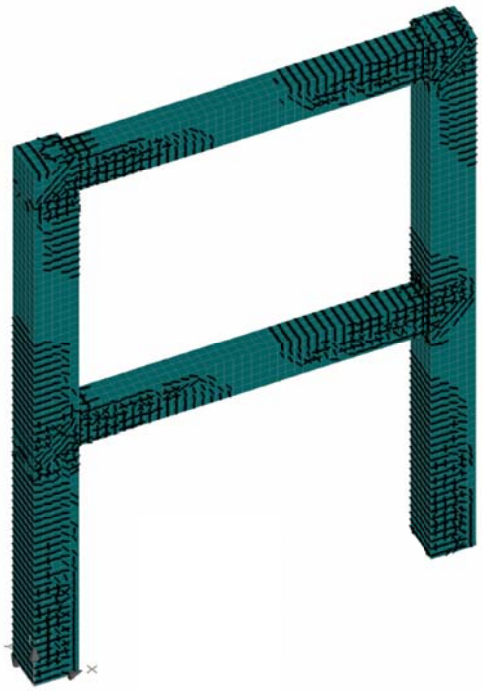

Figure 2.6. 2D test example-cracked structure.

The 16, 50 and 84 percentile IDA curves for all damage indices are given in Figures 2.7(a) to 2.7(h). Although, maximum drift and relative with reference to the base maximum floor acceleration seems to have an almost linear trend and the hazard levels considered, the other DIs have a fully nonlinear trend. The DIs have a similar trend in pairs; in particular, Park and Ang with Kunnath et al. DIs have a similar trend, while the maximum and final softening damage indices have also a similar trend to each other as well as Chung et al. and Banon and Veneziano.

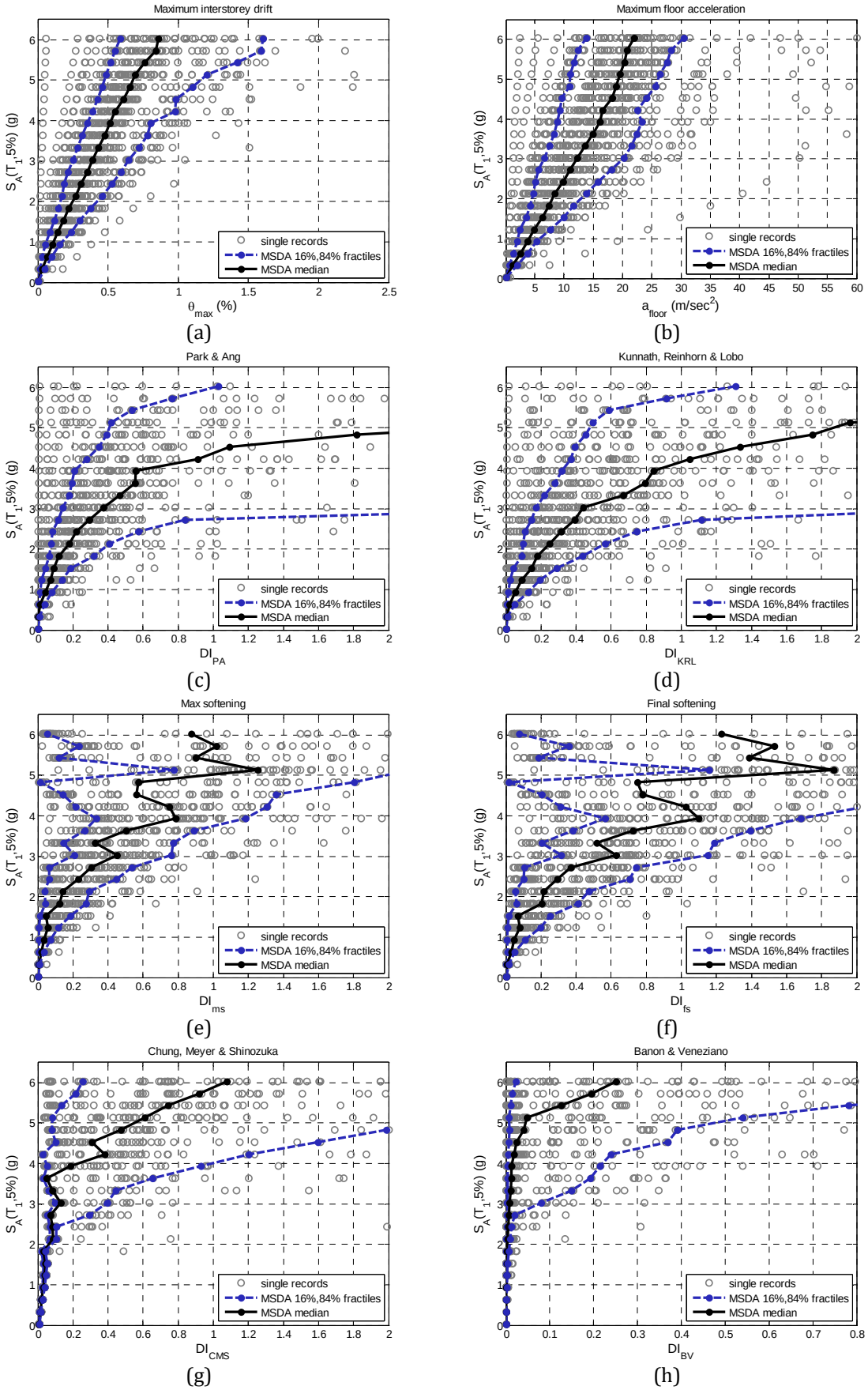

Figure 2.7. 2D test example-IDA curves.

Based on the procedure described in subsection 2.7.1 and for the four damage states considered in Table 2.4, as these were defined according to the crack width the five damage indices, namely maximum softening (DI_{ms}) and final softening (DI_{fs}) by DiPasquale and Cakmak (1988), Park and Ang (DI_{PA}) and its modified version (DI_{KRL}) proposed by Kunnath et al. (1992) and the Chung, Meyer and Shinozuka damage index (DI_{CMS}), are calibrated. The values for the five damage states are given in Table 2.6.

Apart from the calibrated values of the five damage indices defined on the basis of the 50% fractile IDA curve, the COV for each DI and for each damage state are defined. These values are given in Table 2.7, where it can be observed that for the first (no damage), second (slight) and third (moderate) damage states the Chung, Meyer and Shinozuka damage indices (DI_{CMS}) depict the lower COV values, while in the fourth (extensive) damage state the Kunnath et al. (1992) damage index (DI_{KRL}) is the one that depicts the lower COV values. Furthermore, only the maximum floor acceleration has a similar COV value for all four damage states. Worth mentioning, is the fact that for the third (moderate) damage state all DIs depicts their lowest COV values.

Table 2.6. 2D test example-Damage state with reference to crack width.

Damage state	θ_{max} (%)	a_{floor} (m/sec^2)	DI_{ms}	DI_{fs}	DI_{PA}	DI_{KRL}	DI_{CMS}
No damage	0.12	4.28	0.05	0.06	0.06	0.07	0.03
Slight	0.24	7.82	0.13	0.21	0.14	0.21	0.05
Moderate	0.47	14.53	0.44	0.66	0.52	0.75	0.06
Extensive	0.63	18.57	0.57	0.77	1.40	1.51	0.38

Table 2.7. 2D test example- Coefficient of variation of the damage indices in percentages.

Damage state	θ_{max}	a_{floor}	DI_{ms}	DI_{fs}	DI_{PA}	DI_{KRL}	DI_{CMS}
No damage	34.85	41.50	55.53	43.16	44.82	41.97	17.42
Slight	39.35	36.66	47.05	44.36	26.08	31.02	16.15
Moderate	13.55	33.38	14.61	13.31	0.00	9.34	2.79
Extensive	17.54	36.24	25.36	17.79	0.01	9.01	23.11

2.6.3. 3D test example

The second test example employed in order to calibrate the five damage indices by means of the IDA procedure described in previous section of this chapter is a two storey 3D RC frame. The front and layout views of the test example are shown in Figures 2.8(a) and 2.8(b) while the roof displacement-base shear curve is shown in Figure 2.8(c). The number of the hexaedral finite elements for the analyses performed is provided in Table 2.8 below. In particular, Table 2.8 shows the number of elements (hexahedral and steel reinforcement), the number of nodes and the number of degrees of freedom. Additionally, the dimensions of the solid finite elements are 10×10×10 cm^3. The floor area of 5×5 m^2 was considered for the calculation of loads and masses on each floor. Furthermore, rayleigh damping is used for the first and the second mode (T_1= 0.167 sec, T_2= 0.167 sec and $\xi_1=\xi_2$=5.0%).

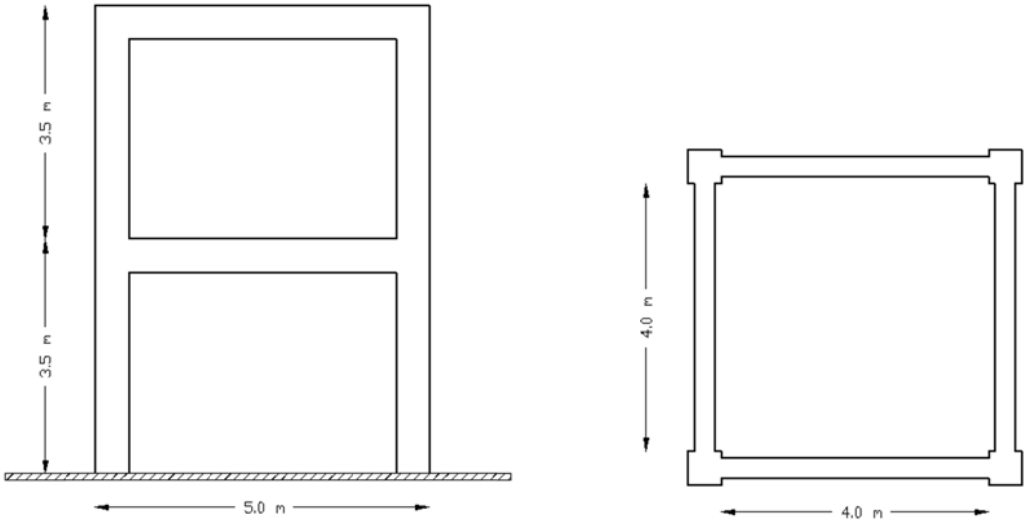

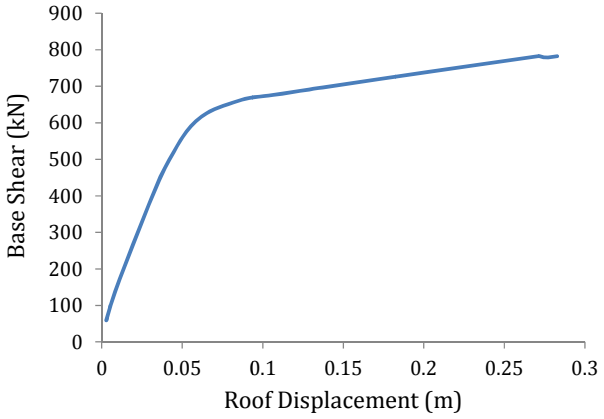

(b)

Figure 2.8. 3D test example – (a) front, (b) side views and (c) roof displacement-base shear curve.

The cross sections of the beams and the columns along with the longitudinal and transverse reinforcement of the 3D test example are shown in Figure 2.9. The dimensions of the beams are 30×50cm^2, with longitudinal reinforcement LR: 3Ø18 top and bottom, and

transverse reinforcement TR: (2)Ø8/10cm. The dimensions of the columns are 50×50cm^2 with longitudinal reinforcement LR: 12Ø22 and transverse reinforcement TR: (2)Ø8/20cm. The solid finite element discretization along with the longitudinal and transverse reinforcement for the 2D test example are shown in Figures 2.10(a) and 2.10(b), respectively. In order to calibrate the five damage indices the IDA procedure has been performed over the bin of sixty records (see Tables A.1 to A.3 of Appendix A for details regarding the bin of records). Based on these analyses the crack openings given in Table 2.4 have been correlated with the various damage indices and thus their median limits have been obtained (Figure 2.11 depicts a cracked structure for the 3D test example).

Table 2.8. 3D test example - number of elements, nodes, degrees of freedom.

Element	No of elements	Nodes	DOFs
Embedded	13,280	13,120	78,720
Hexahedral	12,400	19,056	57,168

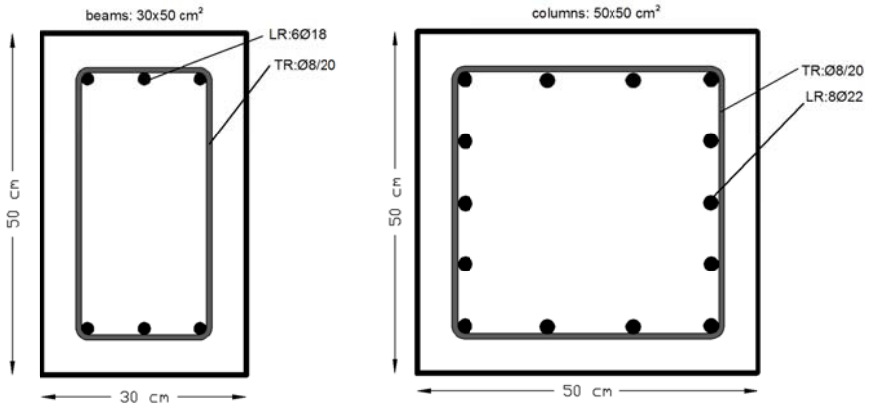

Figure 2.9. 3D test example – cross sections.

The 16, 50 and 84 percentile IDA curves for all damage indices are given in Figures 2.12(a) to 2.12(h). These are similar to the 2D test example presented in the previous section of this chapter, although, maximum drift and relative with reference to the base maximum floor acceleration seem to have a bilinear trend and the hazard levels considered, the other DIs have a fully nonlinear trend. The DIs have the following trend: Park and Ang with Kunnath et al. DIs have a similar trend, while Maximum and final softening damage indices have also a similar trend as well as Chung et al. and Banon and Veneziano damage indices.

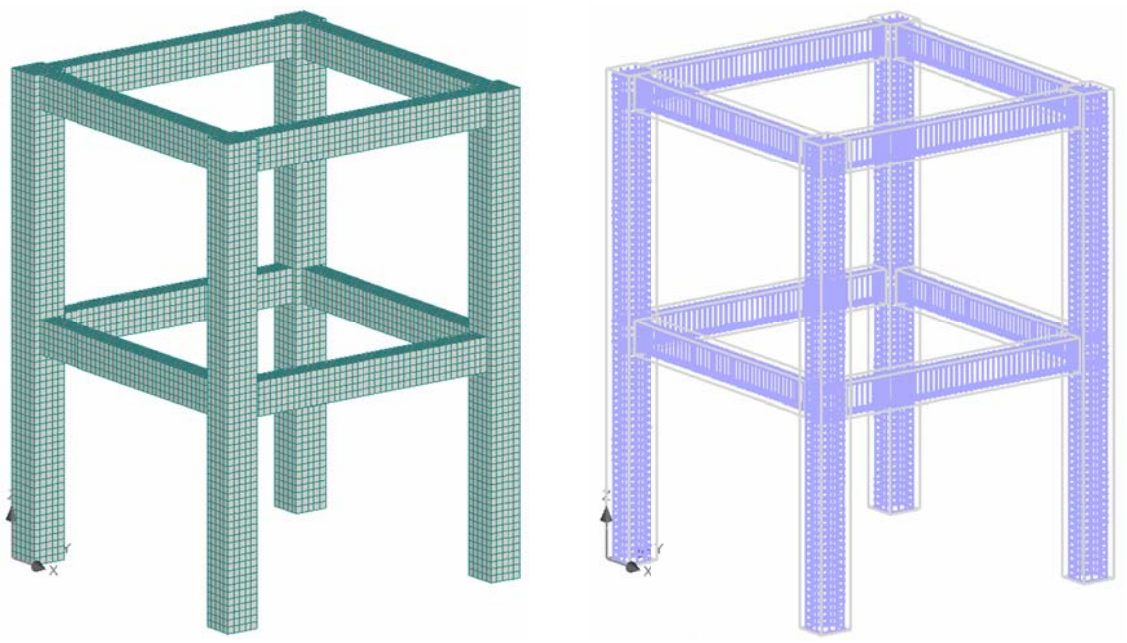

(a) (b)

Figure 2.10. 3D test example-(a) FE mesh and (b) steel reinforcement.

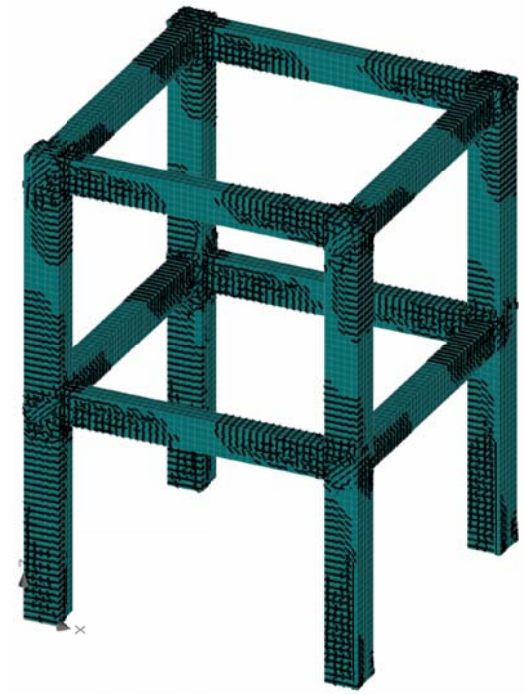

Figure 2.11. 3D test example-cracked structure.

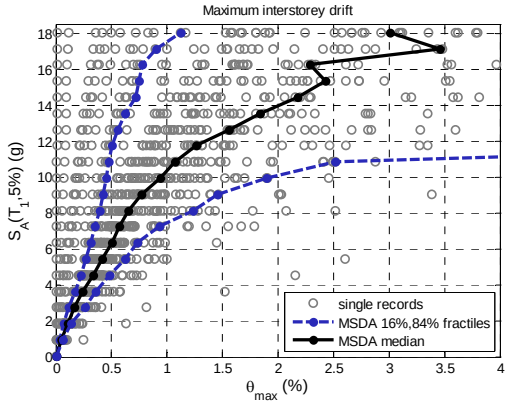

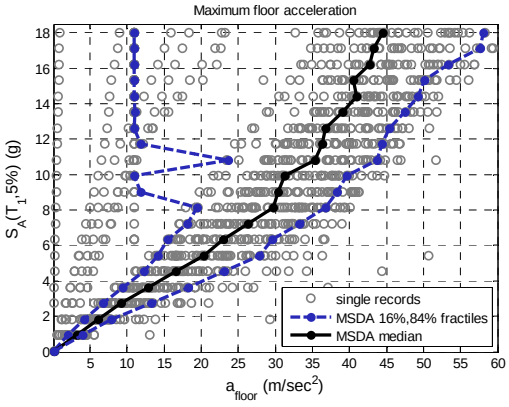

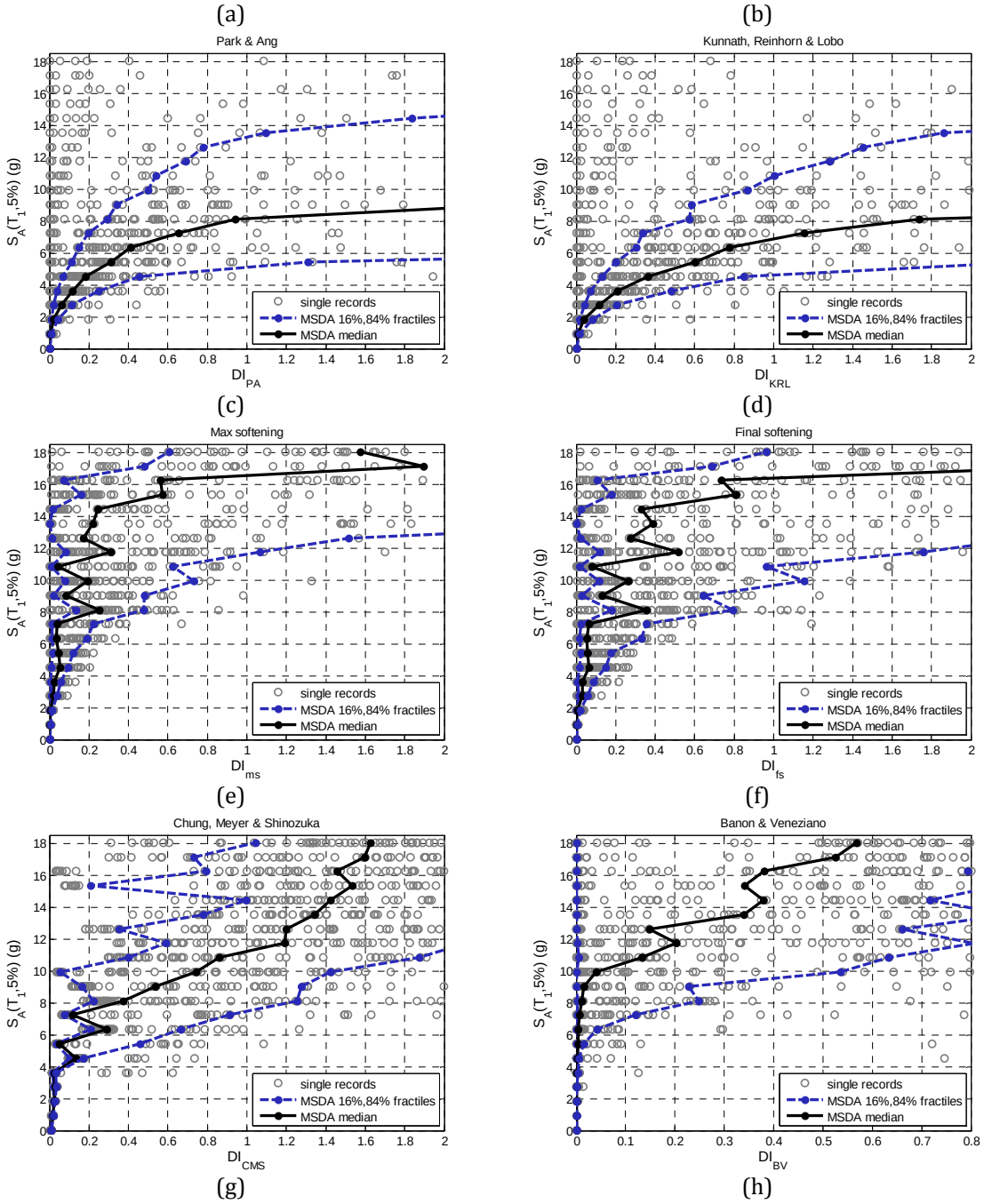

Figure 2.12. 3D test example-IDA curves.

Based on the procedure described in previous section of this chapter and for the four damage states, as these were defined according to the crack width in Table 2.4, the five DIs, namely Maximum Softening (DI_{ms}) and Final Softening (DI_{fs}) by DiPasquale and Cakmak (1988), Park and Ang (DI_{PA}) and its modified version (DI_{KRL}) proposed by Kunnath et al. (1992) and the Chung, Meyer and Shinozuka damage index (DI_{CMS}) have been calibrated. The calibrated values for the five damage states are given in Table 2.9.

Table 2.9. 3D test example-Damage state with reference to crack width.

Damage state	θ_{max} (%)	a_{floor} (m/sec^2)	DI_{ms}	DI_{fs}	DI_{PA}	DI_{KRL}	DI_{CMS}
No damage	0.13	6.92	0.01	0.01	0.03	0.06	0.02
Slight	0.26	12.88	0.02	0.03	0.12	0.21	0.02
Moderate	1.31	21.54	0.04	0.06	0.36	0.68	0.16
Extensive	1.46	28.89	0.20	0.28	0.87	1.59	0.31

In addition to the calibrated values of the five DIs defined on the basis of 50% fractile IDA curve, the COV for each DI and for each damage state are defined. These values are given in Table 2.10, where it can be observed that for all damage states, i.e. first (no damage), second (slight), third (moderate) fourth (extensive) one DI_{ms}, DI_{fs}, DI_{PA}, DI_{KRL} and DI_{CMS} depict similar trend with reference to the lower COV values, which is much lower than the corresponding values for the case of maximum interstorey drift and maximum floor acceleration.

Table 2.10. 3D test example-Coefficient of variation of the damage indices in percentages.

Damage state	θ_{max}	a_{floor}	DI_{ms}	DI_{fs}	DI_{PA}	DI_{KRL}	DI_{CMS}
No damage	23.16	25.43	8.94	7.71	5.02	5.38	5.08
Slight	11.57	26.24	0.39	0.42	1.15	1.19	1.05
Moderate	9.80	30.29	0.66	0.61	0.00	0.82	0.49
Extensive	7.46	41.19	0.12	0.14	0.00	0.76	0.38

2.7. Discussion

In this chapter an overview on the damage indices proposed by various researchers is presented. Damage may be quantified by using several damage indices whose values can be related to particular structural damage states. The idea of describing the state of damage of the structure by one parameter on a prescribed scale in the form of a damage index is attractive because of its simplicity. In the framework of this dissertation, five damage indices belonging to the group of maximum deformation and cumulative damage have been considered and have been calibrated numerically with reference to the level of structural damage. In particular, the Park and Ang damage index and its modified version by Kunnath et al. (1992), the Chung, Meyer and Shinozuka damage index, along with the maximum

softening and final softening by DiPasquale and Cakmak (1988) have been considered for the parametric study performed. The numerical calibration of the five damage indices was based on the incremental dynamic analysis (IDA) procedure. The ultimate goal of this study is to identify the proper DI (with reference to the coefficient of variation, the lower the better) in order to be incorporated into a performance-based design framework (as it will be presented in Chapter 4). Furthermore, in order to be incorporated into the framework, calibrated values of the DIs for different damage levels are required.

The proposed numerical calibration procedure for the of the five damage indices was based on the IDA procedure where multiple nonlinear dynamic analyses were performed in earthquake hazard levels of increasing intensity. The seismic demand used for calibrating the damage indices DI_i (i=1,2,...,n) was considered with reference to the characterization of the damage state defined with respect to the crack openings. In particular, 60 records were scaled in multiple hazard levels and the 16%, 50% and 84% fractile curves were obtained, the calibrated values of the DIs were defined based on the 50% fractile and were computed with reference to the seismic demand. The seismic demand was obtained by means of a single IDA curve using a detailed discretization with solid finite elements and a single artificial accelerogram generated on the basis of the mean response spectrum of the 60 natural records. The 60 IDA curves were obtained by the IDA performed on the discredited structure with beam element. Based on the proposed procedure the five damage indices have been calibrated.

In addition to the calibrated values of the five damage indices defined on the basis of the 50% fractile IDA curve, the COV for each DI and for each damage state were defined. It was found that for the 2D test example examined in the framework of this study, for the first (no damage), second (slight) and third (moderate) damage state the Chung, Meyer and Shinozuka damage index (DI_{CMS}) depicts the lower COV values, while in the fourth (extensive) one it is the Kunnath et al. (1992) damage index (DI_{KRL}) which depicts the lower COV values. Furthermore, the maximum floor acceleration had a similar COV value for all four damage states. Worth mentioning is also the fact that for the third (moderate) damage state all DIs reach depicts their lowest COV values. On the other hand, for the second test example it was observed that for all damage states, i.e. first (no damage), second (slight), third (moderate) fourth (extensive), all damage indices DI_{ms}, DI_{fs}, DI_{PA}, DI_{KRL} and DI_{CMS} show a similar trend with reference to the lower COV values, which was much lower than the corresponding values for the case of maximum interstorey drift and maximum floor acceleration.

2.8. References

Allahabadi, R., Powell, G.H.(1988) DRAIN-2DX User Guide. Technical Re No. UCB/EERC-88-06, Earthquake Engineering Research Center, Univ. of California, Berkeley, CA.

ATC-40, Seismic evaluation and retrofit of concrete buildings, Applied Technology Council, Redwood City, 1996.

Ayala G., Xianguo Y. (1995) Analytical evaluation of the structural seismic damage of reinforced concrete frames, 7th Canadian Conf. on Earthquake Engineering, Montreal, Canada, pp. 389-396.

Balaguru P, Shah S. A method of predicting crack widths and deflections for fatigue loading. ACI Special Pub 1982; 75(5):153–175.

Banon H., Veneziano D. (1982) Seismic safety of reinforced members and structures, Earthquake Engineering and Structural Dynamics 10(2), 179-193. (A2), A23

Beck, J. L. and Jennings, P. C. Structural identification using linear models and earthquake records, Earthquake Engineering and Structural Dynamics, 1980, 8, 145-160

Beck, J. L. Determining models of structure from earthquake records, Report No. EERL 78-01, California Institute of Technology, 1978.

Caughey, T. K. Equivalent linearization technique, J. Ac. Soc. Am., 1963, 27(4), 1706-1711.

Červenka V, Jendele L, Červenka J, ATENA Theory Manual. Cervenka Consulting; 2009.

Chai YH, Fajfar P, Romstad KM. Formulation of duration dependent inelastic seismic design spectrum. Journal of Structural Engineering ASCE 1998; 124(8):913–921.

Chung Y.S., Meyer C., Shinozuka M. Seismic damage assessment of reinforced concrete members, Report NCEER-87-0022, National Center for Earthquake Engineering Research, State University of New York at Buffalo, Buffalo, NY, 1987.

Chung YS, Hatamoto H, Meyer C, Shinozuka M. Seismic safety improvement of damage-controlled reinforced concrete frames. Adv Eng Software 1993;18(2):95-102.

Chung, Y.S., Meyer, C. and Shinozuka, M. Modelling of concrete damage. ACI Struct. J., 1989, 86(3).

DiPasquale E., Çakmak A.S. Identification of the serviceability limit state and detection of seismic structural damage, Report NCEER-88-0022, National Center for Earthquake Engineering Research, State University of New York at Buffalo, NY, 1988.

DiPasquale, E. and Çakmak, A.S. Detection and assessment of seismic structural damage, Report NCCER-87-O015, National Center for Earthquake Engineering Research, State University of New York at Buffalo, August 1987.

Estekanchi, H. E. and Arjomandi, K (2007), Comparison of damage indexes in nonlinear time history analysis of steel moment frames, Asian Journal of Civil Engineering, V. 8, No. 6, p 629-646.

Eurocode 3: Design of steel structures, part 1.8: Design of joints. Brussels: EN1993-1-8, European Committee for Standardization; 2004.

FEMA-273. NEHRP Guidelines for the Seismic Rehabilitation of Buildings, Building Seismic Safety Council for the Federal Emergency Management Agency, Washington, DC, 1997.

FEMA-350: Recommended Seismic Design Criteria for New Steel Moment-Frame Buildings. Federal Emergency Management Agency, Washington DC, 2000.

FEMA-356, Prestandard and Commentary for the Seismic Rehabilitation of Buildings, Federal Emergency Management Agency, Washington, DC, 2000.

FEMA-440: Improvement of Nonlinear Static Seismic Analysis Procedures. Federal Emergency Management Agency: Washington, DC, 2005.

Fujikake, K., Ohno, T. and Nishioka, T. Experimental study on energy absorption capacity of reinforced concrete frame. Proc. JSCE, 1988, 8(390).

Ghobarah, A., Abou-Elfath, H., Biddah, A. (1999). Response-based damage assessment of structures. Earthquake Engineering and Structural Dynamics, 28(1), 79-104.

Grigoriu M. 'Damage models for seismic analysis', Technical Report 87-4, Department of Structural Engineering, Cornell University, Ithaca, NY, 1987.

Hassan, A.F. and Sozen, M.A. 1997, "Seismic vulnerability assessment of low-rise buildings in regions with infrequent earthquakes", ACI Structural Journal, vol. 94, no. 1, pp. 31-39.

Kunnath S.K., Reinhorn A.M., Lobo R.F. IDARC Version 3.0: a program for the inelastic damage analysis of reinforced concrete structures, Technical Report NCEER-92-0022, National Center for Earthquake Engineering Research, Buffalo, NY, 1992.

Lynn, A.C., Moehle, J.P., Mahin, S.A. & Holmes, W.T. 1996, "Seismic evaluation of existing reinforced concrete building columns", Earthquake Spectra, vol. 12, no. 4, pp. 715-739.

Mahin, S. A., Bertero. V.V. 1974. Nonlinear seismic response evaluation - Charaima building. ASCE J Struct Div 100, no. ST6: 1225-1242.

McCabe SL, Hall WJ. Assessment of seismic structural damage. Journal of Structural Engineering ASCE 1989; 115(9):2166–2183.

Mitropoulou, Ch.Ch., Lagaros, N.D., Papadrakakis, M. (2010) Economic building design based on energy dissipation: a critical assessment, Bulletin of Earthquake Engineering, 8(6): 1375-1396.

Mitropoulou, Ch.Ch., Papadrakakis, M. (2011), Fragility Analysis of Structures: A computationally efficient approach with Neural Network predictions, *Engineering Structures*, (accepted for publication).

Newmark N.M., Rosenblueth E. Fundamentals of Earthquake Engineering, Prentice-Hall, Englewood Cliffs, NJ, 1971.

Park Y.J., Ang A.H.-S. (1985) A Mechanistic seismic damage model for reinforced concrete, J. Struct. Div. ASCE 111(4), 722-739.

Park YJ, Reinhorn AM, Kunnath SK. IDARC: Inelastic damage analysis of reinforced concrete frame-shear-wall structures. Technical report NCEER-87-0008. Buffalo, NY: National Center for Earthquake Engineering Research; 1987.

Petryna YS, Kratzig W, Stangenberg F. Structural damage: simulation and assessment. Tech Rep, Computational Structural Technology, Stirling, Scotland 2002.

Powell GH, Allahabadi R. Seismic damage prediction by deterministic methods: Concepts and procedures. Earthquake Engineering and Structural Dynamics 1988; 16: 719–734.

Qin F, Fung TC, Soh CK. Hysteretic behaviour of completely overlap tubular joints. Journal of Constructional Steel Research 2001; 57(7):811–829.

Roufaiel M.S.L., Meyer C. Analysis of damaged concrete frame buildings, Technical Report No. NSF-CEE-81- 21359-1, Columbia University, New York, NY, 1981.

Roufaiel, M.S.L. and Meyer, C. Analytical modelling of hysteretic behaviour of R/C frames. J. Struct. Eng., ASCE, 1987, 113(3).

Saiidi, M. & Sozen, M.A. 1981, "Simple nonlinear seismic analysis of RC structures", ASCE J Struct Div, vol. 107, no. 5, pp. 937-952.

Shahrooz, B.M. & Moehle, J.P. 1990, "Evaluation of seismic performance of reinforced concrete frames", Journal of structural engineering New York, N.Y., vol. 116, no. 5, pp. 1403-1422.

Sozen MA. Review of earthquake response of reinforced concrete buildings with a view to drift control. In: State-of-the-Art in earthquake engineering. Istanbul (Turkey): Turkish National Committee on Earthquake Engineering; 1981. p. 383–418.

Stephens J.E. A damage function using structural response measurements, Structural Safety 5, 22-39 (1985).

Stephens J.E., Yao J.T.P. (1987) Damage assessment using response measurements, Journal of Structural Engineering ASCE 113(4), 787-801.

Toussi, S. and Yao, J.T.P., (1983). Assessment of structural damage using the theory of evidence. Structural Safety, 1, 107–121. .

Toussi, S., and Yao, J.T.P. (1982) Hysteresis identification of existing structures, J. Engng. Mech. ASCE 109(5), 1189-1203.

Valdimarsson, H., Shah, A.H. and McNiven, H.D. Linear models to predict the nonlinear seismic behaviour of a one-storey steel frame, Report No. UCB/EERC-81/13, September 1981, Berkeley, CA.

Wang W, Chen YY. Hysteretic behaviour of tubular joints under cyclic loading. Journal of Constructional Steel Research 2007; 63(10):1384–1395.

Yao, J.P.T., Kozin, F., Wen, Y.-K., Yang, J.-N., Schueller, G.I., Ditlevensen, O. (1986) Stochastic Fatigue, Fracture and Damage Analysis, Structural Safety, 3: 231-267.

Yin, Y., Han, Q.H., Bai, L.J., Yang, H.D., Wang, S.P. Experimental Study on hysteretic behaviour of tubular N-joints, Journal of Constructional Steel Research (2008).

Zeris, C.A., Vamvatsikos, D., Giannitsas, P., Alexandropoulos, K. Impact of FE modelling in the seismic performance prediction of existing RC buildings, COMPDYN 2007, June 13-16, 2007, Rethymno, Crete, Greece.

Zhang, X., Wong, K.K.F. , Wang, Y. Performance assessment of moment resisting frames during earthquakes based on the force analogy method, Engineering Structures 29 (2007) 2792–2802.

Chapter 3

Structural Design Optimization: Formulations & Methods

3.1. Introduction

Nowadays the term “optimum design of structures” can be interpreted in many ways. In order to avoid any misunderstanding, it is important to define the term “structure” according to the baselines of structural mechanics. The term “structure” is used to describe the arrangement of the elements and/or the materials in order to create a system capable to undertake the loads imposed by the design requirements. The process implemented for the design of structures is an iterative procedure aiming to reach the optimum design. The goal of the structural engineering science is the construction of structural systems like bridges, buildings, aircrafts etc. The progress of computer technology created more demands in structural engineering. The design of a structural system that satisfies the structural requirements related to safety is not enough anymore. Nowadays it is crucial that the structural system is optimally designed. The term “optimum design” is used for a design that not only satisfies the serviceability requirements but also complies with criteria like the cost or the weight of the system to have the less possible values.

The aim of the engineer is to find a combination of independent variables that take real or integer values, called parameters or design variables, so as to optimize the objective function of the problem. The optimization problems in the scientific field of computational mechanics, usually are imposed on restrictions, like the range within which the design parameters are defined (search space), and other constraint functions, like those imposed on stresses and strains, which determine the space of acceptable solutions for the problem at hand.

To calculate the optimal designs it is necessary to perform two steps: the mathematical formulation of the optimization problem and the implementation of an optimization

algorithm. The first step involves the definition of the design parameters, the relationship between these parameters, to determine the optimization function as well as defining the constraints of the problem. The optimization process is completed by choosing a suitable optimization algorithm and its combination with the structural and the optimization models. A basic premise for the case of structural optimal design is to express in mathematical terms the structural behaviour (structural model). In the case of structural systems behaviour this refers to the response under static and dynamic loads, such as displacements, stresses, eigenvalues, buckling loads, etc.

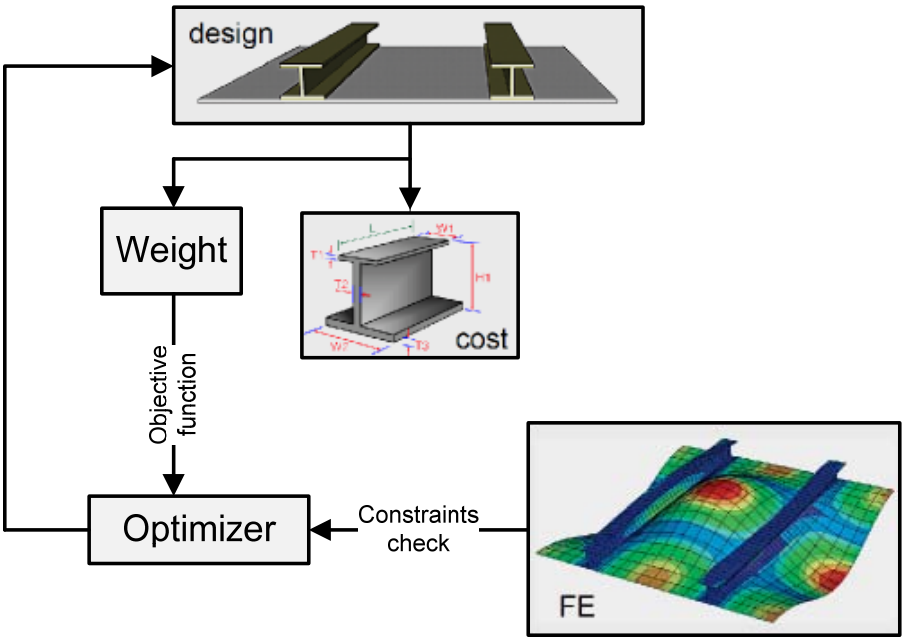

Figure 3.1. The structural optimization procedure.

The existence of efficient optimization algorithms does guaranty that the problem of optimal design will be successfully addressed. The experience of the engineer is important parameter for the proper use of these algorithms. The design procedure is an iterative process where repetition is considered as the sequential test of candidate designs and evaluates whether they are superior or not compared to the past ones, while satisfying the constraints of the problem. The conventional procedure used by engineers is that of "trial and error". Of course, with increased the complexity and magnitude of the problems the use of such empirical techniques does not lead to the optimal solution. So it became necessary to automate the design of buildings by exploiting the developments in computer technology and the advances in optimization algorithms. Today, these tests can be performed automatically and with greater speed and accuracy. The optimum design procedure for structural systems is presented in Figure 3.1.

3.2. History of optimization

The history of optimization dates several hundreds of years during which remarkable progress has been made in developing new and more efficient methods. Euclid (300B.C.) tackled with the problem of finding the shortest distance which may be drawn from a point to a line (Russo, 2004), while Heron of Alexandria (100B.C.) studied the optimization problem of light travelling between two points by the shortest path (Russo, 2004). Fermat in 1657 developed the more general principle that light travels between two points in a minimum time (Veselago, 2002), while Cauchy (1847) presented for the first time a minimization procedure (Steepest Descent Method) implementing function derivatives. The development of calculus provided the means for the development of the mathematical theory for optimization. The pioneering works of Courant (1943) on penalty functions, Dantzig (1951) on linear programming, Karush (1939) as well as Kuhn and Tucker (1951) on optimality conditions for constrained problems initiated the modern era of optimization.

Particularly in the 60's, several optimization methods for solving nonlinear problems were introduced. Rosenbrock (1960) presented the method of orthogonal directions, Rosen (1960) suggested the gradient projection method, Zoutendijk (1960) formed the feasible directions method, Hooke and Jeeves (1961) developed the pattern search method, Davidon, Fletcher and Powell (1963) stated the variable metric method, Fletcher and Reeves (1964) presented the Conjugate Gradient method, Powell (1964) introduced the method of conjugate directions, Nelder and Mead (1965) suggested their Simplex method, Box (1965) introduced his homonymous technique, while Fiacco and McCormick (1966) formed the so called Sequential Unconstrained Minimization technique.

Since 1970 structural optimization has been the subject of intensive research and several different approaches for optimal design of structures have been advocated (Gallagher and Zienkiewicz, 1973; Haug and Arora, 1974; Moses, 1974; Pope and Schmit, 1971; Sheu and Prager, 1968; Spunt, 1971; Venkayya et al., 1973). All the aforementioned methods are of deterministic character; that is, when applied to the same initial design vector, they always result to the same final design vector. The reason for this is the fact that the element of randomness is non-existent. As a result, there is probability of getting trapped in local minima. Mathematical programming methods make use of local curvature information derived from linearization of the original functions by using their derivatives with respect to the design variables at points obtained in the process of optimization to construct an approximate model of the initial problem. On the other hand the application of combinatorial optimization methods based on probabilistic searching do not need gradient

information and therefore avoid to perform the computationally expensive sensitivity analysis step. Gradient based methods present a satisfactory local rate of convergence, but they cannot assure that the global optimum can be found, while combinatorial optimization techniques are in general more robust and present a better global behaviour than the mathematical programming methods. They may suffer, however, from a slow rate of convergence towards the global optimum.

In contrast to the deterministic optimization methods, the stochastic optimization procedures allow for randomness to appear. In this way, it is possible to get different final design vectors, even though the initial vector is the same. In this category, the most known and widely applied methods are the GA, originating from Holland (1975) and Goldberg (1989), the SA by Kirkpatrick (1984), EP (Fogel et. al, 1966), and the ES (Rechenberg, 1973; Schwefel, 1981). The main characteristic of these methods is the wider exploration and exploitation of the domain, which in turn increases both the probability of locating the global minimum and the computational cost. Both GA and ES imitate biological evolution and combine the concept of artificial survival of the fittest with evolutionary operators to form a robust search mechanism. Apart from the pure deterministic or pure stochastic procedure, hybrid schemes have been introduced as well. The main idea behind the hybridism is to combine the advantages of both categories of methods for a better result to be obtained (Papadrakakis et. al, 1999; Lagaros et. al, 2002).

3.3. Formulation of the structural optimization problem

In general a structural optimization problem may be continuous or discrete, depending on the type of the design space that the design parameters take values. Due to code requirements often the range of the design space is discrete. The mathematical model of a continuous optimal design problem can be formulated as follows:

$$
\begin{aligned}
&F(\mathbf{s}) \to \min \\
&\mathbf{s} = \{s_1, s_2, ..., s_n\}^T \\
&l_i \le s_i \le u_i, i = 1, 2, ..., n \\
&g_j(\mathbf{s}) \ge 0, j = 1, 2, ..., m \\
&h_j(\mathbf{s}) = 0, j = m+1, m+2, ..., t
\end{aligned}
\tag{3.1}
$$

where $\mathbf{s}$ is the vector of design variables, l_i and u_i are the lower and upper bound of design variable s_i, respectively, $F(\mathbf{s})$ is the objective function to be minimized while $g_j(\mathbf{s})$, $h_j(\mathbf{s})$ are the inequality and equality constraint functions, respectively.

Many of the problems that arise in the scientific area of structural design optimization may include discrete or mixed design variables. A typical optimal design problem with

mixed design variables is the shape-sizing design optimization problem of a truss structure. In such a problem, the coordinates of the nodes of the panel, which determine the optimum shape of the structural system can take continuous values, however, standardization reasons require that sectional bars to be defined from a discrete design space. Such problem is called as a mixed-discrete design optimization problem.

In accordance to the problem described in Eq. (3.1), a discrete optimal design problem can be written as follows:

$$\begin{aligned} &F(\mathbf{s}) \to \min \\ &\mathbf{s} = \{s_1, s_2, \ldots, s_n\}^T \\ &l_i \le s_i \le u_i, i = 1,2,\ldots,n \\ &s_i \in R^d, \ \ i = 1,2,\ldots,n \\ &g_j(\mathbf{s}) \ge 0, j = 1,2,\ldots,m \\ &h_j(\mathbf{s}) = 0, j = m+1, m+2,\ldots,t \end{aligned} \tag{3.2}$$

where R^d is the design space of the discrete design variables $\mathbf{s}$. The design variables s_i (i=1,2,...,n) can take values only from the design set R^d.

To address a problem of mixed optimal design many methods have been developed. Usually in the case of a mixed-discrete or a purely discrete problem the design variables are dealt as though they were continuous design variables; while at the end of the process, once the optimal values of all design variables have been determined, appropriate values derived from the discrete design space are assigned to the continuously defined design variables (Hager and Balling, 1988). For the case of a discrete optimal design problem in which the design space can be sorted according to all cross sectional characteristics (cross section area, main and secondary moments of inertia, etc.) in a strictly monotonic sequence, this technique provides a better approximation of the optimal solution. But in practical problems this is not the case. The work of Bremicker et al. (1990) presents an overview of the main methods for the treatment of the mixed-discrete optimum design problems. Most of these methods transform the mixed-discrete problem of optimal design into a series of continuous optimal design problems which are solved iteratively (Cai and Thierauf, 1993; Fu et. al, 1991).

3.3.1. Design Variables

The parameters, that when their values are obtained the design if fully defined, are called design variables. If a design does not fulfil the design requirements of the problem then it is called infeasible, otherwise it is known as a feasible design. One feasible design is not necessarily the best but it is always able to be implemented. A very important first step for

proper formulation of a problem is the correct selection of the design variables. In cases where the selection of the design variables is not correct then the formulation may be incorrect or in the worst case, the optimal design obtained from the optimization algorithm is not feasible. Although this way the "degrees of freedom" of the formulation of the optimization problem of the system is increased, there are cases that it is desirable to select more design variables that are necessary for the proper formulation of the problem. In such problems it is possible to remove the additional design variables by designating to them specific values for the next steps of the optimization procedure. Another important issue that needs to be taken into account in the selection of design variables is their relative independence.

During the formulation of the mathematical optimization model the function to be optimize should be sufficiently dependent on all the design parameters. Let as consider the case that the objective function is the weight of the structure, where the minimum value is to be obtained and let assume that the magnitude of the weight is at the order of 1,000 Kg. If the weight of a structural member is in the order of 10^{-3} Kg or less and let as consider that this member represents one of the design variables of the problem, then if the value is changed by 100% the influence on the value of the objective function is negligible. To avoid conditions, such as those mentioned above, it is necessary that linkage between the design variables is imposed. Therefore, some members of the structure can be represented by a common design parameter. Therefore, it is recommended to conduct a sensitivity analysis in order to estimate the sensitivity of the objective function over all the design parameters before the final choice of the optimization model. Through the sensitivity analysis it is possible to detect design parameters that have negligible influence on the objective function.

3.3.2. Objective Function

Every optimization problem is described by a large number of feasible designs and some of them are better and some others are worst while only one is the best solution. To make this kind of distinction between good and better designs it is necessary to have a criterion for comparing and evaluating the designs. This criterion is defined by a function that takes a specific value for any given design. This function is called as objective function which depends on the design variables (see Eqs. (3.1) and (3.2)). With no violation of the generality the formulations given in Eqs. (3.1) and (3.2) refers to a minimization problem. A maximizing problem of the function $F(\mathbf{s})$ can be transformed into a minimization problem of the objective function $-F(\mathbf{s})$. An objective function that is to be minimized it is often called as the cost function.

The appropriate selection of the objective function is a very important step in the process of mathematical model to that of the proper selection of the design variables. Some examples of objective functions reported in the literature are: minimizing the cost, the weight optimization problem, the energy losses problem and maximizing the profit. In many cases the formulation of the optimization problem is defined with the simultaneous optimization of two or more objective functions that are conflicting against each other. As an example, of this type of optimization problem is the case where the objective is to find an optimum design with minimum weight and simultaneously to have minimum stress or displacement in some parts of the structural system. These type of problems are called optimization problems with multiple objective functions (multi-objective design or Pareto optimum design).

3.3.3. Constraint Functions

The design of a structural system is achieved when the design parameters take specific values. Design can be considered any arbitrarily defined structural system, such as a circular cross section with a negative radius, or a ring cross section with a negative wall thickness, as well as any non-constructible building system. All engineering or code provisions are introduced in the mathematical optimization model in the form of inequalities and equalities which are called constraint functions. These constraint functions in order to have meaningful contribution on the mathematical formulation of the problem should be at least dependent on one design variable. The constraint functions that are usually imposed on structural problems are stress and strain constraints, whose values are not allowed to exceed certain limits. Sometimes the engineers impose additional constraint functions that may be useless, which they are either dependent on others or they remain forever in the safe area, this is due to the existence of uncertainties on the definition of the problem or due to inexperience. The use of additional constraint functions may result to calculations requiring additional computational effort without any benefit especially in the case of mathematical programming methods that they require to perform sensitivity analysis.

One inequality constraint function $g_j(\mathbf{s})\leq 0$ is considered as active at the point $\mathbf{s}^*$ in the case that the equality is satisfied, i.e. $g_j(\mathbf{s}^*)=0$. Accordingly, the above constraint function is considered as inactive for the design $\mathbf{s}^*$ for the case that the inequality is strictly satisfied, i.e. $g_j(\mathbf{s}^*)<0$. The inequality constraint function is considered that it is violated for the design $\mathbf{s}^*$ if a positive value that $g_j(\mathbf{s}^*)>0$, corresponds to the value of the constraint function. Similarly, an equality constraint function $h_j(\mathbf{s})=0$ is considered that it is violated for the design $\mathbf{s}^*$ if the equality is not satisfied, i.e. $h_j(\mathbf{s}^*)\neq 0$. Therefore, an equality constraint

function might be active or violated. From all the description provided related to the active or the inactive constraint functions it is clear that any feasible design is defined by active or inactive inequality constraint functions and active equality constraint functions.

At each step of the optimization process it is unlikely that all constraint functions are active. The engineers are not able to determine in advance which of these functions will become active and which of them will become inactive at each step. For this reason, when solving optimization problems it is necessary to use different techniques to address more effectively the constraint functions, techniques that greatly improves the efficiency of the optimization procedure and reduce significantly the time required for the calculations. Especially when the problem is relatively large, i.e. the formulation of the problem is defined with many design variables and constraint functions, any possibility of reducing the calculations of the values required and the derivatives of constraint functions has significant impact on the efficiency of the performance of the optimization procedure. So it is crucial to identify at each step of the optimization procedure the constraint functions that are located within the safe area, i.e. they are inactive, which they do not affect the process of finding of an improved design in order to continue the optimization process with only the active constraint functions.

An active constraint function suggests that its presence significantly affects the improvement of the current design. By definition, the equality constraint functions should be fulfilled at each step of the optimization procedure; therefore, they are considered always among the active constraint functions (Arora, 1989; Gill and Murray, 1981). An active inequality constraint function means that at this stage should be fulfilled as equality or even approximately. When a constraint function is inactive then it means that its presence is not important at that part of the optimization procedure, since the active constraint functions fulfil the needs of the design. This does not mean, though, that this constraint function is redundant as in another optimization step can be activated. Usually, in order to increase the effectiveness of the mathematical algorithms, only the active constraint functions are taken into account. On the other hand other optimal design methods like the fully-stressed design method, are based on exploiting the presence of active constraint functions.

In order to identify the active constraint functions the values of the constraint functions should be normalized first (Vanderplaats, 1984) to have a single reference system regardless of the type of the constraint function. For example, it is likely that the value of a displacement constraint function to take values in the order of 0.1-2.0 cm, while the value of a stress displacement constraint function to take values is in the order of 25,000 kPa, so readily it is apparent that it is necessary to homogenize the sizes of the two constraint

functions. The normalization of the value constraint functions takes place in accordance with the following relations:

$$g_j^N(\mathbf{s}) = \frac{g_j^l - g_j}{\left|g_j^l\right|} \le 0 \tag{3.3}$$

for a constraint function limited with a *lower bound,* $g_j \ge g_j^l$, and:

$$g_j^N(\mathbf{s}) = \frac{g_j - g_j^u}{\left|g_j^u\right|} \le 0 \tag{3.4}$$

for a constraint function limited with an *upper bound*, $g_j \le g_j^u$. Thus, if the normalized value of the constraint function is equal to +0.50 then it violates its permissible value by 50%, while if its normalized value is equal to -0.50 then this constraint is 50% below the allowable value. Usually among the active constraint functions are included those with normalized value greater than -0.1 to -0.01 (Arora, 1989). Furthermore, it is also allowed a small tolerance when the constraint functions violate the minimum allowable value (-0.005 to 0.001) since the process of simulation, analysis, design and construction involves many uncertainties.

3.3.4. Global and local minimum

A common problem for all mathematical optimization methods is that due to the deterministic nature of the operators used they may be directed to identifying a local minimum, in contrast to the methods that are based on probabilistic operators where random search procedures are implemented and they are more likely to locate the global minimum of the problem at hand. The definitions of the local and the global minimum in mathematical terms can be as follows:

Local minimum. A point $\mathbf{s}^*$ in the design space is considered as a local or a relative minimum if this design satisfies the constraint functions and the relationship $F(\mathbf{s}^*) \le F(\mathbf{s})$ is valid for every feasible design point in a small region around the point $\mathbf{s}^*$. If only the inequality is valid, $F(\mathbf{s}^*) < F(\mathbf{s})$, then the point $\mathbf{s}^*$ is called as a strict or a unique or a strong local minimum.

Global minimum. A point $\mathbf{s}^*$ the design space is defined as the global or absolute minimum for the problem at hand if this design satisfies the constraint functions and the relation $F(\mathbf{s}^*) \le F(\mathbf{s})$ is valid for every feasible design point. If only the inequality is valid, $F(\mathbf{s}^*) < F(\mathbf{s})$, then the point $\mathbf{s}^*$ is called as a strict or a unique or a strong global minimum.

If there is no constraint functions then the same definitions can be used, but they are valid throughout the design space and they are not restricted only in the region of feasible designs. Generally it is difficult to foretell in advance the existence of local or global minimum in every optimal design problem. However, if the objective function F(**s**) is continuous and the region of feasible designs is nonempty, closed and bounded, then there is a global minimum for the objective function F(**s**) (Arora, 1994). The region of feasible designs is defined as not empty when there are no conflicting constraint functions or when there are not redundant constraint functions. If the optimization algorithm cannot to identify any feasible point then it can be said that the region of feasible designs is empty and therefore the problem should be reformulated by removing or defining some constraint functions to be more flexible. The region of feasible designs is defined as closed and fixed when the constraint functions are continuous and there are not "strict" inequality constraint functions (g(**s**)<0). The existence of minimum designs is not cancelled if these conditions are not satisfied, simply the minimum designs cannot be established mathematically, but these optimum designs can be obtained during the optimization process.

3.4. Classes of Optimization

There are mainly three classes of structural optimization problems: sizing, shape and topology or layout. Initially structural optimization was focused on sizing optimization, such as optimizing cross sectional areas of truss and frame structures, or the thickness of plates and shells. The next step was to consider finding the optimum boundaries of a structure, and therefore to optimize its shape. In the former case the structural domain is fixed, while in the latter case it is not fixed but it has a predefined topology. In both cases a non-optimal starting topology can lead to sub-optimal results. To overcome this deficiency structural topology optimization needs to be employed, which allows the designer to optimize the layout or the topology of a structure by detecting and removing the low-stressed material in the structure which is not used effectively.

3.4.1. Sizing Optimization

In sizing optimization problems the aim is usually to minimize the weight of the structure under certain behavioural constraints on stresses and displacements. The design variables are most frequently chosen to be dimensions of the cross-sectional areas of the members of the structure. Due to engineering practice demands the members are divided into groups having the same design variables. This linking of elements results in a trade-off between the use of more material and the need of symmetry and uniformity of the structures due to

practical considerations. Furthermore, it has to be taken into account that due to fabrication limitations the design variables are not continuous but discrete since cross-sections belong to a certain set. A discrete structural optimization problem can be formulated in the following form:

$$\begin{aligned} &\min && F(\mathbf{s}) \\ &\text{subject to} && g_j(\mathbf{s}) \le 0,\ j = 1,...,m \\ & && s_i \in R^d, i = 1,...,n \end{aligned} \tag{3.5}$$

Where R^d is a given set of discrete values representing the available structural member cross-sections and design variables s_i (i=1,...,n) can take values only from this set.

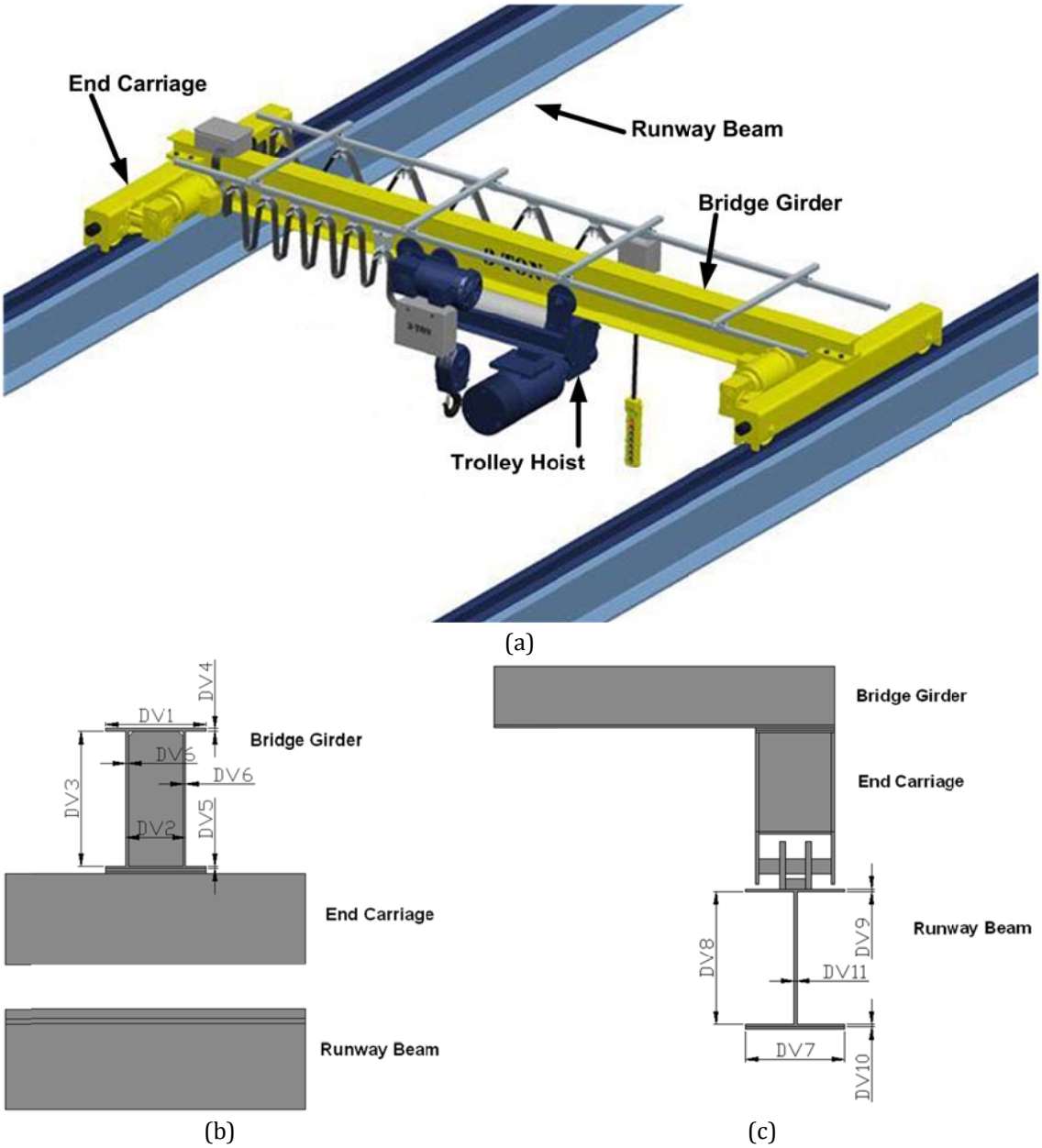

Figure 3.2. Sizing optimization problem (a) Components of an overhead travelling crane, design variables in the (b) bridge girder and (c) runway beam.

The sizing optimization methodology proceeds with the following steps: (i) At the outset of the optimization the geometry, the boundaries and the loads of the structure under investigation have to be defined. (ii) The design variables, which may or may not be independent to each other, are also properly selected. Furthermore, the constraints are also defined in this stage in order to formulate the optimization problem as in Eq. (3.5). (iii) A finite element analysis is then carried out and the displacements and the stresses are evaluated. (iv) If a gradient-based optimizer is used then the sensitivities of the constraints and the objective function to small changes of the design variables are computed. (v) The design variables are being optimized. If the convergence criteria for the optimization algorithm are satisfied, then the optimum solution has been found and the process is terminated, else the optimizer updates the design variable values and the whole process is repeated from step (iii). A typical sizing optimization problem is presented in Figure 3.2.

3.4.2. Shape Optimization

In structural shape optimization problems the aim is to improve the performance of the structure by modifying its boundaries. This can be numerically achieved by minimizing an objective function subjected to certain constraints (Hinton and Sienz, 1994; Ramm et al., 1994). All functions are related to the design variables, which are some of the coordinates of the key points in the boundary of the structure.

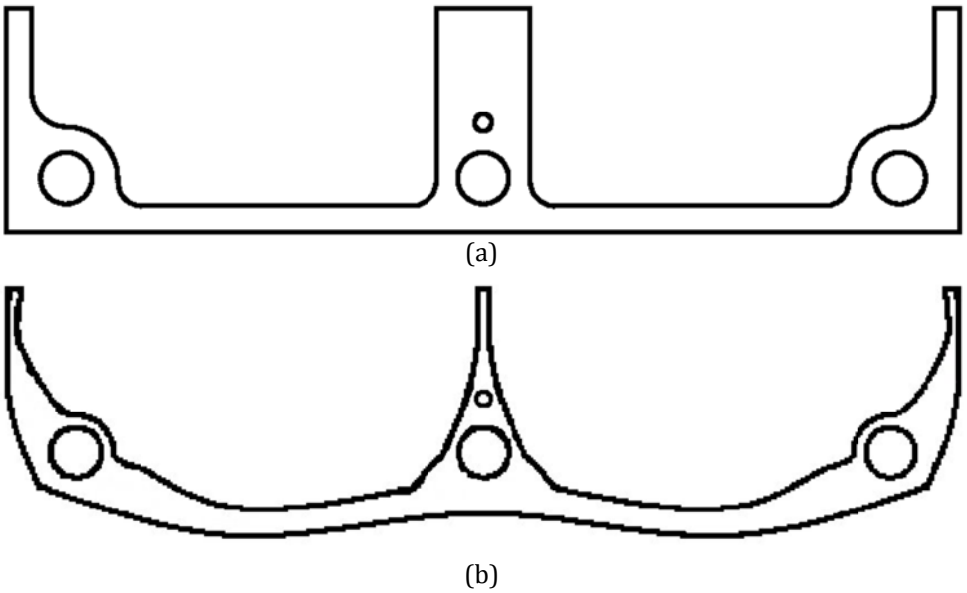

Figure 3.3. Shape optimization problem (a) engine block-initial shape and (b) engine block-final shape.

More specifically the shape optimization methodology proceeds with the following steps: (i) At the outset of the optimization, the geometry of the structure under investigation has to be

defined. The boundaries of the structure are modelled using cubic B-splines that, in turn, are defined by a set of key points. Some of the coordinates of these key points will be the design variables which may or may not be independent to each other. (ii) An automatic mesh generator is used to create a valid and complete finite element model. A finite element analysis is then carried out and the displacements and stresses are evaluated. In order to increase the accuracy of the analysis an h-type adaptivity analysis may be incorporated in this stage. (iii) If a gradient-based optimizer is used then the sensitivities of the constraints and the objective function to small changes of the design variables are computed either with the finite difference, or with the semi-analytical method. (iv) The optimization problem is solved; the design variables are being optimized and the new shape of the structure is defined. If the convergence criteria for the optimization algorithm are satisfied, then the optimum solution has been found and the process is terminated, else a new geometry is defined and the whole process is repeated from step (ii). A typical shape optimization problem is presented in Figure 3.3.

3.4.3. Topology Optimization

Structural topology optimization assists the designer to define the type of structure, which is best suited to satisfy the operating conditions for the problem in question. It can be seen as a procedure of optimizing the rational arrangement of the available material in the design space and eliminating the material that is not needed. Topology optimization is usually employed in order to achieve an acceptable initial layout of the structure, which is then refined with a shape optimization tool. The topology optimization procedure proceeds step-by-step with a gradual "removal" of small portions of low stressed material, which are being used inefficiently. This approach is treated in this study as a typical case of a structural reanalysis problem with small variations of the stiffness matrix between two subsequent optimization steps.

Many researchers have presented solutions for structural topology optimization problems. Topological or layout optimization can be undertaken by employing one of the following main approaches, which have evolved during the last few years (Hinton and Sienz, 1993): (i) Ground structure approach (Pedersen, 1993; Shieh, 1994), (ii) Homogenization method (Bendsoe and Kikuchi, 1988; Hinton and Hassani 1995; Suzuki and Kikuchi, 1993), (iii) Bubble method (Eschenauer, 1993) and (iv) Fully Stressed design technique (Van Keulen and Hinton, 1996; Xie and Steven, 1993). The first three approaches have several things in common. They are optimization techniques with an objective function, design variables, constraints and they solve the optimization problem by using an algorithm based

on Sequential Quadratic Programming (approach (i)), or on an Optimality Criterion concept (approaches (ii) and (iii)). However, inherently linked with the solution of the optimization problem is the complexity of these approaches. The Fully Stressed design technique on the other hand, although it is not an optimization algorithm in the conventional sense, proceeds by removing inefficient material, and therefore optimizes the use of the remaining material in the structure, in an evolutionary process.

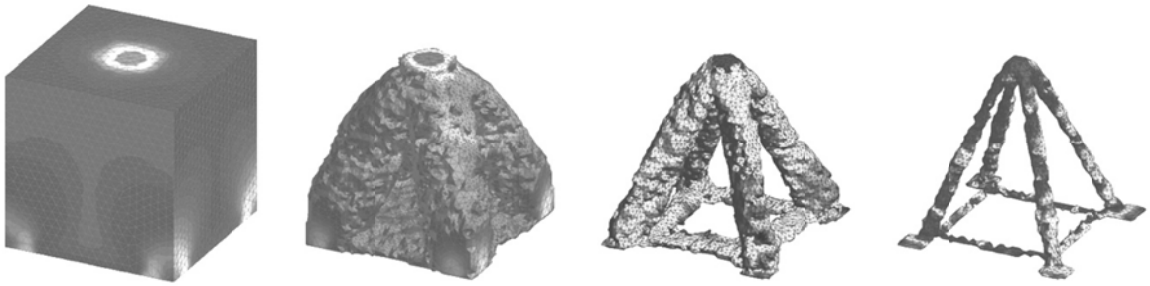

Figure 3.4. Topology optimization for a single loading.

A limited number of studies is devoted to 3-D optimal topology design of structures. For this type of problems the main difficulty when a Homogenization method is used is the orientation of the material voids which is more complicated than in the 2-D case. This difficulty is not present in the case of the Fully Stressed design technique. An efficient method for dealing with such problems is the evolutionary FSD technique proposed by Hinton and Sienz (1993) and the improved implementation presented by Papadrakakis et al. (1996) for 2-D topology optimization problems. This methodology is extended to 3-D topology optimization problems using solid finite elements. Furthermore an investigation was performed (Papadrakakis *et al.* 1996) on the impact of using effective domain decomposition solution techniques on the overall performance of the FSD topology optimization approach. This algorithm for topology optimization is based on the simple principle that material which has small stress levels is used inefficiently and therefore it can be removed. Thus, by removing small amounts of material at each optimization step the layout of the structure evolves gradually. In order to achieve convergence of the whole optimization procedure, it is important the amount of material removed at each stage to be small and to maintain a smooth transition from one layout of the structure to the subsequent one.

The domain of the structure, which is called the reference domain, can be divided into the design domain and the non-design domain. The non-design domain covers regions with stress concentrations, such as supports and areas where loads are applied, and therefore it cannot be modified throughout the whole topology optimization process. After the

generation of the finite element mesh, the evolutionary fully stressed design cycle is activated, where a linear elastic finite element analysis is carried out. The maximum principal stress for each element can be computed which for convenience is called stress level and is denoted as σ_{evo}. The maximum stress level σ_{max} of the elements in the structure at the current optimization step is defined, and all elements that fulfil the condition:

$$\sigma_{evo} < \text{ratre} \times \sigma_{max} \tag{3.6}$$

are removed, or *switched-off,* where *ratre* is the rejection rate parameter (Papadrakakis *et al.* 2001). The elements are removed by assigning them a relatively small elastic modulus which is typically:

$$E_{off} = 10^{-5} \times E_{on} \tag{3.7}$$

In this way the elements switched-off virtually do not carry any load and their stress levels are accordingly small in subsequent analyses. This strategy is called "hard kill", since the low stressed elements are immediately removed, in contrast with the "soft kill" method where the elastic modulus varies linearly and the elements are removed more gradually. The remaining elements are considered *active* and they are sorted in ascending order according to their stress levels before a subsequent analysis is performed.

The iterative process of element removal and addition, if element growth is allowed, is continued until one of several specified convergence criteria are met: (i) All stress levels are larger than a certain percentage value of the maximum stress. This criterion assumes that a fully stressed design has been achieved and the material is used efficiently. (ii) The number of active elements is smaller than a specified percentage of the total number of elements. For uniform meshes, which are commonly used in topology optimization problems, this criterion is equivalent to an area or volume fraction of the initial design, which will be in use in the final layout. (iii) When element growth is allowed the evolutionary process is completed when more elements are switched-on than they are switched-off.

3.5. Evolutionary Algorithms

The two most widely used optimization algorithms belonging to the class of EA that imitate nature by using biological methodologies are the GA and ES. In this work the ES method is used as the optimization tool for addressing the present problem, based on previous experience regarding the relative superiority of ES over the mathematical programming and GA methods in some specific problems (Papadrakakis et. al, 1999; Lagaros et. al, 2002). ES imitate biological evolution in nature and have three characteristics that make them differ from the gradient based optimization algorithms: (i) in place of the usual deterministic

operators, they use randomized operators: recombination, mutation, selection; (ii) instead of a single design point, they work simultaneously with a population of design points; (iii) they can handle continuous, discrete and mixed optimization problems (Papadrakakis et. al, 1998). In the ES algorithm, each individual is equipped with a set of parameters:

$$\begin{aligned} &a = [(s_d, \gamma), (s_c, \sigma, \alpha)] \in (I_d, I_c) \\ &I_d = D^{n_d} \times R_+^{n_\gamma} \\ &I_c = R^{n_c} \times R_+^{n_\sigma} \times [-\pi, \pi]^{n_a} \end{aligned} \tag{3.8}$$

where s_d and s_c are the vectors of discrete and continuous design variables, respectively. Vectors γ, σ and α are the distribution parameter vectors. Vector γ corresponds to the variances of the Poisson distribution, Vector $\sigma \in R_+^{n_\sigma}$ corresponds to the standard deviations ($1 \le n_\sigma \le n_c$) of the normal distribution while vector $\alpha \in [-\pi, \pi]^{n_a}$ corresponds to the inclination angles ($n_\alpha = (n_c - n_\sigma/2)(n_\sigma - 1)$) defining linearly correlated mutations of the continuous design variables s_c. Let $P_p^{(t)} = \{a_1, \ldots, a_\mu\}$ denotes a parent population of individuals at the t-th generation. The genetic operators used in the ES method are denoted by the following mappings:

$$\begin{aligned} &rec : (I_d, I_c)^\mu \to (I_d, I_c)^\lambda \text{ (recombination)} \\ &mut : (I_d, I_c)^\lambda \to (I_d, I_c)^\lambda \text{ (mutation)} \\ &sel_\mu^k : (I_d, I_c)^k \to (I_d, I_c)^\mu \text{ (selection, } k \in \{\lambda, \mu + \lambda\}) \end{aligned} \tag{3.9}$$

A single iteration of the ES, which is a step from the parent population $P_p^{(t)}$ to the next generation parent population $P_p^{(t+1)}$ is modelled by the mapping:

$$opt_{EA} : (I_d, I_c)^\mu \to (I_d, I_c)^\mu \tag{3.10}$$

3.5.1. Recombination

In any generation the μ-membered parent population $\mathbf{P}_p^{(t)}$ produces an λ-membered offspring population $P_0^{(t)}$. For every offspring vector a temporary parent vector is first built by means of recombination. In our implementation the following recombination scheme has been used, $rec_h : R^{n_h} \to R^{n_h}$ recombines the values of the vector *h*, where *h* corresponds to either a design variable vector or a distribution parameter vector:

$$rec_h(h) := (h_{a,1} \text{ or } h_{b,1}, \ldots, h_{a,n_h} \text{ or } h_{b,n_h}) \tag{3.11}$$

$h_{a,i}$ and $h_{b,i}$ are the i-th components of the vector h_a and h_b which are two parent vectors randomly chosen from the population.

3.5.2. Mutation

The Poisson distribution is controlled by the variance γ_i which coincides with the mean value of this distribution. The vector of variances γ controls the Poisson distribution which is used for exploring the discrete part of the design space $n_\gamma = 0.20n_d$. On the other hand, parameters σ and α determine the variances and covariances of the n_c-dimensional normal distribution, which is used for exploring the continuous part of the design space. The amount of parameters attached to an individual can vary, depending on the degree of freedom required by the objective function in question. The setting that is used in the current dissertation is: $n_\sigma = n_c$, $n_\alpha = n_c(n_c\text{-}1)/2$, that corresponds to the correlated mutation operator with a complete covariance matrix for each individual. According to the generalized structure of the individuals of the populations in the proposed mixed-discrete ES algorithm, the mutation operator, mut: $(I_d,I_c)^\lambda \rightarrow (I_d,I_c)^\lambda$, is defined as follows:

$$\mathrm{mut} = \left[\mathrm{mu}_{s_d} \mathrm{o} \mathrm{mu}_\gamma, \mathrm{mu}_{s_c} \mathrm{o} (\mathrm{mu}_\sigma \times \mathrm{mu}_\alpha) \right] \tag{3.12}$$

The mutation operator is applied to the intermediate individuals obtained through the recombination operator. The distribution parameters of the structure of an individual are mutated first:

(i) $\mathrm{mu}_\gamma : R_+^{n_\gamma} \rightarrow R_+^{n_\gamma}$ mutates the recombined vector γ:

$$\mathrm{mu}_\gamma(\gamma) := (\gamma_1 b_1^e, \ldots, \gamma_{n_\gamma} b_{n_\gamma}^e) \tag{3.13}$$

where $b_i \approx U([0,1])$. If, in a sequence of two generations, successful trials occur $e = e\text{-}1$, else $e = e+1$.

(ii) $\mathrm{mu}_{s_d} : D^{n_d} \rightarrow D^{n_d}$ mutates the recombined values of the vector of discrete design variables s_d, using the already mutated values of the vector of variances γ:

$$\mathrm{mu}_{s_d}(s_d) := (s_1 + z_1, \ldots, s_{n_d} + z_{n_d}) \tag{3.14}$$

where z_i follows the Poisson distribution with mean value and variance from the vector γ.

(iii) $\mathrm{mu}_\sigma : R_+^{n_\sigma} \rightarrow R_+^{n_\sigma}$ mutates the recombined values of the vector of standard deviation σ:

$$\mathrm{mu}_\sigma(\sigma) := (\sigma_1 \exp(z_1 + z_0), \ldots, \sigma_{n_\sigma} \exp(z_{n_\sigma} + z_0)) \tag{3.15}$$

where $z_0 \approx N(0, \tau_0^2), z_i \approx N(0, \tau^2) \forall \boldsymbol{i} \in \{1,2,\ldots,n_\sigma\}$ and $\tau_0 = (\sqrt{2n_s})^{-1}, \tau = (\sqrt{2\sqrt{n_s}})^{-1}$.

(iv) Mutation operator $\mathrm{mu}_\alpha : R^{n_\alpha} \rightarrow R^{n_\alpha}$ mutates the recombined values of the vector of inclination angles α:

$$\mathrm{mu}_\alpha(\alpha) := (\alpha_1 + z_1, \ldots, \alpha_1 + z_{n_\alpha}) \tag{3.16}$$

where $z_i \approx N(0, \beta^2) \forall i \in \{1,2,\ldots,n_\alpha\}$ with $\beta \cong 0.0873 (\cong 5^o)$.

(v) Mutation operator $mu_s : R^n \to R^n$ mutates the recombined values of the vector of continues design variables *s*, using the already mutated values of the σ and a:

$$mu_s(s) := (s_1 + cor_1(\sigma,\alpha),\ldots,s_{n_s} + cor_{n_s}(\sigma,\alpha)) \tag{3.17}$$

where *cor* is a random vector with normally distributed correlated components. The vector *cor* can be calculated according to $cor=T\cdot z$ where $z=[z_1,\ldots,z_{n_\sigma}]^T$ with $z_i \approx N(0,\sigma_i^2)\ \forall i \in \{1,\ldots,n_\sigma\}$ and:

$$T=\prod_{p=1}^{n_\sigma-1}\prod_{q=p+1}^{n_\sigma} T_{pq}(\tilde{a}_j) \tag{3.18}$$

where $j = l/2(2n_\sigma-p)(p+l)-2n_\sigma+q$ (Rosenbrock, l960). The rotation matrices $T_{pq}(a_j)$ are unit matrices expect of the diagonal terms where $t_{pp} = t_{qq} = cos(a_j)$ and $t_{pq} = -t_{qp} = -sin(a_j)$.

3.5.3. Selection

There are two different types of selection schemes that are implemented in the case of Evolution Strategies:

***(μ+λ)*-ES**: Where the best μ individuals are selected from a temporary population of (μ+λ) individuals to form the parents of the next generation.

***(μ,λ)*-ES**: Where the μ individuals produce λ offsprings (μ≤λ) and the selection process defines a new population of μ individuals from the set of λ offsprings only.
Combining the recombination, mutation and selection operators the main loop for the case of (μ,λ)-ES is formulated as follows:

$$opt_{(\mu,\lambda)\text{-}ES}(P^{(g)}) = sel_\mu^\lambda\left(\cup_{i=1}^{\lambda}\{mut(rec(P^{(g)}))\}\right) \tag{3.19}$$

While for the case of the (μ+λ)-EA scheme the main loop is formulated as follows:

$$opt_{(\mu+\lambda)\text{-}ES}(P^{(g)}) = sel_\mu^{\mu+\lambda}\left(\cup_{i=1}^{\lambda}\{mut(rec(P^{(g)}))\}\cup P^{(g)}\right) \tag{3.20}$$

The optimization procedure terminates when the following termination criterion is satisfied: the ratio μ_b/μ has reached a given value ε_d (=0.8 in the current study) where μ_b is the number of the parent vectors in the current generation with the best objective function value.

3.5.4. The ES algorithm

In Figure 3.5 a pseudo-code of the ES algorithm is depicted. At the beginning of the procedure in generation t = 0 the initial parent population $P_p^{(t)}$, composed by μ design vectors, is generated randomly (*step 3* of the pseudo-code). *Steps 5* to *12* correspond to the

main part of the ES algorithm, where in every generation λ offspring vectors are generated by means of recombination and mutation. D_l is a sub-population with two members selected from the parent population of the current generation $P_p^{(t)}$ (*Step 6*) which is used by the recombination operator. Recombination and mutation operators, described in *steps 7* to *10*, act on both design variable vectors s_l and distribution parameter vectors σ_l and α_l (both distribution parameter vectors denoted as y_l in the pseudo-code). In *step 11* the objective and constraint functions are calculated in order to assess the design vectors in terms of the objective function value and feasibility.

1. **Begin**
2. $t := 0$
3. initialize$\left(P_p^{(0)} := \left\{\left(y_m^{(0)}, s_m^{(0)}, F(s_m^{(0)})\right), m = 1, ..., \mu\right\}\right)$
4. **Repeat**
5. **For** $l := 1$ **To** λ **Do Begin**
6. $D_l := \text{marriage}\left(P_p^{(t)}\right)$
7. $s_l := \text{s\_recombination}\left(D_l\right)$
8. $y_l := \text{y\_recombination}\left(D_l\right)$
9. $\tilde{s}_l := \text{s\_mutation}\left(s_l\right)$
10. $\tilde{y}_l := \text{y\_mutation}\left(y_l\right)$
11. $\tilde{F}_l := F\left(\tilde{s}_l\right)$
12. **End**
13. $P_o^{(t)} := \left\{\left(y_l^{(t)}, s_l^{(t)}, F(s_l^{(t)})\right), l = 1, ..., \lambda\right\}$
14. **Case** selection_type **Of**
15. $\left(\mu, \lambda\right) : P_p^{(t+1)} := \text{selection}\left(P_o^{(t)}, \mu\right)$
16. $\left(\mu + \lambda\right) : P_p^{(t+1)} := \text{selection}\left(P_o^{(t)}, P_p^{(t)}, \mu\right)$
17. **End**
18. $t := t + 1$
19. **Until** termination_criterion
20. **End**

Figure 3.5. Pseudo-code of the ES algorithm.

3.5.5. ES for structural optimization problems

Structural optimization problems have been treated traditionally with mathematical programming algorithms, such as the SQP method, which need gradient information. In structural optimization problems, where the objective function and the constraints are particularly highly non-linear functions of the design variables, the computational effort spent in gradient calculations is usually large. On the other hand EA optimization methods require more optimization steps.

In a number of studies (Papadrakakis et al., 1998; Papadrakakis et al., 1999; Lagaros et al., 2002) it was found that EA optimization methods in structural optimization are computationally efficient even if large number of optimization steps is required to reach the optimum. These optimization steps are computationally less expensive than in the case of mathematical programming algorithms since they do not need gradient information. This property of probabilistic search methods is of greater importance in the case of Deterministic and Reliability based optimization problems since the calculation of the derivatives of the constraints is very time-consuming especially in the case of probabilistic constraints. Furthermore, probabilistic methodologies are considered as global optimization methods. Due to their random search they are capable of finding the global optimum, whereas mathematical programming algorithms may be trapped in local optima.

3.6. Differential Evolution

Storn and Price (1997) proposed a new floating point evolutionary algorithm for global optimization and named it DE, by implementing a special kind operator which invoked to create new offspring from parent chromosomes. DE is a novel parallel direct search method which utilizes a population of NP parameter vectors $\boldsymbol{s}_{i,g}$ (i=1,..,NP) for each generation g. DE generates new vectors by adding the weighted difference vector between two population members to a third member. If the resulting vector corresponds to a better objective function value than a population member, the newly generated vector replaces this member. The comparison is performed between the newly generated vector and all the members of the population excluding the three ones used for its generation. Furthermore, the best parameter vector $\boldsymbol{s}_{best,g}$ is evaluated in every generation in order to keep track of the progress achieved during the optimization process. The flowchart of the DE algorithm is presented in Figure 3.6. Several variants of DE have been proposed so far, the two most widely used are subsequently presented.

The initial population is chosen randomly if nothing is known about the system. As a rule, we will assume a uniform probability distribution for all random decisions unless otherwise stated. In case a preliminary solution is available, the initial population is often generated by adding normally distributed random deviations to the nominal solution $\boldsymbol{s}_{nom,0}$. The crucial idea behind DE is a new scheme for generating trial parameter vectors. DE generates new parameter vectors by adding the weighted difference vector between two population members to a third member. If the resulting vector yields a lower objective function value than a predetermined population member, the newly generated vector replaces the vector with which it was compared. The comparison vector can, but need not be part of the

generation process mentioned above. In addition the best parameter vector $\boldsymbol{s}_{best,g}$ is evaluated for every generation G in order to keep track of the progress that is made during the minimization process. Extracting distance and direction information from the population to generate random deviations results in an adaptive scheme with excellent convergence properties. Several variants of DE have been tested, the two most promising of which have been presented subsequently in greater detail.

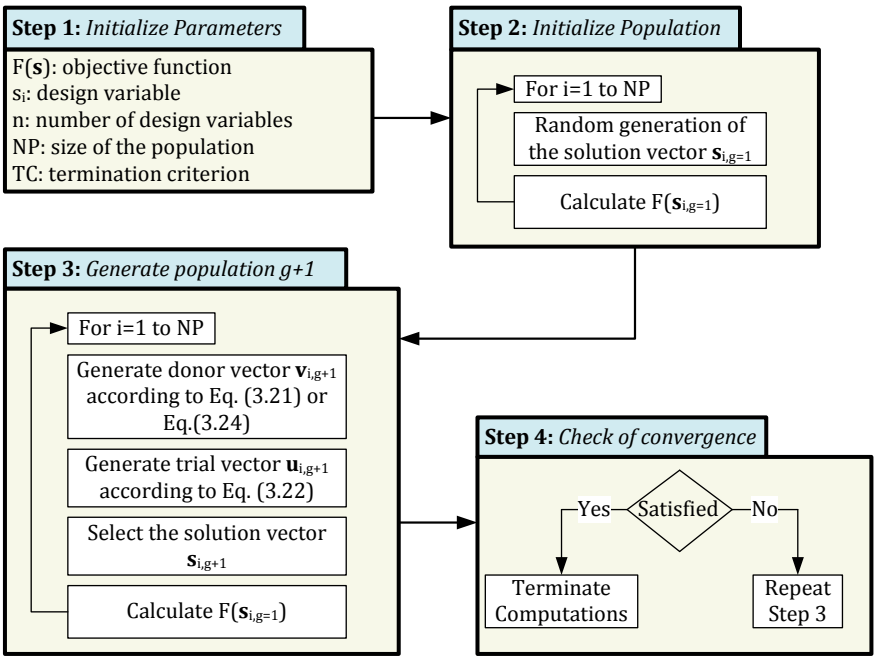

Figure 3.6. Flowchart of the differential evolution algorithm.

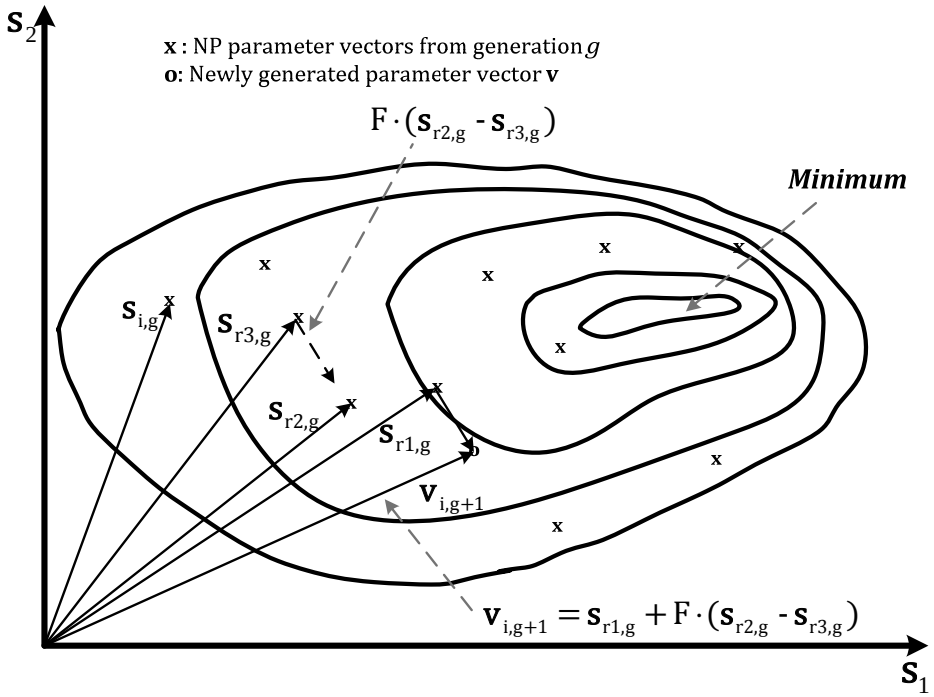

Figure 3.7. Two dimensional example of an objective function showing its contour lines and the process for generating v in scheme DE1.

3.6.1. Scheme DE1

Scheme DE1. In the first variant, a donor vector $\boldsymbol{v}_{i,g+1}$ is generated first according to:

$$\mathbf{v}_{i,g+1} = \mathbf{s}_{r1,g} + F \cdot (\mathbf{s}_{r2,g} - \mathbf{s}_{r3,g}) \tag{3.21}$$

before the computation of the i[th] parameter vector $\boldsymbol{s}_{i,g+1}$. This step is equivalent to the mutation operator step of genetic algorithms or evolution strategies. The integers *r1*, *r2* and *r3* are chosen randomly from the interval [1,*NP*] while i≠ *r1*, *r2* and *r3*. *F* is a real constant value, called mutation factor, which controls the amplification of the differential variation ($\boldsymbol{s}_{r2,g}$−$\boldsymbol{s}_{r3,g}$) and is defined in the range [0,2]. Figure 3.7 shows a two dimensional example that illustrates the different vectors which play a part in DE1.

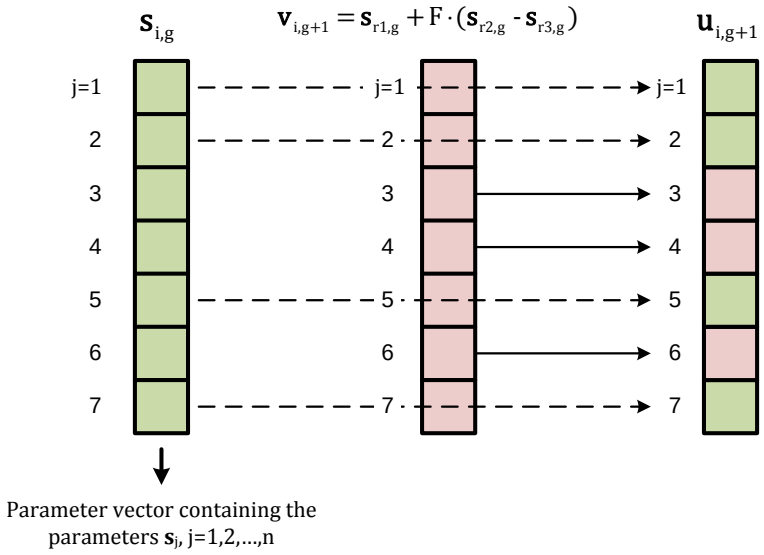

Figure 3.8. Illustration of the crossover process for n=7.

In the next step the crossover operator is applied by generating the trial vector $\boldsymbol{u}_{i,g+1}$ = $[u_{1,i,g+1}, u_{2,i,g+1}, \ldots, u_{D,i,g+1}]^T$ which is defined from the elements of the vector $\boldsymbol{s}_{i,g}$ and the elements of the donor vector $\boldsymbol{v}_{i,g+1}$ whose elements enter the trial vector with probability *CR* as follows:

$$u_{j,i,g+1} = \begin{cases} v_{j,i,g+1} \text{ if } rand_{j,i} \le CR \text{ or } j = I_{rand} \\ s_{j,i,g} \text{ if } rand_{j,i} > CR \text{ or } j \ne I_{rand} \end{cases} \tag{3.22}$$
$$i = 1,2,\ldots,NP \text{ and } j = 1,2,\ldots,n$$

where $rand_{j,i} \sim U[0,1], I_{rand}$ is a random integer from [1,2,...,n] that ensures that $\mathbf{v}_{i,g+1} \ne \mathbf{s}_{i,g}$. i.e. a certain sequence of the vector elements of u are identical to the elements of **v**, the other elements of u acquire the original values of $\mathbf{s}_{i,g}$. Choosing a subgroup of parameters for mutation is similar to a process known as crossover in evolution theory. This idea is illustrated in Figure 3.8 for n=7, where CR∈[0,1] is the crossover probability and constitutes a control variable for the DE1-scheme.

The last step of the generation procedure is the implementation of the selection operator where the vector $\mathbf{s}_{i,g}$, is compared to the trial vector $\boldsymbol{u}_{i,g+1}$:

$$\mathbf{s}_{i,g+1} = \begin{cases} \mathbf{u}_{i,g+1} \text{ if } f(\mathbf{u}_{i,g+1}) \le f(\mathbf{s}_{i,g}) \\ \mathbf{s}_{i,g} \text{ otherwise} \end{cases} \qquad (3.23)$$

where $i = 1,2,...,NP$

3.6.2. Scheme DE2

Scheme DE2. In the second variant the donor vector $\boldsymbol{v}_{i,g+1}$ is generated first according to:

$$\mathbf{v}_{i,g+1} = \mathbf{s}_{i,g} + \lambda \cdot (\mathbf{s}_{best,g} - \mathbf{s}_{i,g}) + F \cdot (\mathbf{s}_{r2,g} - \mathbf{s}_{r3,g}) \qquad (3.24)$$

before the computation of the i[th] parameter vector $\boldsymbol{s}_{i,g+1}$, by introducing an additional control variable λ. The idea behind λ is to provide a means to enhance the greediness of the scheme by incorporating the current best vector $\boldsymbol{s}_{best,g}$. Figure 3.9 illustrates the vector-generation process defined by (3.24). The generation of the trial vector $\boldsymbol{u}_{i,g+1}$ as well as the decision process are identical to those of DE1. In this study the second version has been implemented. The construction of $\boldsymbol{u}$ from $\boldsymbol{v}$ and $\boldsymbol{s}_{i,g}$ as well as the decision process are identical to DE1.

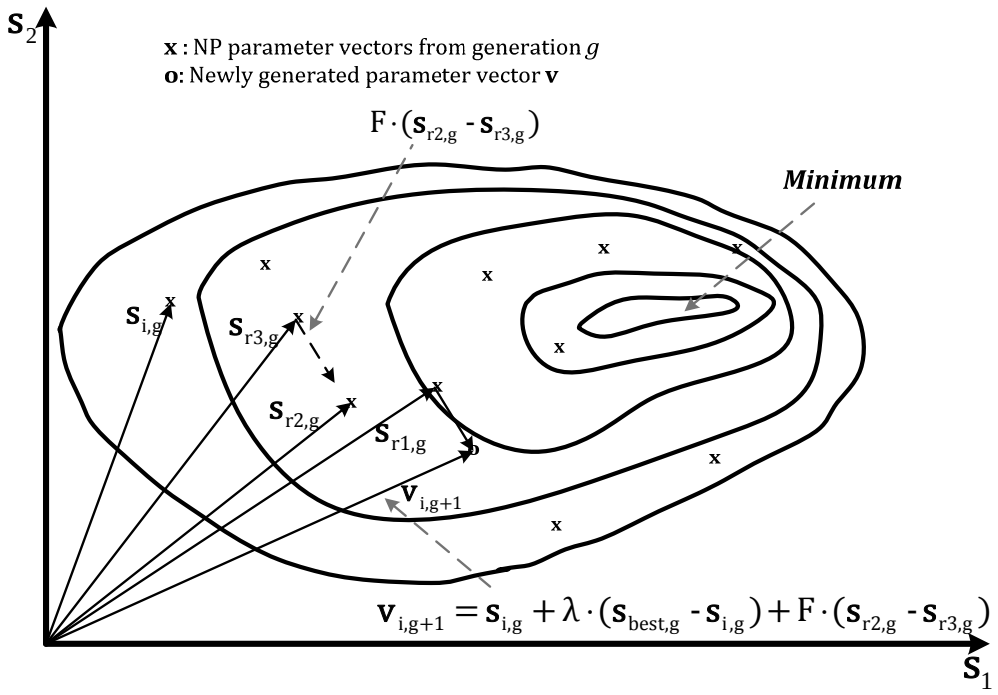

Figure 3.9. Two dimensional example of an objective function showing its contour lines and the process for generating v in scheme DE2.

The DE method for minimizing continuous space functions has been introduced and shown to be superior to adaptive simulated annealing proposed by Ingber (1993) as well as the Annealed Nelder & Mead approach (Press et. al, 1992). DE was the only technique to

converge for all of the functions in the test function suite (Storn and Price, 1995). For those problems where ASA or ANM could find the minimum, DE usually converged faster, especially in the more difficult cases. Since DE is inherently parallel, a further significant speedup can be obtained if the algorithm is executed on a parallel machine or a network of computers. This is especially true for real world problems where computing the objective function requires a significant amount of time. Despite these already promising results, DE is still in its infancy and can most probably be improved. Further research might include a mathematical convergence proof like the one that exists for Simulated Annealing. A theoretically sound analysis to determine why DE converges so well would also be of great interest. Whether or not an annealed version of DE, or the combination of DE with other optimization approaches is of practical use, is still unanswered. Finally, it is important for practical applications to gain more knowledge on how to choose the control variables for DE.

3.7. Particle Swarm Optimization algorithm

Many probabilistic-based search algorithms have been inspired by natural phenomena, such as evolutionary programming, genetic algorithms, evolution strategies, among others. Recently, a family of optimization methods has been developed based on the simulation of social interactions among members of a specific species looking for food or resources in general. One of these methods is the PSO method proposed by Kennedy and Eberhart (1995) that is based on the behaviour reflected in flocks of birds, bees and fish that adjust their physical movements to avoid predators and seek for food. The method has been given considerable attention in recent years among the optimization research community.

A swarm of birds or insects or a school of fish searches for food, resources or protection in a very typical manner. If a member of the swarm discovers a desirable path to go, the rest of the swarm will follow quickly. Every member searches for the best in its locality, learns from its own experience as well as from the others typically from the best performer among them. Even human beings show a tendency to behave in this way as they learn from their own experience, their immediate neighbours and the ideal performers in the society. The PSO method mimics the behaviour described above. It is a population-based optimization method built on the premise that social sharing of information among the individuals can provide an evolutionary advantage.

PSO has been found to be highly competitive for solving a wide variety of optimization problems (Perez and Behdinan, 2007; Bochenek and Foryś, 2006; He and Wang, 2007; Liang and Suganthan, 2006; Mezura-Montes and Lopez-Ramirez, 2007; Munoz-Zavala et al., 2007;

Ye, et al., 2007). It can handle nonlinear, non-convex design spaces with discontinuities. Compared to other non-deterministic optimization methods it is considered efficient in terms of number of function evaluations as well as robust since it usually leads to better or the same quality of results. Its easiness of implementation makes it more attractive as it does not require specific domain knowledge information, while being a population based algorithm, it can be straight forward implemented in parallel computing environments leading to a significant reduction of the total computational cost. PSO has been successfully applied to many fields, such as mathematical function optimization, artificial neural network training and fuzzy system control.

In a PSO formulation, multiple candidate solutions coexist and collaborate simultaneously. Each solution is called a "particle" that has a position and a velocity in the multidimensional design space. A particle "flies" in the problem search space looking for the optimal position. As "time" passes through its quest, a particle adjusts its velocity and position according to its own "experience" as well as the experience of other (neighbouring) particles. Particle's experience is built by tracking and memorizing the best position encountered. As every particle remembers the best position it has visited during its "flight", the PSO possesses a memory. A PSO system combines local search method (through self experience) with global search method (through neighbouring experience), attempting to balance exploration and exploitation.

3.7.1. Relationship of PSO with Evolutionary Algorithms

PSO shares many similarities with evolutionary computation techniques, such as GA, but the conceptual difference lies in its definition which is given in a social rather than a biological context. The common features of the two optimization approaches include the population concept of the design vectors, initialization with a population of random solutions, a fitness value to evaluate performance, searching for optima by updating iterations (generations) based on a stochastic process, no requirement for gradient information or user-defined initial estimates and no guaranteed final success. However, unlike GA, PSO has no genetic operators such as crossover and mutation. In PSO, the potential solutions, fly through the problem space by following a velocity update rule. The information sharing mechanism in PSO is significantly different compared to GA. In GA chromosomes share information with each other, so the whole population moves like one group towards an optimal area. In PSO, only G_{best} (the global best particle) communicates the information to the others, forming a one-way information sharing mechanism. Compared to genetic algorithms, according to the study of Hassan et al. (2005), PSO and GA can both obtain high quality solutions, yet the

computational effort required by PSO to arrive to such high quality solutions is less than the corresponding effort required by GA. According to Angeline (1998), two main distinctions can be made between PSO and an evolutionary algorithm:

i. EAs rely on three mechanisms in their processing: parent representation, selection of individuals and the fine tuning of their parameters. In contrast, PSO only relies on two mechanisms, since PSO does not adopt an explicit selection function. The absence of a selection mechanism in PSO is compensated by the use of leaders to guide the search. However, there is no notion of offspring generation in PSO as with EAs.
ii. The manipulation of the individuals is different in EAs and PSO. PSO uses an operator that sets the velocity of a particle to a particular direction. This can be seen as a directional mutation operator in which the direction is defined by both the particle's personal best and the global best (of the swarm). If the direction of the personal best is similar to the direction of the global best, the angle of potential directions will be small, whereas a larger angle will provide a larger range of exploration. In contrast, EAs use a mutation operator that can set an individual in any direction (although the relative probabilities for each direction may be different). In fact, the limitations exhibited by the directional mutation of PSO has led to the use of mutation operators similar to those adopted in EAs.

3.7.2. Mathematical formulation of PSO

Each particle maintains two basic characteristics, velocity and position, in the multi-dimensional search space that are updated as follows

$$\mathbf{v}^{j}(t+1) = w\mathbf{v}^{j}(t) + c_1\mathbf{r}_1 o\left(\mathbf{s}^{Pb,j} - \mathbf{s}^{j}(t)\right) + c_2\mathbf{r}_2 o\left(\mathbf{s}^{Gb} - \mathbf{s}^{j}(t)\right) \tag{3.25}$$

$$\mathbf{s}^{j}(t+1) = \mathbf{s}^{j}(t) + \mathbf{v}^{j}(t+1) \tag{3.26}$$

where $\boldsymbol{v}^{j}(t)$ denotes the velocity vector of particle j at time t, $\boldsymbol{s}^{j}(t)$ represents the position vector of particle j at time t, vector $\boldsymbol{s}^{Pb,j}$ is the personal 'best ever' position of the j^{th} particle, and vector $\boldsymbol{s}^{Gb}$ is the global best location found by the entire swarm. The acceleration coefficients c_1 and c_2 indicate the degree of confidence in the best solution found by the individual particle (c_1 - cognitive parameter) and by the whole swarm (c_2 - social parameter), respectively, while $\boldsymbol{r}_1$ and $\boldsymbol{r}_2$ are two random vectors uniformly distributed in the interval [0, 1]. The symbol "$\circ$" of Eq. (3.25) denotes the Hadamard product, i.e. the element-wise vector or matrix multiplication.

Figure 3.10 depicts a particle's movement, in a two-dimensional design space, according to Eqs. (3.25) and (3.26). The particle's current position $\boldsymbol{s}^{j}(t)$ at time t is represented by the

dotted circle at the lower left of the drawing, while the new position $\boldsymbol{s}^j(t+1)$ at time $t+1$ is represented by the dotted bold circle at the upper right hand of the drawing. It can be seen how the particle's movement is affected by: (i) it's velocity $\boldsymbol{v}^j(t)$; (ii) the personal best ever position of the particle, $\boldsymbol{s}^{Pb,j}$, at the right of the figure; and (iii) the global best location found by the entire swarm, $\boldsymbol{s}^{Gb}$, at the upper left of the figure. In the above formulation, the global best location found by the entire swarm up to the current iteration ($\boldsymbol{s}^{Gb}$) is used. This is called a fully connected topology (fully informed PSO), as all particles share information with each other about the best performer of the swarm. Other topologies have also been used in the past where instead of the global best location found by the entire swarm, a local best location of each particle's neighbourhood is used. Thus, information is shared only among members of the same neighbourhood.

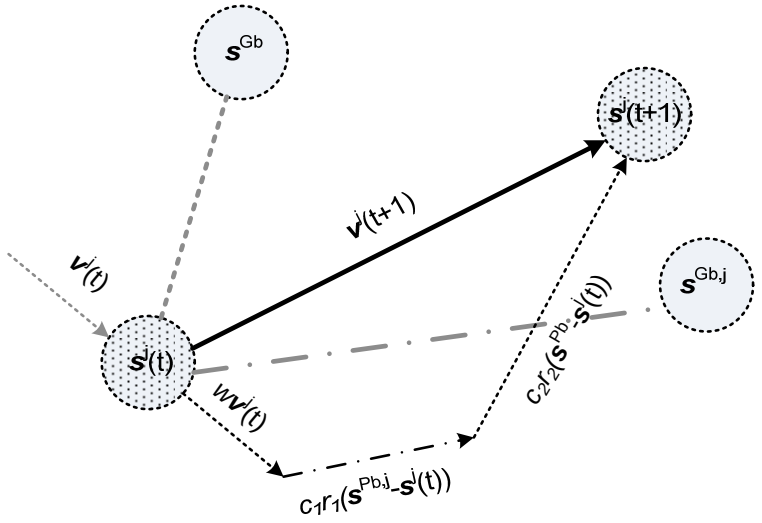

Figure 3.10. Visualization of the particle's movement in a two-dimensional design space.

The term w of Eq. (3.25) is the inertia weight, essentially a scaling factor employed to control the exploration abilities of the swarm, which scales the current velocity value affecting the updated velocity vector. The inertia weight was not part of the original PSO algorithm (Kennedy and Eberhart, 1995), as it was introduced later by Shi and Eberhart (1998) in a successful attempt to improve convergence. Large inertia weights will force larger velocity updates allowing the algorithm to explore the design space globally. Similarly, small inertia values will force the velocity updates to concentrate in the nearby regions of the design space. The inertia weight can also be updated during iterations. A commonly used inertia update rule is the linearly-decreasing, calculated by the formula:

$$w_{t+1} = w_{max} - \frac{w_{max} - w_{min}}{t_{max}} \times t \tag{3.27}$$

where t is the iteration number, w_{max} and w_{min} are the maximum and minimum values, respectively, of the inertia weight. In general, the linearly decreasing inertia weight has shown better performance than the fixed one.

Table 3.1. Main PSO parameters.

Symbol	Description	Details
$\boldsymbol{NP}$	Number of particles	A typical range is 10 – 40. For most problems 10 particles is sufficient enough to get acceptable results. For some difficult or special problems the number can be increased to 50-100.
$\boldsymbol{n}$	Dimension of particles	It is determined by the problem to be optimized.
$\boldsymbol{w}$	Inertia weight	Usually is set to a value less than 1, i.e. 0.95. It can also be updated during iterations.
$\boldsymbol{s^L}$, $\boldsymbol{s^U}$	Vectors containing the lower and upper bounds of the n design variables, respectively	They are determined by the problem to be optimized. Different ranges for different dimensions of particles can be applied in general.
$\boldsymbol{v^{max}}$	Vector containing the maximum allowable velocity for each dimension during one iteration	Usually is set half the length of the allowable interval for the given dimension: $v^{max}_i = (s^U_i - s^L_i)/2$. Different values for different dimensions of particles can be applied in general.
$\boldsymbol{c_1}$, $\boldsymbol{c_2}$	Cognitive and social parameters	Usually c_1=c_2=2. Other values can also be used, provided that $0 < c_1+c_2 < 4$.

Particles' velocities in each dimension i (i=1, …,n) are restricted to a maximum velocity v^{max}_i. The vector $\boldsymbol{v}^{max}$ of dimension n holds the maximum absolute velocities for each dimension. It is more appropriate to use a vector rather than a scalar, as in the general case different velocity restrictions can be applied for different dimensions of the particle. If for a given particle j the sum of accelerations of Eq. (3.25) causes the absolute velocity for dimension i to exceed v^{max}_i, then the velocity on that dimension is limited to $\pm v_{max,i}$. The vector parameter $\boldsymbol{v}^{max}$ is employed to protect the cohesion of the system, in the process of amplification of the positive feedback. The basic PSO has only few parameters to adjust. In Table 3.1 there is a list of the main parameters, their typical values as well as other information.

3.7.3. Convergence criteria

Due to the repeated process of the PSO search, convergence criteria have to be applied for the termination of the optimization procedure. Two widely adopted convergence criteria are the maximum number of iterations of the PSO algorithm and the minimum error requirement on the calculation of the optimum value of the objective function. The selection

of the maximum number of iterations depends, generally, on the complexity of the optimization problem at hand. The second criterion presumes prior knowledge of the global optimal value, which is feasible for testing or fine-tuning the algorithm in mathematical problems when the optimum is known a priori, but this is certainly not the case in practical structural optimization problems where the optimum is not known a priori.

Table 3.2. PSO convergence parameters.

Symbol	Description	Details
t_{max}	Maximum number of iterations for the termination criterion.	Determined by the complexity of the problem to be optimized, in conjunction with other PSO parameters (n, NP).
k_f	Number of iterations for which the relative improvement of the objective function satisfies the convergence check.	If the relative improvement of the objective function over the last k_f iterations (including the current iteration) is less or equal to f_m, convergence has been achieved.
f_m	Minimum relative improvement of the value of the objective function.	

In this study, together with the maximum number of iterations, we have implemented the convergence criterion connected to the rate of improvement of the value of the objective function for a given number of iterations. If the relative improvement of the objective function over the last k_f iterations (including the current iteration) is less or equal to a threshold value f_m, convergence is supposed to have been achieved. In mathematical terms, denoting as Gbest_t the best value for the objective function found by the PSO at iteration t, the relative improvement of the objective function can be written for the current iteration t as follows:

$$\frac{\text{Gbest}_{t-k_f+1} - \text{Gbest}_t}{\text{Gbest}_{t-k_f+1}} \leq f_m \tag{3.28}$$

In Table 3.2 there is a list of the convergence parameters of the PSO used in this study with description and details. A pseudo code of the PSO procedure is given in Figure 3.11.

3.7.4. PSO for integer optimization

For the solution of the problem described in Eq. (3.2) a discrete optimization algorithms are required. In the continuous version of the PSO method, both particle positions and velocity are initialized randomly. In this work, the particle positions are generated randomly over the design space using discrete LHS, thus guaranteeing that the initial particle positions will

be integers in the acceptable range. Furthermore, in the case of discrete optimization and in particular in integer programming, at every step of the optimization procedure, integer particle positions should also be generated. In order to satisfy this, Eq. (3.25) is modified as follows

$$\mathbf{v}^{j}(t+1) = \text{round}\left[w\mathbf{v}^{j}(t) + c_1\mathbf{r}_1 o\left(\mathbf{s}^{Pb,j} - \mathbf{s}^{j}(t) \right) + c_2\mathbf{r}_2 o\left(\mathbf{s}^{Gb} - \mathbf{s}^{j}(t) \right) \right] \tag{3.29}$$

where the vector function *round*(***s***) rounds each element of the vector ***s*** into the nearest integer.

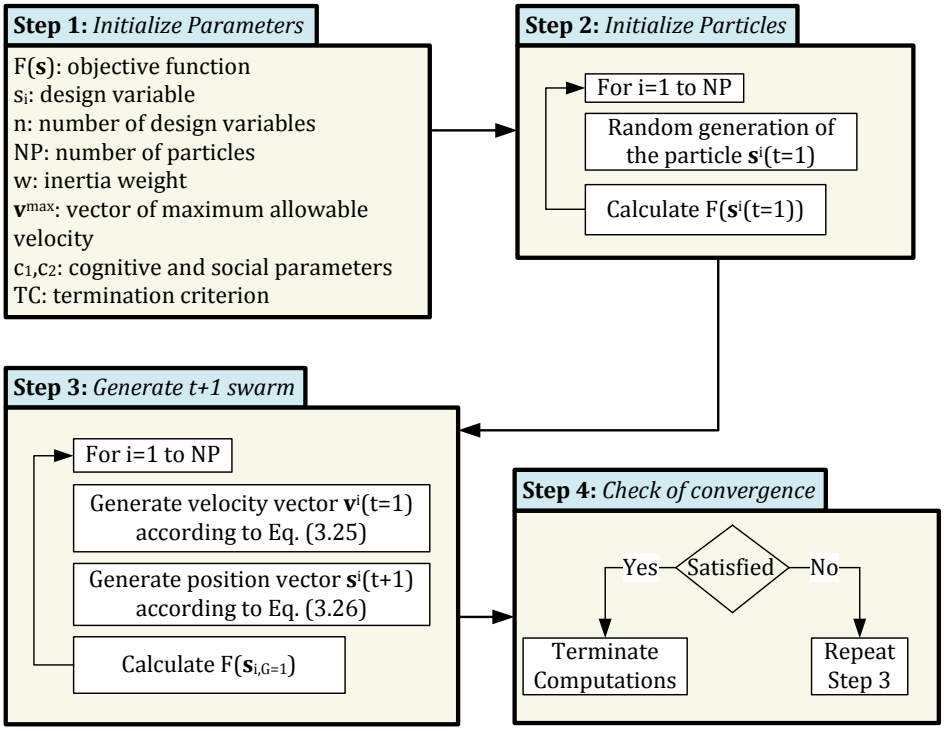

Figure 3.11. Flowchart of the particle swarm optimization algorithm.

3.8. Harmony Search

The HS algorithm was originally inspired (Geem et al., 2001) by the improvisation process of Jazz musicians. According to the analogy between improvisation and optimization each musician (saxophonist, bassist, guitarist etc) corresponds to each decision variable; while musical instrument's pitch range corresponds to decision variable's value range. Figure 3.12 shows the analogy between improvisation and optimization: Each musician corresponds to each decision variable; musical instrument's pitch range corresponds to decision variable's value range; musical harmony at certain time corresponds to solution vector at certain iteration; and audience's aesthetics corresponds to objective function. Just like musical harmony is improved time after time, the solution vector is improved iteration by iteration.

This section introduces each step of the HS algorithm in detail, including 1) algorithm parameter setting, 2) random tuning for memory initialization, 3) harmony improvisation (random selection, memory consideration, and pitch adjustment), 4) memory update and 5) performing termination. Musical harmony at certain time corresponds to solution vector at certain iteration, and audience's aesthetics corresponds to the objective function. According to the above algorithmic concept, the HS algorithm consists of the following five steps: parameter initialization; harmony memory initialization; new harmony improvisation; harmony memory update; and termination criterion check. The flowchart of the HS algorithm is presented in Figure 3.13.

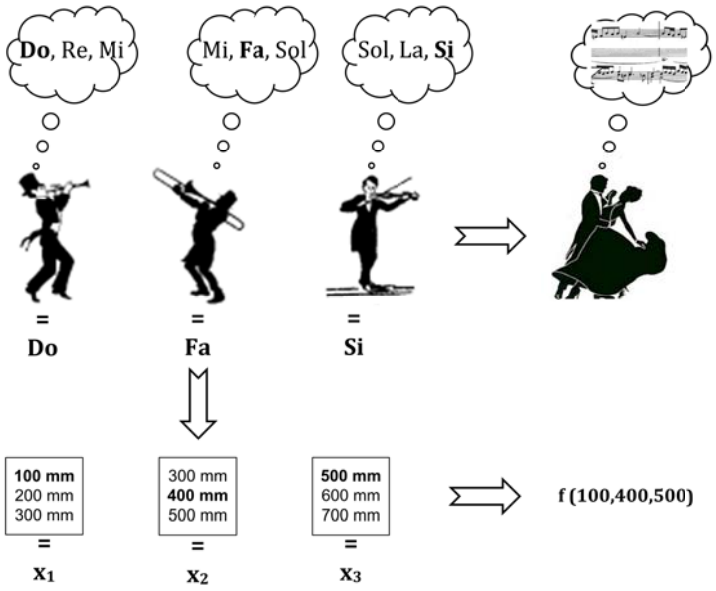

Figure 3.12. Analogy between improvisation and optimization.

3.8.1. Algorithm Parameter Setting

Parameter initialization: In the first step, the optimization problem is specified (Eq. (3.1)) where n is the number of decision variables (equivalent to the number of music instruments), while $s_i^L \le s_i \le s_i^U, i = 1,2,...,n$ determines the range of the i^{th} decision variable's value. The HS algorithm parameters are also specified in this step: HMS is the harmony memory size that corresponds to the number of simultaneous solution vectors stored in harmony memory, HMCR defines the harmony memory considering rate, while PAR is the pitch adjusting rate.

Once the problem formulation is ready, the algorithm parameters should be set with certain values. HS contains algorithm parameters including HMS, HMCR, PAR, MI, and FW. HMS is the number of solution vectors simultaneously handled in the algorithm; HMCR is the rate ($0 \le HMCR \le 1$) where HS picks one value randomly from musician's memory. Thus, (1-HMCR) is the rate where HS picks one value randomly from total value range; PAR ($0 \le$

PAR ≤ 1) is the rate where HS tweaks the value which was originally picked from memory. Thus, (1-PAR) is the rate where HS keeps the original value obtained from memory; MI is the number of iterations. HS improvises one harmony vector at each iteration; and FW is arbitrary length only for continuous variable, which was formerly called as BW.

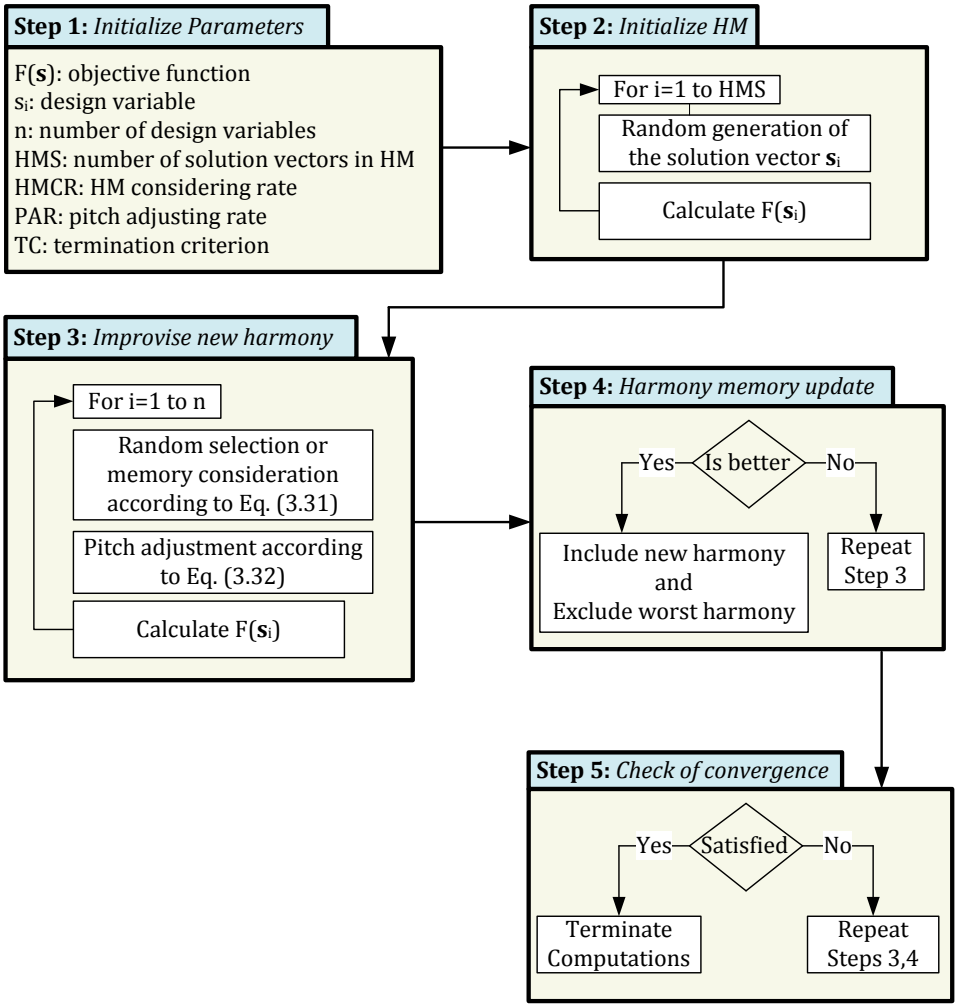

Figure 3.13. Flowchart of the harmony search algorithm.

For more information of the term fret, it is the metallic ridge on the neck of a string instrument (such as guitar), which divides the neck into fixed segments, and each fret represents one semitone. In the context of the HS algorithm, frets mean arbitrary points which divide the total value range into fixed segments, and FW is the length between two neighbouring frets. Uniform FW is normally used in HS. Originally fixed parameter values were used. However, some researchers have proposed changeable parameter values. Mahdavi et al. (2007) suggested that PAR increase linearly and FW decrease exponentially with iterations:

$$\mathrm{PAR(I)} = \mathrm{PAR_{min}} + (\mathrm{PAR_{max}} - \mathrm{PAR_{min}}) \cdot \frac{1}{\mathrm{MI}} \tag{3.30}$$

$$\mathrm{FW(I)} = \mathrm{FW_{max}} \cdot \exp\left[\ln\left(\frac{\mathrm{FW_{min}}}{\mathrm{FW_{max}}} \right) \cdot \frac{\mathrm{I}}{\mathrm{MI}} \right] \tag{3.31}$$

Mukhopadhyay et al. (2008) suggested that FW be the standard deviation of the current population when HMCR is close to 1.

$$\mathrm{FW}(\mathrm{I}) = \sigma(\mathbf{s}_i) = \sqrt{\mathrm{var}(\mathbf{s}_i)} \tag{3.32}$$

Geem (2006) tabulated fixed parameter values, such as number of variables, HMS, HMCR, PAR, and MI, after surveying various literatures. FW normally ranges from 1% to 10% of total value range. Furthermore, some researchers have proposed adaptive parameter theories that enable HS to automatically have best parameter values at each iteration (Geem 2006 and 2009).

3.8.2. Harmony memory initialization

Harmony memory initialization: In the second step, the HM is initialized with HMS randomly generated solution vectors defining the musician's harmony memory matrix:

$$\mathrm{HM} = \begin{bmatrix} \mathrm{s}_1^1 & \mathrm{s}_2^1 & \mathrm{s}_3^1 \ldots & \mathrm{s}_n^1 \\ \mathrm{s}_1^2 & \mathrm{s}_2^2 & \mathrm{s}_3^2 \ldots & \mathrm{s}_n^2 \\ \ldots & \ldots & \ldots & \ldots \\ \mathrm{s}_1^{\mathrm{HMS}} & \mathrm{s}_2^{\mathrm{HMS}} & \mathrm{s}_3^{\mathrm{HMS}} \ldots & \mathrm{s}_n^{\mathrm{HMS}} \end{bmatrix} \tag{3.33}$$

3.8.3. Harmony Improvisation

New harmony improvisation: In the third step, a new harmony vector is improvised following three rules: random selection, memory consideration and pitch adjustment. According to the random selection, the value of the decision variable s_i is chosen randomly from the pitches stored in $\mathrm{HM} = [\mathrm{s_i^1}, \mathrm{s_i^2}, \ldots, \mathrm{s_i^{HMS}}]$ with probability of HMCR ($0 \leq \mathrm{HMCR} \leq 1$) or according to the memory consideration it is randomly chosen with a probability of (1-HMCR) within its value range, as a musician plays any pitch within the instrument's pitch range:

$$\mathrm{s_i} = \begin{cases} \mathrm{s_i} \in [\mathrm{s_i^1}, \mathrm{s_i^2}, \ldots, \mathrm{s_i^{HMS}}] \text{ with probability HMCR} \\ \mathrm{s_i^L} \leq \mathrm{s_i} \leq \mathrm{s_i^U} \text{ with probability } (1 - \mathrm{HMCR}) \end{cases} \tag{3.34}$$

After the value s_i is randomly picked according to the above memory consideration process, it can be further adjusted into neighbouring values by adding certain amount to the value, with probability of HMCR × PAR ($0 \leq$ PAR ≤ 1) while the original pitch obtained in HM consideration is just kept with a probability of HMCR × (1-PAR):

$$s_i = \begin{cases} s_i(k+m) \text{ with probability } HMCR \times PAR \\ s_i \text{ with probability } HMCR \times (1-PAR) \end{cases} \quad (3.35)$$

In Jazz improvisation, a musician plays a note by randomly selecting it from total playable range, from musician's memory, or by tweaking the note obtained from musician's memory. Likewise, the HS algorithm improvises a value by choosing it from total value range or from HM, or tweaking the value which was originally chosen from HM.

For discrete design variables, the HS algorithm has the following stochastic partial derivative which consists of three terms such as random selection, memory consideration and pitch adjustment

$$\frac{df}{ds_i} = \frac{1}{K_i}(1-HMCR) + \frac{n(s_i(k))}{HMS} HMCR(1-PAR) + \frac{n(s_i(k-m))}{HMS} HMCR(PAR) \quad (3.36)$$

Also, the HS algorithm can consider the relationship among decision variables using ensemble consideration just as there exists stronger relationship among specific musicians. The value s_i^{new} can be determined based on if the s_j^{new} two has the strongest relationship

$$s_i^{new} \leftarrow fn(s_j^{new}) \text{ where } \max\left\{\left[Corr(s_i, s_j)\right]^2\right\} \quad (3.37)$$

If the newly improvised harmony $\mathbf{s}^{New}$ violates any constraint, HS abandons it or still keeps it by adding penalty to the objective function value just like musicians sometimes still accept rule-violated harmony.

3.8.4. Memory Update

Harmony memory update: If the new generated harmony vector, is better than the worst harmony vector of the HM, with reference to the objective function value, the worst harmony is replaced by the new harmony vector:

$$s^{New} \in HM \cap s^{Worst} \notin HM \quad (3.38)$$

However, for the diversity of harmonies in HM, other harmonies (in terms of least-similarity) can be considered. Also, maximum number of identical harmonies in HM can be considered in order to prevent premature. If the New Harmony $\mathbf{s}^{New}$ is the best one when compared with every harmony in HM, the New Harmony can consider an additional process named *accidentaling*. In music, an accidental is a note whose pitch is not a member of a scale and the accidental sign raise (#) or lowers (b) the following note from its normal pitch. Likewise, HS can further pitch-adjust every note of the new harmony if it is the ever-best harmony, which may find an even better solution:

$$s^{New} = \left\{ \begin{matrix} s_i \left(k \pm m \right) & \text{for discrete variables} \\ s_i \pm \Delta s & \text{for continious variables} \end{matrix} , i = 1,....,n \right\} \tag{3.39}$$

3.9. References

Angeline, P.J., (1998), Evolutionary optimization versus particle swarm optimization: Philosophy and performance differences in Evolutionary Programming VII. Springer Berlin / Heidelberg. pp. 601-610.

Arora, J.S., (1989), Introduction to optimum design, McGraw-Hill, New York.

Arora, J.S., (1994), Methods for optimization of large-scale systems, in Papadrakakis, M. (ed.), Solving Large-Scale Problems in Mechanics, John Wiley, pp. 391-430.

Bendsoe M.P., and Kikuchi N., (1988), Generating optimal topologies in structural design using a homogenization method, Computer Methods in Applied Mechanics and Engineering, 71, 197-224.

Bochenek, B. and Foryś, P. (2006) Structural optimization for post-buckling behavior using particle swarms. Structural and Multidisciplinary Optimization, 32(6): 521-531.

Box, M.J. (1965). A New Method of Constrained Optimization and a Comparison with Other Methods. Computer J, Vol.8, pp.42-52.

Bremicker, M., Papalambros, P.Y., and Loh, H.T., (1990), Solution of Mixed-Discrete Structural Optimization Problems with a New Sequential Linearization Algorithm, Computers & Structures, vol. 37, No. 4, pp. 451-461.

Cai, J., and Thierauf, G., (1993), Discrete optimization of structures using an improved penalty function method, Engineering Optimization Journal, vol. 21, pp. 293-306, 1993.

Cauchy, A. (1847). Methode generale pour la resolution des systemes d'equations simultanes. Compt. Rend., Vol.25, pp.536-538.

Courant R. (1943). Variational methods for the solution of problems of equilibrium and vibrations. Bull Amer. Math. Soc., Vol. 49, pp.1–23.

Dantzig, G. B., (1951). Maximization of a linear function of variables subject to linear inequalities. Activity Analysis of Production and Allocation, Koopman (Ed.), Cowles Commission Monograph, 13, John Wiley and Sons, New York.

Davidson, R., Fletcher, R., Powell, M.J.D. (1963). A rapidly convergent descent method for minimization. Computer J., Vol. 6(2), pp.163-l68.

Eschenauer H.A., Schumacher A., and Vietor T., (1993), Decision makings for initial designs made of advanced materials, in Bendsoe M.P. and Soares C.A.M. (eds.), NATO ARW 'Topology design of structures', Sesimbra, Portugal, Kluwer Academic Publishers, Dordrecht, Netherlands, 469-480.

Fiacco, A.V., McCormick, G.P. (1966). Extension of SUMT for nonlinear programming: equality constraints and extrapolation. Management Science, Vol. 12, pp.816-828.

Fletcher, R., Reeves, C.M (1964). Function Minimization by Conjugate Gradients. Computer J., Vol.7, pp.149-154.

Fogel L.J., Owens A.J., and Walsh M.J., (1966), Artificial intelligence through simulated evolution, Wiley, New York.

Fu, J., Fenton, R.G., and Cleghorn, W.L., (1991), A mixed integer-discrete-continuous programming method and its applications to engineering design optimization, Engineering Optimization Journal, vol. 17, pp. 263-280.

Gallagher R.H. and Zienkiewicz O.C., (1973), Optimum Structural Design: Theory and Applications, John Wiley & Sons, New York, USA.

Geem, Z.W. (2006), Optimal cost design of water distribution networks using harmony search, *Engineering Optimization* 38, 259–280.

Geem, Z.W. (2009), Music-inspired harmony search algorithm: theory and applications, Springer, Berlin.

Geem, Z.W., Kim, J.H., Loganathan, G.V. (2001). A new heuristic optimization algorithm: harmony search. *Simulation*, 76: 60-68.

Gill, P.E, Murray, W., and Wright, M.H., (1981), Practical Optimization, Academic Press.

Goldberg, D.E, (1989), Genetic Algorithms in search, optimization and machine learning. Addison-Wesley.

Hassan, R., et al., (2005) A Comparison of Particle Swarm Optimization and the Genetic Algorithm, in Proceedings of the 46th AIAA/ASME/ASCE/AHS/ASC structures, structural dynamics and materials conference. Austin, Texas, USA.

Haug E.J. and Arora J.S., 'Optimal mechanical design techniques based on optimal control methods', ASME paper No 64-DTT-l0, Proceedings of the 1st ASME design technology transfer conference, 65-74, New York, October, 1974.

He, Q. and L. Wang, (2007), An effective co-evolutionary particle swarm optimization for constrained engineering design problems. Engineering Applications of Artificial Intelligence, 20(1): 89-99.

Hinton E., and Hassani B., (1995). Some experiences in structural topology optimization, in B.H.V. Topping (ed.) Developments in Computational Techniques for Structural Engineering, CIVIL-COMP Press, Edinburgh, 323-333.

Hinton E., and Sienz J., (1993). Fully stressed topological design of structures using an evolutionary procedure, Journal of Engineering Computations, 12, 229-244.

Hinton E., and Sienz J., (1994) Aspects of adaptive finite element analysis and structural optimization, in Topping B.H.V. and Papadrakakis M. (eds) Advances in Structural Optimization, CIVIL-COMP Press, Edinburgh, 1-26.

Holland J., (1975), Adaptation in natural and artificial systems, University of Michigan Press, Ann Arbor, USA.

Hooke, R., Jeeves, T.A. (1961). Direct Search Solution of Numerical and Statistical Problems. J of the ACM, Vol.8, pp.212-229.

Ingber, L., (1993), Simulated Annealing: Practice Versus Theory, J. Mathematical Computational Modelling, Vol. 18, No. 11, pp. 29 - 57.

Karush, W. (1939). Minima of Functions of Several Variables with Inequalities as Side Conditions. MS Thesis, Dept. of Mathematics, University of Chicago, Chicago, IL.

Kennedy, J., Eberhart, R. (1995), Particle swarm optimization. IEEE Int. Conf. on Neural Networks. Piscataway, NJ, USA. IV, 1942–1948.

Kirkpatrick, S. (1984), Optimization by simulated annealing: quantitative studies. J Statist Phys, Vol. 34, pp. 975-986.

Kuhn, H.W., Tucker A.W. (1951). Non-linear Programming. in J. Neyman (Ed.), Proceedings of the Second Berkeley Symposium on Mathematical Statistics and Probability, University of California Press, Berkeley, CA , pp. 481-493.

Lagaros, N.D., Papadrakakis, M., Kokossalakis, G., (2002). Structural optimization using evolutionary algorithms, Computer & Structures, 80 (7-8), 571-587.

Liang, J.J. and P.N. Suganthan, (2006), Dynamic Multi-Swarm Particle Swarm Optimizer with a Novel Constraint-Handling Mechanism, in Evolutionary Computation, 2006. CEC 2006. IEEE Congress on. pp. 9-16

Mahdavi, M., Fesanghary, M., Damangir, E. (2007). An improved harmony search algorithm for solving optimization problems, *Applied Mathematics and Computation*, 188, 1567–1579.

Mezura-Montes, E. and B.C. Lopez-Ramirez, (2007), Comparing bio-inspired algorithms in constrained optimization problems, in Evolutionary Computation, 2007. CEC 2007. IEEE Congress on. p. 662-669.

Moses F., Mathematical programming methods for structural optimization, ASME Structural Optimisation Symposium AMD Vol. 7, 35-48, 1974.

Mukhopadhyay, A., Roy, A., Das, S., Das, S., Abraham, A. (2008). Population-variance and explorative power of harmony search: an analysis, Proceedings of 3rd IEEE International Conference on Digital Information Management, pp. 13–16.

Munoz-Zavala, A.E., et al., PESO for Constrained Optimization, in Evolutionary Computation, 2006. CEC 2006. IEEE Congress on. 2006. pp. 231-238.

Nelder, J.A., Mead, R. (1965). A Simplex Method for Function Minimization. Computer Journal, Vol.7, pp. 308-313.

Papadrakakis M., Tsompanakis Y., Hinton E., and Sienz J., (1996) Advanced solution methods in topology optimization and shape sensitivity analysis, Journal of Engineering Computations, Vol. 3, No. 5, 57-90.

Papadrakakis, M., Lagaros, N.D., Thierauf, G., Cai, J., (1998). Advanced solution methods in structural optimization based on evolution strategies, Journal of Engineering Computations, 15 (1), 12-34.

Papadrakakis, M., Lagaros, N.D., Tsompanakis, Y., Plevris, V. Large scale structural optimization: Computational methods and optimization algorithms, Archives of Computational Methods in Engineering (State of the art reviews), Vol. 8, No. 3, pp 239-301, 2001.

Papadrakakis, M., Tsompanakis, Y., Lagaros, N.D., (1999). Structural shape optimization using Evolution Strategies, Engineering Optimization, 31, 515-540.

Pedersen P., (1993). Topology optimization of three dimensional trusses, in Bendsoe M.P., and Soares C.A.M. (eds.), NATO ARW `Topology design of structures', Sesimbra, Portugal, Kluwer Academic Publishers, Dordrecht, Netherlands, 19-31.

Perez, R.E., Behdinan, K., (2007) Particle swarm approach for structural design optimization, Computers and Structures 85, 1579-1588.

Pope G.G. and Schmit L.A. (eds.) (1971), Structural Design Applications of Mathematical Programming Techniques, AGARDO graph 149, Technical Editing and Reproduction Ltd., London.

Powell, M.J.D. (1964). An efficient Method for finding the minimum of a function of several variables without calculating derivatives. Computer Journal, Vol.7 (4), pp.303-307.

Press, W.H., Teukolsky, S.A., Vetterling, W.T. and Flannery, B.P., (1992), Numerical Recipes in C, Cambridge University Press.

Ramm E., Bletzinger K.-U., Reitinger R., and Maute K., (1994) The challenge of structural optimization, in Topping B.H.V. and Papadrakakis M. (eds) Advances in Structural Optimization, CIVIL-COMP Press, Edinburgh, 27-52.

Rechenberg I., (1973), Evolution strategy: optimization of technical systems according to the principles of biological evolution, Frommann-Holzboog, Stuttgart.

Rosen, J. (1960). The Gradient Projection Method for Nonlinear Programming, I. Linear Constraints. Journal of the Society for Industrial and Applied Mathematics, Vol.8, pp. 181–217.

Rosenbrock, H.H. (1960). An Automatic Method for finding the Greatest or Least Value of a Function. Comp J, Vol.3, pp.175-184.

Russo, L. (2004). The forgotten revolution: How science was born in 300BC and why it had to be reborn. Springer, Berlin.

Schwefel H.P., (1981) Numerical optimization for computer models, Wiley & Sons, Chichester, UK.

Sheu C.Y. and Prager W., (1968), Recent development in optimal structural design, Applied Mechanical Reviews, 21(10), 985-992.

Shi, Y., Eberhart, R. (1998), A modified particle swarm optimizer. IEEE World Congress on Computational Intelligence. Anchorage, AK, USA, 69-73.

Shieh R.C., (1994). 'Massively parallel structural design using stochastic optimization and mixed neural net/finite element analysis methods', Computing Systems in Engineering, Vol. 5, No. 4-6, pp. 455-467.

Spunt L., (1971), Optimum Structural Design, Prentice-Hall, Englewood Cliffs, New Jersey, 41-42.

Storn R, Price K, (1995), Differential Evolution - A simple and efficient adaptive scheme for global optimization over continuous spaces, TR-95-012 March 1995.

Storn, R.M., Price, K.V. (1997). Differential evolution - a simple and efficient heuristic for global optimization over continuous spaces. Journal of Global Optimization 11: 341-359

Suzuki K., and Kikuchi N., (1993). Layout optimization using the homogenization method, in Rozvany G.I.N. (ed.), NATO/DFG ASI `Optimization of large structural systems', Berchtesgaden, Germany, Kluwer Academic Publishers, Dordrecht, Netherlands, 157-175.

Van Keulen F. and Hinton E., (1996). Topology design of plate and shell structures using the hard kill method, in B.H.V. Topping (ed.) Advances in optimization for Structural Engineering, CIVIL-COMP Press, Edinburgh, 177-188.

Vanderplaats, G.N., (1984), Numerical optimization techniques for engineering design", McGraw-Hill, New York, USA.

Venkayya V.B., Khot N.S. and Berke L., (1973), Application of optimality criteria approaches to automated design of large practical structures, 2nd Symposium on Structural Optimisation AGARD-CP-123, Milan, Italy.

Veselago, V.G. (2002). Formulating Fermat's principle for light travelling in negative refraction materials. PHYS-USP, Vol. 45(10), pp. 1097-1099.

Xie Y.M., and Steven G.P., (1993). A simple evolutionary procedure for structural optimization, Computers & Structures, Vol. 49, 885-896.

Ye, D., Z. Chen, and J. Liao, (2007). A New Algorithm for Minimum Attribute Reduction Based on Binary Particle Swarm Optimization with Vaccination, in Advances in Knowledge Discovery and Data Mining. pp. 1029-1036.

Zoutendijk, G. (1960). Methods of Feasible Directions. Elsevier.

Chapter 4

Seismic Design Procedures: Prescriptive vs Performance-Based Design

4.1. Introduction

In the past the requirements and provisions of the seismic design codes for buildings have been based on experience and they were periodically revised after disastrous earthquakes. Most of the current seismic design codes define a single design earthquake for assessing the structural performance against the earthquake hazard. These codes adopt many inherent assumptions built in the design procedure regarding the behaviour of the structure against earthquake loading. Severe damages caused by recent earthquakes made the engineering community to question the effectiveness of the current seismic design codes (Panagiotakos and Fardis, 2004; Browning, 2002; Xue, 2000). Given that the primary goal of contemporary seismic design is the protection of human life it is evident that additional performance targets and earthquake intensities should be considered in order to assess the structural performance at many hazard levels. During the last decade, the concept of PBD for structures subjected to seismic loading conditions was introduced (ATC-40, 1996; FEMA-273, 1997; SEAOC-Vision 2000, 1995). Using PBD, more accurate, but time consuming, analysis procedures are employed based on nonlinear structural response. The progress that took place in the last two decades in the fields of computational mechanics as well as in computer hardware technology, made possible the use of these PBD procedures.

Most of the current seismic design codes belong to the category of the prescriptive design procedures (or limit state design procedures), where if a number of checks, expressed in terms of forces or deformations are satisfied, the structure is considered safe and consequently it will not collapse. Typical limit state based designs rely on one (i.e. ultimate strength) or two (i.e. serviceability and ultimate strength) limit state approach. All modern

seismic design procedures are based on the principle that a structure will avoid collapse if it is designed to absorb and dissipate the kinetic energy produced during the seismic excitation. Most of the modern seismic codes allow the ability of the structure to absorb energy through inelastic deformation which is quantified with the reduction or behaviour factor q. The capacity of a structure to resist seismic actions in the nonlinear range generally permits these to be designed with seismic loads smaller than those corresponding to a linear elastic response. The seismic loads are reduced using the behaviour factor q. The numerical confirmation of the behaviour factor became a subject of research work during the past decade (Fajfar, 1998; Mazzolani and Piluso, 1996) in order to check the validity of the design assumptions.

ATC-40 (1996) and FEMA-273 (1997) were the first guidelines for performance-based seismic rehabilitation of existing buildings, while in the report Vision 2000 (1995) these ideas were extended to the design process of new buildings. The main objective of this kind of design procedures is to achieve more predictable and reliable levels of safety and operability against natural hazards. According to PBD procedures, the structures should be able to resist earthquakes in a quantifiable manner and to present target performance levels of possible damages. PBD procedures are multi-level design approaches where various levels of structural performance are considered. For example, FEMA-356 (2000) suggests the following performance levels: operational level, immediate occupancy, life safety and collapse prevention. For assessing the structural performance the guidelines suggest the use of various types of analysis methods: linear static, nonlinear static, linear dynamic and nonlinear dynamic. The most commonly used approach is the NSA, also called as pushover analysis. Pushover analysis allows for the direct evaluation of the performance of the structure at each limit state as opposed to the prescriptive design procedures, such as those of Eurocode 2 (1992) or the 2000 GNDC for RC buildings (EKOS, 2000), where the structure is designed for the ultimate limit strength state.

4.2. Seismic Design Procedures

The majority of the seismic design codes belong to the category of the prescriptive building design codes, which include: site selection and development of conceptual, preliminary and final design stages. According to a prescriptive design code the strength of the structure is evaluated at one or two limit states between life-safety and near collapse using the corresponding response spectrum (EAK, 2000; EC8, 2004). In addition, serviceability limit state is usually checked in order to ensure that the structure will not deflect or vibrate

excessively during its functioning. On the other hand, PBD is a different approach for the seismic design which includes, apart from the site selection and the development of the design stages, the construction and maintenance of the building in order to ensure reliable and predictable seismic performance over its life.

4.2.1. Prescriptive design procedures

The current seismic design philosophy for RC structures relies on energy dissipation through inelastic deformations. Proper design of an earthquake resistant RC building should provide the structure with adequate deformation capacity to dissipate energy without a substantial reduction of its overall resistance against horizontal and vertical loading. According to EC2 (2004) and EC8 (2004), or EKOS (2000) and EAK (2000), the fundamental design requirements that should be satisfied with an adequate degree of reliability are the requirements of no-collapse, damage limitation and minimum level of serviceability. In order to ensure that the structure will meet these requirements a number of checks must be satisfied: strength (all types of load effect combinations), second-order effects (P-Δ effects), capacity design, limitation of inter-storey drift, stress levels, crack width and deflection control.

The study performed in the framework of this dissertation is based on EC8 (2004) and EC2 (2004), with the following assumptions: (i) The seismic load is an EDRs with 10% probability of being exceeded in 50 years (475 years return period), reduced by a behaviour factor q. (ii) The characteristic material strength is reduced by a partial safety factor γ_s=1.15 for steel reinforcement and by a partial safety factor γ_c=1.50 for concrete. (iii) The analysis procedure employed is either the simplified modal or the multi-modal response spectrum analysis.

According to the Eurocodes or the Greek national design codes a number of checks must be considered in order to ensure that the structure will meet the design requirements. Each candidate design is assessed using the following constraints. All EC2 (2004) or EKOS (2000) checks must be satisfied for various combinations of the gravity loads, e.g. the following load combinations:

$$S_d = 1.35\sum_j G_{kj}" + "1.50\sum_i Q_{ki} \quad (4.1a)$$

$$S_d = 1.0\sum_j G_{kj}" + "1.50\sum_i Q_{ki} \quad (4.1b)$$

where "+" implies "to be combined with", the summation symbol "Σ" implies "the combined effect of", G_{kj} denotes the characteristic value "k" of the permanent action j and Q_{ki} refers to the characteristic value "k" of the variable action i. If the above constraints are satisfied,

multi-modal response spectrum analysis is performed according to EC8 (2004) or EAK (2000), and earthquake loading is considered using the following load combination:

$$S_d = \sum_j G_{kj}" + "E_d" + "\sum_i \psi_{2i} Q_{ki} \quad (4.2a)$$

$$E_d = E_X + 0.30E_Y \; or \; E_d = E_Y + 0.30E_X \quad (4.2b)$$

where E_d is the design value of the seismic action for the three components (longitudinal, transverse and vertical) respectively and ψ_{2i} is the combination coefficient for the quasi-permanent action *i*, here taken equal to *0.30*.

4.2.2. Response modification factors (q or R)

Although, life safety under high seismic risk is the main objective of contemporary seismic design codes like EC8 (2004) and ATC-34 (1995), economic considerations permit the assumption that the structure will behave inelastically and could tolerate damages up to a certain level given that life safety is ensured. Since damage levels that a structure should tolerate cannot be predicted through linear analysis procedures, behaviour or response modification factors are used in order to account for nonlinear response of structures. The behaviour factors are used to scale down the linear elastic design response spectrum ordinates, corresponding to the maximum earthquake expected at the site, to the inelastic design response spectrum (Palazzo and Petti, 1996). Difficulties in evaluating behaviour factors, that are generally applicable to various structural systems, materials, configurations and input motions, are well documented and the inherent drawbacks in code specified factors are widely accepted (Tassios, 1986; Kappos, 1991; Uang, 1991; Zeris et al., 1991; Moroni et al., 1996; Lam et al., 1998; Kappos, 1999; Whittaker et al., 1999; Borzi and Elnashai, 2000; Elnashai and Mwafy, 2002; Balendra and Huang, 2003). No matter how difficult or unreliable may be the prediction of its value, the behaviour factor is used both in European design codes (denoted as *q*) and in US design codes, named as response modification factor (denoted as *R*). The *q* factor is eventually an approximation of the ratio of the seismic forces that the structure would experience if its response were completely elastic with 5% viscous damping, to the seismic design forces inducing inelastic response and is in EC8 assumed to be given by the following expression:

$$q = q_0 \cdot k_D \cdot k_R \cdot k_W \geq 1.5 \quad (4.3)$$

where q_0 is the basic value of the behaviour factor influenced by the structural configuration, k_D corresponds to the ductility class, k_R is related to the vertical irregularity and k_W is connected to the main failure mode. According to the US codes the response

modification factor consists of three parameters and is given by the following equation (Borzi and Elnashai, 2000):

$$R = R_S \cdot R_\mu \cdot R_R \tag{4.4}$$

where R_S is the overstrength factor, R_μ is the ductility reduction factor and R_R is known as the redundancy factor, introduced to account for the number and distribution of active plastic hinges. The values of R are larger than those of q due to the differences on the applied ground motions (Borzi and Elnashai, 2000). The theoretical background of reduction factors suffers from shortcomings due to the fact that the physical mechanisms involved are not rigorously defined (Kappos, 1999). For these reasons many researchers have tried to introduce new definitions for q and R factors, trying to take into consideration the uncertainties involved (Lu et al., 2001; Miranda and Bertero, 1994; Lam et al., 1998).

Using the reduction factor, a structural system is designed to have lower strength, in order to absorb energy through its inelastic deformations. Furthermore, since the demand in terms of inelastic deformations is expressed with reference to the ductility, there is a strict correlation between the reduction factor and the available ductility of the structure. Collapse mechanisms due to low energy dissipation should be avoided and adequate supply of local ductility should be provided in the plastic hinges. For this reason, three ductility levels (Low-Medium-High) are defined, each corresponding to different structural requirements in order to ensure the desired ductility level. From the definition of the reduction factor, it is obvious that the higher the ductility level is the lower the seismic design loads are, corresponding to higher value of the reduction factor. Structures designed according to the low ductility class are imposed to higher seismic design actions leading to increased structural cost. However, due to their small ductility and their low inelastic response, less damage is expected. According to the Eurocodes (EC2, 2004 and EC8, 2004) a medium ductility level is recommended since it is considered as a compromise between resistance and economical design (Cuesta et al., 2003).

A number of methods have been proposed in the literature for evaluating the reduction factors based on two structural ingredients: (i) overstrength and (ii) ductility (Tassios, 1989a; Tassios, 1989b). Miranda and Bertero (1994) have found that strength reduction factors are primarily influenced by the maximum tolerable displacement ductility demand, the period of the structural system and the soil conditions of the site. Lam et al. (1998) developed a relationship between the ductility reduction factor (R_μ) and the ductility for linear elasto-perfectly plastic SDOF systems (where $R=R_\mu$) in order to rationalize seismic design provisions for codes of practice. Borzi and Elnashai (2000) employed an earthquake

set to derive values for force reduction factors needed for the structure to reach, and not exceed, a pre-determined level of ductility. It was observed that the force modification factors are only slightly influenced by the shape of the hysteretic model used in their derivation and that they are even less sensitive to strong motion characteristics. Cuesta et al. (2003) unified the results taken from two different approaches for determining the R-μ-T relationships, where the ground motion frequency content is considered. Recently, Lee and Foutch (2006) used different R factors to design steel moment resisting frame structures. In their study it was found that the recommended R factors provide conservative designs for some of the structures considered. Karavasilis et al. (2007) proposed simplified expressions to estimate the behaviour factor of plane steel moment resisting frames, based on statistical analysis of the results of nonlinear dynamic analyses. Karakostas et al. (2007) derived the ductility component of the behaviour factor from statistical analysis of constant ductility spectra, and proposed empirical relationships suitable for design purposes. All these studies however, do not reach any concrete conclusion regarding the reliability of the design philosophy based on the behaviour factors.

4.2.3. Performance-based design procedure

Performance-based seismic design has the following distinctive features with respect to the prescriptive design codes: (i) allows the structural engineer to choose both the appropriate level of seismic hazard and the corresponding performance level of the structure, (ii) the structure is designed to meet a series of combinations of hazard levels in conjunction with corresponding performance levels. The PBD process implemented in this dissertation is a displacement-based design procedure where the design criteria and the capacity demand comparisons are expressed in terms of displacements rather than forces (Sullivan et al., 2003; Panagiotakos and Fardis, 2001, Priestley et al., 2007).

PBEE implies the design, evaluation, construction and maintenance of engineering facilities in order to meet the objectives set by the society and the owners/users of a facility (Krawinkler and Miranda, 2004). In the case of earthquakes, the aim is to make structures having a predictable and reliable performance, or in other words, they should be able to resist earthquakes with quantifiable confidence. Therefore, the modern conceptual approach of seismic structural design is that the structures should meet performance-based objectives for a number of different hazard levels ranging from earthquakes with a small intensity and with a small return period, to more destructive events with large return periods. The current state of practice in performance-based earthquake engineering is defined by the US guidelines (ATC-40, 1996; ASCE-41, 2006). These guidelines do not differ

conceptually and introduce procedures that can be considered as the first significant diversification from prescriptive building design codes. Many of the current codes for the design of new buildings are only partially performance-based, since they attempt to tie all design criteria to one performance level, usually to that of life safety or collapse prevention.

In nonlinear structural analysis procedures it is essential to formulate structural models that incorporate all the essential characteristics of the problem to be examined and can estimate the demand within acceptable accuracy. In order to evaluate the demand, appropriate EDPs are necessary. As an EDP any response variable can be used, such as stress resultants, displacements, chord rotations, among others. According to ASCE-41 the actions can be either force or deformation-controlled depending on the capacity of the members to deform inelastically. The capacity of force-controlled members should be assessed using formulas based on stress resultants (e.g. EC2, 2004); while for deformation-controlled actions an appropriate EDP must be chosen. EDPs may be interstorey drifts, inelastic deformations, section curvatures, floor accelerations and velocities, etc (Fragiadakis and Papadrakakis, 2008; Mitropoulou *et al.* 2010). The main part in a performance-based seismic design procedure is the definition of the performance objectives that will be used. The proposed PBD process can be described with the following two steps:

1) Proportioning of the longitudinal and transverse reinforcement of all members on the basis of the serviceability limit state.
2) Use of pushover analysis in order to estimate the structural capacities of the design in the different intensity levels employed. Revise the reinforcement and the dimension of the members so that the capacities exceed the seismic demands (Panagiotakos and Fardis, 2001).

The completion of *Step 1* is necessary for *Step 2* as the structural capacity depends both on the reinforcement and the dimensions of the members.

The constraints considered for Step 2 of the PBD procedure are related to the maximum interstorey drift limit θ, which is the largest value of the height-wise peak interstorey drift ratio for each hazard level. This is a commonly used measure of both structural and non-structural damage because of its close relationship to plastic rotation demands on individual beam-column connection assemblies. In this part of the dissertation three performance objectives are considered that correspond to hazard levels with 50, 10 and 2 percent probabilities of exceedance in 50 years. The drift limits θ, for the three performance objectives considered, are equal to 0.25, 0.5 and 3.0 percent, respectively. The θ values obtained at the three hazard levels are also used for the calculation of the limit state cost, as

will be described in a following section. The framework for the PBD procedure employed in this study is shown schematically in Figure 4.1.

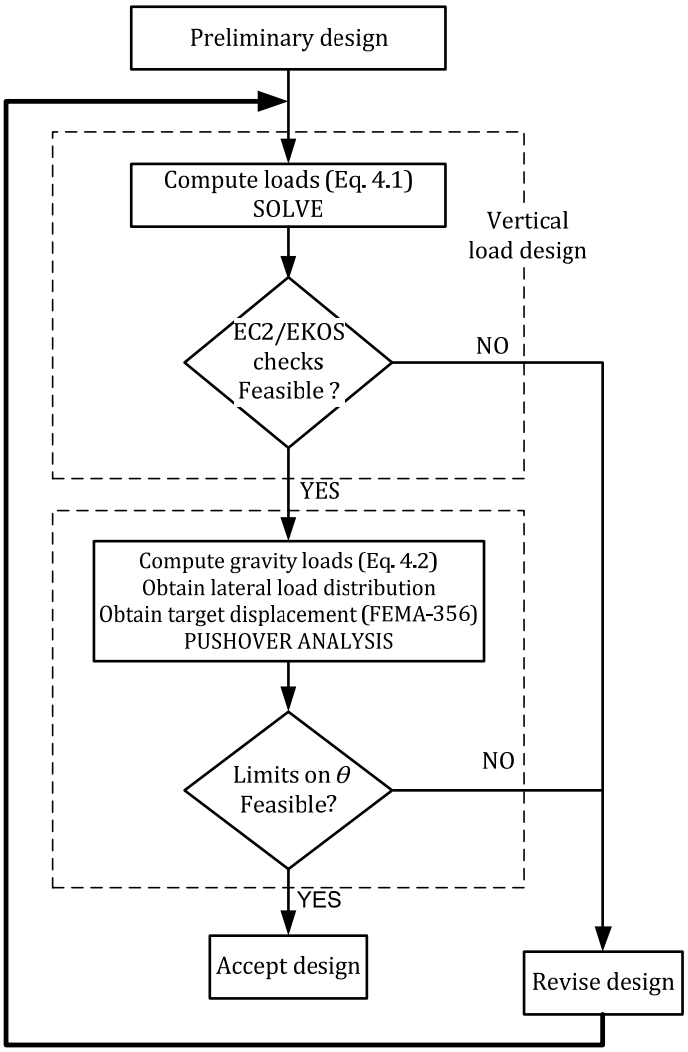

Figure 4.1. Flowchart of the employed PBD design procedure.

A performance objective is defined as the combination of a performance level for a specific hazard level. In this dissertation the three performance objectives considered correspond to the "Enhanced Objectives" of FEMA-356 (2000). The first step in the definition of the performance objectives is the selection of the performance levels. The implemented performance levels are the following:

i) *Operational*: the overall damage level is characterized as very light. No permanent drift is encountered, while the structure essentially retains original strength and stiffness.

ii) *Life Safety*: the overall damage level is characterized as moderate. Permanent drift is encountered while strength and stiffness reserves are encountered in all stories. Gravity-load bearing elements continue to function while there is no out-of plane failure of the walls. The overall risk of life-threatening injury as a result of structural damage is

expected to be low. It should be possible to repair the structure; however, for economic reasons this may not be practical.

iii) *Collapse Prevention*: the overall damage level is characterized as severe. Substantial damage has occurred to the structure, including significant degradation in the stiffness and strength of the lateral-force resisting system. Large permanent lateral deformation of the structure and degradation in vertical-load bearing capacity is encountered. However, all significant components of the gravity load- resisting system continue to carry their gravity load demands. The structure may not be technically practical to be repaired and is not safe for reoccupancy, since aftershock activity could induce collapse.

The second step in the definition of the performance objectives is to determine the earthquake hazard levels. Earthquake hazards according to FEMA-350 (2000) include direct ground fault rupture, ground shaking, liquefaction, lateral spreading and land sliding. Ground shaking is the only earthquake hazard that the structural design provisions of the building codes directly address. Ground shaking hazards are typically characterized by a hazard curve, which indicates the probability that a given value of a ground motion parameter, for example peak ground acceleration, will be exceeded over a certain period of time. The ground shaking hazard levels that have been considered are the following:

i) *Occasional* earthquake hazard level: with probability of exceedance 50% in 50 years with a mean return period 72 years.

ii) *Rare* earthquake hazard level: with probability of exceedance 10% in 50 years with a mean return period 475 years.

iii) *Maximum Considered Event* earthquake hazard level: with probability of exceedance 2% in 50 years with a mean return period 2475 years.

The combination of one performance level with an earthquake hazard level results in a performance objective. Figure 4.2 depicts the performance objectives for three classes of facilities. (i) For Standard Occupancy Facilities three performance objectives are defined: S1, S2 and S3. (ii) For Emergency Response Facilities two performance objectives are defined: E1 and E2. (iii) For Safety Critical Facilities one performance objective is defined: SC1. It can be seen that the PBD step is performed as soon as the structure has satisfied the serviceability limit-state checks.

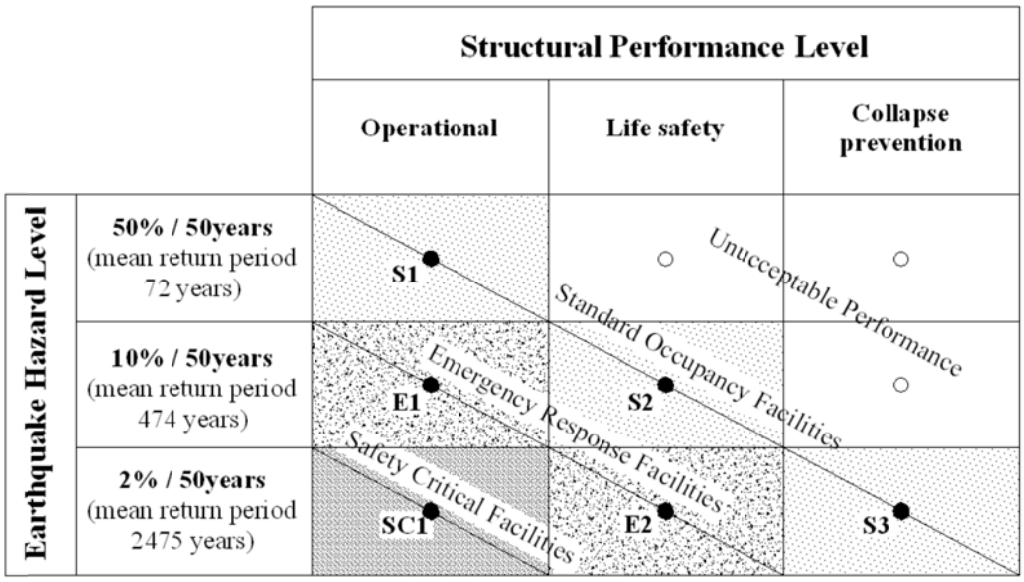

Figure 4.2. The design performances objectives for different importance classes.

4.3. Analysis procedures

According to FEMA-356 (2000) four alternative analytical procedures, based on linear and nonlinear structural response, are recommended for the structural analysis of buildings under earthquake loading. The linear procedures can be either the LSP or the LDP. For the linear dynamic procedures there are two alternatives, the response spectrum method (which in EAK, 2000 is referred as MmRS analysis), and the time history method. In a similar fashion the nonlinear methods are distinguished to the NSP, also known as *pushover* analysis, and the NDP, also referred as inelastic or nonlinear time history analysis. Procedures that are not based on dynamic time history analysis, when applied in the framework of a seismic design code, usually resort to a regional response spectrum. Design procedures based on nonlinear analysis are not so popular due to the increased computational effort needed and the requirement for highly trained engineers to put into practice more elaborate analysis methods. However, when a linear analysis method is employed simplifying assumptions of the structural response are made, resulting either to conservative and therefore to more expensive designs, or to designs with reduced safety since phenomena that have not been accounted for during the design phase may influence the load carrying capacity of the structure during its functioning. In the case of the EAK (2000) and EC8 (2004) seismic design procedure the MmRS analysis method is used, while in the PBD procedure the pushover analysis procedure is used.

4.3.1. Nonlinear Static Procedures-Pushover

The purpose of the nonlinear static procedure is to assess structural performance in terms of strength and deformation capacity globally as well as at the element level. The structural model is "pushed" according to a predefined lateral load pattern. The purpose of pushover analysis procedure is used in order to assess the structural performance in terms of strength and deformation capacity for the whole structure, as well as at the element level. The pushover analysis step is performed as soon as the structure has satisfied the serviceability limit state. For assessing the performance of the structure for the three performance levels considered a lateral load distribution that follows the fundamental mode is adopted, while the pushover analysis is terminated as soon as a target displacement is reached, or earlier if the algorithm fails to converge because a collapse mechanism has been formed. In order to determine the target displacement in multiple hazard levels required by the performance-based design framework, typically one of the following methods is adopted: the Capacity Spectrum method of ATC-40 (1996), the Coefficient method of ASCE-41 (2006) and the N2 method of EC8 (2004). According to ASCE-41 (2006), apart from a first-mode based lateral load pattern, the use of a uniform pattern is also suggested. In the numerical results that follow only the first-mode pattern was taken into consideration. For 3D structures the properties of the lateral load pattern have to be extracted from the mode that refers to the direction under consideration.

Pushover is limited with regard to evaluation of the simultaneous response to ground shaking in different directions. In this work the recommendation of FEMA-350 (2000) is employed where multidirectional excitation effects are accounted for by combining 100% of the response due to loading in the longitudinal direction with 30% of the response due to loading in the transverse direction, and by combining 30% of the response in the longitudinal direction with 100% of the response in the transverse direction. The worst of these two combinations in each of the three hazard levels is used in order to assess the structural performance in the corresponding performance levels.

The displacement coefficient method (ASCE-41)

When pushover analysis, or adopting the ASCE/SEI 41-06 terminology, the NSP is implemented, the analysis is terminated when 150% of the target displacement that correspond to the 2% in 50 years (2/50) hazard level is reached or earlier if the structure has collapsed. The target displacement, which is the displacement during a given seismic event of a characteristic node on the top of a structure, typically in the roof, is defined with the aid of the formula:

$$d_t = C_0 C_1 C_2 C_3 S_a \frac{T_e^2}{4\pi^2} g \quad (4.5)$$

where C_0, C_1, C_2 and C_3 are modification factors. C_0 relates the spectral displacement to the building roof displacement. C_1 relates the expected maximum inelastic displacements to the displacements calculated for linear elastic response. C_2 represents the effect of the hysteresis shape on the maximum displacement response and C_3 accounts for the P-Δ effects. T_e is the effective fundamental period of the building in the direction under consideration and S_a the response spectrum acceleration, corresponding to the T_e period, normalised by g. The FEMA-440 (2005) guidelines introduce updated expressions for the calculation of the effective damping and the period and also for scaling the demand spectrum based on the hysteretic model of the system. In this study it was adopted the new FEMA-440 expressions although we cite the displacement coefficient method as the ASCE/SEI 41-06 method for consistency.

The capacity spectrum method (ATC-40)

The CSM was initially proposed by Freeman (1998). The method compares the capacity of a structure to resist lateral forces to the demand given by a response spectrum in a graphical manner. The response spectrum represents the demand while the pushover curve (or the "capacity curve") represents the available capacity. Both curves are converted and plotted against an acceleration-displacement graph (AD graph) making easy the evaluation of the point of equal demand and supply, also known as performance point. Among the three variations of the method discussed in ATC-40, the Procedure A was examined. The steps of the method are briefly summarized as follows:

(i) Perform pushover analysis and determine the capacity curve in base shear (V_b) versus roof displacement of the building (D). This diagram is then converted to AD terms using an equivalent SDOF. The conversion is performed using the first mode participation factor C_0 ($D^*=D/C_0$) and the modal mass ($A=V_b/M$).

(ii) Plot the capacity diagram on the same graph with the 5%-damped elastic response spectrum that is also in AD format.

(iii) Select a trial peak deformation demand d_t^* and determine the corresponding pseudo-acceleration A from the capacity diagram, initially assuming ζ=5%.

(iv) Compute ductility $\mu=D^*/u_y$ and calculate the hysteretic damping ζ_h as $\zeta_h=2(\mu-1)/\pi\mu$. The equivalent damping ratio is evaluated from a relationship of the form:

$$\zeta_{eq} = \zeta_{el} + \kappa\zeta_h \quad (4.6)$$

where κ is a damping modification factor that depends on the hysteretic behaviour of the system. Update the estimate of d_t^* using the elastic demand diagram for ζ_{eq}.

(v) Check for convergence the displacement d_t^*. When convergence has been achieved the target displacement of the MDOF system is equal to $d_t = C_0 d_t^*$.

The N2 method (EC8)

The N2 method was initially proposed by Fajfar (Fajfar and Fischinger, 1988), Fajfar and Gaspersic, 1996)) and was later expressed in a displacement-acceleration format (Fajfar, 1999). Recently, the method has been included in the Eurocode 8 (2004). Conceptually the method is a variation of Capacity Spectrum Method that instead of highly damped spectra uses an *R-μ-T* relationship. The method, as implemented in EC8, consists of the following steps:

(i) Perform pushover analysis and obtain the capacity curve in V_b-D terms,

(ii) Convert the pushover curve of the MDOF system to the capacity diagram of an ESDOF system and approximate the capacity curve with an idealized elasto-perfectly plastic relationship to get the period T_e of the ESDOF,

(iii) The target displacement is then calculated as:

$$d_{et}^* = S_a(T_e)\left[\frac{T_e}{2\pi}\right]^2 \tag{4.7}$$

where $S_a(T_e)$ is the elastic acceleration response spectrum at the period T_e. To determine the target displacement d_t^*, different expressions are suggested for the short and the medium to long-period ranges:

$T^* < T_C$ (short period range): If $F_y^* / m^* \geq S_a(T_e)$, the response is elastic and thus $d_t^* = d_{et}^*$ and $d_t = C_0 d_t^*$. Otherwise the response is nonlinear and the ESDOF maximum displacement is calculated as:

$$d_t^* = \frac{d_{et}^*}{q_u}\left(1 + (q_u - 1)\frac{T_C}{T_e}\right) \geq d_{et}^* \tag{4.8}$$

where q_u is the ratio between the acceleration in the structure with unlimited elastic behaviour $S_e(T^*)$ times the modal mass m^* over its yield force, or simply:

$$q_u = S_a(T_e) m^* / F_y^* \tag{4.9}$$

$T^* \geq T_C$ (medium and long period range): The target displacement of the inelastic system is equal to that of an elastic structure, thus $d_t^* = d_{et}^*$. The displacement of the MDOF system is always calculated as $d_t = C_0 d_t^*$.

4.3.2. Nonlinear Dynamic Procedures

In the seismic assessment of structures a wide range of seismic records and more than one performance levels should be considered in order to take into account the uncertainties that the seismic hazard introduces into a performance-based seismic assessment or design problem. The methods used for the performance-based assessment implementing non-linear dynamic analyses are classified as single and multiple hazard level methods. IDA and MSDA are the two most applicable methods, both considering multiple hazard levels.

Incremental Dynamic Analysis

IDA, with its 3D implementation called MIDA, was based on a primary idea of Bertero (1977) and then it was presented under different approaches from other researchers (for example Luco and Cornell, 2000; Mwafy and Elnashai, 2001). The main objective of an IDA study is to develop a curve through a relation between the seismic intensity level and the corresponding maximum response of the structural system (Vamvatsikos and Cornell 2002). The intensity level and the structural response are described through an IM and an EDP, respectively. The IDA study is implemented through the following steps: (i) define the nonlinear FE model required for performing nonlinear dynamic analyses; (ii) select a suit of natural records; (iii) select a proper intensity measure and an engineering demand parameter; (iv) employ an appropriate algorithm for selecting the record scaling factor in order to obtain the IDA curve performing the least required nonlinear dynamic analyses and (v) employ a summarization technique for exploiting the multiple records results.

Selecting IM and EDP is one of the most important steps of the IDA study. In the work by Giovenale et al. (2004) the significance of selecting an efficient IM is discussed while an originally adopted IM is compared with a new one. The IM should be a monotonically scalable ground motion intensity measure like the PGA, PGV, the ξ=5% damped spectral acceleration at the structure's first-mode period ($S_A(T_1,5\%)$) and many others. In the current work the $S_A(T_1,5\%)$ is selected, since it is the most commonly used intensity measure in practice today for the analysis of buildings. An indicative PGA versus drift curve is shown in Figure 4.3.

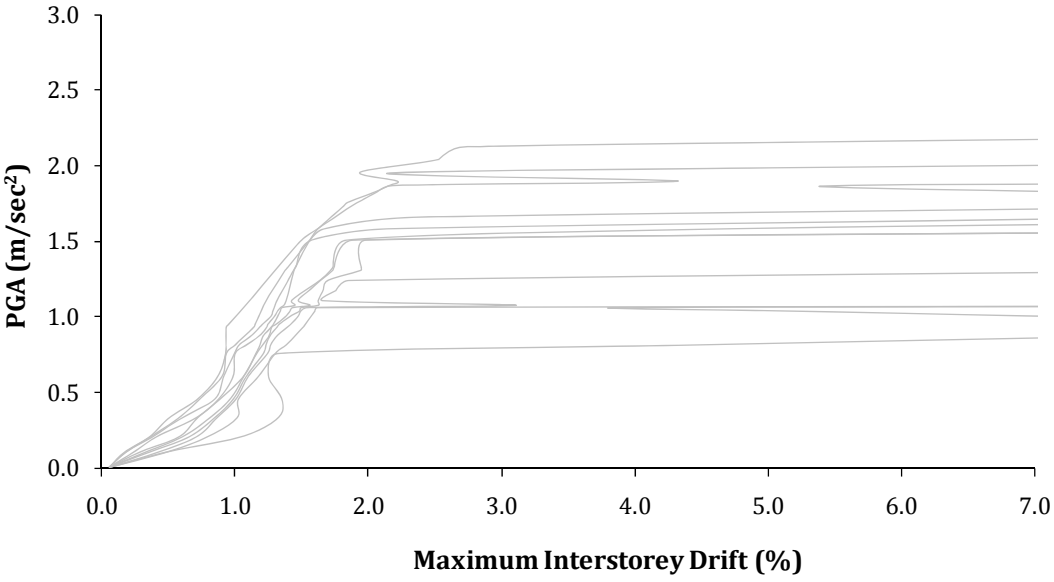

Figure 4.3. Median IDA curve of IDA curves for ten different earthquake records.

On the other hand, the damage may be quantified by using any of the EDPs whose values can be related to particular structural damage states. A number of available response-based EDPs were discussed and critically evaluated in the past for their applicability in seismic damage evaluation (Ghobarah et al., 1999). In the work by Ghobarah et al. (1999) the EDPs are classified into four categories: engineering demand parameters based on maximum deformation, engineering demand parameters based on cumulative damage, engineering demand parameters accounting for maximum deformation and cumulative damage, global engineering demand parameters. In the current study the maximum interstorey drift θ_{max} was chosen. The reason for selecting θ_{max} is because there is an established relation between interstorey drift values and performance-oriented descriptions such as immediate occupancy, life safety and collapse prevention (FEMA-273, 1997). Furthermore, there is a defined relation between drift ratio and damage-states (Ghobarah, 2004). A similar relation between damage-state and other damage indices is defined in this dissertation (see Chapter 2). Based on these relations in the last part of this chapter various PBD problems are formulated in order to define the most efficient damage indices for designing new structures.

IDA is based on the time step integration of each seismic record. Thus, different scaling factors are used for each seismic record and one IDA curve is associated to each seismic record. The median IDA capacity curve for a single structure is derived from the collection of the IDA curves of the whole range of the imposed seismic records. Figure 4.4 depicts three capacity curves corresponding to an RC frame, in which an IDA analysis was performed for

three different seismic records. It is obvious that the capacity curve depends not only on the type of the structure but also on the seismic record that is imposed on the structure. For lower values of the PGA in the vicinity of 0.4 g the response of the structure can be considered almost elastic and the inclination of the curves are almost constant. When the intensity level becomes higher the inclination of the capacity curves decreases in some cases and in other cases becomes higher due to hardening.

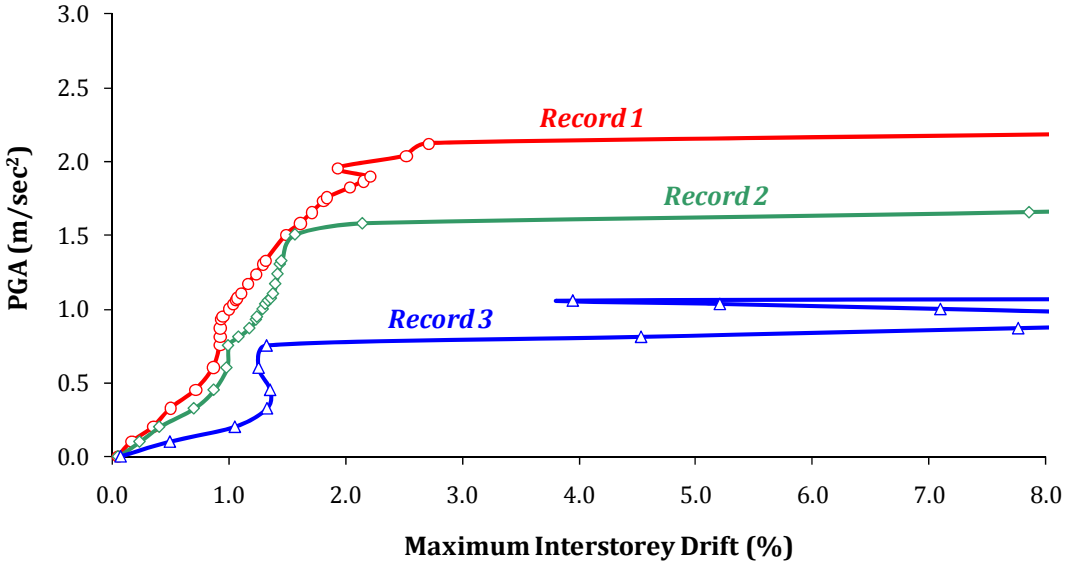

Figure 4.4. IDA curves for different records of seismic hazards.

The increase of the curves' inclination depends on the seismic record and the inelastic response of the structure. This is explained by the fact that as the record is scaled up, weak response cycles in the early part of the response time-history become strong enough to inflict damage (yielding) thus altering the properties of the structure for the subsequent, stronger cycles. For multi-storey buildings, a stronger ground motion may lead to earlier yielding of one floor which in turn acts as a fuse to relieve another (usually higher) one. Even simple oscillators when caused to yield in an earlier cycle, may be proven less responsive in later cycles that had previously caused higher DI values, as it is shown in Record 1 in Figure 4.4, possibly due to "period elongation". The same phenomena account for the structural resurrection, an extreme case of hardening, where a system is pushed all the way to global collapse (i.e. the analysis code cannot converge, producing "numerically infinite" values of the DIs) at some values of the IM, only to reappear as non-collapsing at a higher intensity level, displaying high response but still standing (e.g. Figure 4.4 – Record 3) (Vamvatsikos and Cornell, 2004).

Table 4.1. Limit states values defined by HAZUS (2003).

Maximum Inter-storey Drift	Limit State
$\theta_{max} \leq 0.5\%$	Slight Damage
$0.5\% \leq \theta_{max} \leq 1.0\%$	Moderate Damage
$1.0\% \leq \theta_{max} \leq 3.0\%$	Extensive Damage
$3.0\% \leq \theta_{max} \leq 8.0\%$	Collapse Limit State

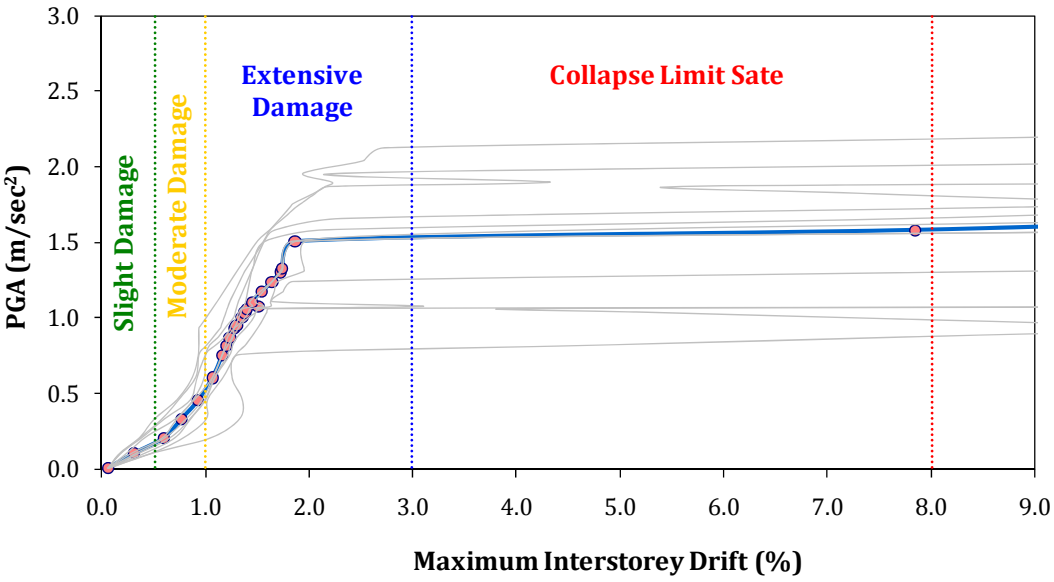

Figure 4.5. Median IDA curve and HAZUS (2003) recommended limit states.

For each seismic record 10 to 15 number of analysis are enough in order to develop an IDA curve. These runs are performed by using the hunt and fill tracing algorithm, described in detail by Vamvatsikos and Cornell (2004), which performs increasingly larger steps, attempting to bound the IM parameter space, and then fills in the gaps, both capacity and demand-wise (Vamvatsikos and Cornell, 2004). Hunt and fill tracing algorithm ensures that the record scaling levels are appropriately selected to minimize the number of required runs: Analyses are performed at rapidly increasing levels of IM until numerical nonconvergence is encountered (signaling global dynamic instability), while additional analyses are run at intermediate IM levels to sufficiently bracket the global collapse and increase the accuracy at lower IMs. The user only needs to specify the desired accuracy for demand and capacity, select the maximum tolerable number of dynamic analyses, and then wait for a few hours to get the results.

Since the collapse point is reached, additional runs are used to fill in the IDA at lower levels, being sequentially placed in the middle of the largest IM gaps. Thus the large gaps left by the initial increasing steps to the flatline are filled in; this step increases the demand resolution and, given enough runs, it ensures that the algorithm has not missed an earlier

collapse (Vamvatsikos and Cornell, 2004). For the estimation of the demanded performance levels, it is essential the limit states be defined on the IDA curves. For example in Figure 4.5 and Table 4.1 the four limit states are depicted for RC buildings according to HAZUS (2003).

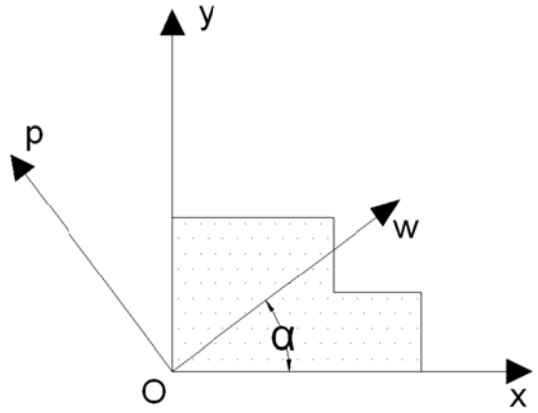

Figure 4.6. Definition of the incident angle α (Lagaros, 2010).

Multicomponent Incremental Dynamic Analysis

In order to take into account damage and other earthquake losses a reliable tool for estimating the capacity for any structural system in multiple earthquake hazard levels is required. Among others (Fajfar, 2000; Chopra and Goel, 2002), IDA (Vamvatsikos and Cornell, 2002) is considered as an analysis procedure for obtaining good estimates of the structural performance in the case of earthquake hazard and it is considered as an appropriate method. In view of the complexity and the computational effort required by the 3D models, that are employed to represent real buildings, simplified 2D structural simulations are implemented during the design procedure. This is mainly encountered in plan-symmetric buildings and mostly in the case of steel framed buildings since they are composed by 2D moment resisting frames. In 3D RC buildings, however, the columns belong to two or more intersecting lateral-force-resisting systems, therefore it is not possible to employ a 2D simulation since the bidirectional orthogonal shaking effects should be taken into account. Moreover, 3D models should also be considered in the case of plan-nonsymmetric steel or RC buildings are examined. IDA has mainly been implemented in 2D structures (Jalayer et al., 2007; Mander et al., 2007). MIDA, proposed by Lagaros (2010), is performed in a similar way of the 2D implementation of IDA, i.e. a suit of records is selected and for each record a MIDA representative curve is derived. The 50% fractile MIDA curve is then calculated using the representative curves of all the records. Selecting the IDA representative curve in its 2D implementation is, in most cases, a straightforward procedure. On the other hand, in its 3D implementation this is not an easy task, since the incident angle selected for applying the two components of the records might influence

considerably the product of MIDA, and consequently the results of design and assessment procedure. MIDA is performed over a set of record-incident angle pairs generated using the LHS (Olsson et al., 2003).

A structure subjected to the simultaneous action of two orthogonal horizontal ground accelerations along the directions *Ow* and *Op* is illustrated in Figure 4.6. The orthogonal system *Oxyz* defines the reference axes of the structure (structural axes). The angle defined with a counter clock wise rotation of the structural axis *Ox* to coincide with the ground motion axis *Ow* is called as incident angle of the record.

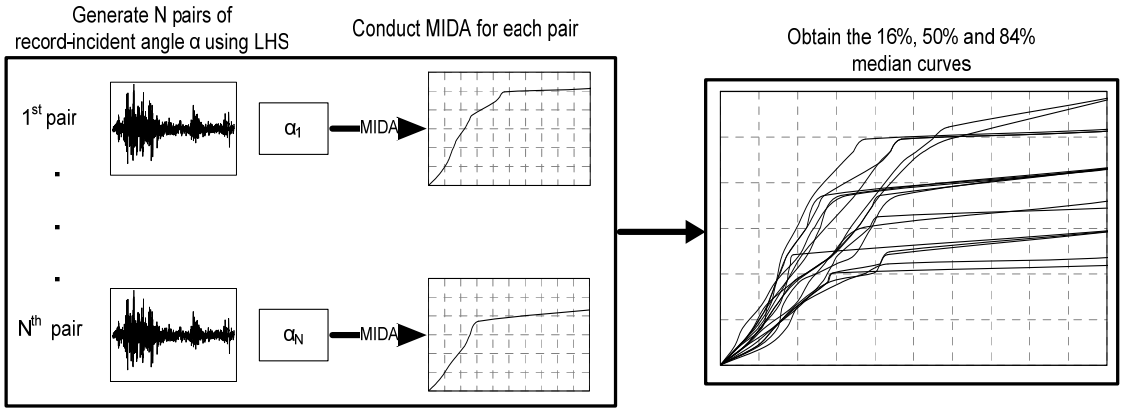

Figure 4.7. The MIDA procedure (Lagaros, 2010).

According to the MIDA framework a set of natural records, each one represented by its longitudinal and transverse components, are applied to the structure in order to account for the randomness on the seismic excitation. The difference of the MIDA procedure from the original component version of IDA, proposed by Vamvatsikos and Cornell (2002), stems from the fact that for each record a number of MIDA representative curves can be defined depending on the incident angle selected, while in most cases of the one component version of IDA only one IDA representative curve is obtained. MIDA is based on the idea of considering variable incident angle for each record, taking into account randomness both on the seismic excitation and the incident angle. In MIDA the relation of IM-EDP is defined similarly to the one component version of the IDA, i.e. both horizontal components of each record are scaled to a number of intensity levels to encompass the full range of structural behaviour from elastic to yielding that continues to spread leading finally to global instability. In order to preserve the relative scale of the two components of the records, the component of the record having the highest $S_A(T_1,5\%)$ is scaled first, while a scaling factor that preserves their relative ratio is assigned to the second component.

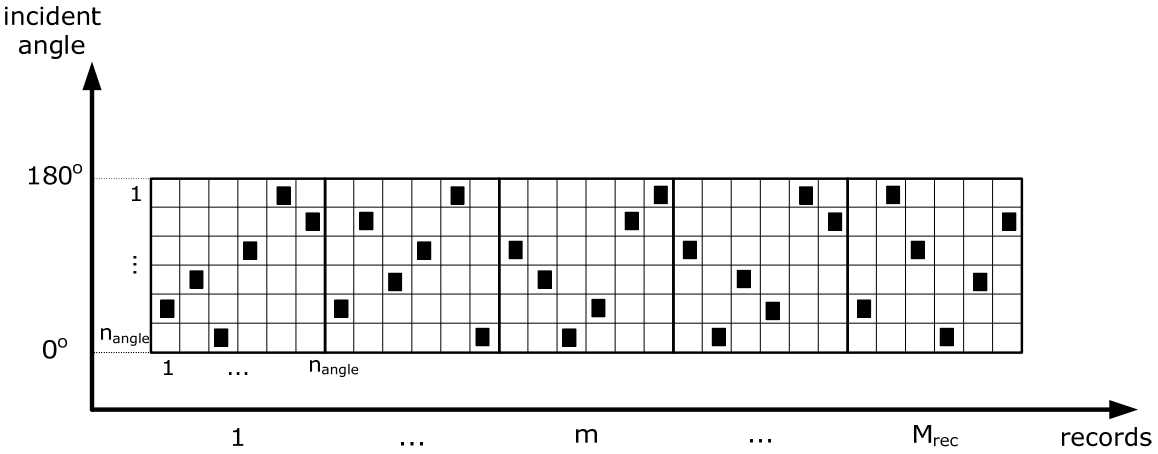

Figure 4.8. Latin hypercube sampling of record-incident angle pairs.

MIDA is implemented over a set of record-incident angle pairs. A schematic representation of its implementation can be found in Figure 4.7. According to MIDA a sample of N pairs of record-incident angles is generated by means of LHS (Olsson et al., 2003), MIDA is conducted for each pair and a representative curve is developed. Subsequently all these representative MIDA curves are used in order to define the 16%, 50% and 84% median curves. LHS is a strategy for generating random sample points ensuring that every part of the random space is represented. Latin hypercube samples are generated by dividing each random variable into N non-overlapping segments of equal probability. Thus, if M random variables are considered, the random variable space is partitioned into N^M cells. For each random variable, a single value is randomly selected from each segment, producing a set of N values. The values of each random variable are randomly matched with each other to create N samples. In the current implementation both record and incident angle are considered as uniformly distributed random variables over a set of M_{rec} records and in the range 0 to 180 degrees, respectively. In order to implement the proposed procedure the number of simulations N_{sim} (pairs of record-incident angle) should be a whole multiplier of the number of records M_{rec}. The number of incident angles combined with each record m=1, 2, ..., M_{rec} is equal to $n_{angle} = M_{rec}/N_{sim}$, hence for each record n_{angle} angles uniformly distributed in the range of 0 to 180 degrees are generated in order to define the N_{sim} pairs, this is schematically shown in Figure 4.8.

Multiple-Stripe Dynamic Analysis

Multiple-stripe analysis is a nonlinear dynamic analysis method that can be used for performance-based seismic assessment of structures for a wide range of ground motions and more than one performance levels. Similar to IDA the main objective of a MSDA study is to define a relation between the seismic intensity level and the corresponding maximum

response of the structural system. The intensity level and the structural response are described through an IM and an EDP, respectively. The method refers to groups of inelastic dynamic analyses (stripes) performed at multiple spectral acceleration levels (Figure 4.9), where at each stripe analysis a number of dynamic structural analyses are performed for a group of ground motion records that are scaled to a single value of spectral acceleration. The suite of ground motion records used for performing each stripe analysis should ideally be representative of the seismic threat at the corresponding spectral acceleration; however, it is common, but not necessarily always justified (e.g. Jalayer and Cornell, 2009), to use the same suite of records for all the spectral acceleration levels.

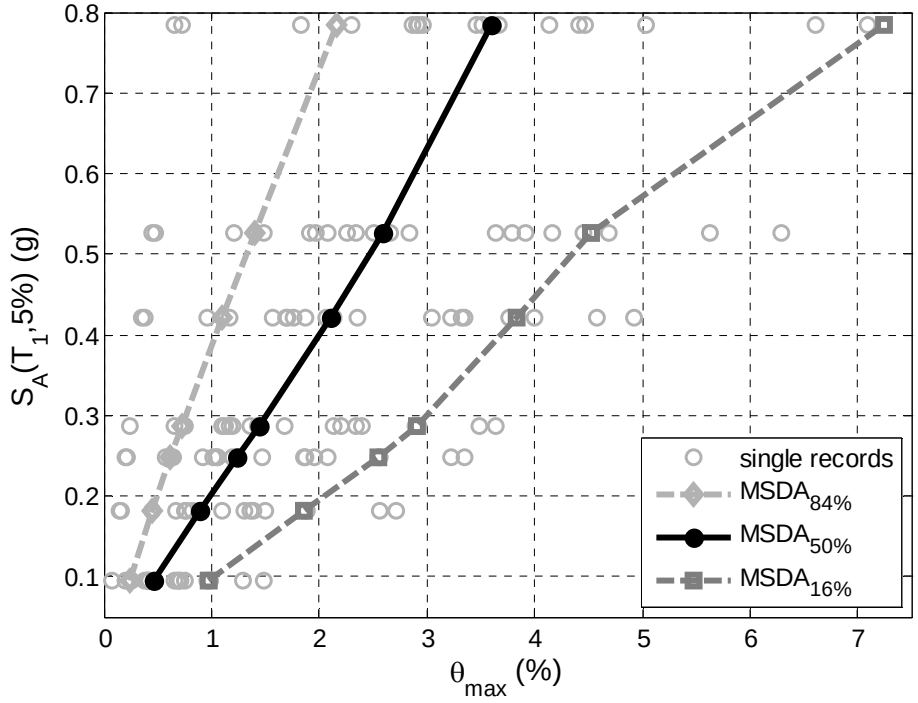

Figure 4.9. Multi-stripe dynamic analysis.

For a MSDA the intensity measure is usually the first mode spectral acceleration $S_A(T_1,5\%)$ for damping equal to 5%. The maximum inter-storey drift, as recommended by FEMA-350 (2000), is used in this study. Depending on the problem and the performance that is needed to be calculated different intensity measures and performance factors can also be used. In the case of the $S_A(T_1,5\%)$ intensity measure, two types of scaling can be used: scaling all ground motion records to the same value of spectral acceleration, or using a common scaling factor for all ground motion records (Vamvatsikos and Cornell, 2002). The $S_A(T_1,5\%)$ is calculated from the hazard curve of the area of interest.

Table 4.2. Natural records representing the 50% in 50 year hazard level (Somerville and Collins, 2002).

Earthquake	Station	Distance	Site
Honeydew (PT) 17 August 1991	Cape Mendocino	20	rock
	Petrolia	17	soil
Cape Mendocino (CM) 25 April 1992	Bunker Hill	8.8	rock
	Butler Valley	37	rock
	Centerville	16	soil
	Eureka College	21	soil
	Eureka School	24	soil
	Ferndale	14	soil
	Fortuna	13	soil
	Loleta	17	soil
	Rio Dell	13	soil
Cape Mendocino (C1) aftershock, 26 April 1992 0741GMT	Bunker Hill	27	rock
	Centerville	27	soil
	Eureka College	46	soil
	Eureka School	48	soil
	Ferndale	34	soil
	Fortuna	43	soil
	Loleta	41	soil
Cape Mendocino (C2) aftershock, 4/26/92 1118GMT	Bunker Hill	27	rock
	Centerville	28	soil
	Ferndale	34	soil
	Fortuna	43	soil

4.4. Assessment of seismic design procedures

Two are the main objectives of this investigation: (i) to examine a number of values of the behaviour factor q and compare the initial and life-cycle cost of a RC building designed to meet either the EAK (2000) ($q=3.5$) provisions or its variations depending on the value of the behavioural factor and (ii) to compare the EAK (2000) prescriptive design code with a performance-based seismic design procedure. The proposed PBD procedure employs three performance objectives.

4.4.1. Definition of Seismic Response Spectra

The most common approach for the definition of the seismic action is the use of design code response spectrum. This is a general approach which is easy to implement. However if a more realistic design is required the use of spectra derived from natural earthquake records is more appropriate. Since significant dispersion on the structural response, has been observed due to the use of different natural records, these spectra must be scaled to the

same desired earthquake intensity. The most commonly applied scaling procedure is based on the PGA.

Table 4.3. Natural records representing the 10% in 50 year hazard level (Somerville and Collins, 2002).

Earthquake	Station	Distance	Site
Tabas (TB) 16 September 1978	Dayhook	14	rock
	Tabas	1.1	rock
Cape Mendocino (CM) 25 April 1992	Cape Mendocino	6.9	rock
	Petrolia	8.1	soil
Chi-Chi (CC), Taiwan 20 September 1999	TCU052	1.4	soil
	TCU065	5.0	soil
	TCU067	2.4	soil
	TCU068	0.2	soil
	TCU071	2.9	soil
	TCU072	5.9	soil
	TCU074	12.2	soil
	TCU075	5.6	soil
	TCU076	5.1	soil
	TCU078	6.9	soil
	TCU079	9.3	soil
	TCU089	7.0	rock
	TCU101	4.9	soil
	TCU102	3.8	soil
	TCU129	3.9	soil

Table 4.4. Natural records representing the 2% in 50 year hazard level (Somerville and Collins, 2002).

Earthquake	Station	Distance	Site
Valparaiso (VL), Chile 3 May 1985	Vina del Mar	30	soil
	Zapaller	30	rock
Michoacan (MI), Mexico 19 September 1985	Caleta de Campos	12	rock
	La Union	22	rock
	La Villita	18	rock
	Zihuatenejo	21	rock

Table 4.5. Seismic hazard levels (Papazachos et al., 1993).

Event	Recurrence Interval	Probability of Exceedance	PGA (g)
Frequent	21 years	90% in 50 years	0.06
Occasional	72 years	50% in 50 years	0.11
Rare	475 years	10% in 50 years	0.31
Very Rare	2475 years	2% in 50 years	0.78

In this study three sets of natural records, i.e. sets with their longitudinal and their transverse components, are used. The records have been selected from the database of Somerville and Collins (2002). The basic characteristics of these records are provided in Tables 4.2, 4.3 and 4.4 corresponding to the three hazard levels, 50, 10 and 2 percent in 50 years, respectively. It can be seen that each record corresponds to different earthquake magnitudes and soil properties. The records are scaled to the same PGA in order to ensure compatibility between the records, according to the hazard curves for Greece obtained from the work of Papazachos et al. (1993) (Table 4.5). The response spectra for the 10% in 50 years scaled records are shown in Figures 4.10(a) and 4.10(b). It has been observed that the response spectra follow the lognormal distribution (Chintanapakdee and Chopra, 2003). Therefore the median spectra, also shown in Figures 4.10(a) and 4.10(b) are calculated from the above set of spectra using the following expression

$$\hat{x} = \exp\left[\frac{\sum_{i=1}^{n} \ln(R_{d,i}(T))}{n}\right] \tag{4.10}$$

where $R_{d,i}(T)$ is the response spectrum value for period equal to T of the i-th record (i=1,…,n). n = 22 for the 50% in 50 years hazard level, n = 19 for the 10% in 50 years and n = 6 for the 2% in 50 years.

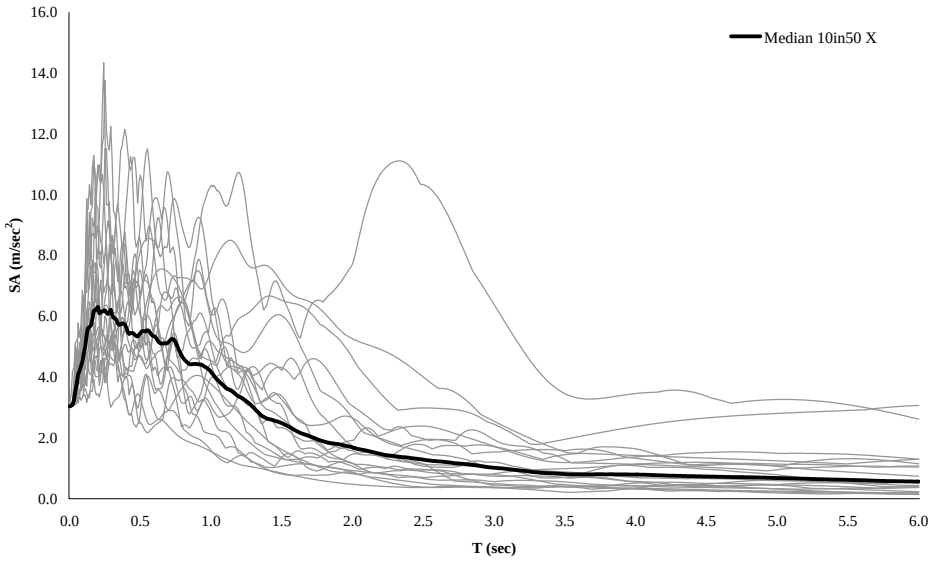

(a)

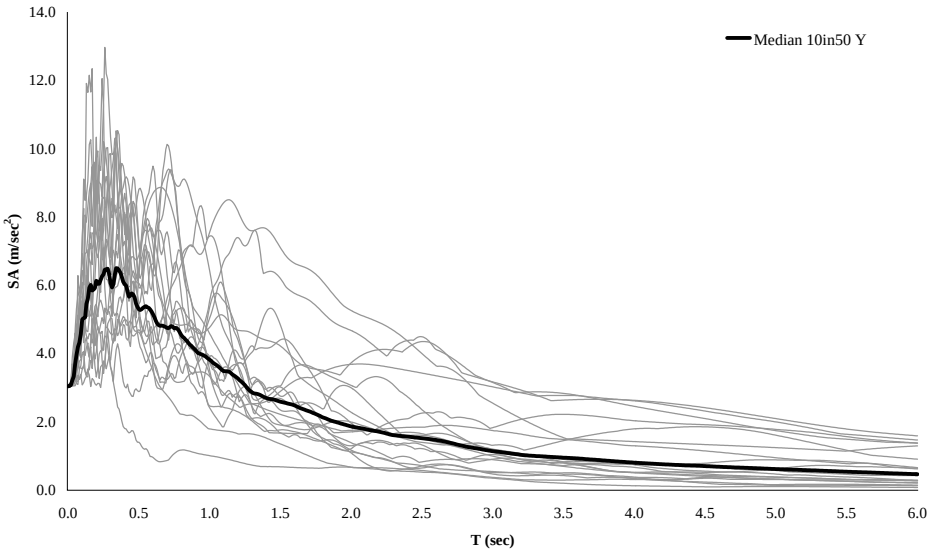

(b)

Figure 4.10. Response spectra and median (a) component X, (b) component Y for the records of Table 4.3.

4.4.2. Case study

The three storey 3D RC building, shown in Figure 4.11, has been employed for the comparative study performed in this work. The 3D RC building has been designed to meet the EKOS 2000 and EAK 2000 requirements for different values of the behaviour factor q ranging from 1.0 to 6.0 with a step size equal to 0.5. The lateral forces were derived from the design response spectrum (5%-damped elastic spectrum divided by the behaviour factor q) at the fundamental period of the building. Concrete of class C16/20 (characteristic cylindrical strength of 16MPa) and class S500 steel (yield stress of 500MPa) are assumed. The base shear is obtained from the response spectrum for soil type B (stiff soil $\theta = 1.0$, with characteristic periods $T_1 = 0.15$sec and $T_2 = 0.60$sec) and a PGA of 0.31 g. Moreover, the importance factor γ_I was taken equal to 1.0 (importance category Σ2), while damping correction factor is equal to 1.0, since a damping ratio of 5% has been considered (as it is suggested by EAK, 2000 for RC structures).

The slab thickness is equal to 15 cm and is considered to contribute to the moment of inertia of the beams with an effective flange width according to EKOS 2000. In addition to the self weight of the beams and the slab, a distributed dead load of 1.5 kN/m^2 due to floor finishing and movebale partitions and an imposed live load with nominal value of 2.0 kN/m^2 are considered. In the combination of gravity loads ("persistent design situation") nominal dead and live loads are multiplied with load factors of 1.35 and 1.5, respectively (Eq. 4.1).

Following EAK (2000), in the seismic design combination, dead loads are considered with their nominal value while live loads with 30% of the nominal value (Eq. 4.2).

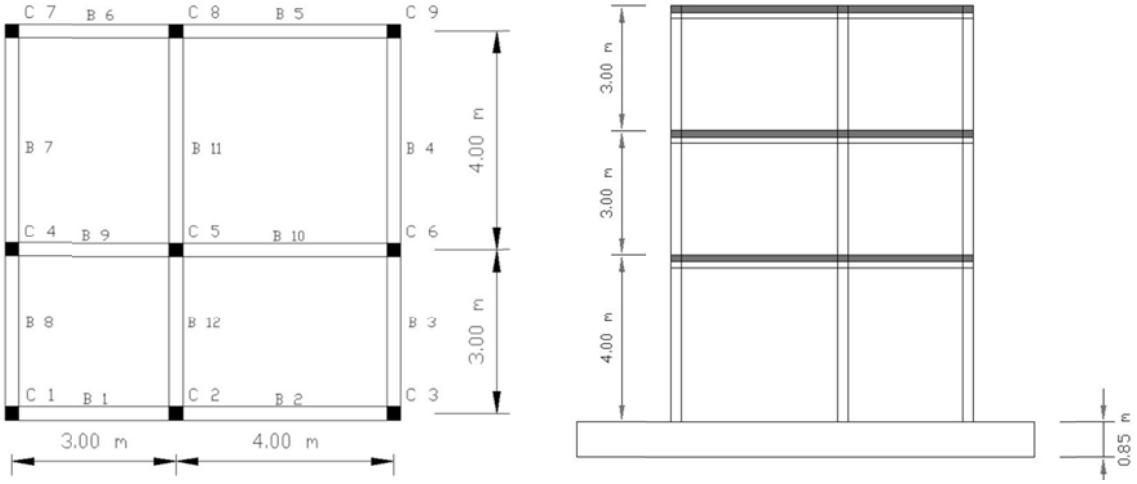

(a) (b)

Figure 4.11. Geometry of the three storey 3D building (a) layout, (b) front view.

4.4.3. Design with Greek national design codes and PBD

The parametric study resulted in eleven different designs depending on the value of the behavioural factor q, plus one design resulting from the proposed PBD procedure. Thus, in total twelve designs have been obtained. The design process both for the Greek design code and the PBD procedure started with the same initial design having the same minimum dimensions for the beams and the columns. The minimum dimensions that have been considered were the following: columns 25x25 cm^2 and beams 25x30 cm^2. The dimensions of the columns and the beams were increased until the fulfilment of the requirements and provisions of either the EAK 2000 for the current value of the behaviour factor q or the requirements of the proposed PBD procedure. Beams and columns that fail to meet the constraints imposed by EAK and EKOS design codes were increased in size according to the following procedure: (i) *columns*: increase the size of the smallest dimension by 5 cm and if column constraints are not yet satisfied increase the size of the second dimension by 5 cm, this rule is processed until satisfying all the constraints, (ii) *beams*: increase the size of the height of the beam by 5 cm and if constraints are not yet satisfied the width of the web is increased by 5 cm (the width of the web was restricted not to exceed 35 cm) until satisfying all the constraints. While for both beam and columns the longitudinal steel reinforcement was increased by 0.5%. Furthermore, the lower and upper bounds for steel reinforcement quantities and cross-section dimensions imposed by the codes are implemented in all designs; while depending on the behavioural factor value the proper design checks are implemented. For example, in the case of $q \leq 1.5$ no capacity checks are implemented, while for $q \geq 3.5$ capacity design is considered. For the case that $1.5 < q < 3.5$, although no

guidelines are provided by EAK (2000), capacity design is also considered. A similar procedure was followed for the case of the PBD starting with same initial design, the only requirement imposed by the PBD procedure are those of the *Step 1* and *Step 2* described in subsection 4.2.4.

Table 4.6. Comparison of steel and concrete quantities in the twelve designs.

Design procedure	Columns		Beams	
	Steel (kg.)	Concrete (m^3)	Steel (kg.)	Concrete (m^3)
$D_{q=1}$	12700	32	6940	27
$D_{q=1.5}$	10030	26	5330	21
$D_{q=2}$	7720	21	4180	17
$D_{q=2.5}$	6510	18	3490	15
$D_{q=3}$	5730	15	3170	13
$D_{q=3.5}$	5210	15	2640	13
$D_{q=4}$	4600	14	2490	11
$D_{q=4.5}$	4280	14	2260	11
$D_{q=5}$	4010	12	2140	11
$D_{q=5.5}$	3870	12	2050	10
$D_{q=6}$	3750	11	1940	10
D_{PBD}	8657	17	4685	14

Table 4.7. Detailed breakdown comparison of steel quantity (kg) in the four selected designs.

Design procedure	Columns		Beams	
	Longitudinal	Transverse	Longitudinal	Transverse
$D_{q=1}$	10207	2493	4696	2244
$D_{q=3.5}$	4344	866	1958	682
$D_{q=6}$	3473	277	1627	313
D_{PBD}	6787	1870	3304	1381

In the first part of this study a comparative analysis with the objective to the steel and concrete quantities is performed. Table 4.6 compares the weight of the steel and the concrete quantities required for the eleven designs obtained using the Greek national design codes and the design obtained based on the proposed PBD procedure. The quantities accounted in Table 4.6 are related to the initial cost of the structure that will be examined in the second part of this study. In order to evaluate the performance of the different designs achieved, four characteristic designs were selected. These designs correspond to the two extreme designs with respect to the value of the behaviour factor *q*. The first extreme design, denoted as $D_{q=1}$, is the one corresponding for q=1 (permitting linear behaviour only) and the second extreme design is denoted as $D_{q=6.0}$, corresponding to the largest value of the behaviour factor examined in this study. The third design that is employed, denoted as $D_{q=3.5}$, corresponds to the design obtained for q=3.5 that is the behavioural factor suggested by

EAK 2000 for this type of structures, while the fourth design, denoted as D_{PBD}, corresponds to the design obtained with the PBD procedure.

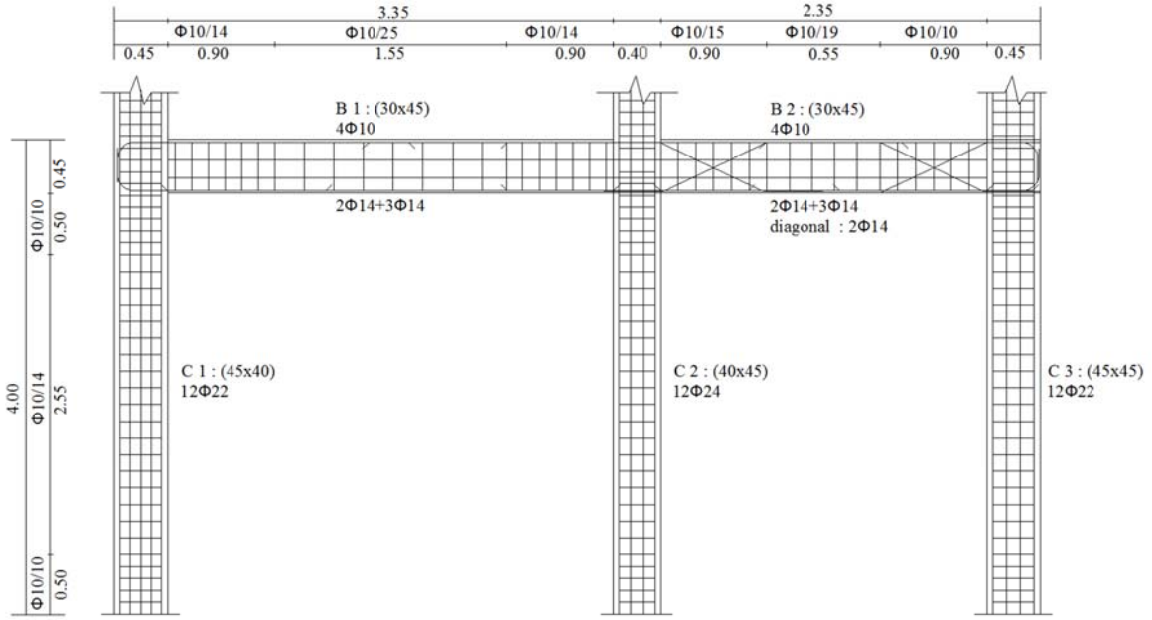

Figure 4.12. Design $D_{q=3.5}$, beam-column reinforcement of a typical frame.

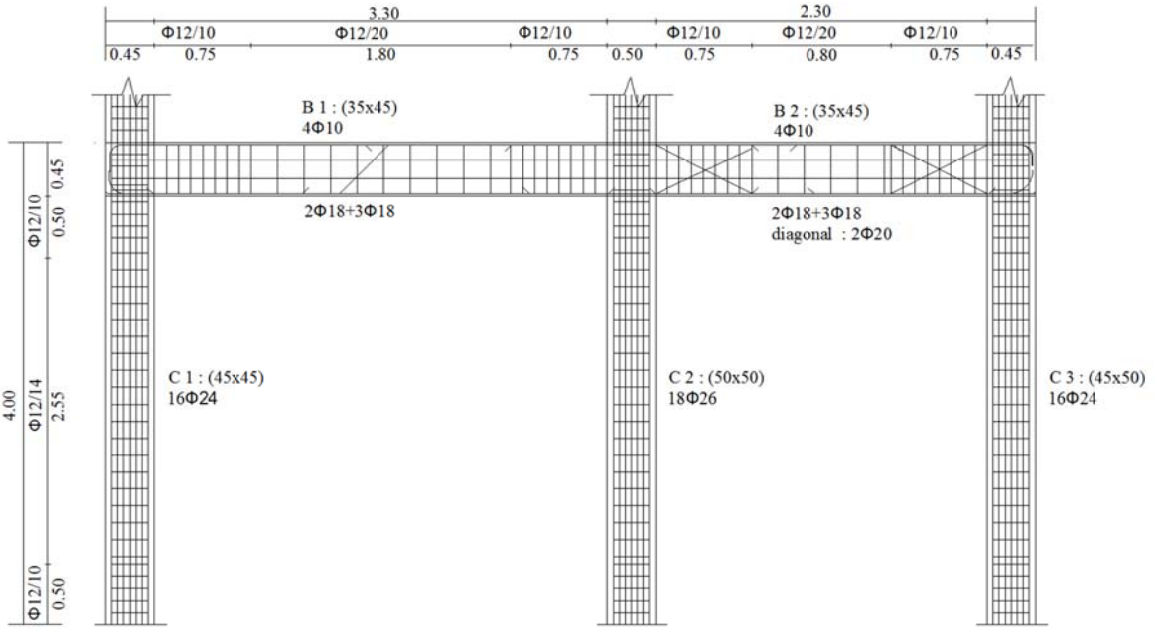

Figure 4.13. Design D_{PBD}, beam-column reinforcement of a typical frame.

The final reinforcement for the $D_{q=3.5}$ and D_{PBD} designs are shown in Figures 4.12 and 4.13, respectively. In Table 4.7 details on the required longitudinal and transverse reinforcement is also provided. D_{PBD} design requests in approximately 30% less longitudinal reinforcement compared to the $D_{q=1}$, while it requests 50% and 35% more compared to the $D_{q=6}$ and $D_{q=3.5}$ designs, respectively. On the other hand D_{PBD} design requires approximately 25% less transverse reinforcement compared to the $D_{q=1}$, while it requires 85% and 70%

more compared to the $D_{q=6}$ and $D_{q=3.5}$ designs, respectively. It should be noted that the findings regarding the initial cost of the design $D_{q=1}$ are in accordance to the results reported by Avramidis *et al.* (2003).

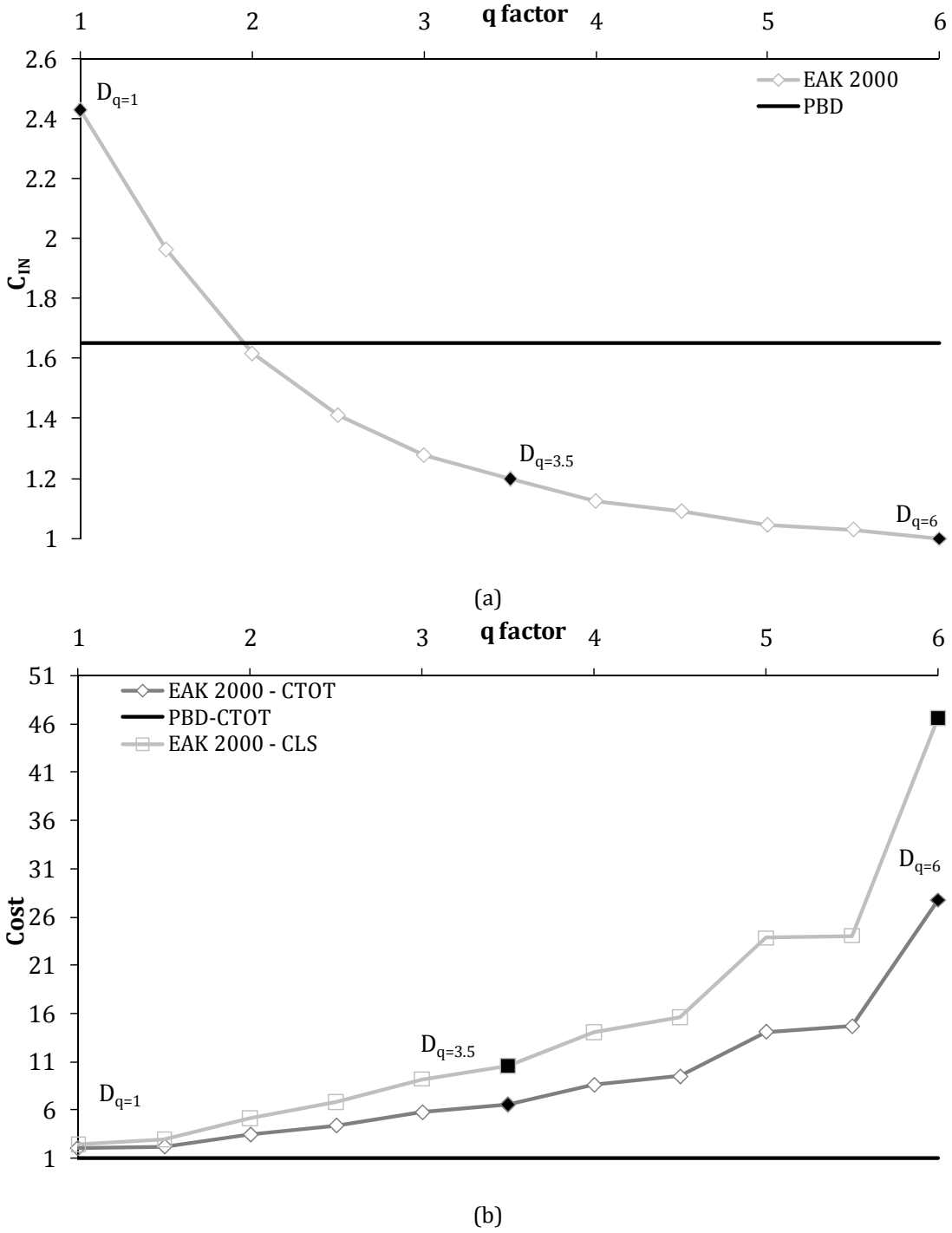

Figure 4.14. Comparison of the designs with respect to (a) the normalized initial, (b) the normalized limit state and total cost.

4.4.4. Comparison with respect to the total cost

In the second part of this study a comparative study with respect to the initial cost is performed. The initial cost is related to the material and the labour cost for the construction

of the building which includes concrete, steel reinforcement, labour cost for placement and the nonstructural components cost. In Figure 4.14 the initial, life-cycle and total cost for each of the twelve designs, are presented. The designs obtained using the EAK 2000 procedure depict, as expected, a reverse trend on the value of the initial and life-cycle cost. $D_{q=6}$ corresponds to the cheapest design with respect to the initial cost, but to the most expensive one with respect to the life-cycle cost, on the other hand, the second extreme design $D_{q=1}$ corresponds to the most expensive design with respect to the initial cost but to the cheapest one with respect to the life-cycle cost. Among the twelve designs, $D_{q=6}$ is the cheapest one with respect to the initial cost, $D_{q=1}$ with respect to the life-cycle cost while D_{PBD} with respect to the total cost.

The code-conforming design obtained according to the EAK (2000) provisions. $D_{q=3.5}$, will be used as the reference point design. $D_{q=3.5}$ is cheaper, with respect to the initial cost, by 51% compared to $D_{q=1}$ and by 27% compared to D_{PBD}, while it is more expensive by 16.5% compared to the $D_{q=6}$. As it can be seen from Figure 4.14 the initial cost for a RC structure, designed to permit elastic behaviour for the response spectrum of the Greek national seismic code ($D_{q=1}$), is not prohibitive. On the other hand $D_{q=3.5}$ is more expensive, with respect to the life-cycle cost, by 77% compared to $D_{q=1}$ and by 91% compared to D_{PBD}, while it is cheaper by 77% compared to the $D_{q=6}$. Ending the comparison $D_{q=3.5}$ is more expensive, with respect to the total cost, by 68% compared to $D_{q=1}$ and by 85% compared to D_{PBD}, while it is cheaper by 76% compared to the $D_{q=6}$. As it can be observed from Figure 4.14(b) the optimum value of the behavioural factor, for the test example considered, lies between *q=1* and *q=1.5*. It can also be seen, from this comparative study, that the life-cycle cost is the dominant part of the total cost. The life-cycle cost contains information about the performance of the design in future earthquake events which is the most crucial factor when designing a building to withstand against earthquake hazard.

4.4.5. Discussion

In this part of the chapter a parametric study has been performed in order to assess the design obtained using either the 2000 Greek national design codes or a performance-based design procedure where three performance objectives are considered. In the case of the 2000 Greek national seismic design code a linear static analysis procedure has been used, while in the performance-based design procedure the nonlinear static analysis procedure has been implemented in order to determine the damage levels for different earthquake intensities. The two design procedures have been applied for the design of a 3D RC building. For the test example considered it has been shown that when designing with the behaviour

factor suggested by the 2000 Greek national seismic design code the resulting design will be more vulnerable to future earthquakes leading to a much higher total cost compared to the design obtained with the performance-based procedure or the design obtained according to the Greek national seismic design code using a behavioural factor between 1 to 1.5. It has also been demonstrated how the concept of performance-based design can be integrated in a structural design procedure in order to obtain a design that fulfil the provisions of contemporary design codes like the three performance objectives employed in this study. Even though these conclusions cannot be generalized, it is an indication about the performance of the designs according to a prescriptive design code and to a performance-based design procedure.

4.5. Structural Optimization: An assessment approach of design procedures against earthquake hazard

A number of studies have been performed in the past dealing with structural optimization of RC structures. One of the earliest studies on this subject is the work by Frangopol (1986) where the general formulation of the deterministic optimization problem was reviewed and a reliability-based optimization approach for the design of both steel and RC framed structures was presented. Moharrami and Grierson (1993) presented a computer-based method for the optimal design of RC buildings, where the width, depth and longitudinal reinforcement of member sections are considered as design variables. A review on the design of concrete structures can be found in the work by Sarma and Adeli (1998), where it was concluded that there is a need to perform further research on cost optimization of realistic three-dimensional structures with hundreds of members, where optimization can result in substantial savings. In the work by Li and Cheng (2001) the optimal decision model of the target value of performance-based structural system reliability of RC frames is established according to the cost-effectiveness criterion. Chan and Zou (2004) presented an optimization technique for the elastic and inelastic drift performance-based design of reinforced concrete buildings, while Lagaros and Papadrakakis (2007) critically assessed the designs of a 3D reinforced concrete building, obtained according to the European seismic design code and a performance-based design procedure, in the framework of a multi-objective optimization problem. The results revealed that the designs based on the European seismic design code violated safety requirements for different hazard levels. The main objective of this part of the chapter is to examine the validity of the behaviour factor q in designing safe and economic RC structures using Eurocode 2 (2004) and Eurocode 8

(2004). Numerical tests are performed on two different types of RC structures, a mid-rise irregular one and a high-rise regular one. The evaluation is performed on the basis of the initial cost optimally designed to meet the EC2 (2004) and EC8 (2004) provisions.

4.5.1. Formulation of the optimization problem

The mathematical formulation of the optimization problem considered in the present work is defined as follows:

$$\begin{aligned} &\min_{\mathbf{s}\in F} && C_{IN}(\mathbf{s}) \\ &\text{where} && C_{IN}(\mathbf{s}) = C_b(\mathbf{s}) + C_{sl}(\mathbf{s}) + C_{cl}(\mathbf{s}) + C_{ns}(\mathbf{s}) \\ &\text{subject to} && g_j^{SERV}(\mathbf{s}) \le 0 \quad j = 1,...,m \\ & && g_j^{ULT}(\mathbf{s}) \le 0 \quad j = 1,...,k \end{aligned} \tag{4.11}$$

where **s** represents the design vector corresponding to the dimensions of columns and beams cross-sections, F is the feasible region where all the serviceability and ultimate constraint functions (g^{SERV} and g^{ULT}) are satisfied. In this work the boundaries of the feasible region are defined according to the recommendations of the EC8. The objective function considered is the total initial construction cost of the structure C_{IN}, while $C_b(\mathbf{s})$, $C_{sl}(\mathbf{s})$, $C_{cl}(\mathbf{s})$ and $C_{ns}(\mathbf{s})$ correspond to the total initial construction cost of beams, slabs, columns and non-structural elements, respectively. The term "initial cost" of a new structure corresponds to the cost just after construction. The initial cost is related to material, which includes concrete, steel reinforcement, and labour costs for the construction of the building. The solution of the resulting optimization problem is performed by means of EA. The optimization procedure was implemented for four characteristic values of behaviour factor *q* in two different buildings resulting into eight optimum designs. In all eight cases the design procedure was based on linear elastic static analysis according to EC8. The designs obtained through the optimization procedure are assessed by performing life-cycle cost analysis.

Table 4.8. Five storey test example - Optimum designs obtained for different values of behaviour factor q.

		Optimum Designs			
		q=1	**q=2**	**q=3**	**q=4**
Columns	**h1×b1**	0.80×0.80, LR: 34Ø32, TR: (4)Ø10/10cm	0.60×0.60, LR:8Ø24+ 12Ø28, TR: (4)Ø10/20cm	0.55×0.55, LR:8Ø20+ 12Ø24, TR: (2)Ø10/20cm	0.55×0.55, LR:8Ø24+ 4Ø28, TR: (2)Ø10/20cm
	h2×b2	0.85×0.85, LR: 34Ø32, TR: (4)Ø10/10cm	0.60×0.60, LR:8Ø24+ 12Ø28, TR: (4)Ø10/20cm	0.55×0.55, LR:8Ø22+ 12Ø26, TR: (2)Ø10/20cm	0.55×0.55, LR:8Ø24+ 4Ø28, TR: (2)Ø10/20cm
	h3×b3	0.80×0.80, LR: 28Ø32, TR:	0.60×0.60, LR:8Ø24+ 12Ø28,	0.50×0.50, LR:4Ø22+ 12Ø26,	0.50×0.50, LR:4Ø26+ 4Ø32, TR:

		(4)Ø10/10cm	TR: (4)Ø10/20cm	TR: (2)Ø10/20cm	(2)Ø10/20cm
	h4×b4	0.70×0.70, LR:8Ø22+ 12Ø26, TR: (4)Ø10/10cm	0.55×0.55, LR:8Ø24+ 12Ø28, TR: (4)Ø10/20cm	0.55×0.55, LR:8Ø18+ 4Ø22, TR: (2)Ø10/20cm	0.55×0.55, LR:8Ø18+ 4Ø22, TR: (2)Ø10/20cm
	h5×b5	0.70×0.70,LR: 26Ø32, TR: (4)Ø10/10cm	0.55×0.55, LR:4Ø28+ 8Ø24, TR: (4)Ø10/20cm	0.55×0.55, LR:8Ø24+ 4Ø28, TR: (2)Ø10/20cm	0.55×0.55, LR:8Ø20+ 4Ø24, TR: (2)Ø10/20cm
	h6×b6	0.70×0.70, LR: 24Ø32, TR: (4)Ø10/10cm	0.50×0.55, LR:12Ø28+ 8Ø24, TR: (4)Ø10/20cm	0.45×0.45, LR:4Ø24+ 4Ø28, TR: (2)Ø10/20cm	0.45×0.45, LR:4Ø26+ 4Ø32, TR: (2)Ø10/20cm
	h7×b7	0.65×0.65, LR:15Ø18+ 16Ø20, TR: (4)Ø10/10cm	0.35×0.60, LR:8Ø18+ 8Ø20, TR: (2)Ø10/20cm	0.35×0.55, LR:7Ø16+ 5Ø20, TR: (2)Ø10/20cm	0.50×0.30, LR:5Ø18+ 6Ø16, TR: (2)Ø10/20cm
	h8×b8	0.60×0.65, LR:24Ø20+ 20Ø18, TR:(4)Ø10/10cm	0.40×0.60, LR: 18Ø18, TR: (2)Ø10/20cm	0.35×0.55, LR:8Ø18+ 5Ø20, TR: (2)Ø10/20cm	0.55×0.30, LR:8Ø18, TR: (2)Ø10/20cm
Beams	**h9×b9**	0.45×0.55,LR: 15Ø20, TR: (2)Ø10/10cm	0.30×0.50, LR: 9Ø18, TR: (2)Ø10/20cm	0.30×0.55, LR:3Ø20+ 4Ø14, TR: (2)Ø10/20cm	0.25×0.45, LR:4Ø16+ 4Ø14, TR: (2)Ø10/20cm
	h10×b10	0.50×0.55, LR: 24Ø18, TR: (2)Ø8/15cm	0.30×0.55, LR: 10Ø18, TR: (2)Ø8/15cm	0.30×0.55, LR:6Ø20, TR: (2)Ø8/15cm	0.25×0.45, LR:4Ø16, TR: (2)Ø8/15cm
$C_{IN,\ RC\ Frame}$ (1000 €)		1.85E+02	1.32E+02	1.11E+02	9.62E+01
C_{IN} (1000 €)		8.10E+02	7.57E+02	7.36E+02	7.21E+02

In this investigation, two 3D RC MRF buildings have been considered in order to study the influence of the behaviour factor *q* on the design of RC buildings. The first test example is a five storey RC building with non-symmetrical plan view while the second one is an eight storey RC building having symmetrical plan view. Both buildings have been designed to meet the Eurocode requirements, i.e. the EC8 (2004) and EC2 (2004) design codes. Concrete of class C20/25 (nominal cylindrical strength of 20 MPa) and class S500 steel (nominal yield stress of 500 MPa) are assumed. The base shear is obtained from the response spectrum for soil type B (characteristic periods T_B = 0.15 sec, T_C = 0.50 sec and T_D = 2.00 sec) while the PGA considered is equal to 0.31 g. Moreover, the importance factor γ_I was taken equal to 1.0, while the damping correction factor is equal to 1.0, since a damping ratio of 5% has been considered.

The slab thickness is equal to 15 cm, for both test examples, while it is considered to contribute to the moment of inertia of the beams with an effective flange width. In addition to the self weight of beams and slabs, a distributed permanent load of 2 kN/m^2 due to floor finishing-partitions and an imposed load with nominal value of 1.5 kN/m^2, are considered. The nominal permanent and imposed loads are multiplied by load factors of 1.35 and 1.5, respectively. Following EC8, in the seismic design combination, dead loads are considered with their nominal values, while live loads with the 30% of their nominal value.

In both test examples the parametric study is performed in two stages: (i) design based on structural optimization and (ii) assessment of the designs. In the first stage the optimum

design is computed employing the ES(μ+λ) optimization scheme (more details can be found in Chapter 3) with ten parent and offspring (μ=λ=10) design vectors for both test examples. Four optimization problems are defined, following the design recommendations of EC8 and EC2, according to the value of the behaviour factor considered. The optimum designs obtained are labelled as $D_{q=i}$ defining the value of the behaviour factor used. In all formulations the initial construction cost is the objective function to be minimized. The columns and beams are of rectangular cross-sectional shape, and are separated into groups. The two dimensions of the columns/beams along with the longitudinal, transverse reinforcement and its spacing are the five design variables that are assigned to each group of the columns/beams. In the second stage, life-cycle cost analysis is performed on the optimum designs by means of nonlinear dynamic analysis where the beam-column members are modelled with the inelastic force-based fibre element (Papaioannou et al., 2005).

4.5.2. Five storey non-symmetrical test example

The plan and front views of the five storey non-symmetrical test example are shown in Figure 4.15. The structural elements (beams and columns) are separated into 10 groups, 8 for the columns and 2 for the beams, resulting into 50 design variables. The optimum designs achieved for different values of the q factor are presented in Table 4.8. It can be seen that the initial construction cost of design $D_{q=1}$ is increased by the marginal quantity of 7% compared to $D_{q=2}$, while it is 10% and 12% more expensive compared to $D_{q=3}$ and $D_{q=4}$, respectively. It can therefore be said that the initial cost of RC structures, designed on the basis of their elastic response for the design earthquake, is not excessive taking into consideration the additional costs of a building structure which are practically the same for all designs q=1 to 4. When the four designs are compared with respect to the cost of the RC skeletal members, design $D_{q=1}$ is increased by 40% compared to $D_{q=2}$ and by 67% and 92% compared to $D_{q=3}$ and $D_{q=4}$, respectively.

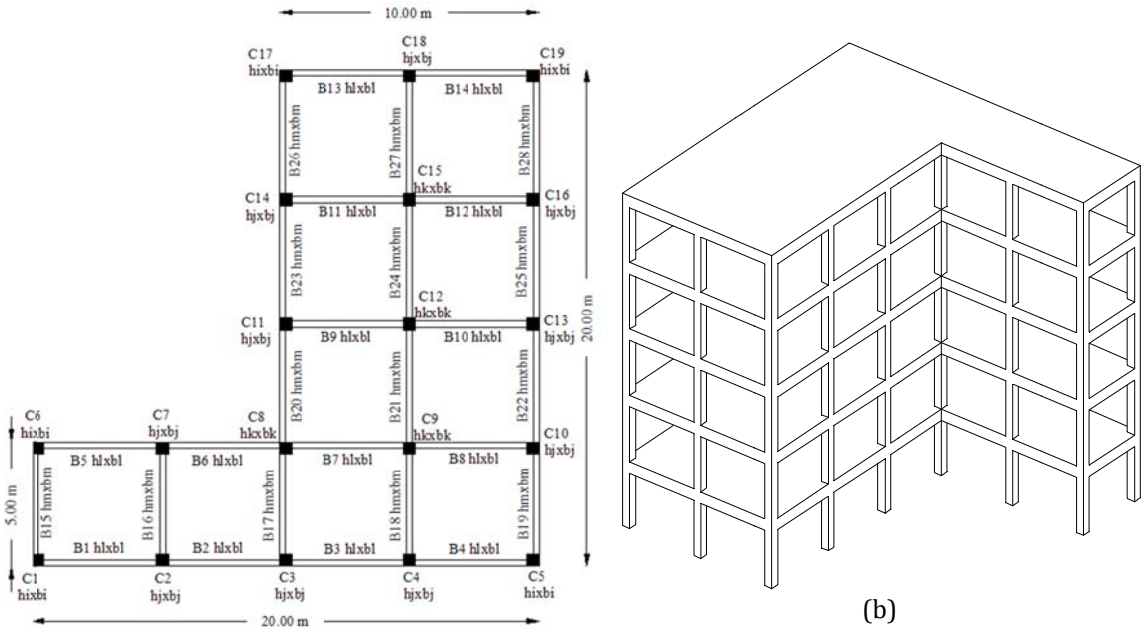

Figure 4.15. Five storey test example - (a) plan view, (b) front view.

4.5.3. Eight storey symmetrical test example

The plan and front views of the eight storey symmetrical test example are shown in Figure 4.16. The structural elements (beams and columns) are separated into 14 groups, 12 groups for the columns and 2 for the beams, resulting into 70 design variables. The optimum designs achieved for different values of the q factor are presented in Table 4.9. It can be seen that, with respect to total initial cost design $D_{q=1}$ is increased by the marginal quantity of 3% compared to $D_{q=2}$ and by 10% and 15% compared to $D_{q=3}$ and $D_{q=4}$, respectively. In the case when the four designs are compared with reference to the cost of the RC skeletal members alone, design $D_{q=1}$ is increased by 12% compared to $D_{q=2}$ and by 65% and 95% compared to $D_{q=3}$ and $D_{q=4}$, respectively. Confirming the results of the first test example, it can be also seen that the initial construction cost of RC structures designed based on elastic response for the design earthquake is by no means prohibitive.

Table 4.9. Eight storey test example - Optimum designs obtained for different values of behaviour factor q.

		Optimum Designs			
		q=1	**q=2**	**q=3**	**q=4**
Columns	**h1×b1**	1.35×1.35, LR: 88Ø30, TR: (5)Ø10/10cm	0.80×0.75, LR: 26Ø32, TR: (4)Ø10/15cm	0.80×0.60, LR: 24Ø28, TR: (4)Ø10/20cm	0.80×0.60, LR:10Ø24+ 12Ø28, TR: (2)Ø10/20cm
	h2×b2	0.90×0.85, LR: 34Ø30, TR: (4)Ø10/10cm	0.80×0.80, LR: 30Ø32, TR: (4)Ø10/10cm	0.65×0.60, LR: 26Ø28, TR: (4)Ø10/20cm	0.75×0.35, LR:8Ø22+ 12Ø26, TR: (2)Ø10/20cm
	h3×b3	1.05×1.10, LR: 50Ø30, TR: (4)Ø10/10cm	0.80×0.80, LR: 30Ø32, TR: (4)Ø10/10cm	0.75×0.65, LR: 28Ø28, TR: (4)Ø10/20cm	0.75×0.70, LR:10Ø22+ 12Ø26, TR: (2)Ø10/20cm

	h4×b4	1.10×1.05, LR: 60Ø30, TR: (4)Ø10/10cm	0.80×0.85, LR: 32Ø32, TR: (4)Ø10/10cm	0.75×0.65, LR: 30Ø28, TR: (4)Ø10/15cm	0.70×0.65, LR:8Ø26+ 12Ø32, TR: (2)Ø10/20cm
	h5×b5	0.85×0.85, LR: 36Ø30, TR: (4)Ø10/10cm	0.65×0.65, LR:8Ø22+ 12Ø26, TR: (4)Ø10/10cm	0.65×0.55,LR:8Ø24+ 4Ø26, TR: (2)Ø10/20cm	0.60×0.55, LR:8Ø20+ 4Ø24, TR: (2)Ø10/20cm
	h6×b6	0.80×0.80, LR: 36Ø30, TR: (4)Ø10/10cm	0.65×0.65, LR: 22Ø32, TR: (2)Ø10/10cm	0.55×0.55, LR:8Ø24+ 12Ø28, TR: (2)Ø10/20cm	0.55×0.40, LR:6Ø22+ 12Ø26, TR: (2)Ø10/20cm
	h7×b7	0.85×0.85, LR: 36Ø30, TR: (4)Ø10/10cm	0.65×0.65, LR: 24Ø32, TR: (2)Ø10/10cm	0.75×0.50, LR: 24Ø28, TR: (2)Ø10/20cm	0.75×0.55, LR:10Ø22+ 12Ø26, TR: (2)Ø10/20cm
	h8×b8	0.85×0.85, LR: 40Ø30, TR: (4)Ø10/10cm	0.70×0.70, LR: 24Ø32, TR: (4)Ø10/10cm	0.55×0.60, LR: 22Ø28, TR: (2)Ø10/20cm	0.55×0.55, LR:8Ø24+ 12Ø28, TR: (2)Ø10/20cm
	h9×b9	0.60×0.60, LR: 8Ø26+ 12Ø30, TR: (4)Ø10/10cm	0.65×0.65, LR:8Ø22+ 4Ø26, TR: (4)Ø10/10cm	0.55×0.55, LR:8Ø18+ 4Ø22, TR: (2)Ø10/20cm	0.60×0.55, LR:8Ø20+ 4Ø24, TR: (2)Ø10/20cm
	h10×b10	0.75×0.75, LR: 28Ø30, TR: (4)Ø10/10cm	0.65×0.65, LR:8Ø22+ 12Ø26, TR: (4)Ø10/10cm	0.55×0.50, LR:6Ø20+ 12Ø28, TR: (2)Ø10/20cm	0.50×0.35, LR:4Ø26+ 4Ø32, TR: (2)Ø10/20cm
	h11×b11	0.75×0.75, LR: 28Ø30, TR: (4)Ø10/10cm	0.65×0.65, LR:8Ø26+ 12Ø32, TR: (4)Ø10/10cm	0.50×0.50, LR:4Ø22+ 12Ø26, TR: (2)Ø10/20cm	0.45×0.45, LR:4Ø22+ 12Ø26, TR: (2)Ø10/20cm
	h12×b12	0.80×0.80, LR: 34Ø30, TR: (4)Ø10/10cm	0.65×0.65, LR:8Ø26+ 12Ø32, TR: (4)Ø10/10cm	0.55×0.55, LR:8Ø22+ 12Ø26, TR: (2)Ø10/20cm	0.55×0.55, LR:8Ø24+ 4Ø28, TR: (2)Ø10/20cm
Beams	**h13×b13**	0.60×0.60, LR: 26Ø20+ 35Ø18, TR: (2)Ø8/15cm	0.65×0.65, LR:31Ø20, TR: (2)Ø8/15cm	0.55×0.55, LR:11Ø18+ 10Ø20, TR: (2)Ø8/15cm	0.60×0.55, LR:6Ø18+ 5Ø20, TR: (2)Ø8/15cm
	h14×b14	0.75×0.75, LR: 26Ø20+ 35Ø18, TR: (2)Ø8/15cm	0.65×0.65, LR:33Ø20, TR: (2)Ø8/15cm	0.55×0.50, LR:9Ø18+ 10Ø20, TR: (2)Ø8/15cm	0.50×0.35, LR:6Ø18+ 3Ø16, TR: (2)Ø8/15cm
$C_{IN,\ RC\ Frame}$ (1000 €)		3.92E+02	3.51E+02	2.40E+02	1.99E+02
C_{IN} (1000 €)		1.59E+03	1.55E+03	1.44E+03	1.40E+03

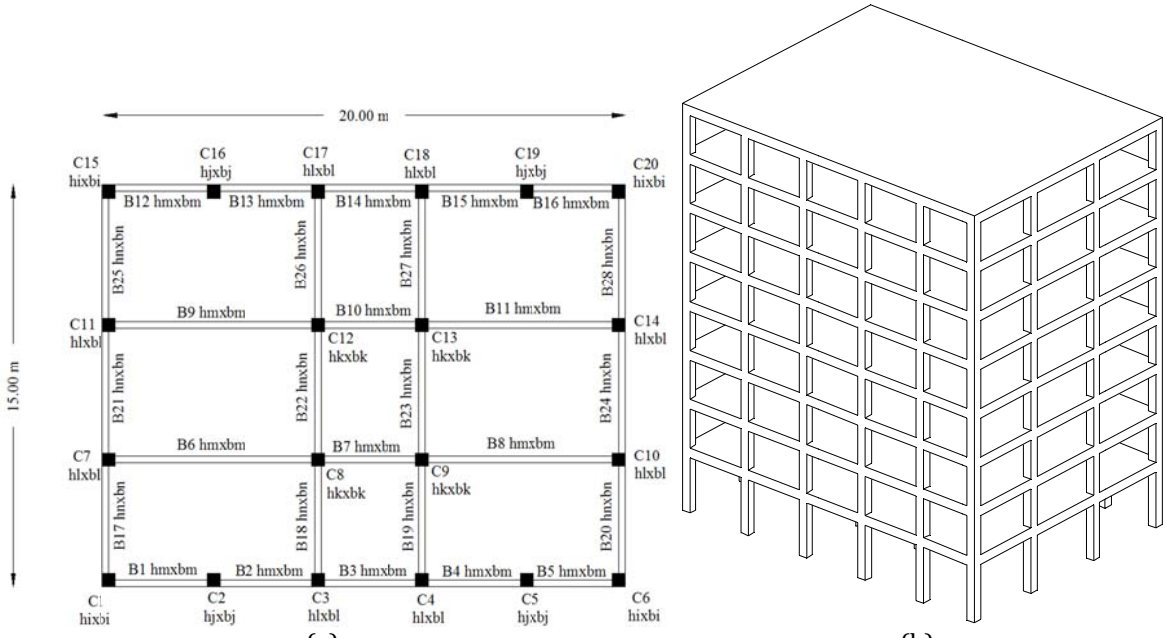

(a) (b)

Figure 4.16. Eight storey test example - (a) plan view, (b) front view.

4.5.4. Discussion

An investigation was performed on the effect of the behaviour factor q in the final design of reinforced concrete buildings under earthquake loading in terms of safety and economy. The numerical tests were performed on two multi-storey reinforced concrete buildings having symmetrical and non-symmetrical plan views which were optimally designed according to the European codes EC2 and EC8. The values of the behaviour factor varied from q=1, representing the elastic response, to q=4. Although the two test examples are different this study resulted in quite similar findings for the two cases considered.

The main finding of this part of the study is that the initial cost of reinforced concrete structures designed based on elastic response $D_{q=1}$ is not excessive since it varies, for the two representative test cases considered, from 3% to 15% compared to the initial cost of the designs $D_{q=2}$ to $D_{q=4}$, respectively. In fact, the designs $D_{q=1}$ are only by 10% more expensive compared to the cost of the designs obtained for the value of the behaviour factor suggested by the Eurocode (q=3). In the case, though, that the four designs are compared with reference to the cost of the RC skeletal members alone, design $D_{q=1}$ is 95% more expensive compared to D_q (q=2,3,4).

4.6. A new performance-based seismic design framework based on damage indices and structural optimization

The main objective of this part of the chapter is to incorporate a number of DIs examined in Chapter 2 into a performance-based design framework and to identify which one is the proper one to be used for designing reinforced concrete structures. In particular the Park and Ang local damage index; its modified variant proposed by Kunnath, Reinhorn and Lobo; the Chung, Meyer and Shinozuka local damage index; along with the maximum softening and final softening damage indices proposed by DiPasquale and Cakmak are used. This was achieved by means of lower bound performance-based design. The ultimate objective of this task was to compare lower-bound designs, or in other words comparing the designs that satisfy the code requirements in the most cost-effective way, i.e. those with minimum cross section and reinforcement dimensions. For this reason, a structural optimization problem was formulated and the designs obtained were then assessed.

4.6.1. Formulation of the optimization problem

The mathematical formulation of the optimization problem considered in the present work is defined as follows:

$$
\begin{aligned}
&\min_{\mathbf{s}\in F} && C_{IN}(\mathbf{s}) \\
&\text{where} && C_{IN}(\mathbf{s}) = C_b(\mathbf{s}) + C_{sl}(\mathbf{s}) + C_{cl}(\mathbf{s}) + C_{ns}(\mathbf{s}) \\
&\text{subject to} && DI^{i}_{HL1}(\mathbf{s}) \le DI^{allow,i}_{HL1} \\
& && DI^{i}_{HL2}(\mathbf{s}) \le DI^{allow,i}_{HL3} \\
& && \vdots \\
& && DI^{i}_{HLn}(\mathbf{s}) \le DI^{allow,i}_{HLn}
\end{aligned}
\tag{4.12}
$$

where **s** represents the design vector corresponding to the dimensions of columns and beams cross-sections, F is the feasible region where the i^{th} DI for a number of hazard levels (HL1, HL2,…,HLn) is below the allowable upper bounds ($DI^{i}_{HLj}(\mathbf{s}) \le DI^{allow,i}_{HLj}$) where i denotes to damage index considered in the formulation (i=1,2,…,m) and j is the hazard level. The boundaries of the feasible region are defined according to the calibrated values of the DIs presented in the Chapter 2 of this dissertation, these boundaries are given in Table 4.10.

The objective function considered is the total initial construction cost of the structure C_{IN}, while $C_b(\mathbf{s})$, $C_{sl}(\mathbf{s})$, $C_{cl}(\mathbf{s})$ and $C_{ns}(\mathbf{s})$ correspond to the total initial construction cost of beams, slabs, columns and non structural elements, respectively. The solution of the resulting optimization problem is performed by means of PSO method (see Chapter 3 for more details on the method).

Table 4.10. Definition of the limit states.

Design procedure	**50/50**	**10/50**	**2/50**
θ_{max}	4.00E-01	1.80E+00	3.00E+00
DI_{ms}	4.57E-02	4.43E-01	5.66E-01
DI_{fs}	6.08E-02	6.55E-01	7.65E-01
DI_{PA}	5.57E-02	5.24E-01	1.40E+00
DI_{KRL}	7.06E-02	7.51E-01	1.51E+00
DI_{CMS}	3.46E-02	6.03E-02	3.77E-01

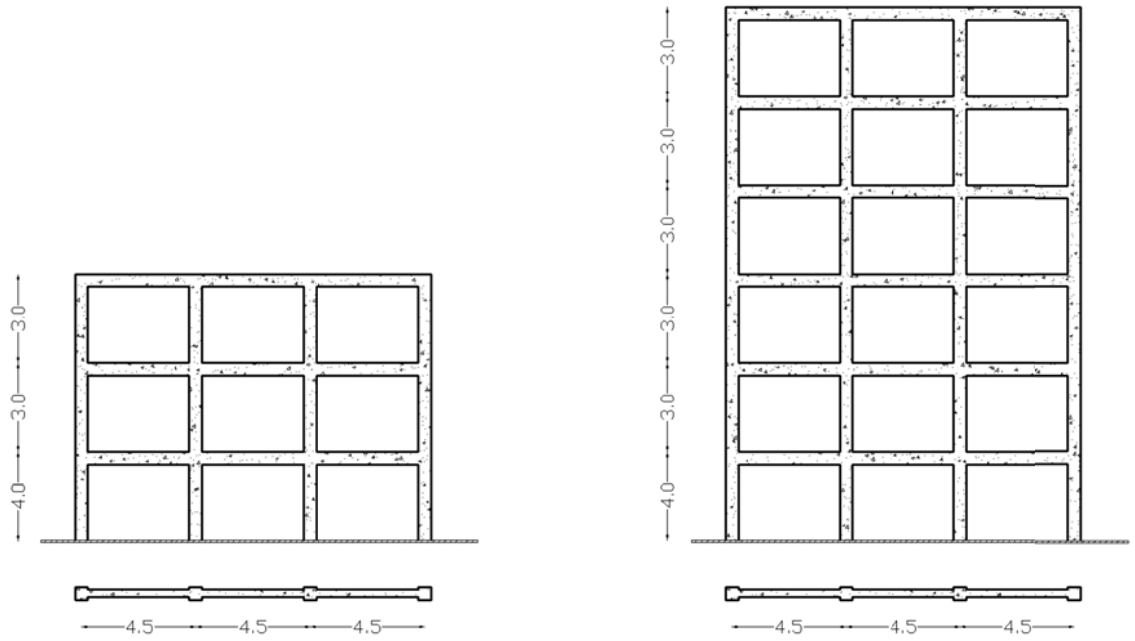

Figure 4.17. Test example - (a) three-storey, (b) six-storey.

In this part of this chapter, the two 2D RC moment resisting framed (MRF) buildings shown in Figure 4.17 have been considered in order to study the influence of the DI incorporated into the PBD framework on the design of RC buildings. The first test example is a three storey RC building while the second one is a six storey RC building. Concrete of class C20/25 (characteristic cylindrical strength of 20 MPa) and class S500 steel (characteristic yield stress of 500 MPa) are assumed. The slab thickness is equal to 15 cm, for both test examples, while it is considered to contribute to the moment of inertia of the beams with an effective flange width. In addition to the self-weight of beams and slabs, a distributed permanent load of 2 kN/m^2 due to floor finishing-partitions and an imposed load with nominal value of 1.5 kN/m^2, are considered, where an effective zone 10×15 m^2 is considered for each storey. The nominal permanent and imposed loads are multiplied by load factors of 1.35 and 1.5, respectively.

In both test examples the parametric study is performed in two stages: (i) design based on structural optimization and (ii) assessment of the designs. In the first stage the optimum design is computed by applying the PSO method, where the number of particles NP = 100, the inertia weight w = –0.6, while the cognitive parameter c_1 = –0.65 and social parameter c_2 = 2.65 based on the parameter study of Pedersen (2010), for both test examples. Six optimization problems are defined, following the PBD framework defined for (i) the interstorey drift, (ii) the Park and Ang damage index; (iii) its modified variant proposed by Kunnath, Reinhorn and Lobo; (iv) the Chung, Meyer and Shinozuka damage index; along with (v) the maximum softening and (vi) final softening damage indices proposed by Di

Pasquale and Cakmak. The optimum designs obtained are labelled as $D_{DI=a}$ defining the value of the behaviour factor used (i to vi). In all formulations the initial construction cost is the objective function to be minimized. The columns and beams are of rectangular cross-sectional shape, and are separated into groups. The dimensions of the columns/beams along with the longitudinal reinforcement are the design variables that are assigned to each group of the columns/beams. In the second stage, multi-stripe analysis is performed on the optimum designs where the beam-column members are modelled with the inelastic force-based fibre element (Papaioanou et al., 2005) and the median values of the MSDA curves, defined for all the damage indices, are compared.

4.6.2. Optimum design results

The structural elements (beams and columns) are separated into 2 and 3 groups for the three-storey and the eight-storey test examples, respectively, resulting into 5 and 7 design variables. The optimum designs achieved for different formulation of the optimization problem, with reference to the concrete and steel quantities for the beams and the columns required, are presented in Table 4.11 and 4.12, respectively. It can be seen that, compared to design $D_{DI=\theta}$ the initial construction cost of the other five designs is increased by 23% to 145% for the three-storey test example and by 26% to 75% for the six-storey one.

Table 4.11. Three-storey test example: Comparison of steel and concrete quantities in the twelve designs.

Design procedure	Columns		Beams		$C_{IN,Frame}$ (MU)
	Concrete (m^3)	Steel (kg.)	Concrete (m^3)	Steel (kg.)	
$D_{DI=\theta}$	10.00	1.81E+03	5.06	7.15E+02	8.11E+03
$D_{DI=ms}$	8.46	1.73E+03	6.75	1.80E+03	1.06E+04
$D_{DI=fs}$	8.46	1.93E+03	7.16	1.63E+03	1.08E+04
$D_{DI=PA}$	14.88	4.21E+03	8.98	2.54E+03	1.97E+04
$D_{DI=KRL}$	13.00	2.24E+03	6.62	1.19E+03	1.10E+04
$D_{DI=CMS}$	7.06	1.27E+03	6.08	9.54E+02	9.99E+03

Table 4.12. Six-storey test example: Comparison of steel and concrete quantities in the twelve designs.

Design procedure	Columns		Beams		$C_{IN,Frame}$ (MU)
	Concrete (m^3)	Steel (kg.)	Concrete (m^3)	Steel (kg.)	
$D_{DI=\theta}$	19.65	2.11E+03	12.69	1.89E+03	1.39E+04
$D_{DI=ms}$	27.32	4.58E+03	14.51	2.05E+03	2.16E+04
$D_{DI=fs}$	28.34	3.29E+03	16.46	1.55E+03	1.75E+04
$D_{DI=PA}$	29.90	3.50E+03	14.85	1.87E+03	1.88E+04
$D_{DI=KRL}$	30.74	3.84E+03	12.69	2.59E+03	2.13E+04
$D_{DI=CMS}$	31.46	4.44E+03	19.53	2.76E+03	2.41E+04

4.6.3. Assessment of the optimum design

In order to compare the capacities of the optimum designs obtained by means of the six performance-based design procedures presented above, multi-stripe analyses is performed over the bin of records described in Tables 4.2 to 4.4, corresponding to records belonging to the 50/50, 10/50 and 2/50 hazard levels. In particular, six optimum designs are obtained, for each test example with reference to different DI. Figures 4.18 and 4.19 shows the median values of the maximum drift, maximum floor acceleration, maximum softening, final softening, Park & Ang damage index, Kunnath, Reinhorn & Lobo damage index and Chung, Meyer & Shinozuka damage index obtained for the three hazard levels and for the optimum designs obtained according to the design frameworks discussed above (see also Table 4.13 and 4.14). For the three-storey test example it is the design obtained from the PBD framework according to the Park & Ang damage index that shows an overall good performance with reference to the seven engineering demand parameters. On the other hand, for the six-storey test example it is the design obtained from the PBD framework according to the Chung, Meyer & Shinozuka damage index that shows an overall good performance with reference to the seven engineering demand parameters. Furthermore, for both test examples the maximum interstorey drift and floor acceleration are increased linearly for all optimum designs, while the behaviour of the six designs is non-linear with reference to the other damage indices.

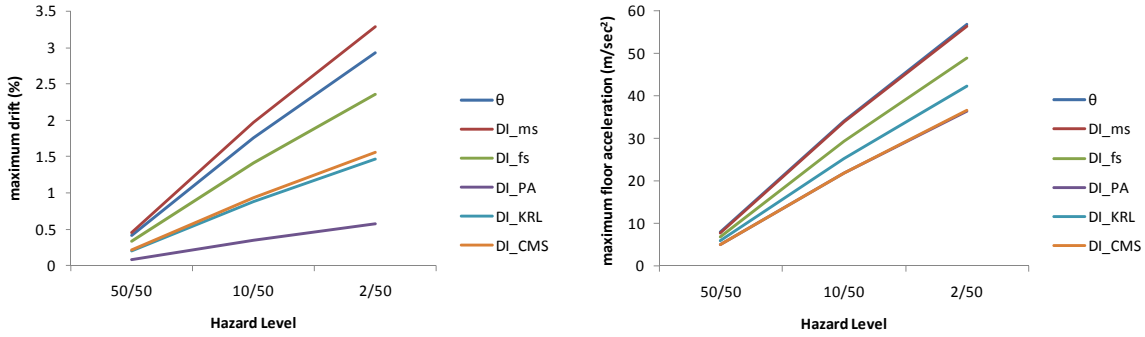

(a)

(b)

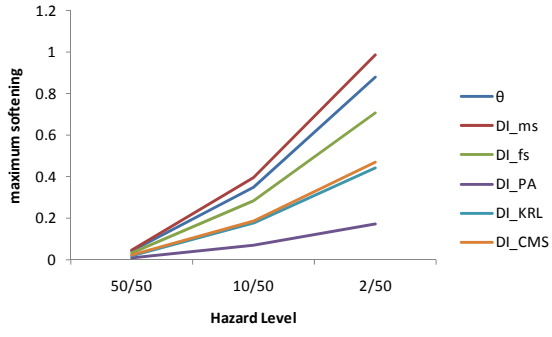

(c)

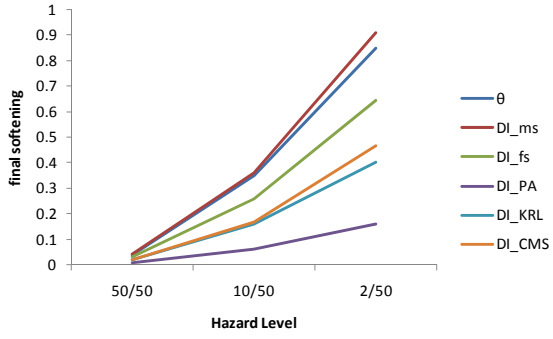

(d)

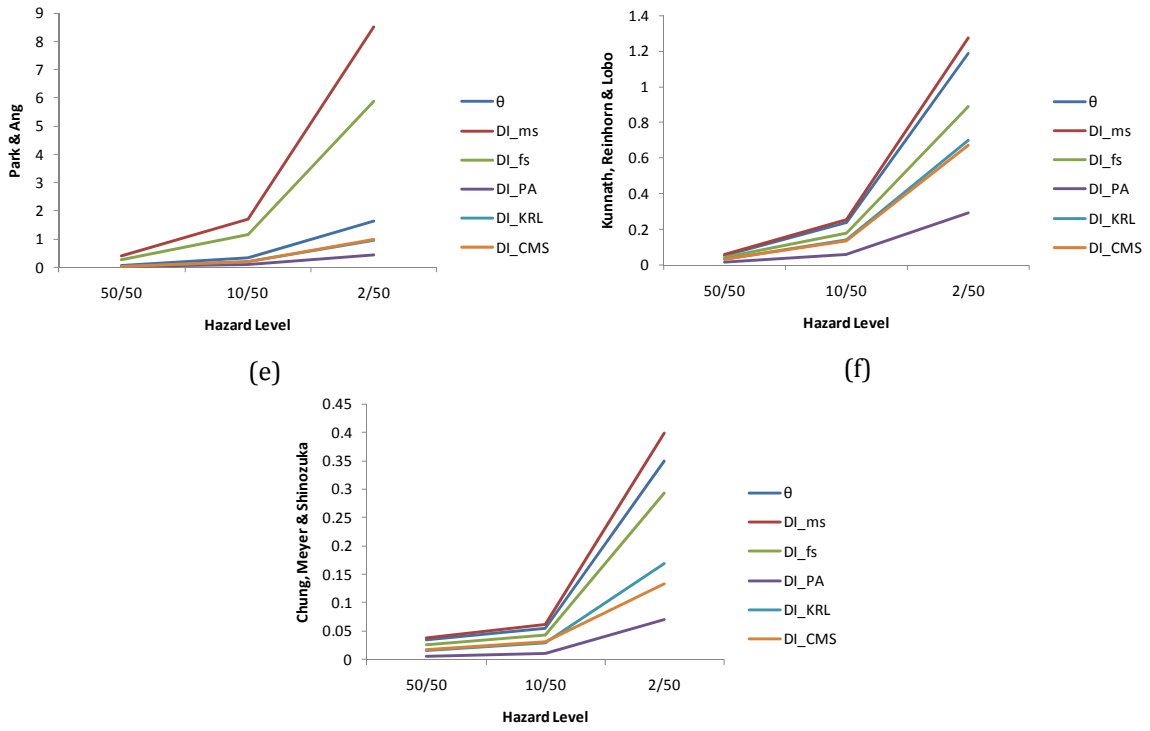

(e)

(f)

(g)

Figure 4.18. Three-storey test example – comparison with reference to (a) maximum drift, (b) maximum floor acceleration, (c) maximum softening, (d) final softening, (e) Park & Ang damage index, (f) Kunnath, Reinhorn & Lobo damage index and (g) Chung, Meyer & Shinozuka damage index.

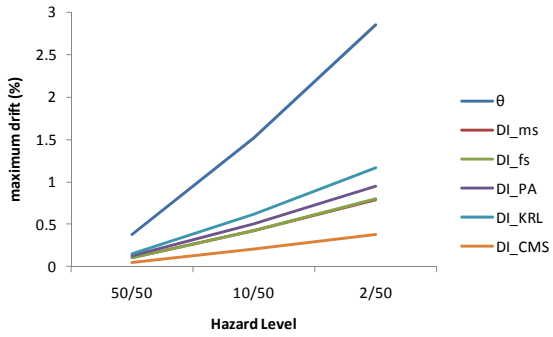

(a)

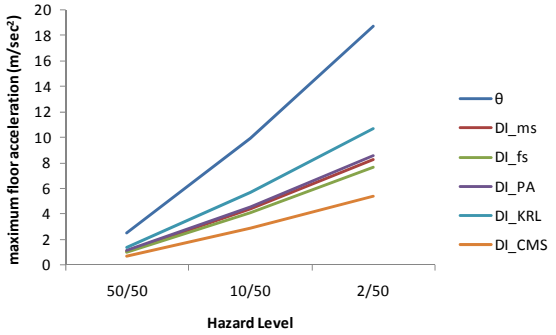

(b)

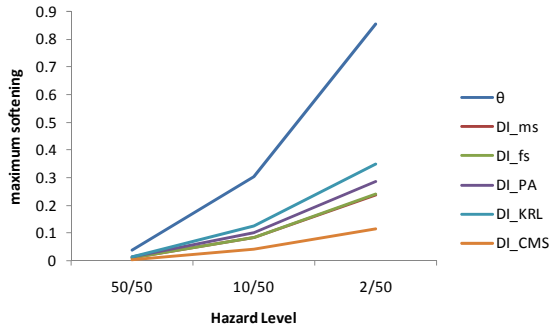

(c)

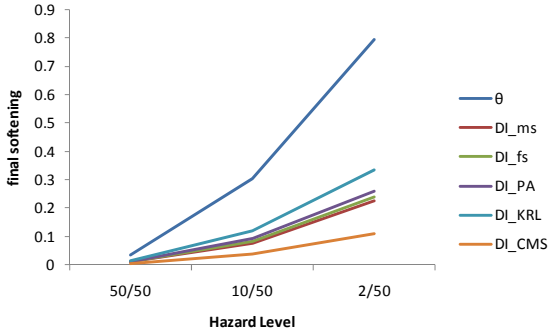

(d)

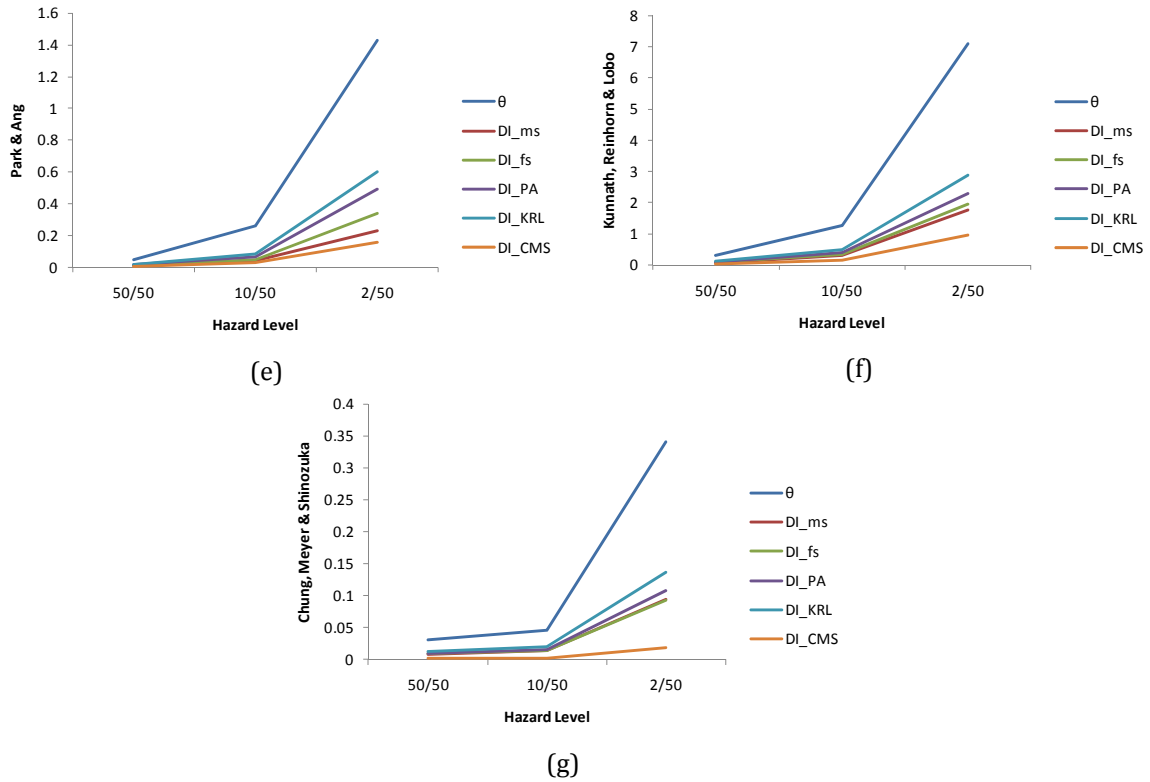

Figure 4.19. Six-storey test example – comparison with reference to (a) maximum drift, (b) maximum floor acceleration, (c) maximum softening, (d) final softening, (e) Park & Ang damage index, (f) Kunnath, Reinhorn & Lobo damage index and (g) Chung, Meyer & Shinozuka damage index.

In general, it can be said that for the two test examples considered it is the Chung, Meyer & Shinozuka damage index that shows an overall good performance with reference to the performance criteria considered.

4.6.4. Discussion

In this part of the study the objective is to incorporate a number of damage indices examined in Chapter 2 into a performance-based design framework and to identify which one is the proper one to be used for designing reinforced concrete structures. For this purpose, six structural optimization problems are formulated with performance-based design criteria for two 2D reinforced concrete buildings.

Table 4.13. Three-storey test example – comparison with reference to the damage indices.

Assessment Criteria	Hazard Level	$D_{DI=\theta}$	$D_{DI=ms}$	$D_{DI=fs}$	$D_{DI=PA}$	$D_{DI=KRL}$	$D_{DI=CMS}$
Drift	50/50	0.41	0.46	0.33	0.08	0.20	0.22
	10/50	1.75	1.97	1.42	0.35	0.88	0.94
	2/50	2.92	3.28	2.36	0.58	1.47	1.57
Floor acceleration	50/50	7.93	7.87	6.84	5.10	5.91	5.13
	10/50	34.07	33.82	29.35	21.83	25.36	21.94
	2/50	56.88	56.46	48.95	36.38	42.31	36.56
Maximum softening	50/50	0.04	0.05	0.03	0.01	0.02	0.02
	10/50	0.35	0.39	0.28	0.07	0.18	0.19

	2/50	0.88	0.98	0.71	0.17	0.44	0.47
Final softening	50/50	0.04	0.04	0.03	0.01	0.02	0.02
	10/50	0.33	0.36	0.27	0.06	0.17	0.18
	2/50	0.81	0.89	0.64	0.17	0.43	0.47
Park & Ang	50/50	0.07	0.39	0.27	0.02	0.04	0.04
	10/50	0.33	1.69	1.17	0.09	0.19	0.20
	2/50	1.64	8.53	5.89	0.43	0.96	1.00
Kunnath, Reinhorn & Lobo	50/50	0.06	0.06	0.04	0.01	0.03	0.03
	10/50	0.24	0.25	0.18	0.06	0.14	0.13
	2/50	1.19	1.27	0.89	0.30	0.70	0.67
Chung, Meyer & Shinozuka	50/50	0.03	0.04	0.03	0.01	0.02	0.02
	10/50	0.05	0.06	0.05	0.01	0.03	0.03
	2/50	0.35	0.38	0.29	0.07	0.18	0.12

Table 4.14. Six-storey test example – comparison with reference to the damage indices.

Assessment Criteria	**Hazard Level**	$\mathbf{D_{DI=\theta}}$	$\mathbf{D_{DI=ms}}$	$\mathbf{D_{DI=fs}}$	$\mathbf{D_{DI=PA}}$	$\mathbf{D_{DI=KRL}}$	$\mathbf{D_{DI=CMS}}$
Drift	50/50	0.38	0.11	0.11	0.13	0.15	0.05
	10/50	1.52	0.42	0.43	0.51	0.62	0.20
	2/50	2.85	0.79	0.80	0.95	1.17	0.38
Floor acceleration	50/50	2.49	1.11	1.02	1.13	1.42	0.72
	10/50	9.97	4.43	4.08	4.57	5.71	2.88
	2/50	18.68	8.30	7.64	8.58	10.71	5.40
Maximum softening	50/50	0.04	0.01	0.01	0.01	0.02	0.01
	10/50	0.30	0.08	0.09	0.10	0.12	0.04
	2/50	0.86	0.24	0.24	0.29	0.35	0.11
Final softening	50/50	0.03	0.01	0.01	0.01	0.01	0.00
	10/50	0.29	0.08	0.08	0.10	0.11	0.04
	2/50	0.81	0.23	0.23	0.28	0.35	0.11
Park & Ang	50/50	0.05	0.01	0.01	0.02	0.02	0.01
	10/50	0.26	0.04	0.05	0.07	0.08	0.03
	2/50	1.43	0.23	0.34	0.49	0.60	0.16
Kunnath, Reinhorn & Lobo	50/50	0.31	0.08	0.09	0.10	0.13	0.04
	10/50	1.26	0.31	0.34	0.40	0.51	0.17
	2/50	7.09	1.77	1.94	2.29	2.88	0.95
Chung, Meyer & Shinozuka	50/50	0.03	0.01	0.01	0.01	0.01	0.00
	10/50	0.05	0.01	0.01	0.02	0.02	0.00
	2/50	0.33	0.09	0.09	0.12	0.14	0.02

An investigation was performed on the effect of the damage index incorporated into a performance-based design procedure. In particular the Park and Ang local damage index; its modified variant proposed by Kunnath, Reinhorn and Lobo; the Chung, Meyer and Shinozuka local damage index; along with the maximum softening and final softening damage indices proposed by Di Pasquale and Cakmak are used. This was achieved by means of lower bound performance-based design. The ultimate objective of this task was to compare lower-bound designs, or in other words comparing the designs that satisfy the code requirements in the most cost-effective way, i.e. those with minimum cross section and reinforcement dimensions. For this reason, a structural optimization problem was formulated and the designs obtained were then assessed.

The main findings of this study can be summarized in the following:

- Six performance-based optimization problems were formulated with reference to different damage indices.
- It was observed that, compared to design $D_{DI=\theta}$, the initial construction cost of the other five designs is increased by 23% to 145% for the three-storey test example and by 26% to 75% for the six-storey one.
- In general, it can be said that for the two test examples considered it is the Chung, Meyer & Shinozuka damage index that shows an overall good performance with reference to the performance criteria considered.

4.7. References

ASCE/SEI Standard 41-06, 2006. Seismic Rehabilitation of Existing Buildings, prepublication edition, Structural Engineering Institute, American Society of Civil Engineers.

ATC-34. A critical review of current approaches to earthquake resistance design. Applied Technology Council: Redwood City, CA, 1995.

ATC-40, Seismic evaluation and retrofit of concrete buildings, Applied Technology Council, Redwood City, 1996.

Avramidis, I.E., Anastasiadis, K., Athantopoulou, A., Katsavelos, A. The myth of the excessive cost of seismic resistant structures designed for elastic behaviour for the design earthquake, 14th National Congress on RC structures, Kos, Greece, 2003.

Balendra, T. & Huang, X. 2003, "Overstrength and ductility factors for steel frames designed according to BS 5950", Journal of Structural Engineering, vol. 129, no. 8, pp. 1019-1035.

Bertero, V.V. (1977). "Strength and deformation capacities of buildings under extreme environments." In Structural Engineering and Structural Mechanics, Pister KS (ed.). Prentice-Hall: Englewood Cliffs, NJ, pp. 211-215.

Borzi, B., Elnashai, A.S. Refined force reduction factors for seismic design. Engineering Structures 2000; 22(10): 1244–1260.

Browning, J. Proportioning earthquake-resistant RC frames in central/eastern U.S., Earthquake Engineering & Structural Dynamics 2002; 31(6): 1267-1280.

Chan, C.-M., Zou, X.-K. Elastic and inelastic drift performance optimization for reinforced concrete buildings under earthquake loads. Earthquake Engineering & Structural Dynamics 2004; 33(8): 929–950.

Chintanapakdee, C, Chopra, AK. Evaluation of modal pushover analysis using generic frames. Earthquake Engineering & Structural Dynamics 2003; 32(3), 417-442.

Chopra AK, Goel RK. A modal pushover analysis procedure for estimating seismic demands for buildings, Earthquake Engineering & Structural Dynamics, 2002; 31(3): 561-582.

Cuesta, I., Aschheim, M.A., Fajfar, P. Simplified R-factor relationships for strong ground motions. Earthquake Spectra 2003; 19(1): 25–45.

EAK 2000, National seismic code of Hellas, 2000.

EC2. Eurocode 2. Design of Concrete Structures—Part 1: General Rules and Rules for Buildings. European Committee for Standardisation: Brussels, Belgium, The European Standard EN 1992-1-1: 2004.

EC8. Eurocode 8: Design of Structures for Earthquake Resistance. European Committee for Standardisation: Brussels, Belgium, The European Standard EN 1998-1: 2004.

EKOS 2000, National code for concrete building structures of Hellas, 2000.

Elnashai, A.S. & Mwafy, A.M. 2002, "Overstrength and force reduction factors of multistorey reinforced-concrete buildings", Structural Design of Tall Buildings, vol. 11, no. 5, pp. 329-351.

Fajfar P. A nonlinear analysis method for performance-based seismic design, Earthquake Spectra 2000; 16(3): 573-592.

Fajfar, P. and Fischinger, M. (1988). N2-a method for non-linear seismic analysis of regular buildings, Proc. 9th World Conf. Earthquake Engng., Maruzen, Tokyo (1989), Kyoto, 111-116.

Fajfar, P. and Gaspersic, P. (1996). The N2 method for the seismic damage analysis for RC buildings, Earthquake Engineering & Structural Dynamics, 25: 23-67.

Fajfar, P. Towards nonlinear methods for the future seismic codes, In Seismic design practice into the next century, Booth (Ed.), Balkema, 1998.

Fajfar, P., (1999) Capacity spectrum method based on inelastic demand spectra, Earthquake Engineering & Structural Dynamics; 28(9): 979-999.

FEMA-273. NEHRP Guidelines for the Seismic Rehabilitation of Buildings, Building Seismic Safety Council for the Federal Emergency Management Agency, Washington, DC, 1997.

FEMA-350: Recommended Seismic Design Criteria for New Steel Moment-Frame Buildings. Federal Emergency Management Agency, Washington DC, 2000.

FEMA-356, Prestandard and Commentary for the Seismic Rehabilitation of Buildings, Federal Emergency Management Agency, Washington, DC, 2000.

FEMA-440: Improvement of Nonlinear Static Seismic Analysis Procedures. Federal Emergency Management Agency: Washington, DC, 2005.

FEMA-National Institute of Building Sciences. HAZUS-MH MR1, Multi-hazard Loss Estimation Methodology Earthquake Model, Washington, DC, 2003.

Fragiadakis, M., Papadrakakis, M. (2008) Modeling, analysis and reliability of seismically excited structures: Computational issues. International Journal of Computational Methods; 5(4): 483-511.

Frangopol, D.M. Computer-automated design of structural systems under reliability-based performance constraints. Engineering Computations 1986; 3(2): 109–115.

Freeman, S. A. 1998. Development and use of capacity spectrum method. Proc.6 US National Conference on Earthquake Engineering.

Ghobarah A, Abou-Elfath H, Biddah A. Response-based damage assessment of structures. Earthquake Engineering & Structural Dynamics 1999, 28(1): 79-104.

Ghobarah, A. On drift limits associated with different damage levels, International Workshop on Performance-Based Seismic Design, June 28-July 1, 2004.

Giovenale P, Cornell CA, Esteva L. Comparing the adequacy of alternative ground motion intensity measures for the estimation of structural responses, Earthquake Engng Struct. Dyn. 2004; 33(8): 951-979.

Jalayer F, Cornell CA. Alternative non-linear demand estimation methods for probability-based seismic assessments. Earthquake Engineering & Structural Dynamics 2009; 38(8): 951-972.

Jalayer F, Franchin P, Pinto PE. A scalar damage measure for seismic reliability analysis of RC frames, Earthquake Engng Struct. Dyn. 2007; 36(13): 2059-2079.

Kappos AJ. Evaluation of behaviour factors on the basis of ductility and overstrength studies. Engineering Structures 1999; 21(9): 823-835.

Kappos, A.J. 1991, "Analytical prediction of the collapse earthquake for R/C buildings: suggested methodology", Earthquake Engineering & Structural Dynamics, vol. 20, no. 2, pp. 167-176.

Karakostas, C.Z., Athanassiadou, C.J., Kappos, A.J., Lekidis, V.A. Site-dependent design spectra and strength modification factors, based on records from Greece. Soil Dynamics and Earthquake Engineering 2007; 27 (11): 1012–1027.

Karavasilis, T.L., Bazeos, N., Beskos, D.E. Behaviour factor for performance-based seismic design of plane steel moment resisting frames. Journal of Earthquake Engineering 2007; 11(4): 531–559.

Krawinkler, H. and Miranda, E. (2004). Performance-base earthquake engineering, In: Earthquake Engineering: From Engineering Seismology to Performance-based Earthquake Engineering (Y. Bozorgnia and Vitelmo V. Bertero (Eds), CRC Press.

Lagaros ND. (2010). Multicomponent incremental dynamic analysis considering variable incident angle, Journal of Structure and Infrastructure Engineering; 6(1-2): 77-94.

Lagaros, N.D., Papadrakakis, M. (2007) Seismic design of RC structures: a critical assessment in the frame-work of multi-objective optimization, Earthquake Engineering and Structural Dynamics, 36(12): 1623-1639.

Lam, N., Wilson, J. & Hutchinson, G. 1998, "The ductility reduction factor in the seismic design of buildings", Earthquake Engineering and Structural Dynamics, vol. 27, no. 7, pp. 749-769.

Lee, K., Foutch, D.A. Seismic evaluation of steel moment frame buildings designed using different R-values. Journal of Structural Engineering 2006; 132(9): 1461–1472.

Li, G., Cheng, G. Optimal decision for the target value of performance-based structural system reliability. Structural & Multidisciplinary Optimization 2001; 22(4): 261–267.

Lu Y, Hao H, Carydis P. G, Mouzakis, H. Seismic performance of RC frames designed for three different ductility levels. Engineering Structures 2001; 23(5): 537–547

Luco N, Allin Cornell C. Effects of connection fractures on SMRF seismic drift demands. Journal of Structural Engineering New York, N.Y. 2000;126(1):127-136.

Mander JB, Dhakal RP, Mashiko N, Solberg KM. Incremental dynamic analysis applied to seismic financial risk assessment of bridges, Engineering Structures 2007; 29(10): 2662-2672.

Mazzolani, FM, Piluso, V. The theory and design of seismic resistant steel frames, E & FN Spon, 1996.

Miranda, E., Bertero, V.V. Evaluation of strength reduction factors for earthquake resistant design. Earthquake Spectra 1994; 10(2): 357–379.

Mitropoulou, Ch.Ch., Lagaros, N.D., Papadrakakis, M. (2010) Economic building design based on energy dissipation: a critical assessment, Bulletin of Earthquake Engineering, 8(6): 1375-1396.

Moharrami, H., Grierson, D.E. Computer-automated design of reinforced concrete frameworks. Journal of Structural Engineering 1993; 119(7): 2036–2058.

Moroni, M.O., Astroza, M., Gómez, J. & Guzmán, R. 1996, "Establishing Rw and Cd factors for confined masonry buildings", Journal of Structural Engineering, vol. 122, no. 10, pp. 1208-1215.

Mwafy, A.M. and Elnashai, A.S. (2001). "Static pushover versus dynamic collapse analysis of RC buildings." Engineering Structures, Vol. 23(5), pp. 407-424.

Olsson A, Sandberg G, Dahlblom O. On latin hypercube sampling for structural reliability analysis. Structural Safety 2003; 25(1), 47-68.

Palazzo B, Petti L. Reduction factors for base isolated structures. Computers and Structures 1996; 60(6): 945–956

Panagiotakos, TB, Fardis, MN. A displacement-based seismic design procedure for RC buildings and comparison with EC8, Earthquake Engineering & Structural Dynamics 2001; 30, 1439-1462.

Panagiotakos, TB, Fardis, MN. Seismic performance of RC frames designed to Eurocode 8 or to Greek Codes 2000, Bulletin of Earthquake Engineering 2004; 2: 221-259.

Papaioannou I, Fragiadakis M, Papadrakakis M. Inelastic Analysis of framed structures using the fiber approach, Proceedings of the 5th International Congress on Computational Mechanics (GRACM 05), Limassol, Cyprus, June 29 - July 1, 2005.

Papazachos, BC, Papaioannou, ChA, Theodulidis, NP. Regionalization of seismic hazard in Greece based on seismic sources, Natural Hazards 1993; 8(1), 1-18.

Pedersen, M.E.H. (2010). Good Parameters for Particle Swarm Optimization, Hvass Laborato-ries Technical Report no. HL1001.

Priestley, M.J.N., Calvi, G.M., Kowalsky, M.J. Displacement Based Seismic Design of Structures, IUSS Press (2007).

Sarma, K.C., Adeli, H. Cost optimization of concrete structures. Journal of Structural Engineering 1998; 124(5): 570–578.

Somerville, P, Collins, N. Ground motion time histories for the Humboldt bay bridge, Pasadena, CA, URS Corporation, 2002, www.peertestbeds.net/humboldt.htm.

Structural Engineers Association of California (SEAOC), Vision 2000 a framework for performance-based seismic engineering, Structural Engineers Association of California, Sacramento, California, 1995.

Sullivan, TJ, Calvi, GM, Priestley, MJN, Kowalsky, MJ. The limitations and performances of different displacement based design methods, Journal of Earthquake Engineering, 2003; 7(1): 201-241.

Tassios TP (1989a), 'Specific Rules for Concrete Structures - Justification Note No. 6: Required Confinement for Columns', Background Document for Eurocode 8 - Part 1, Vol. 2 - Design Rules, CEC DG III/8076/89 EN, 23-49.

Tassios TP (1989b), 'Specific Rules for Concrete Structures - Justification Note No. 13: Confined Concrete Constitutive Law', Background Document for Eurocode 8 - Part 1, Vol. 2 - Design Rules, CEC DG III/8076/89 EN, 104-116.

Tassios, T. 1986. Estimation of behaviour factor of RC structures. Rep., EC8. Study Group, NTUA.

Uang, C. 1991, "Establishing R (or Rw) and Cd factors for building seismic provisions", Journal of structural engineering New York, N.Y., vol. 117, no. 1, pp. 19-28.

Vamvatsikos D., Cornell CA. (2002) Incremental dynamic analysis. Earthquake Engineering and Structural Dynamics; 31(3): 491-514.

Vamvatsikos, D. Cornell, C.A. (2004). Applied Incremental Dynamic Analysis, Earthquake Spectra, Vol. 20(2), pp. 523 – 553.

Whittaker A, Hart G, Rojahn C. Seismic response modification factors. Journal of Structural Engineering 1999; 125(4): 438–444

Xue, Q. Need of performance-based earthquake engineering in Taiwan: a lesson from the Chichi earthquake, Earthquake Engineering & Structural Dynamics 2000; 29(11): 1609-1627.

Zeris, C., Tassios, T., Lu, T., Zhang, G. (1991) A parametric study of the strength reduction factor of Irregular RC frames, Proceedings of the International Meeting on Earthquake Protection of Buildings, University of Ancona, June 6-8, pp. 87B-98B.

Chapter 5

Seismic Hazard Analysis: ground excitation for design and assessment

5.1. Introduction

Seismic hazard analysis involves the quantitative estimation of ground shaking hazards at a particular area. It describes the possibility of a natural hazard related an earthquake occurrence. Seismic hazards can be analyzed deterministically when a particular earthquake scenario is assumed, or probabilistically, where uncertainties in earthquake size, location, and time of occurrence are explicitly considered (Kramer, 1996). The deterministic approach of a seismic hazard analysis is defined as: "The earthquake hazard for the site of interest is a peak ground acceleration of A_G resulting from an earthquake of magnitude M on the *X Fault* at a distance of R miles from the site.", while in the case of a probabilistic approach the definition is "The earthquake hazard for the site of interest is a peak ground acceleration of A_G with a P probability (i.e. probability 10%) of being exceeded in a T-year period (i.e. 50 years)". An important factor in seismic hazard analysis is the determination of the amplitude parameters of a ground motion, therefore the determination of *PGA* and response acceleration (spectral acceleration) for an area/site. S_A is preferred for the design of civil engineering structures. It is an accepted trend in engineering practice to develop design response spectrum for different types of foundation materials such as rock, hard soil and weak soils. Analysis of lineaments and faults helps in understanding the regional seismotectonic activity of the area. Lineaments are linear features seen on the surface of earth which represents faults, features, shear zones, joints, litho contacts, dykes, and are of great relevance to geoscientists.

As it will be described in detail in Chapter 6 the principles of LCCA are based on economic theories, and have been used as decision-support tools in industrial and commercial projects. LCCA has been frequently implemented to energy and water

conservation projects as well as to transportation projects, including highways, bridges, etc. When it comes to building structures, the application of LCCA is considered particularly important in the case of retrofitted deteriorating structures, especially for those situated in seismic regions, since LCCA takes into account future damages due to earthquakes. Furthermore, it is also used as a decision making tool for selecting the most cost-effective solution related to the design of new structures in seismic regions. In a previous work (Iervolino et. al, 2009) it was shown the significant influence of some parameters on the estimation of the life-cycle cost of structural systems. In the framework of LCCA work it is proved that the efficiency of implementing LCCA is highly dependent on the set of records selected for the evaluation of the cost.

Despite the increasing availability of databanks with natural records it is difficult to obtain code-compliant sets of natural records for design and assessment purposes. In particular, the guidelines provided by code provisions on the selection of ground motion input for dynamic analysis are poor. The main guideline refers to the compatibility with the design spectrum in a specified range of periods (Gasparini and Vanmarke, 1976). This is why artificial accelerogram generation procedures, compatible with an assigned design spectrum, are still very popular for both practice and research purposes. The usual procedure which is followed for the generation of an artificial accelerogram is to perform iterations for the achievement of the spectral matching by adjusting the Fourier amplitude spectrum. The spectral matching technique is carried out in the frequency domain using an appropriate power spectral density function. However, the variance of a hazard curve and consequently its implication to the seismic load is not taken into account.

In this chapter the artificial accelerograms are generated by producing stationary signals that are subsequently enveloped in a trapezoidal shape to roughly simulate the non-stationary characteristics of ground motion (Mitropoulou et. al, 2010). The artificial accelerograms are generated through design spectra based on the mean hazard curve of the region. The mean hazard curve is derived by taking into consideration important uncertainties, such as maximum magnitude, earthquake recurrence rate, distribution of seismicity between faults, attenuation relationships, etc.

In the framework of LCCA implemented in this study, three different classes of seismic records are considered in this study and their influence on the LCCA performance is examined by analysing two typical 3D reinforced concrete buildings. One having symmetrical plan view and the other having irregular plan view. The first class of ground motion excitations is composed by a number of natural records associated to the region of interest (set NAT). The second class comprises a number of artificial accelerograms

generated according to the corresponding elastic response spectrum (set ART). Previous studies have shown that artificial accelerograms underestimate the maximum drift and the maximum floor acceleration, leading to an overestimation of structural response under seismic loads. In this dissertation it was found that this underestimation is associated with a significantly faulty reduction of the estimated life-cycle cost, thus overestimation of the safety. On the other hand, the number of natural records required for the reliable calculation of the life-cycle cost is excessive leading to an analogous increase of the computational effort. In order to combine robustness and computational efficiency, a procedure for selecting the most representative artificial seismic excitations at each hazard level is proposed leading to reduction of the required computational effort for performing a LCCA. More specifically, the proposed procedure leads to a reduced number of randomly generated representative artificial accelerograms by taking into consideration the stochastic characteristics of the peak ground acceleration (set UART).

5.2. Deterministic Seismic Hazard Analysis

Deterministic methods consider the effect at a site of either a single scenario earthquake, or a relative small number of individual earthquakes. The drawback of a DSHA is the selection of a representative earthquake on which the hazard assessment would be based. This drawback usually involves the identification of an earthquake that satisfies code requirements.

Krinitzsky (2003) highlights that a DSHA uses geology and seismic history to identify earthquake sources and interprets the strongest earthquake each source is capable of producing, regardless of time, because that earthquake might happen tomorrow. Those are the MCEs, the largest earthquakes that can reasonably be expected. As we cannot safely predict when an earthquake will happen, the MCEs are what a critical structure should be designed for if the structure is to avoid catastrophe failure. Deterministic seismic hazard assessment is carried out to identify the MCE that will affect a site. Consequently, the MCE is the largest earthquake that appears possible along a recognized fault under the presently known or presumed tectonic activity, which will cause the most severe consequences to the site.

The steps of a DSHA are presented in the flowchart of Figure 5.1. The DSHA process initiates with the definition of the seismic sources in Step 1, following the identification of an earthquake from a predefined seismic source through a specific value of magnitude and distance from source to site in Step 2, in Step 3 is defined the value of the amplitude parameter of a ground motion given the distance and the magnitude, while in Step 4 is

presented the result of a deterministic seismic hazard analysis (Benjamin & Cornell, 1970).

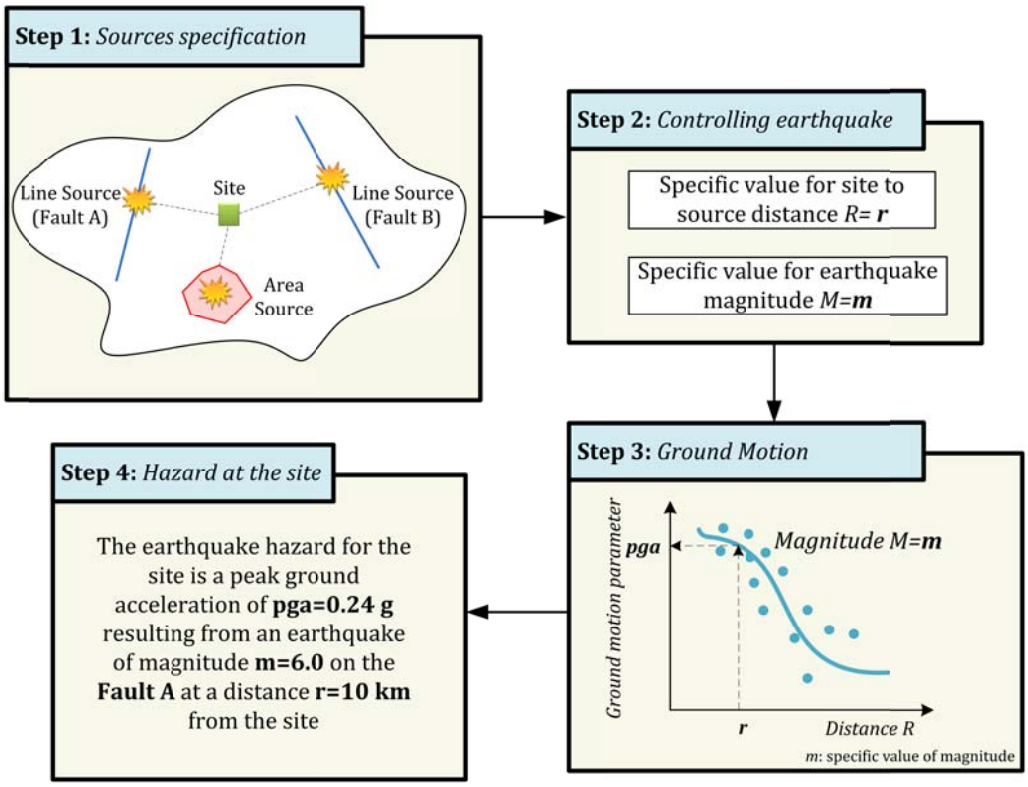

Figure 5.1. Steps in deterministic seismic hazard analysis (Kramer, 1996).

An example of a DSHA for a site surrounded by three sources, two faults and an area source is presented in Figure 5.2 by Kramer (1996). The result of the DSHA is the maximum PGA value equal to 0.57g given from the Fault B, therefore "the earthquake hazard for the site of interest is a *peak ground acceleration of 0.57g* resulting from an earthquake of *magnitude 7.7* on the *Fault B* at a *distance of 25 kilometers* from the site."

5.3. Probabilistic Seismic Hazard Analysis

The goal of PSHA is to quantify the hazard (the probability of exceeding various ground motion levels) at a site from all earthquakes of all possible magnitudes, at all significant distances from the site of interest, as a probability, by taking into account their frequency of occurrence. Deterministic earthquake scenarios, therefore, are a subset of the probabilistic methodology. The numerical/analytical approach to PSHA was first formalized by Cornell (1968). PSHA can be expressed as:

$$\lambda(X \geq x) \approx \sum_{\text{Sources i}} v_i \int_{M_0}^{M_{max}} \int_{R|M} P(X \geq x \,|\, M,R) f_M(m) f_{R|M}(r \,|\, m) dr\, dm \qquad (5.1)$$

where $\lambda(X \geq x)$ is the annual frequency that ground motion at a site exceeds the chosen level X=x; v_i is the annual rate of occurrence of earthquakes on seismic source i, having magnitude

between M_0 and M_{max}; M_0 is the minimum magnitude of engineering significance; M_{max} is the maximum magnitude assumed to occur on the source; $P(X \geq x \mid M,R)$ denotes the conditional probability that the chosen ground motion level is exceeded for a given magnitude and distance; $f_M(m)$ is the probability density function of earthquake of earthquake magnitude; $f_{R|M}(r \mid m)$ is the probability density function of distance from the earthquake source to the site of interest. In practice, this expression is solved for each seismic source i of a seismotectonic model.

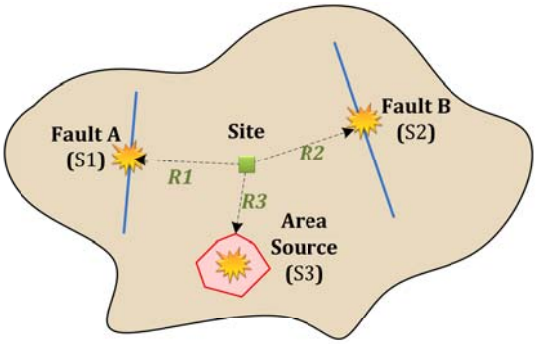

Source	Magnitude (max)	Distance (km)	PGA (g)
S1	7.3	R1=23.7	0.42
S2	7.7	R2=25.0	0.57
S3	5.0	R3=60.0	0.02
	↑ Maximum on source	↑ Closest distance	↑ From attenuation relationship

Figure 5.2. Example of deterministic seismic hazard analysis (Kramer, 1996).

In general it can be said that PSHA illustrates four probabilistic modesl for the estimation of the ground motion hazard:

- Seismic sources
- Earthquake recurrence frequency
- Ground motion model (attenuation relationship)
- Ground motion occurrence probability at a site

In Figure 5.3 the models considered in a PSHA are presented. The procedure begins with the definition of the seismic sources. The definition of the number of the earthquakes exceeding a multiple values of magnitude M for each site, called as earthquake recurrence frequency follows in Step 2. The third step refers to the definition of the attenuation curves, namely the relation among the ground motion intensity parameters and the site-to-source, geometry and seismic region characteristics. The final step is the probabilistic calculation of the ground motion occurrence at a site.

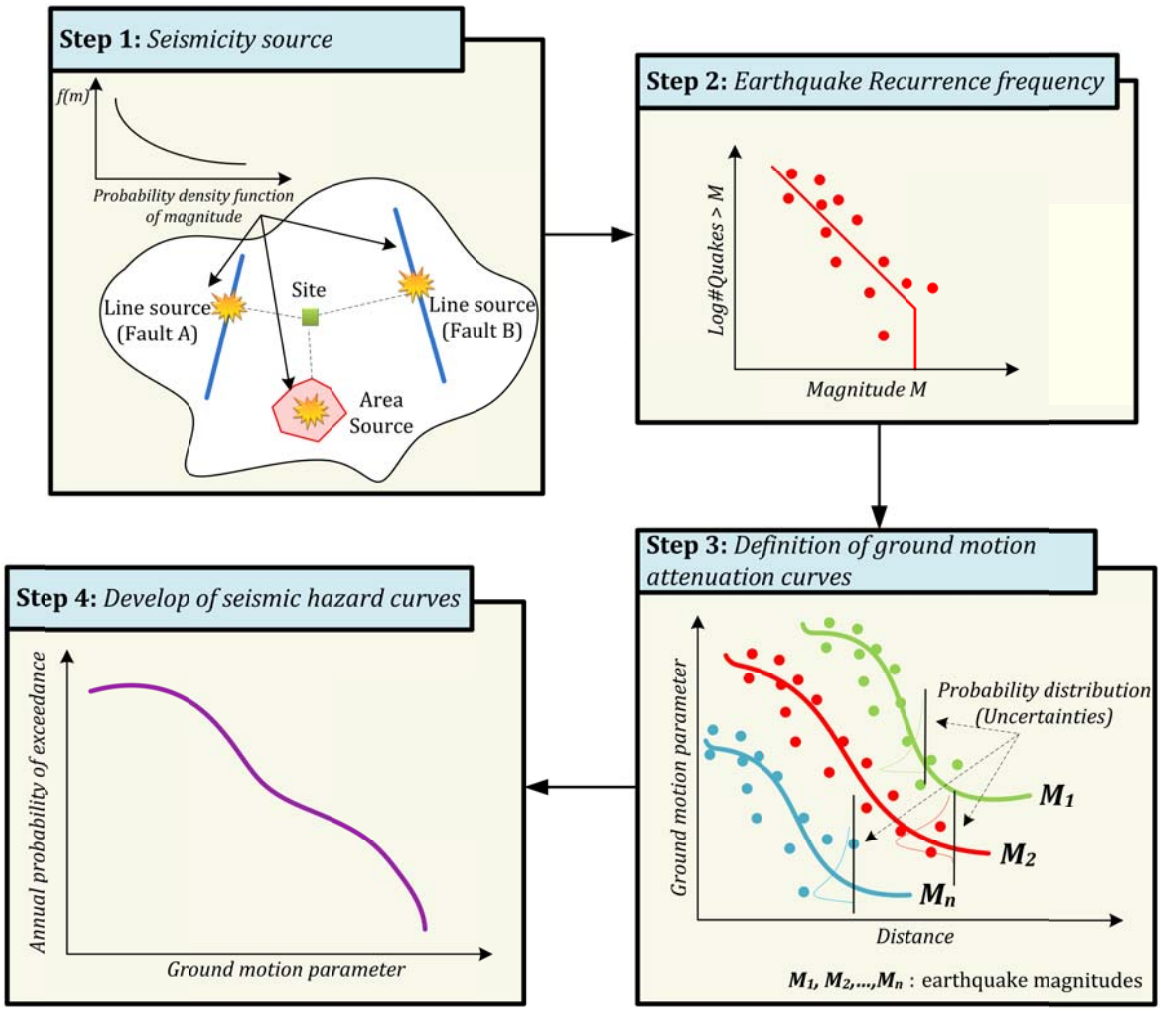

Figure 5.3. Steps in probabilistic seismic hazard analysis.

5.3.1. Seismic Source Model

Seismic source characterization is generally rooted in geoscience knowledge that relates earthquakes to geological structure. The defined geographic distribution of seismic sources and the specification of all source characteristics required for the seismic hazard analysis is defined as the seismotectonic model. The seismotectonic model provides a complete description of earthquake occurrence in time and space. Hence, the seismic source model is a description of the magnitude, location, and timing of all earthquakes (usually limited to those that pose a significant threat). For example, a source model might be composed of N earthquake scenarios (E_n), where each has its own magnitude (m_n), location (L_n) and the annual rate of the earthquake scenario (r_n):

$$E = E(m, L, r) \tag{5.2}$$

The fundamental assumptions in a defined seismic source are that (i) earthquake occurrence is uniformly distributed for a given magnitude within the source, and (ii) earthquake occurrence is only considered between a minimum earthquake magnitude of

engineering interest (M_0) and a maximum magnitude (M_{max}) that is representative of the entire source (Reiter, 1990). Therefore, *m* might represent the single characteristic magnitude of a specific fault, or it might represent a discrete value sampled from a fault or region that has a continuous (e.g., Gutenberg-Richter) distribution of events.

The seismic sources are shown as map representations of lines (fault sources) and area source zones based on the interpretation of multiple geological, geophysical, and seismological data. Line sources are defined as map-view representations of three-dimensional active fault planes for the purpose of accurate representation of faults that are considered capable of earthquake rupture. Area seismic sources define regions of the Earth's crust that are assumed to have uniform seismicity characteristics, they are distinct from neighboring zones, and are limited from active faults. So, the location term *L* is usually given as a point or a rectangular surface or an arbitrarily complex surface.

5.3.2. Earthquake recurrence frequency

The assessment of the earthquake recurrence frequency of the defined seismic sources in PSHA is based on two approaches: historical and geological frequency assessment. Historical frequency assessment is based on statistical analyses of the historical earthquakes that have occurred within a region. Geological frequency assessment is based on a prehistoric list of earthquake occurrence on faults (termed paleoseismicity) for the most tectonical active regions of the world. Earthquake frequency estimates in PSHA typically assume independence of earthquake events, or Poisson arrival times.

5.3.3. Ground Motion Model (Attenuation Relationship)

The ground motion attenuation relationships provide the estimation of a strong ground motion parameter of interest from specified seismological parameters, such as magnitude of an earthquake, source-to-site distance, faulting mechanism, local site conditions, etc. This relationship is a particularly important element in PSHA because it states the requirements of the seismic source definition, the ground motion parameters that can be estimated and contribute significantly to the uncertainty in the PSHA results, as it can be seen in Eq. (5.3) (McGuire and Shedlock, 1981, Bender, 1984). A logarithmic form of an attenuation relationship is:

$$\ln Y = c_1 + c_2 M - c_3 \ln D - c_4 D + c_5 F + c_6 S + \varepsilon \tag{5.3}$$

where, *Y* is the strong motion parameter of interest, *M* is the earthquake magnitude, *F* is the faulting mechanism of the earthquake, *S* is a description of the local site conditions beneath the site, ε is a random error term with a mean of zero and a standard deviation of $\sigma_{\ln Y}$, *D =f*

(d,M) is the distance term and *d* is a measure of the shortest distance from the site to the source of the earthquake. The coefficients c_1 to c_6, are defined in terms of *M* and *D* and they are dependent on the tectonic environment of the regions in which the earthquakes occurred (Chen and Scawthorn, 2003).

A wide variety of empirical ground motion attenuation relationships is available for application in PSHA and research has shown the ground motion attenuation to be regionally dependent. The most basic attenuation relationship gives the ground motion level as a function of magnitude and distance, but many attenuation laws include other parameters, as well to allow for different site types (i.e. soil type) or fault mechanisms. Different relationships have also been developed for different tectonic structures. All are developed by fitting an analytical expression to observations or to synthetic data in case of lack of observations. Empirical ground motion attenuation relationships are widely used to define the amplitude of earthquake ground motion at a site of interest and are expected to evolve as more data become available. In engineering applications, the ground motion parameters of interest are *PGA* and the response S_A, which gives the maximum acceleration experienced by an inelastic, single degree-of-freedom oscillator which is a crude representation of building response.

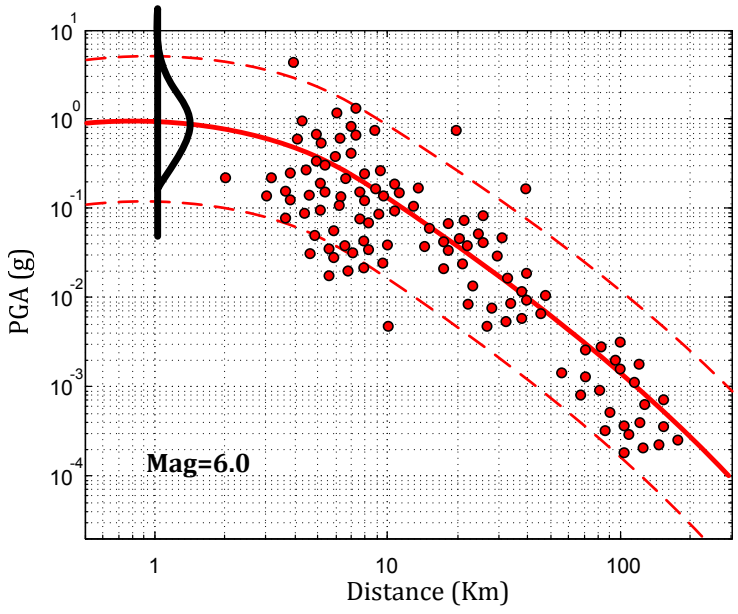

(a)

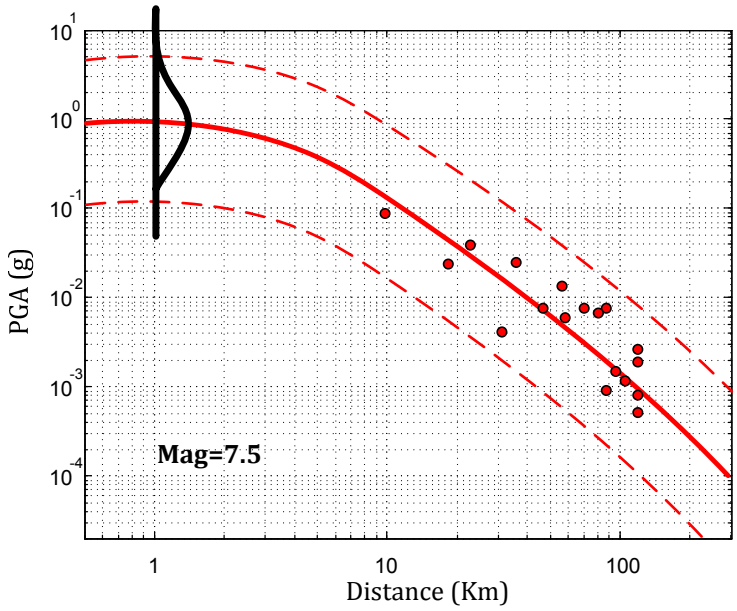

Figure 5.4. Median value and 95% confidence region predicted by the Boore, Joyner, and Fumal (1997) attenuation relationship for strike slip earthquakes and soil site conditions (taken from Field, 2010).

An example of the relationship proposed by Boore, Joyner, and Fumal (1997) is shown in Figure 5.4. The analytical expression for this particular expression is described as follows:

$$\ln(\mathrm{PGA}) = 0.53 \cdot (\mathrm{M} - 6) - 0.39 \cdot \ln\left(\mathrm{D}^2 + 31\right) + 0.25 \tag{5.4}$$

where D is the epicentral distance. The red dots are southern California observations for events within 0.2 magnitude units of that computed. The black normal curve represents the distribution of predicted values at 1 km distance.

5.3.4. Handling Uncertainties

It is common in earthquake risk analysis to distinguish between uncertainty that reflects the variability of the outcome of a repeatable experiment and uncertainty due to ignorance. This uncertainty is sometimes referred as "randomness", commonly known as "aleatory uncertainty", which cannot be reduced. However, both deterministic and probabilistic approaches are built on a number of model assumptions and model parameters that are based on what is currently known about the physics of the relevant processes and the behaviour of systems under given conditions. There is uncertainty associated with these conditions, which depends upon the state of knowledge that is referred to as "epistemic uncertainty". Both types of uncertainty (epistemic and aleatory) are implemented in PSHA, for example the mean and standard deviation of the magnitude of an event recorded at a specific distance is an epistemic uncertainty (handled with logic trees), while the scatter,

about the mean, of PGAs observed from all magnitude of the events recorded at a specific distance is an aleatory uncertainty (handled with probability distributions).

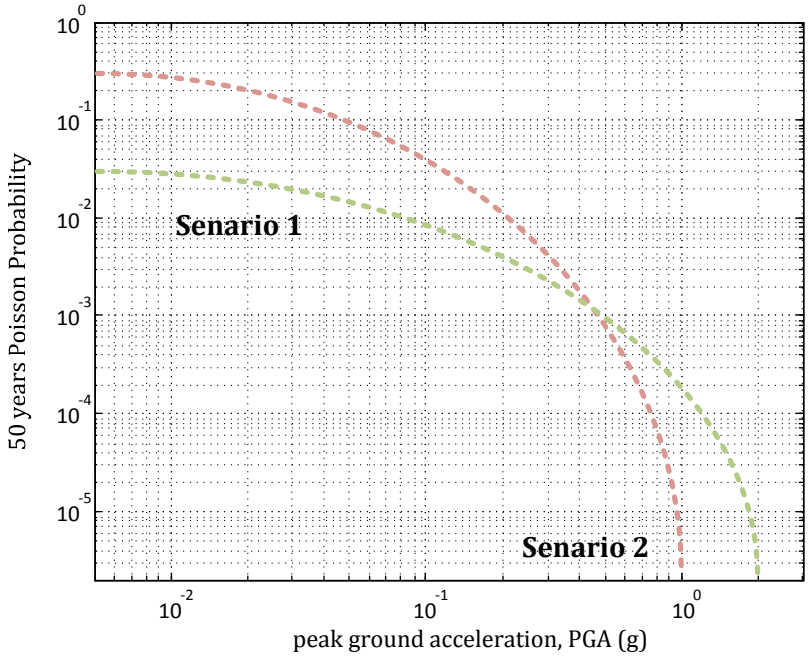

Figure 5.5. Hazard curves for the two scenarios treated as epistemic uncertainties (Field, 2010).

In the case of the attenuation relationships that mainly introduce the uncertainty in the PSHA procedure, which can be either epistemic or aleatory. The aleatory uncertainty is depicted in the scatter of the PGA values given by a single attenuation relationship due to the different models defined with reference to the earthquake magnitude, the faulting mechanism of the earthquake, the description of the local site conditions beneath the site etc (as an example see Figure 5.5 obtained by Field, 2010). The epistemic uncertainty is defined by the dispersion ($\sigma_{\ln Y}$) of the predicted values of ground motion parameter (by the attenuation relationship model) from the observed one. Improving the attenuation relationships (ground motion models) the epistemic uncertainty is reduced. Therefore, due to uncertainties a family of hazard curves is obtained and the representative one is either the average one or fractiles of the distribution (e.g., 95% fractile) (Field, 2010).

5.4. Ground Motion Excitation

The selection of the proper seismic loading for design and/or assessment purposes is not an easy task due to the uncertainties involved in the very nature of seismic excitations. A rigorous treatment of the seismic loading is to assume that the structure is subjected to a set of records that are more likely to occur in the region where the structure is located. The

seismic excitations that are more likely to occur are considered either as a set of natural or as a series of artificial accelerograms.

5.4.1. Natural records

For the implementation of the nonlinear dynamic analysis procedures like IDA, MIDA or MSDA (see for details in Chapter 4) a scale factor is calculated for each hazard level and for each one of the natural records selected. In order to preserve the relative scale of the two components of the records in the longitudinal and transverse directions, the component of the record having the highest $S_A(T_1,5\%)$ is scaled first, while the scaling factor that preserves their relative ratio is assigned to the second component. The records are selected randomly from a list of records (like the three lists of records given in Tables A.1 to A.3 of Appendix A). These records have been chosen from the PEER strong-motion database (2010) according to the following features: (i) events occurred in specific area (longitude -124^o to -115^o, latitude 32^o to 41^o); (ii) moment magnitude (M) is equal to or greater than 5; (iii) epicentral distance (R) is smaller than 150 km.

5.4.2. Generation of artificial accelerograms

In order for the artificial accelerograms that will load the structure to be representative these accelerograms have to match some requirements imposed by the seismic codes. The most essential one is that the accelerograms have to be compatible with the elastic design response spectrum of the region where the structure is located. It is well known that each accelerogram corresponds to a single response spectrum for a given damping ratio. On the other hand, on each response spectrum corresponds an infinite number of accelerograms. Gasparini and Vanmarke (1976) were the first to propose the creation of artificial accelerograms based on a specific response spectrum. In this dissertation, the implementation presented by Taylor (1989) for the generation of statistically independent artificial acceleration time histories is adopted. This method is based on the fact that any periodic function can be expanded into a series of sinusoidal waves:

$$x(t) = \sum_k A_k \sin(\omega_k t + j_k) \tag{5.5}$$

where A_k is the amplitude, ω_k is the cyclic frequency and φ_k is the phase angle of the k^{th} contributing sinusoid uniformly distributed in the range $[0,2\pi]$. By fixing an array of amplitudes and then generating different arrays of phase angles, different motions can be generated that match the same elastic response spectra. The amplitudes A_k are related to the spectral density function in the following way:

$$G(\omega_k)\Delta\omega = \frac{A_k^{\,2}}{2} \tag{5.6}$$

where $G(\omega_k)\Delta\omega$ may be interpreted as the contribution to the total power of the motion from the sinusoid with frequency ω_k. The power of the motion produced by Eq. (5.5) does not vary with time. To simulate the transient character of real earthquakes, the steady-state motion are multiplied by a deterministic envelope function I(t):

$$Z(t) = I(t)\sum_k A_k \sin(\omega_k t + j_k) \tag{5.7}$$

The resulting motion is stationary in frequency content with peak acceleration close to the target peak acceleration. In this study a trapezoidal intensity envelope function is adopted for defining the shape of the artificial accelerogram. The generated peak acceleration is artificially modified to match the target peak acceleration, which corresponds to the chosen elastic design response spectrum. An iterative procedure is implemented to smooth the calculated spectrum and improve the matching (Gasparini, 1976). A target response spectrum and the corresponding response spectrum of an artificial accelerogram are depicted in Figures 5.6(a) and 5.6(b).

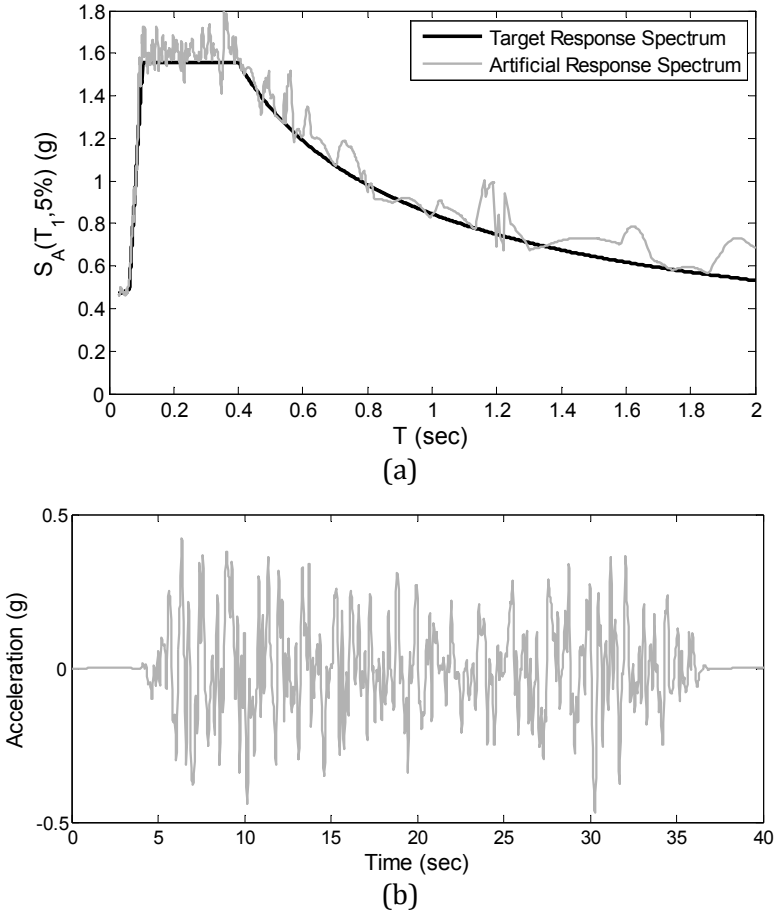

Figure 5.6. (a) Target (elastic design) response spectrum and response spectrum of the artificial accelerogram and (b) artificial accelerogram.

The mean (μ) response spectrum along with its dispersion ($\mu+\sigma$ and $\mu-\sigma$ denoted with dotted lines) are depicted in Figure 5.7, for the case of the NAT and ART generated according to the procedure described in this section.

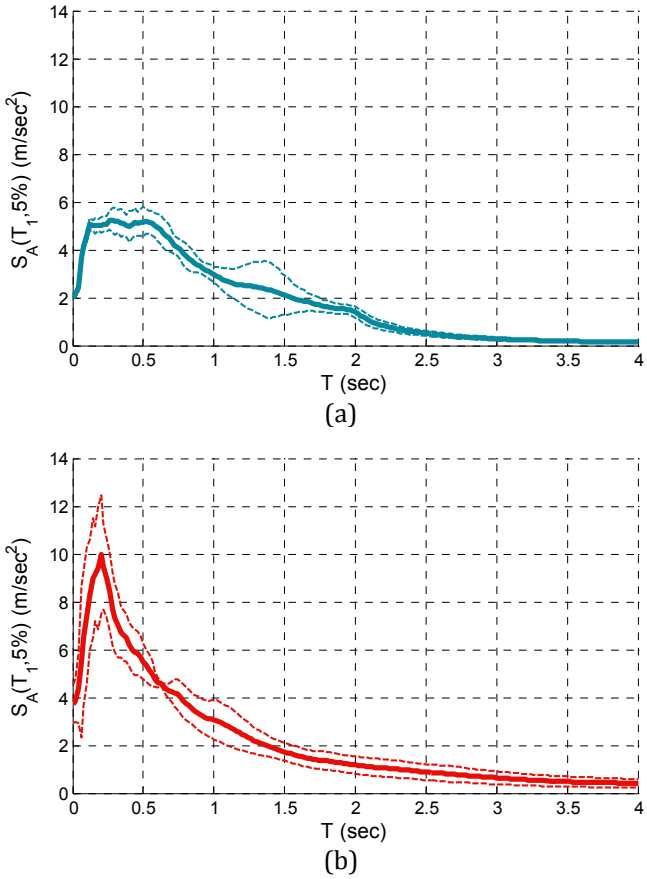

Figure 5.7. Mean response spectra of the 60 records for the class of (a) Artificial accelerograms and (b) Natural records (The dotted lines represent the μ+σ and μ-σ response spectra).

The three response spectra for the NAT class of records were obtained after scaling the 60 records of Tables A.1 to A.3 (of Appendix A) to the same $S_A(T_1,5\%)$, where T_1=0.628 sec for the 38.28/50 hazard level, in accordance to the hazard curve of the city of San Diego, California. Comparing NAT and ART class of accelerograms it can be seen that the dispersion of the response spectra for the ART class of accelerograms is lower to that of the NAT class (see Figure 5.7). This is due to the fact that a significant number of uncertain parameters are ignored in the case of ART.

5.4.3. Probabilistic definition of the artificial ground motion characteristics

The definition of the seismicity of a region under examination is very critical for earthquake engineering purposes. The seismic risk of a region is defined by conducting PSHA. As it was mentioned in detail earlier in this chapter, PSHA involves the assessment of the probability of exceeding a specified seismic intensity at a particular site in some period of interest and it is defined through the calculation of a MHC. A MHC gives the annual probability or

frequency that a seismic ground motion at a specific region exceeds a chosen level (see Figure 5.8). The calculation procedure of the MHC involves many uncertainties and for this reason multiple seismotectonic models or a single seismic hazard model are developed in the form of a logic tree. This logic tree collects all the knowledge and information related to seismic sources, earthquake recurrence frequency, ground motion attenuation and ground motion occurrence probability at a site. The partial logic tree of the California seismic hazard model (2002) used in the current study for the generation of artificial accelerograms taking into account various sources of randomness is depicted in Figure 5.9.

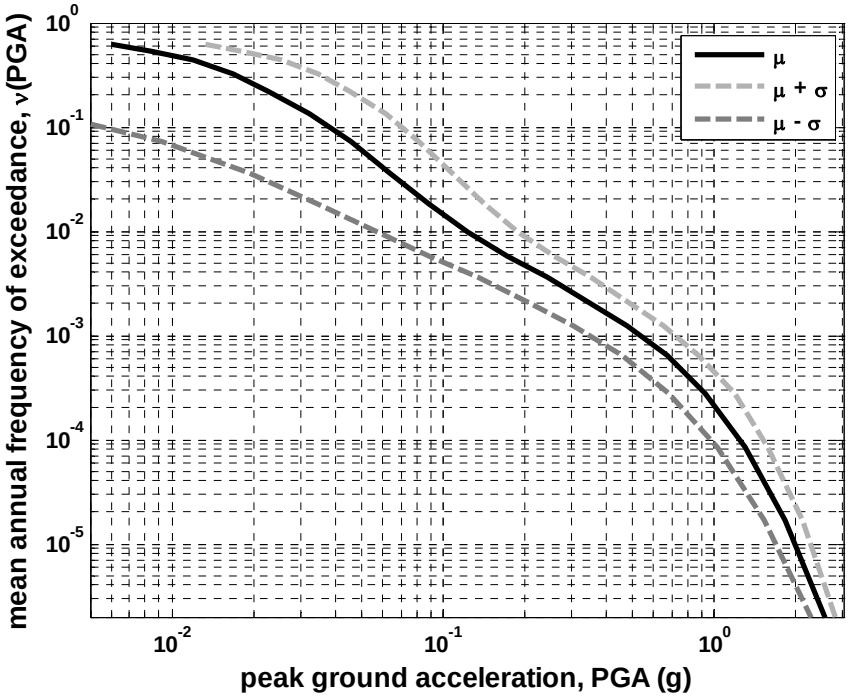

Figure 5.8. Mean and dispersion hazard curves of the city of San Diego, California (Latitude (N) 32.7°, Longitude (W) -117.2°).

The two main components of a seismic hazard model are the earthquake rupture forecast (*fault rupture area-magnitude relations*) and the intensity measure relationship (*attenuation relations*). The first one gives an inventory of all possible earthquake – rupture events in the region, and their associated probabilities, over a specified time span and above a threshold magnitude, while the latter provides the probability that an amplitude intensity measure will exceed a specified value at a site given the occurrence of an earthquake rupture event (Field et. al, 2005). The *fault rupture area-magnitude relations* are derived from statistical analyses of the historical records of earthquakes for tectonically active areas where paleoseismic studies of active faults have been performed. The *attenuation relations* are empirical relations which provide the mean value of the estimation of an amplitude of a strong motion parameter from the parameters of the earthquake, i.e. magnitude, source to site distance, faulting mechanisms, local site conditions, etc. The *attenuation relations* are site dependent and it is therefore critical to establish an appropriate relation according to

the tectonic setting of the site of interest. The characteristics of an *attenuation relation* and its site dependence declare its important role in the PSHA due to the introduction of most of the uncertainties involved in the whole hazard estimation procedure.

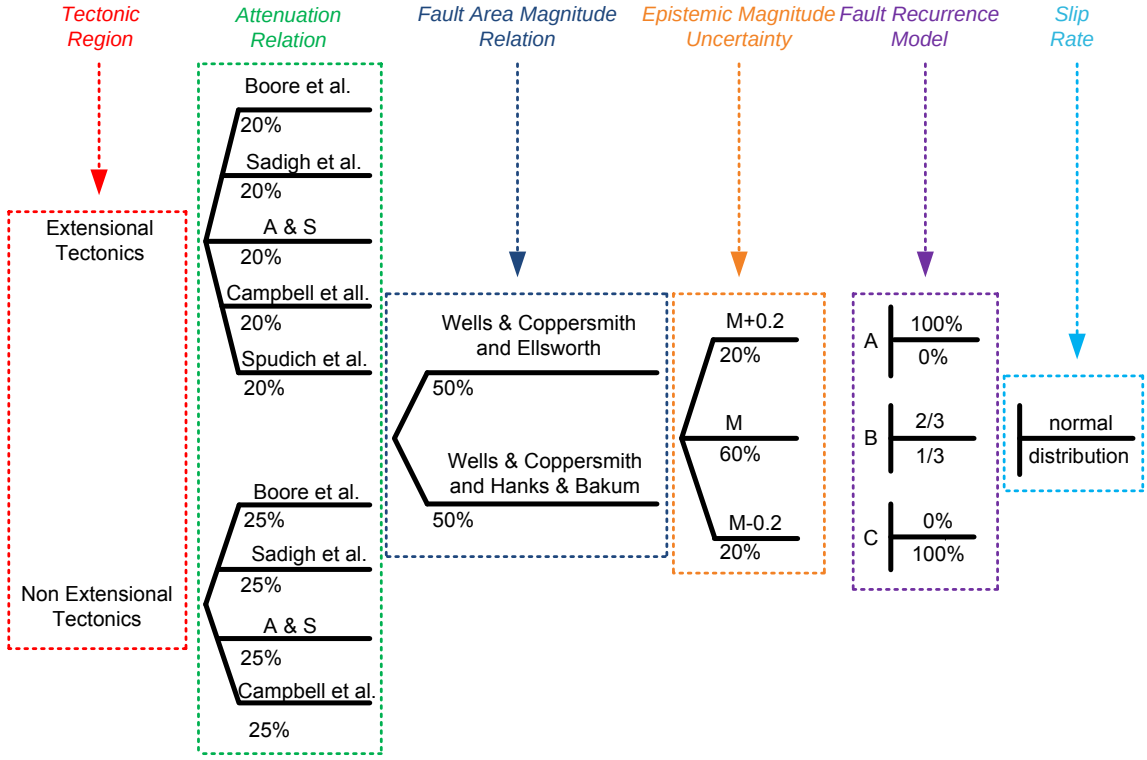

Figure 5.9. Partial logic tree for the 2002 update of the California seismic hazard model (Cao et. al, 2002).

Each branch of the logic tree represents alternative hypotheses, for each one of the *seismic source, earthquake recurrence frequency, ground motion attenuation* and *ground motion occurrence probability at a site*, and their weight factors in PSHA. The weight factors represent the probability of each alternative option being correct. The most appropriate method for sampling a logic tree is the Monte Carlo Simulation method, since each branch refers to an uncertain factor important for the PSHA. The hazard models or seismic scenarios sampled from a logic tree using Monte Carlo simulation produce a hazard curve for the specific hazard model at a particular site, based on the branches and the respective weight factors that describe each hazard model. The MHC is derived from the curves coming from the multiple hazard models. The uncertainties of a seismic hazard model are separated into **random** or **aleatory** and **model** or **epistemic**. *Aleatory* are defined the uncertainties that are associated with the empirical data based on nature, i.e. the variability in earthquake sources and ground shaking parameters. The standard deviation included in an attenuation relation is an aleatory uncertainty. *Epistemic* are called the uncertainties that are associated with the interpretation and characterization of the empirical data and their correct representation through appropriate formulas and predictive models. For example, the use of

attenuation relations and fault rupture area-magnitude relations, refers to an epistemic uncertainty. In a PSHA framework the main uncertainties refer to maximum magnitude, earthquake recurrence rate, location and segmentation of seismogenic faults, distribution of seismicity between faults, and attenuation relationships (Chen and Scawthorn, 2003).

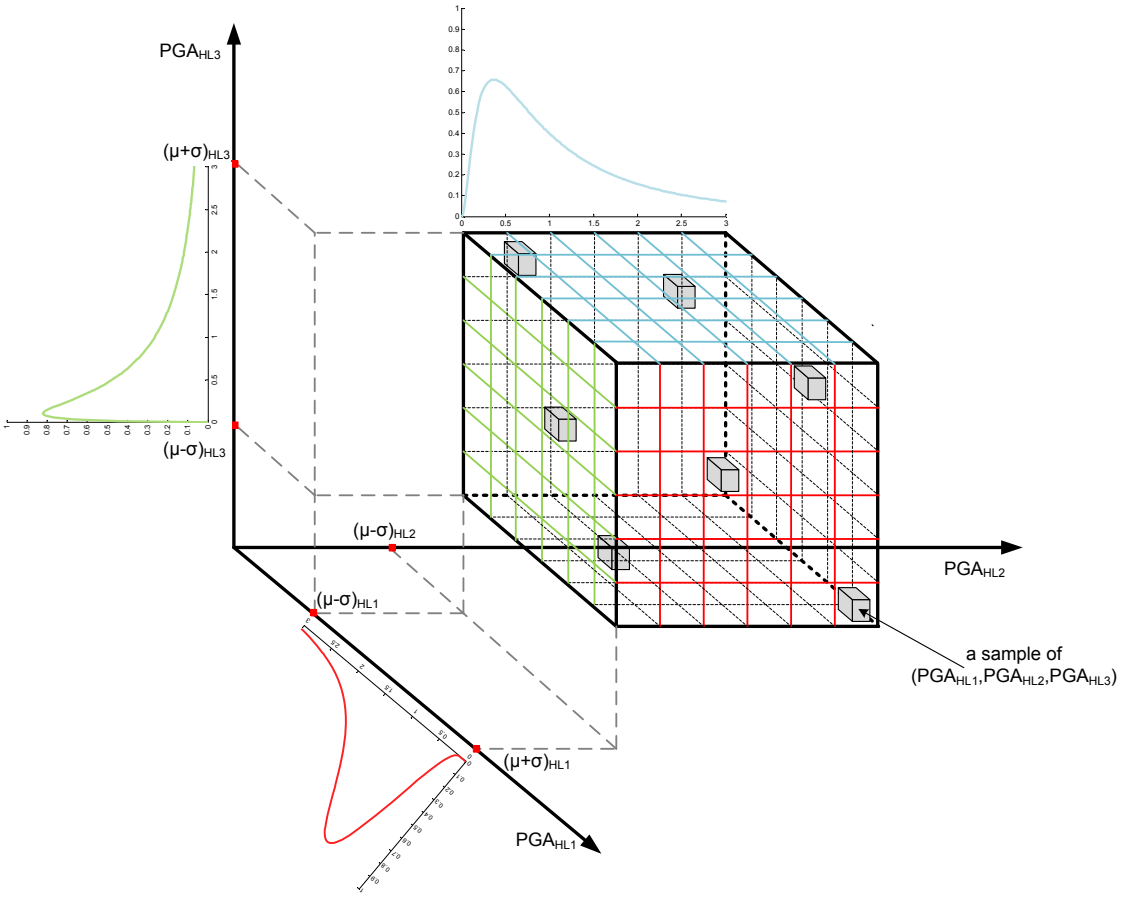

Figure 5.10. The UART procedure for generating artificial accelerograms based on LHS (M=3).

One of the main products of a MHC is the constant probability response spectrum that is used in seismic design codes and is presented by a plot of response to probabilistic PGAs (ground motion acceleration) over a number of oscillator periods at a constant return period. The derivation of the MHC relies on the response spectrum defined by its mean values. When it comes to the production of artificial ground motions, the generation procedure is based on the successful fitting of the artificial accelerogram response spectrum with the response spectrum obtained from the hazard curve of a site. Due to the fact that the uncertainties following the MHC are propagated through its generated products, such as the response spectrum, a new methodology is developed in the framework of this dissertation in the field of artificial ground motion generation by taking into consideration the covariance of the MHC values due to the uncertainties involved in a PSHA.

The region under examination is chosen to be the city of San Diego, California (Latitude (N) 32.7^{o}, Longitude (W) -117.2^{o}). The COV of the PGA for 2% and 10% probability of

exceedance was selected in distance of 100 km and was obtained by the study of Cao *et al.* (2002) where a part of the 2002 California Seismic Hazard logic tree (USGS) at a site along San Andreas fault is used (see Figure 5.9). Based on the fact that the COV is increasing with the increase of the probability of exceedance, the probabilities of exceedance for other hazard levels were derived through a fitting curve. Based on these characteristics the MHC along with the $\mu+\sigma$ and the $\mu-\sigma$ hazard curves for the region under investigation are shown in Figure 5.8. The uncertainties involved in the seismic scenarios for the generation of the hazard curves are: (i) tectonic region; (ii) attenuation relation; (iii) fault rupture area-magnitude relation; (iv) epistemic magnitude; (v) fault recurrence model (characteristic and Gutenberg-Richter) and (vi) slip rate (Figure 5.9).

In this dissertation a procedure for taking into account the uncertainties described above in the generation procedure of artificial accelerograms is proposed and it is denoted as UART. This procedure is based on the LHS technique and it is presented schematically in Figure 5.10. LHS is a strategy for generating random sample points ensuring that every part of the random space is adequately represented. Latin hypercube samples are generated by dividing each random variable into N non-overlapping segments of equal probability. Thus, if M random variables are considered the random variable space is partitioned into N^M cells. For each random variable, a single value is randomly selected from each segment, producing a set of N values. The values of each random variable are randomly matched with each other to create N samples. LHS is, therefore, used in order to generated N samples of PGA values for the HL in question. The samples (PGA_{HL1}, PGA_{HL2}, PGA_{HL3}) correspond to the three hazard levels, where PGA_{HLi} is a random variable following the lognormal distribution (Aslani and Miranda, 2005) with mean value obtained from MHC and standard deviation obtained from the study of Cao et al. (2002) and best fit as it was described above.

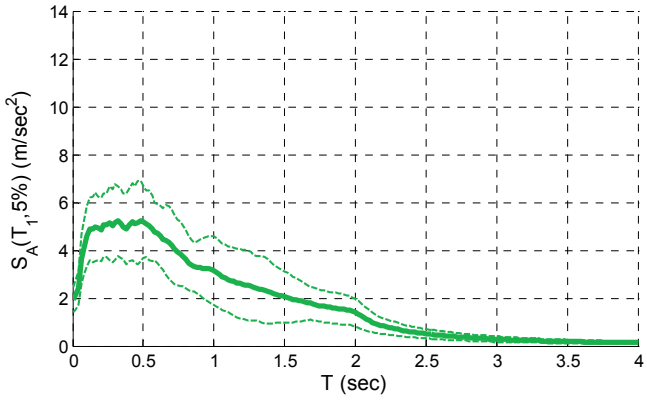

Figure 5.11. Artificial accelerograms with uncertainty (The dotted lines represent the μ+σ and μ-σ response spectra).

Significant dispersion was observed on the structural response with the use of different natural records (Iervolino et. al, 2009), while the implementation of artificial accelerograms

tends to underestimate seismic response (Iervolino et. al, 2010). This underestimation can be justified by the fact that uncertainties are ignored in the generation of the artificial accelerograms resulting to a small dispersion on the ground acceleration values as shown in Figures 5.7(a) and (b) for the conventionally generated artificial accelerograms and the natural records, respectively. Figure 5.11 provides the mean (μ) response spectrum along with its dispersion for the class of artificial accelerograms generated according to the proposed procedure, denoted as set UART. The proposed procedure UART results to an increased dispersion on the response spectra and consequently to an increased dispersion on the values of the ground acceleration, as it can be seen comparing Figures 5.7(a) and 5.13, this is because a significant number of uncertain parameters are ignored in the case of ART generated artificial accelerograms. It is worth mentioning that the size of the variance is similar to that of the NAT class of records (see response spectra of Figure 5.11 compared to those of Figure 5.7(b)).

5.5. Structural Models and Numerical Simulation

The two multi-storey 3D RC buildings considered are the same with those presented in Chapter 4 (sections 4.5.2 and 4.5.3) while the designs obtained for q=3 are used.

5.6. Intensity Measures

Earthquake engineering is a scientific field strongly connected with the effect of strong ground motions on people and environment. Strong ground motions are extremely complicated and a lot of data are required for their complete description. The definition of a number of ground motion parameters, named IM, simplifies the description of a strong ground motion and links the seismic hazard with the structural data required for the solution of earthquake engineering problems. The most significant characteristics of a ground motion from an earthquake engineering point of view are the *amplitude* (acceleration, velocity and displacement), the *frequency content* and the *motion duration*. Some of the IM are related to amplitude or to frequency content, to duration, or to more that one of the three essential ground motion characteristics. The IMs that are related to the effect of more than one ground motion characteristics are considered more reliable for the description of a ground motion and are most suitable to reflect the potential damage that a ground motion can produce.

The most commonly used *amplitude* IM derived from an accelerogram are the peak ground acceleration (high frequency component), peak velocity (intermediate frequency component), peak displacement (low frequency component), sustained maximum

acceleration and velocity and the effective design acceleration. Amplitude IMs are used for the derivation of empirical attenuation relationships used in PHA, because their production is based on IMs' dependence, on the magnitude of the earthquake and on the site-to-source distance. *Frequency content* IMs describe through different types of spectra, how the amplitude of a ground motion is distributed among different frequencies. IMs related to frequency content are Fourier spectra and power spectra that correspond to the frequency content of the ground motion itself, and the response spectra, that correspond to the influence of the ground motion on structures with different firstmode eigenperiods. Among this type of IMs are spectral parameters, like the predominant period, bandwidth, central frequency, shape factor, Kanai-Tajimi parameters and the ratio v_{max}/a_{max} which describes the frequency content of a ground motion. The most commonly used *duration* IM is the bracketed duration which is defined as the time between the first and the last exceedance of a threshold acceleration, usually equal to 0.05g.

Arias Intensity (I_A), *Characteristic intensity* (I_C) and *Cumulative Absolute Velocity* (CAV) are three IMs that reflect the amplitude, the frequency content and the duration of a strong ground motion respectively and they correlate well with structural damage. *Arias Intensity* (I_A) is defined as the time-integral of the square of the ground acceleration:

$$I_A = \frac{\pi}{2g}\int_0^{\infty}\left[a(t)\right]^2 dt \quad (m\cdot \sec^{-1}) \tag{5.8}$$

where *a(t)* is the ground acceleration, g is the acceleration due to gravity (9.81 m/sec^2), π is a mathematical constant equal to 3.1415926 and is expressed in units of velocity i.e. meter per second. The symbol of infinity in the time integration means that I_A is calculated over the entire duration and not over the duration of the strong ground motion T_d that is defined through specific methods.

Characteristic intensity (I_C) is defined as:

$$I_C = a_{rms}^{1.5} T_d^{0.5} \quad \left(\frac{m^{1.5}}{\sec^{2.5}}\right) \tag{5.9}$$

where α_{rms} is the *rms acceleration* (root mean square acceleration) ground motion parameter and T_d is the duration of the strong motion.

Cumulative Absolute Velocity (*CAV*) is defined as the integral of the absolute acceleration in a time history and it is obtained through the following equation:

$$CAV = \int_0^{T_d}\left|a(t)\right| dt \quad (m\cdot \sec^{-1}) \tag{5.10}$$

where $|a(t)|$ is the absolute value of the acceleration time series at time t and T_d is the duration of the strong motion. *CAV* expresses the absolute area under the absolute accelerogram and corresponds to the cumulative absolute velocity that is well correlated with structural damage (Kramer, 1996).

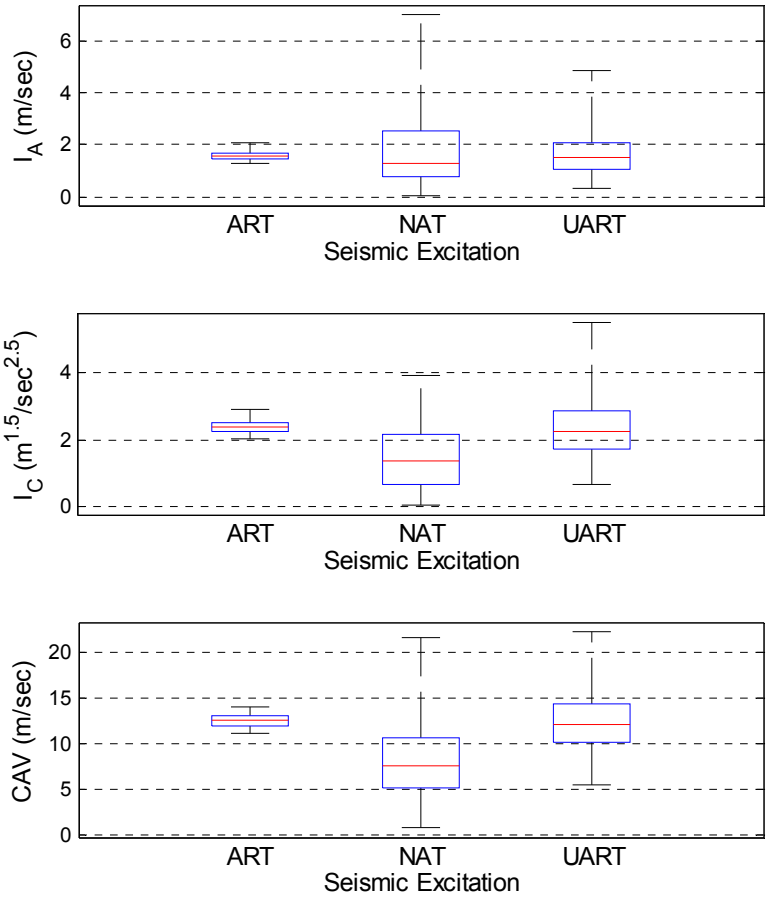

Figure 5.12. Mean and 25%, 75% confidence bounds for the values of I_A, I_C and CAV obtained for the classes of records considered.

These three IMs presented in this chapter of the dissertation are employed in the study for investigating their dispersion with reference to the three classes of seismic excitations considered. In particular, the *Characteristic intensity* is a measure that is related to a damage index that quantifies the damage due to the maximum deformation and the absorbed hysteretic energy (Kramer, 1996). In order to examine the influence of the class of seismic excitations considered on the values of the three IMs, the box plots depicted in Figure 5.12 have been generated for the 38.28/50 hazard level when 60 records are considered. For each IM considered and for each class of seismic excitation a box plot was created. On each box, the central mark denoted with a red line is the median value of the IM in question. The edges of the blue box represent the 25% and 75% percentiles while the whiskers denoted with black lines extend to the most extreme data points i.e. represent the range of the IMs

values. For all three IMs, ART class of accelerograms, has the narrower range and confidence bounds. On the other hand, the median values of ART and UART are close to each other while NAT varies significantly for the case of I_C and CAV. For the case of I_A the three median values are quite close. For the 25% and 75% percentiles, I_C and CAV, for NAT and UART classes of seismic excitations have similar box sizes. On the other hand, in the case of I_A the range of the values for the case of the UART is narrower compared to that of NAT. It is therefore anticipated that using the proposed UART class of seismic excitations similar range of values to that of the NAT class are achieved.

5.7. Numerical Tests

In this section the two 3D RC buildings described previously, have been considered in order to study the influence of the three classes of seismic excitations in the framework of LCCA. Multiple-stripe dynamic analysis was performed for both RC buildings while for each class of seismic excitations, sets of 15, 20, 30 and 60 records, have been applied. The performance of the two buildings was assessed with reference to the maximum inter-storey drift and floor acceleration induced by three hazard levels for each class of ground motions. The results of 360 nonlinear time-history analyses, (2 buildings times 60 artificial records-random variable samples times 3 hazard levels), were postprocessed in order to create a response databank with the maximum interstorey drift ratio along the height of the buildings and the maximum floor accelerations.

5.8. Implementation of the LCCA

The life-cycle cost calculation procedure (as it will be described in detail in Chapter 6) involves the assessment of the structural capacity at a number of three hazard levels of increasing intensity based on the definition of the corresponding three pairs of annual probability of exceedance $(\overline{P}_i)$ and maximum value of the damage index in question (DI_i). In this work the *abscissa* values of the $(\overline{P}_i - DI_i)$ pairs, corresponding to the maximum values of the damage index for a number of hazard levels in question, are obtained by means of a MSDA, while the *ordinate* values correspond to the annual probabilities of exceedance.

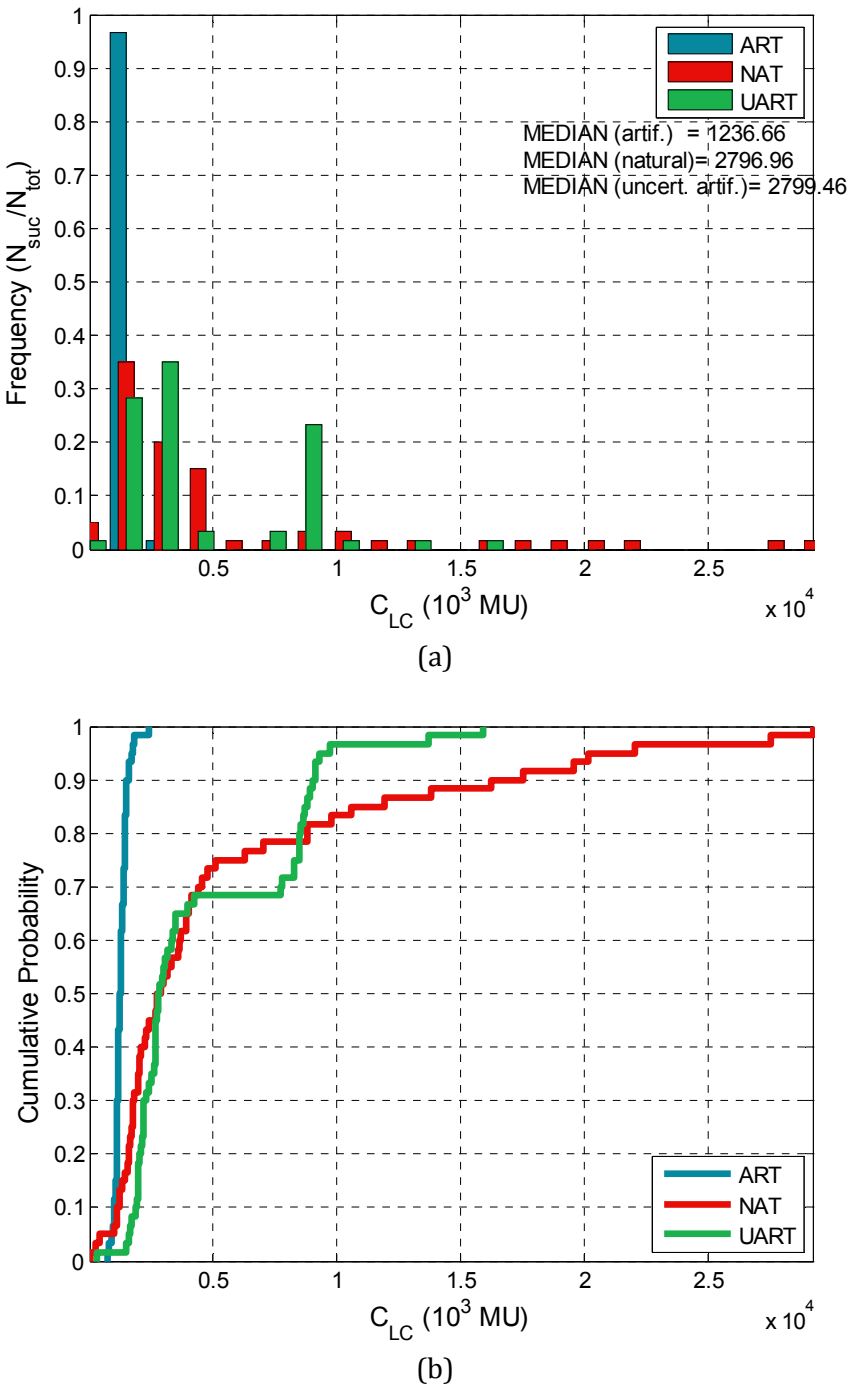

Figure 5.13. Eight storey test example: (a) frequency of occurrence for the case of MSDA(60) and (b) cumulative density function.

Three hazard levels are considered, namely the: 100/50, 38.28/50 and 5.90/50 hazard levels, corresponding to discrete values of annual probabilities of exceedance, obtained from the USGS ground motion parameter calculator (USGS, 2010) in accordance to the hazard curve of the city of San Diego, California (Latitude (N) 32.7°, Longitude (W) -117.2°, Figure 5.8). For the implementation of the MSDA, multiple nonlinear dynamic analyses have to be performed in order to assess the test buildings' structural performance in all three hazard

levels. The application of MSDA incorporated into LCCA (see Chapter 6 for details) results in a time-consuming and computationally-demanding procedure since, as it was shown by Iervolino *et al*., (2009), several records are required for obtaining reliable estimation of the life-cycle cost of a structural system. Therefore, the main objective of the investigation presented in this Chapter is to propose an attenuative procedure for generating the smallest feasible set of accelerograms, capable of providing a reliable evaluation of the structural performance in the minimum possible computing time.

The class of seismic excitations (ART, NAT or UART) determines the corresponding implementation of LCCA in conjunction to MSDA. In particular, in the case of ART class 15, 20, 30 or 60 artificial accelerograms are generated for each hazard level and they are combined by means of LHS. In the case of NAT, in order to make sure that the randomly selected number of records *no_recs* (where *no_recs* = 15, 20 or 30) of *MSDA* are not dominated by a few events, an equal number of records from each earthquake was applied. This was performed by means of LHS by selecting one, two or more records from the same earthquake event depending on the number of records used. In the case of UART 15, 20, 30 or 60 artificial accelerograms are generated for each hazard level, as in the case of ART. However, the uncertainties on the PGA values are considered using a combination of the mean value and the coefficient of variation by means of the LHS technique as proposed in the previous section. The mean value is obtained from the hazard curve of Figure 5.8, while the coefficient of variation was obtained by the work of Cao *et al*., (2002).

5.9. Uncertainty on the seismic excitation

The influence of the three classes of seismic excitation on the LCCA evaluation is examined with reference to the computational efficiency and the robustness on the obtained results. The histograms in Figures 5.13(a) and 5.14(a) show the probabilistic distribution of the life-cycle cost values corresponding to ART, NAT and UART class of seismic records implemented in the MSDA for the two test examples, respectively. The frequency of C_{LS} value occurrence is defined as the ratio of the number of simulations (N_{suc}), corresponding to life-cycle cost values in a specific range, over the total number of simulations (N_{tot}), where N_{tot} is equal to 60. Comparing the histograms of Figure 5.13(a) it can be noticed that the dispersion for the case of NAT class of records is significant.

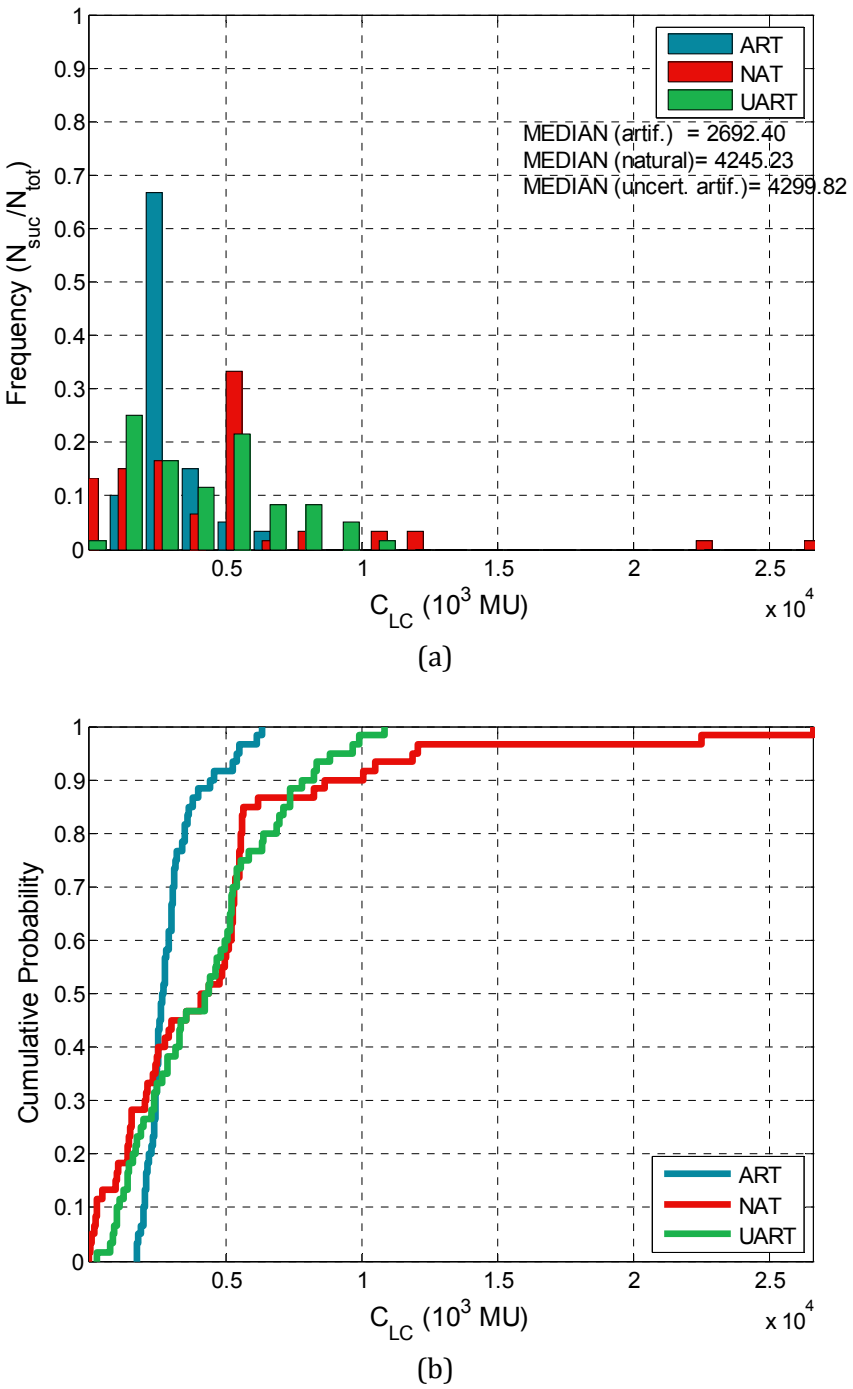

Figure 5.14. Five storey test example: (a) frequency of occurrence for the case of MSDA(60) and (b) cumulative density function.

On the other hand, there is almost no dispersion on the results of ART class of seismic excitations. However, the estimated median value of the life-cycle cost for the ART is half of that estimated for the NAT class which is considered the correct one (Iervolino et. al, 2010). This is due to the fact that the artificial accelerograms underestimate the structural response. On the other hand, the proposed procedure UART for generating artificial accelerograms taking into account uncertainty on the PGA values proved to be capable for

estimating with acceptable accuracy the life-cycle cost value, compared to that estimated by the NAT class of seismic excitations, achieving significantly less dispersion. Similar conclusions can be drawn for the second test example as it is presented in Figure 5.14(a).

The cumulative density function (CDF) curves, corresponding to the three classes of records (ART, NAT and UART) for the symmetrical and irregular test example, are depicted in Figures 5.13(b) and 5.14(b). These two plots confirm the findings shown in Figures 5.13(a) and 5.14(a), where the dispersion of the ART class of seismic excitations is very small, in the range of 2 to 3.5 million of monetary units (MU, corresponding to Dollars or Euros) for the symmetric building (see Figure 5.13(b)) and in the range of 3 to 6.5 million of monetary units for the irregular building (see Figure 5.14(b)). On the other hand, the dispersion of the NAT class of seismic excitations is in the range of 1 to 25 million monetary units for the symmetric building and in the range of 1 to 20 million monetary units for the irregular building with cumulative probability 95%. For the case of UART a small dispersion is confirmed since LCC varies in the range of 1 to 8 million monetary units for the symmetric building and in the range of 1 to 7 million monetary units for the irregular building with cumulative probability 95%.

Figure 5.15 provides evidence of the robustness on the calculation of the life-cycle cost of the three classes of seismic excitations for the symmetric and the irregular building, respectively. Due to the significant dispersion on the estimation of the seismic response, when the NAT class of seismic excitations is implemented, the variation on the estimation of the life-cycle cost extends to 60% for the symmetric building and 25% for the irregular one. On the other hand, as a result of the similarity of the characteristics of the artificial accelerograms generated according to ART and UART the dispersion in the estimation of the life-cycle cost is in the range of 0.5 to 3.0% for ART and in the range of 0.5 to 8.0% for UART. Therefore UART and ART are not influenced by the number of records. It is worth mentioning that 15 records of the UART class result to the same accuracy, in terms of life-cycle cost estimation, as the 60 records of the NAT class. Consequently, the computational cost required, is reduced by four times when implementing the proposed procedure with the UART generated seismic excitations. This reduction has a significant impact on the life-cycle cost estimation of real world structures.

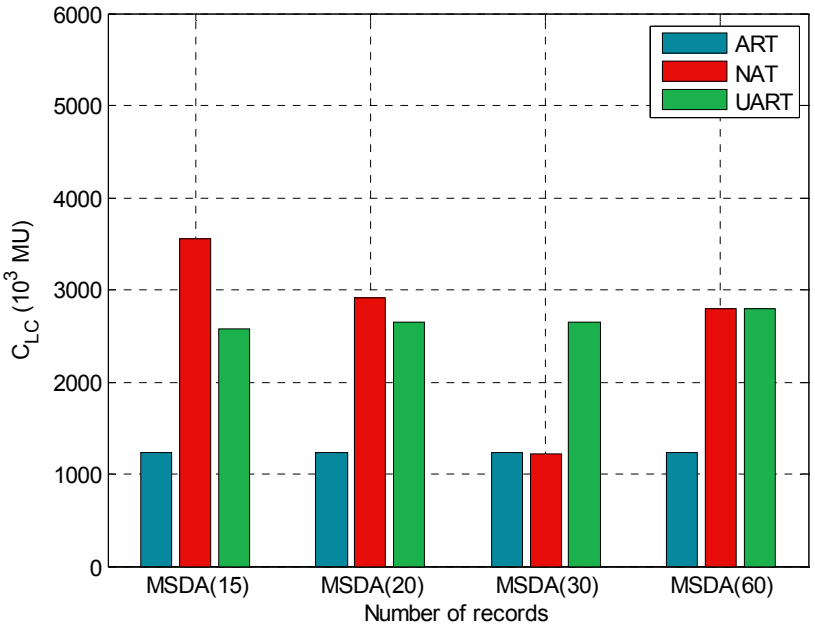

(a)

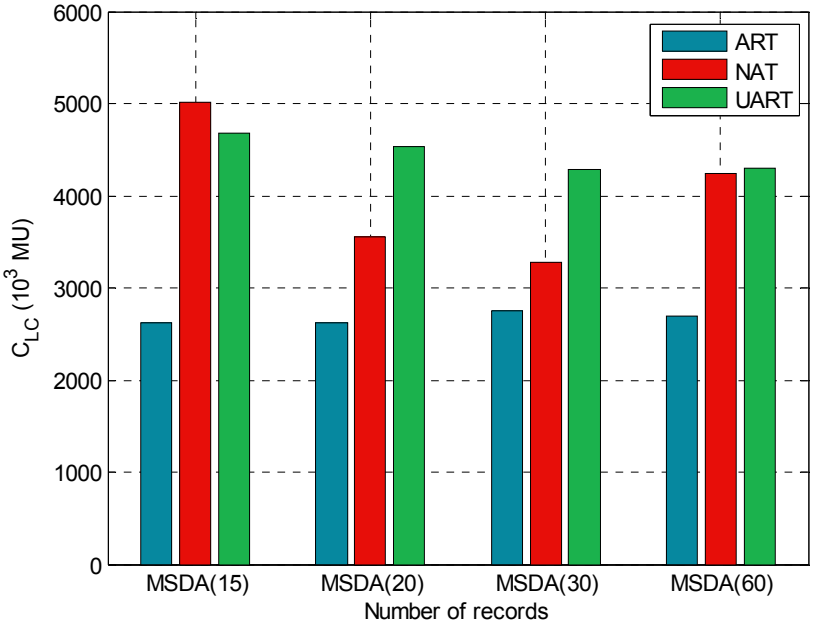

(b)

Figure 5.15. Variation with reference to the number of records (10^3 MU): (a) eight storey test example (b) five storey test example

5.10. Discussion

In the construction industry, the decision making for structural systems situated in seismically active regions involves a consideration of the cost of damage and other losses costs resulting from earthquakes occurring during the lifespan of the structures. The initial cost is related to the material and the labour cost for the construction of the building which

includes both structural and non-structural components. The life-cycle cost refers to the potential damage cost from earthquakes that may occur during the life of the structure. Thus, the life-cycle cost assessment becomes an essential component of the design process in order to control the initial and the future cost of building ownership for investment purposes. The life-cycle cost is calculated on the basis of the damage repair cost and loss of contents cost, due to structural damage associated with the maximum inter-storey drift, the loss of rental cost, the income loss cost, the cost of injuries as well as the cost of human fatality and the loss of contents cost due to floor acceleration expressed in today's values, based on an assumed interest rate time model.

A procedure for taking into account a number of uncertainties in the generation of artificial accelerograms is proposed in this chapter of the dissertation in an effort to increase the representativity of the seismic records and reduce the resulting computational cost in assessing the structural performance in the framework of the life-cycle cost assessment. This procedure is based on the Latin hypercube sampling technique used for generating N samples of the PGA, corresponding to the hazard levels considered three types of accelerograms. The value of PGA for each hazard level is a random variable following the lognormal distribution with mean value obtained from the mean hazard curve. The uncertainties considered in the hazard curves are related to: (i) tectonic region, (ii) attenuation relation, (iii) fault-rupture relation, (iv) epistemic magnitude, (v) characteristic and Gutenberg-Richter recurrence processes and (vi) slip rate. The numerical study for the calculation of the life-cycle cost using the three types of accelerograms denoted as NAT, ART and UART, was performed on 3D RC building structures with regular and irregular plan views. Multiple stripe dynamic analysis, a variant of the incremental dynamic analysis, was applied, to compute the performance criteria above namely as maximum inter-storey drift and floor acceleration.

It was confirmed that a significant dispersion on the structural performance was observed due to the use of a set of natural records, while on the other hand the artificial accelerograms underestimated the seismic response of the structure. However, the proposed procedure for generating a minimum set of artificial accelerograms required for a reliable structural assessment and design leads to a reliable and cost efficient estimation of the life-cycle cost of reinforced concrete buildings subjected to seismic actions.

5.11. References

Anderson, J.G. and J.N. Brune (1999). Probabilistic hazard analysis without the ergodic assumption, Seism. Res. Lett. 70, 19-23.

Arditi DA, Messiha HM. Life-cycle costing in municipal construction projects, Journal of Infrastructure Systems 1996; 2(1):5-14.

Asiedu Y, Gu P. Product life cycle cost analysis: state of the art review, Int. J. Prod. Res. 1998; 36: 883-908.

Aslani H, Miranda E. Probability-based seismic response analysis. Eng Struct 2005; 27(8): 1151-1163.

ATC-13. Earthquake Damage Evaluation Data for California. Applied Technology Council: Redwood City, CA, 1985.

Bender, B., 1984, "Incorporating Acceleration Variability into Seismic Hazard Analysis," Bull. Seismol. Soc. Am. , 74, 1451–1462.

Benjamin JR, and Cornell CA., 1970. Probability, Statistics, and Decision for Civil Engineers. McGraw-Hill: New York

Cao T, Petersen MD, Frankel AD. Model uncertainties of the 2002 update of California seismic hazard maps. Bulletin of the Seismological Society of America 2005; 95(6):2040-2057.

Chen Wai-Fah and Scawthorn Charles, Earthquake Engineering Handbook, CRC Press 2003

Chen, W.F., Scawthorn, C. (2003) Earthquake Engineering Handbook. CRC Press, New York.

Cornell, C.A. (1968). Engineering seismic risk analysis, Bull. Seism. Soc. Am., 58, 1583-1606.

Cornell, C.A. and S.R. Winterstein, 1988, "Temporal and Magnitude Dependence in Earthquake Recurrence models," Bull. Seismol. Soc. Am. , 78, 1522–1537.

Elenas A, Meskouris K. Correlation study between seismic acceleration parameters and damage indices of structures, Engineering Structures 2001; 23:698-704.

Ellingwood BR, Wen Y-K. Risk-benefit-based design decisions for low-probability/high consequence earthquake events in mid-America. Progress in Structural Engineering and Materials 2005; 7(2):56–70.

FEMA 227. A Benefit–Cost Model for the Seismic Rehabilitation of Buildings. Federal Emergency Management Agency, Building Seismic Safety Council: Washington, DC, 1992.

FEMA 273. NEHRP Guidelines for seismic rehabilitation of buildings. Federal Emergency Management Agency, Washington, DC, 1997.

Field E.H. (2010), Probabilistic Seismic Hazard Analysis (PSHA) A Primer, www.opensha.org/sites/opensha.org/files/PSHA_Primer_v2_0.pdf, (last accessed December 2010).

Field E.H., Gupta N., Gupta V., Blanpied M., Maechling P., and Thomas J.H. Hazard Calculations for the WGCEP-2002 Earthquake Forecast Using OpenSHA and Distributed Object Technologies. Seismological Research Letters Volume 76, Number 2 March/April 2005.

Fragiadakis, M., Papadrakakis, M. Modeling, analysis and reliability of seismically excited structures: Computational issues. International Journal of Computational Methods, 5(4): 483–511, 2008

Gasparini DA, Vanmarke EH. Simulated earthquake motions compatible with prescribed response spectra, Massachusetts Institute of Technology (MIT), Department of Civil Engineering, Publication No. R76-4, Cambridge (MA), January 1976.

Gasparini DA. SIMQKE, A program for artificial motion generation, User's manual and documentation, Massachusetts Institute of Technology (MIT), Department of Civil Engineering, November 1976.

Ghobarah A, Abou-Elfath H, Biddah A. Response-based damage assessment of structures, Earthquake Engng Struct. Dyn. 1999; 28(1):79-104.

Ghobarah A. On drift limits associated with different damage levels. International Workshop on Performance- Based Seismic Design, June 28 - July 1, 2004.

Giovenale P, Cornell CA, Esteva L. Comparing the adequacy of alternative ground motion intensity measures for the estimation of structural responses, Earthquake Engng Struct. Dyn. 2004; 33(8):951-979.

http://earthquake.usgs.gov/hazards/designmaps/ US Geological Survey (USGS) (last accessed February 2010).

http://peer.berkeley.edu/smcat/search.html/ Pacific Earthquake Engineering Research (PEER). (last accessed February 2010).

Iervolino I, De Luca F., Cosenza E. Spectral shape-based assessment of SDOF nonlinear response to real, adjusted and artificial accelerograms. Eng Struct 2010; 32(9):2776-2792.

Iervolino I, Maddaloni G, Cosenza E. A note on selection of time-histories for seismic analysis of bridges in Eurocode 8. J Earthq Eng 2009; 13(8):1125-1152.

Jalayer F, Cornell CA. Alternative non-linear demand estimation methods for probability-based seismic assessments. Earthquake Engng Struct. Dyn. 2009; 38(8):951-972.

Kent DC, Park R. Flexural members with confined concrete. Journal of Structural Division 1971; 97(7):1969-1990.

Kramer S.L., Geotechnical Earthquake Engineering, Prentice Hall, 1996.

Krinitzsky EL. How to combine deterministic and probabilistic methods for assessing earthquake hazards. Eng Geol 2003;70(1-2):157-163.

Lagaros ND. Multicomponent incremental dynamic analysis considering variable incident angle, Journal of Structure and Infrastructure Engineering 2010; 6(1-2):77-94.

Lagaros, ND. Life-cycle cost analysis of construction practices, Bulletin of Earthquake Engineering 2007; 5:425-442.

Marini A, Spacone E. Analysis of reinforced concrete elements including shear effects. ACI Structural Journal 2006; 103(5): 645-655.

McGuire, R.K. and K.M. Shedlock, 1981, "Statistical Uncertainties in Seismic Hazard Evaluations in the United States," Bull. Seismol. Soc. Am., 71, 1287–1308.

McKenna F, Fenves GL. The OpenSees Command Language Manual - Version 1.2, Pacific Earthquake Engineering Research Centre, University of California, Berkeley, 2001.

Menegotto M, Pinto PE. Method of analysis for cyclically loaded reinforced concrete plane frames including changes in geometry and non-elastic behaviour of elements under combined normal force and bending. Proceedings, IABSE Symposium on Resistance and Ultimate Deformability of Structures Acted on by Well Defined Repeated Loads: 15-22, 1973.

Mitropoulou Ch.Ch., Lagaros ND, Papadrakakis M. Economic building design based on energy dissipation: a critical assessment, Bulletin of Earthquake Engineering, 2010; 8(6): 1375-1396.

Mitropoulou ChCh, Lagaros ND, Papadrakakis M. Life-cycle cost assessment of reinforced concrete buildings subjected to seismic actions, Earthquake Engineering and Structural Safety, 2010; (submitted for publication).

Mitropoulou ChCh, Papadrakakis M. Selection of seismic excitations for the life-cycle cost assessment of structures, Structural Dynamics and Earthquake Engineering, 2010; (submitted for publication).

Rackwitz R, Lentz A, Faber M. Socio-economically sustainable civil engineering infrastructures by optimization. Structural Safety 2005; 27(3): 187-229.

Rackwitz R. The effect of discounting, different mortality reduction schemes and predictive cohort life tables on risk acceptability criteria, Reliability Engineering and System Safety 2006; 91(4):469-484.

Reiter, L. (1990). Earthquake Hazard Analysis, Issues and Insights, Columbia University Press, New York.

Sanchez-Silva M, Rackwitz R. Socioeconomic implications of life quality index in design of optimum structures to withstand earthquakes, J. of Str. Engng. 2004; 130(6):969-977.

SSHAC (Senior Seismic Hazard Analysis Committee). Recommendations for Probabilistic Seismic Hazard Analysis: Guidance on Uncertainty and Use of Experts, US Nuclear Regulatory Commission report CR-6372, Washington DC.

Taylor CA. EQSIM, A program for generating spectrum compatible earthquake ground acceleration time histories, Reference Manual, Bristol Earthquake Engineering Data Acquisition and Processing System, December 1989.

Thenhaus, P.C., 1983, "Summary of Workshops Concerning Regional Seismic Source Zones of Parts of the Conterminous United States, Convened 1979–1980, Golden, Colorado," U.S. Geological Survey, Circular 898 .

Thenhaus, P.C., 1986, "Seismic Source Zones in Probabilistic Estimation of the Earthquake Ground Motion Hazard: A Classification with Key Issues," Proceedings of Conference 34: Workshop on Probablistic Earthquake Hazards Assessments, pp. 53–71.

Wen YK, Kang YJ. Minimum building life-cycle cost design criteria. II: Applications. J. of Str. Engng. 2001; 127(3):338-346.

Wen YK, Kang YJ. Minimum building life-cycle cost design criteria. I: Methodology. J. of Str. Engng. 2001; 127(3):330-337.

WGCEP (Working Group on California Earthquake Probabilities) (1995). Seismic hazards in southern California: probable earthquakes, 1994 to 2024. Bull. Seism. Soc. Am., 85, 379-439.

Chapter 6

Life-Cycle Cost Assessment of Structures

6.1. Introduction

LCCA is a tool used for calculating the cost required for keeping an object like, a product, an enterprise or a structure, for a specific time period, which is defined as the lifetime of the object, in its initial condition. LCCA is an important procedure in the scientific field of structural engineering, because it can be used as an assessment tool of the structural response during its life and assess its influence on the structural system in economic terms and as an evaluation tool based on the economic impact of a structure on the community and also as a decision making tool in cases related to the performance of a structure.

The life-cycle cost of a building consists of the sum of the present value of all expected costs concerning the construction plus all the expenses related to maintenance and management of the structure during its life. Life-cycle cost usually refers to the deterioration of the structural components' capacity over time due to phenomena such as corrosion or weakening of the joints or the bearings (Frangopol et al., 1997). Moreover, life-cycle cost may refer to the risk related to natural hazards, such as wind or earthquake. In general the life-cycle cost is related to the possible losses due to unsatisfactory performance of the structure under loadings with random occurrence and intensity during its life. The design process should take into account both direct economic and human life losses within a given social context (Sanchez-Silva and Rackwitz, 2004).

In order to take into account damage and other earthquake losses into the LCCA procedure a reliable tool for estimating the capacity of any structural system in multiple earthquake hazard levels is required. IDA (Vamvatsikos & Cornell, 2002) is proven to be an analysis procedure for obtaining good estimates of the structural performance in the case of earthquake hazards and it is considered, among others (Fajfar, 2000, Chopra et al., 2002), an

appropriate method to be incorporated into the LCCA procedure. In view of the complexity and the computational effort required by the 3D structural analysis models simplified 2D structural simulations are usually used during the design procedure. This is mainly justified in plan-symmetric buildings and mostly in the case of steel framed buildings composed by 2D moment resisting frames. In 3D RC buildings, however, the columns belong to two or more intersecting lateral-force-resisting systems, therefore it is not possible to implement a 2D simulation since the bidirectional orthogonal shaking effects are significant and should be taken into account. Moreover, 3D models should also be considered in the case of non-symmetric in plan steel or RC buildings. More details on the analysis procedures are provided in Chapter 4 of this dissertation.

In this chapter the basic principles of LCCA are presented while 3D RC buildings with regular and irregular plan views were analysed in order to examine the sensitivity of life-cycle cost with reference to the analysis procedure (static or dynamic), the number of seismic records imposed, the performance criterion used and the structural type (regular or irregular). In particular, nonlinear static analysis and multiple stripe analysis, which is a variation of IDA, were applied with respect to the maximum interstorey drift and the maximum floor acceleration. Both in the regular and irregular in plan test examples, the life-cycle cost was calculated taking into consideration the damage repair cost, the cost of loss of contents due to structural damage that is quantified by the maximum interstorey drift and floor acceleration, the loss of rental cost, the income loss cost, the cost of injuries and the cost of human fatalities.

6.2. Literature Survey

The LCCA principles are based on economic theories, and have been used as decision-support tools in industrial and commercial projects. LCCA is mainly implemented to energy and water conservation projects as well as transportation projects, including highways, bridges, and pavements. When it comes to building structures, the application of LCCA is considered particularly important in the case of retrofitted/deteriorating structures. Especially in the case of steel and reinforced concrete building structures in seismic regions, LCCA is applied as a structural performance criterion for taking into account future damages due to earthquakes. Furthermore, it is also used as a decision making tool for the most cost-effective solution related to the construction of building structures in seismic regions.

In early 1960s LCCA was applied in the commercial area in the design of products considering the total cost of developing, producing, using and retiring. The introduction of LCCA was made in the field of infrastructures as an absolute investment assessment tool. In

particular, in early 1980s it was used in USA as an appraisal tool for the total cost of ownership over the lifespan of an asset (Arditi et al., 1996, Asiedu et al., 1998). Later, in view of large losses due to extreme hazards, like earthquakes and hurricanes, there was a need for new design procedures of facilities that could lead to life protection and reduction of damage and economical impact of such hazards to an acceptable level (Wen & Kang, 2001a). In this context LCCA was introduced in the field of constructions as a complex investment appraisal tool incorporating a structural performance criterion (Sanchez-Silva & Rackwitz, 2004).

A considerable amount of work has been done in estimating losses due to earthquakes. In particular in the work by Beck et al. (2003) a measure, to be incorporated into the seismic risk assessment framework for economic decision-making of buildings, was introduced, denoted as the probable frequent loss, which is defined as the mean loss resulting from shaking with 10% exceedance probability in 5 years. Liu et al. (2003) presented a two-objective optimization procedure for designing steel moment resisting frame buildings within a performance-based seismic design framework, where initial material and lifetime seismic damage costs are treated as two separate objectives. In the work by Sanchez-Silva and Rackwitz (2004) it is concluded that structures should be optimal with respect to economic investment, benefits derived from their use, expected consequences in case of failure and the degree of protection to human life. Lagaros *et al.* (2006) have adopted the limit state cost in order to compare descriptive and performance based design procedures. Frangopol and Liu (2007) reviewed the recent development of life-cycle maintenance and management planning for deteriorating civil infrastructure with emphasis on bridges. Kappos and Dimitrakopoulos (2008) implemented decision making tools, namely cost-benefit and life-cycle cost analyses, in order to examine the feasibility of strengthening reinforced concrete buildings. A probabilistic framework to estimate long-term earthquake-induced economical loss for wood frame structures was proposed and demonstrated in the work by Pei and Van De Lindt (2009).

Moreover the LCCA is used lately in the framework of a cost optimization problem. In general, it is introduced in the formulation of the problem optimization procedure as an objective function. Among others, in the work by Wen and Kang (2001a and 2001b) building design criteria are developed to protect life and to reduce damage and loss to an acceptable level for this purpose a minimization problem of the total life-cycle cost is considered. Sarma and Adeli (2002) addressed the life-cycle optimization of steel structures, solving a four criteria optimization problem. Their study is based on a detailed breakdown of all factors that influence the life-cycle cost of steel structures. Khajehpour and Griersson (2003)

investigated the trade-off between life-cycle profitability and load-path safety for a high-rise office building. Takahashi *et al.* (2004) presented a decision methodology for the management of seismic risk of a building. The decision criterion aims at minimizing the expected life-cycle cost, including the initial cost of the design and the expected cost of damage due to future earthquakes. Liu *et al*. (2005) proposed a multiobjective structural optimization formulation where the present capital investment and the future seismic risk are treated simultaneously as separate objectives. In the work by Rackwitz *et al*. (2005) an appropriate objective function for cost-benefit analyses based on a renewal model is established while various renewal models for deteriorating structures including multiple failure modes are examined.

6.3. Life-cycle Cost Analysis

The total cost C_{TOT} of a structure, may refer either to the design-life period of a new structure or to the remaining life period of an existing or retrofitted structure. This cost can be expressed as a function of time and the design vector $\boldsymbol{s}$ as follows (Wen & Kang, 2001a)

$$C_{TOT}(t,\boldsymbol{s}) = C_{IN}(\boldsymbol{s}) + C_{LC}(t,\boldsymbol{s}) \tag{6.1}$$

where C_{IN} is the initial cost of a new or retrofitted structure, C_{LC} is the present value of the life-cycle cost; $\boldsymbol{s}$ is the design vector corresponding to the design loads, resistance and material properties that influence the performance of the structural system, while t is the time period. The term "initial cost" of a new structure refers to the cost required for construction. The initial cost is related to the material and the labour cost for the construction of the building which includes concrete, steel reinforcement, labour cost for placement as well as the non-structural component cost, in the case of a RC building. The term "life-cycle cost" refers to the potential damage cost from earthquakes that may occur during the life of the structure. It should be mentioned that in the calculation of C_{LC} a regularization factor is used that transforms the costs in present values. The estimation of the cost of exceedance of the collapse prevention damage state will vary considerably according to which approach is adopted by the three steps of the life-cycle cost analysis is presented in the flowchart of Figure 6.1.

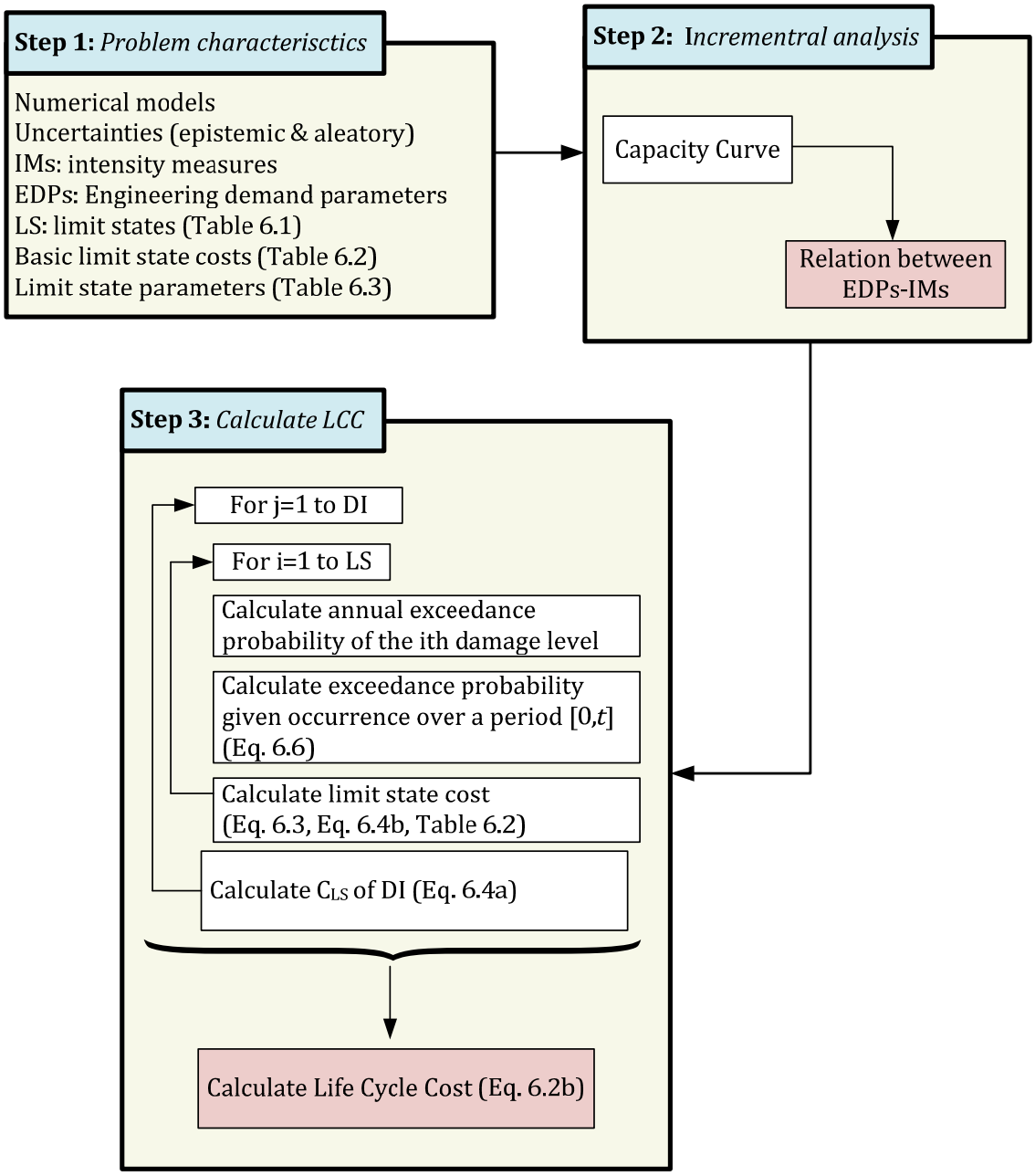

Figure 6.1. Flowchart of the life-cycle cost analysis framework.

6.3.1. Calculation of the life-cycle cost

The calculation of C_{LC} demands first the detection and quantification of the damage that a structure sustains during an earthquake. Damage may be quantified by using several DIs whose values can be related to particular structural damage states, also called limit states. The idea of describing the state of damage of the structure by a specific quantity, on a defined scale in the form of a damage index, is attractive because of its simplicity. So far a significant number of researchers have studied various DIs for reinforced concrete or steel structures, a detailed survey can be found in the Chapter 2 of this dissertation. Damage, in the context of life-cycle cost assessment, refers not only to structural damage but also to

non-structural damage. The latter including the case of architectural damage, mechanical, electrical and plumbing damage and also the damage of furniture, equipment and other contents. The maximum inter-story drift (θ) has been considered as the response parameter which best characterises the structural damage, associated with all types of losses. It is generally accepted that interstorey drift can be used as a reliable limit state criterion to determine the expected damage. The relation between the drift ratio limits with the limit state, employed in this dissertation (Table 6.1), is based on the work of Ghobarah (2004) for ductile RC moment resisting frames. On the other hand, the intensity measure which has been associated with the loss of contents, like furniture and equipment, is the maximum response floor acceleration (*acc*). The relation between the limit state and the values of the floor acceleration (Table 6.1) are based on the work of Elenas and Meskouris (2001).

Considering the way that the potential damage is detected, the life-cycle cost (C_{LC}) configuration involves the sum of functions time of the corresponding costs based on different *DI*, where *DI* is the number of the damage indices that used to quantify the damage of a structure (Eq. 6.1b). Each damage cost based on a *DI* is a function of the sum of the limit state costs (C_{LS}), since each DI is quantified in six limit states, where *n* is the number of the considered limit states, which differ according to the damage index:

$$C_{LC}(t,\boldsymbol{s}) = \sum_{i=1}^{DI} {C_{LS}}^{i}(t,\boldsymbol{s}) \tag{6.2a}$$

$${C_{LS}}^{DI}(t,\boldsymbol{s}) = \sum_{i=1}^{n} f({C_{LS}}^{i},t,\boldsymbol{s}) \tag{6.2b}$$

The C_{LS} accounts for the cost of repair, the cost of loss of contents, related to loss of contents, rental and income, after an earthquake. The quantification of these losses in economical terms depends on several socio-economic parameters. The most difficult cost to quantify is the cost corresponding to the loss of a human life. There are a number of approaches for its estimation, ranging from purely economic reasoning to more sensitive that consider the loss of a human being irreplaceable.

The limit state cost (C_{LS}), for the *i*-th limit state, can thus be expressed as follows:

$$C_{LS}^{i} = C_{dam}^{i} + C_{con}^{i} + C_{ren}^{i} + C_{inc}^{i} + C_{inj}^{i} + C_{fat}^{i} \tag{6.3a}$$

$$C_{con}^{i} = C_{con}^{i,\theta} + C_{con}^{i,acc} \tag{6.3b}$$

where C_{dam}^{i} is the damage repair cost, $C_{con}^{i,\theta}$ is the loss of contents cost due to structural damage that is quantified by the maximum interstorey drift while $C_{con}^{i,acc}$ is the loss of contents cost due to floor acceleration (Mitropoulou *et al*., 2010), C_{ren}^{i} is the loss of rental

cost, C_{inc}^{i} is the income loss cost, C_{inj}^{i} is the cost of injuries and C_{fat}^{i} is the cost of human fatality. These cost components are related to the damage of the structural system. A more detailed description of the different cost evaluation for each limit state cost can be found in Table 6.2 (Wen & Kang, 2001) given in MU (corresponding to Dollars or Euros). The values of the mean damage index, loss of function, down time, expected minor injury rate, expected serious injury rate and expected death rate used in this study are based on (Lagaros, 2007, Ellingwood & Wen, 2005). Table 6.3 provides the ATC-13 (1985) and FEMA-227 (1992) limit state dependent damage consequence severities.

Table 6.1: Damage indices limits for bare moment resisting frames.

Limit State	**Interstorey Drift (%)** (Ghobarah, 2004)	**Floor Acceleration (g)** (Elenas & Meskouris, 2001)
(I) - None	θ ≤0.1	$\ddot{u}_{floor}$ ≤0.05
(II) - Slight	0.1< θ ≤0.2	0.05< $\ddot{u}_{floor}$ ≤0.10
(III) - Light	0.2< θ ≤0.4	0.10< $\ddot{u}_{floor}$ ≤0.20
(IV) - Moderate	0.4< θ ≤1.0	0.20< $\ddot{u}_{floor}$ ≤0.80
(V) - Heavy	1.0< θ ≤1.8	0.80< $\ddot{u}_{floor}$ ≤0.98
(VI) - Major	1.8< θ ≤3.0	0.98< $\ddot{u}_{floor}$ ≤1.25
(VII) - Collapsed	θ >3.0	$\ddot{u}_{floor}$ >1.25

Table 6.2. Limit state cost - calculation formulas (Wen & Kang, 2001a, and 2001b).

Cost Category	**Calculation Formula**	**Basic Cost**
Damage/repair (C_{dam})	Replacement cost × floor area × mean damage index	1500 MU/m^2
Loss of contents (C_{con})	Unit contents cost × floor area × mean damage index	500 MU/m^2
Rental (C_{ren})	Rental rate × gross leasable area × loss of function	10 MU/month/m^2
Income (C_{inc})	Rental rate × gross leasable area × down time	2000 MU/year/m^2
Minor Injury ($C_{inj,m}$)	Minor injury cost per person × floor area × occupancy rate × expected minor injury rate	2000 MU/person
Serious Injury ($C_{inj,s}$)	Serious injury cost per person × floor area × occupancy rate × expected serious injury rate	2×10^4 MU/person
Human fatality (C_{fat})	Human fatality cost per person × floor area × occupancy rate × expected death rate	2.8×10^6 MU/person

* Occupancy rate 2 persons/100 m^2

Table 6.3. Limit state parameters for cost evaluation.

Limit State	FEMA-227 (1992)				ATC-13 (1985)	
	Mean damage index (%)	Expected minor injury rate	Expected serious injury rate	Expected death rate	Loss of function (%)	Down time (%)
(I) - None	0	0	0	0	0	0
(II) - Slight	0.5	3.0E-05	4.0E-06	1.0E-06	0.9	0.9
(III) - Light	5	3.0E-04	4.0E-05	1.0E-05	3.33	3.33
(IV) - Moderate	20	3.0E-03	4.0E-04	1.0E-04	12.4	12.4
(V) - Heavy	45	3.0E-02	4.0E-03	1.0E-03	34.8	34.8
(VI) - Major	80	3.0E-01	4.0E-02	1.0E-02	65.4	65.4
(VII) - Collapsed	100	4.0E-01	4.0E-01	2.0E-01	100	100

Based on a Poisson process model of earthquake occurrences and an assumption that damaged buildings are immediately retrofitted to their original intact conditions after each major damage-inducing seismic attack, Wen and Kang (2001) proposed the following formulae for the limit state cost function considering *N* limit states

$$C_{LS}^{\ DI}(t,\boldsymbol{s}) = C_{LS}^{\theta}(t,\boldsymbol{s}) + C_{LS}^{acc}(t,\boldsymbol{s}) \tag{6.4a}$$

$$C_{LS}^{\theta}(t,\boldsymbol{s}) = \frac{\nu}{\lambda}\left(1-e^{-\lambda t}\right)\sum_{i=1}^{N} C_{LS}^{i,\theta}\cdot P_i^{\theta} \tag{6.4b}$$

$$C_{LS}^{acc}(t,\boldsymbol{s}) = \frac{\nu}{\lambda}\left(1-e^{-\lambda t}\right)\sum_{i=1}^{N} C_{LS}^{i,acc}\cdot P_i^{acc} \tag{6.4c}$$

where

$$P_i^{DI} = P(DI > DI_i) - P(DI > DI_{i+1}) \tag{6.5}$$

and

$$P(DI > DI_i) = (-1/t)\cdot\ln[1-\bar{P}_i(DI-DI_i)] \tag{6.6}$$

P_i is the probability of the ith limit state being violated given the earthquake occurrence and C_{LS}^{i} is the corresponding limit state cost; $P(DI-DI_i)$ is the exceedance probability given occurrence; DI_i, DI_{i+1} are the damage indices (maximum interstorey drift or maximum floor acceleration) defining the lower and upper bounds of the ith limit state; $\bar{P}_i(DI-DI_i)$ is the annual exceedance probability of the maximum damage index DI_i; ν is the annual occurrence rate of significant earthquakes modelled by a Poisson process and t is the service life of a new structure or the remaining life of a retrofitted structure. Thus, for the calculation of the

limit state cost of Eq. (6.4b) the maximum interstorey drift DI is considered, while for the case of Eq. (6.4b) the maximum floor acceleration is used. The first component of Eqs. (6.4b) or (6.4c), with the exponential term, is used in order to express C_{LS} in present value, where λ is the annual monetary discount rate. Various studies have proposed values of the discount rate λ in the range of 3 to 6% (Ellingwood & Wen, 2005). In this dissertation the annual monetary discount rate λ is taken to be constant and equal to 5%, since considering a continuous discount rate is accurate enough for all practical purposes according to Rackwitz (2006) and Rackwitz et al. (2005).

Each limit state is defined by the drift ratio limits or the floor acceleration, as listed in Table 6.1. When one of the *DIs* is exceeded the corresponding limit state is assumed to be reached. The annual exceedance probability $\overline{P}_i(DI > DI_i)$ is obtained from a relationship of the form:

$$\overline{P}_i(DI > DI_i) = \gamma (DI_i)^{-k} \tag{6.7}$$

where the parameters γ and k are obtained by best fit of known $\overline{P}_i$ - DI_i pairs for each of the two *DIs*. According to Poisson's law the annual probability of exceedance of an earthquake with a probability of exceedance p in t years is given by the formula

$$\overline{P} = (-1/t) \cdot \ln(1-p) \tag{6.8}$$

This means that the 2/50 earthquake has a probability of exceedance equal to $\overline{P}_{2\%}$ = - ln(1-0.02)/50 = 4.04×10^{-4} (4.04×10^{-2} %).

6.3.2. Implementation of the analysis procedures in the LCCA framework

The limit state cost calculation procedure requires the assessment of the structural capacity in at least three hazard levels of increased intensity with the definition of at least three pairs of annual probability of exceedance $(\overline{P}_i)$ and maximum value of the damage index in question (DI_i). In this work the abscissa values of the $(\overline{P}_i - DI_i)$ pairs, corresponding to the maximum values of the damage index, are obtained either by means of nonlinear static or dynamic analysis procedure, while the ordinate values correspond to the annual probabilities of exceedance.

These probabilities correspond to discrete values of annual probabilities of exceedance obtained from a hazard curve (see Chapter 5), which describe the seismic risk of a region. An example of a hazard curve in the city of San Diego, California (Latitude (N) 32.7°, Longitude (W) -117.2°) is presented in Figure 6.2, which was obtained from the USGS. From this curve three or more pairs of the intensity measure and the corresponding annual probability of exceedance $(IM - \overline{P}_i)$ can be derived, where the IM will be applied to the

structure in order to give the corresponding (DI_i). In the case of nonlinear static analysis (NSA) procedure the damage index considered is the maximum interstorey drift, while in the case of NDA procedure two damage indices are employed, namely the maximum interstorey drift and maximum floor acceleration.

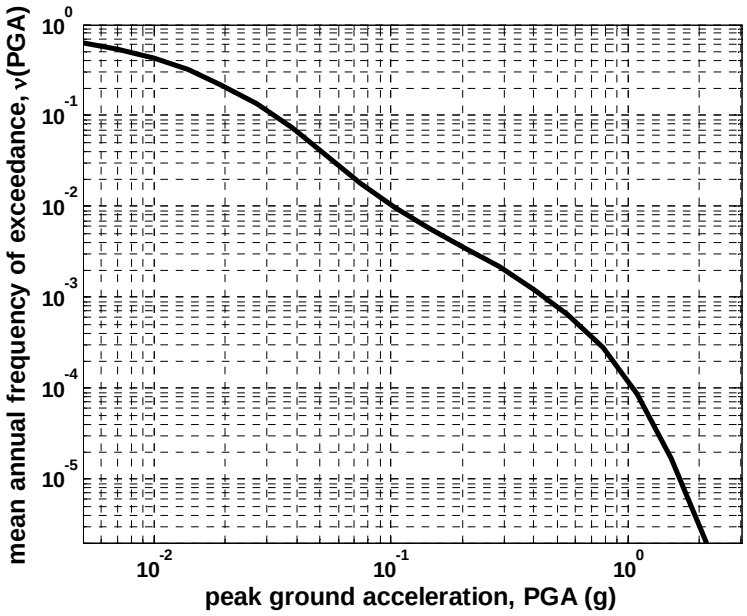

Figure 6.2. Hazard curve of the city of San Diego, California (Latitude (N) 32.7°, Longitude (W) -117.2°).

The implementation of results of a structural analysis in the LCCA procedure depends on the type of the analysis implemented (incremental nonlinear static or incremental nonlinear dynamic). Significant role in that step of the LCCA framework plays the selection procedure of the seismic actions, as it was presented in Chapter 5.

Nonlinear static analysis procedure

NSA is based on the assumption that the response of the structure is described by an equivalent single degree of freedom system with properties proportional to the first mode of the structure. For the implementation of NSA a lateral load distribution that follows the fundamental mode is adopted. The analysis is terminated when 150% of the target displacement that correspond to the 2% in 50 years (2/50) hazard level is reached, or earlier if the structure has collapsed (FEMA-356, 2006).

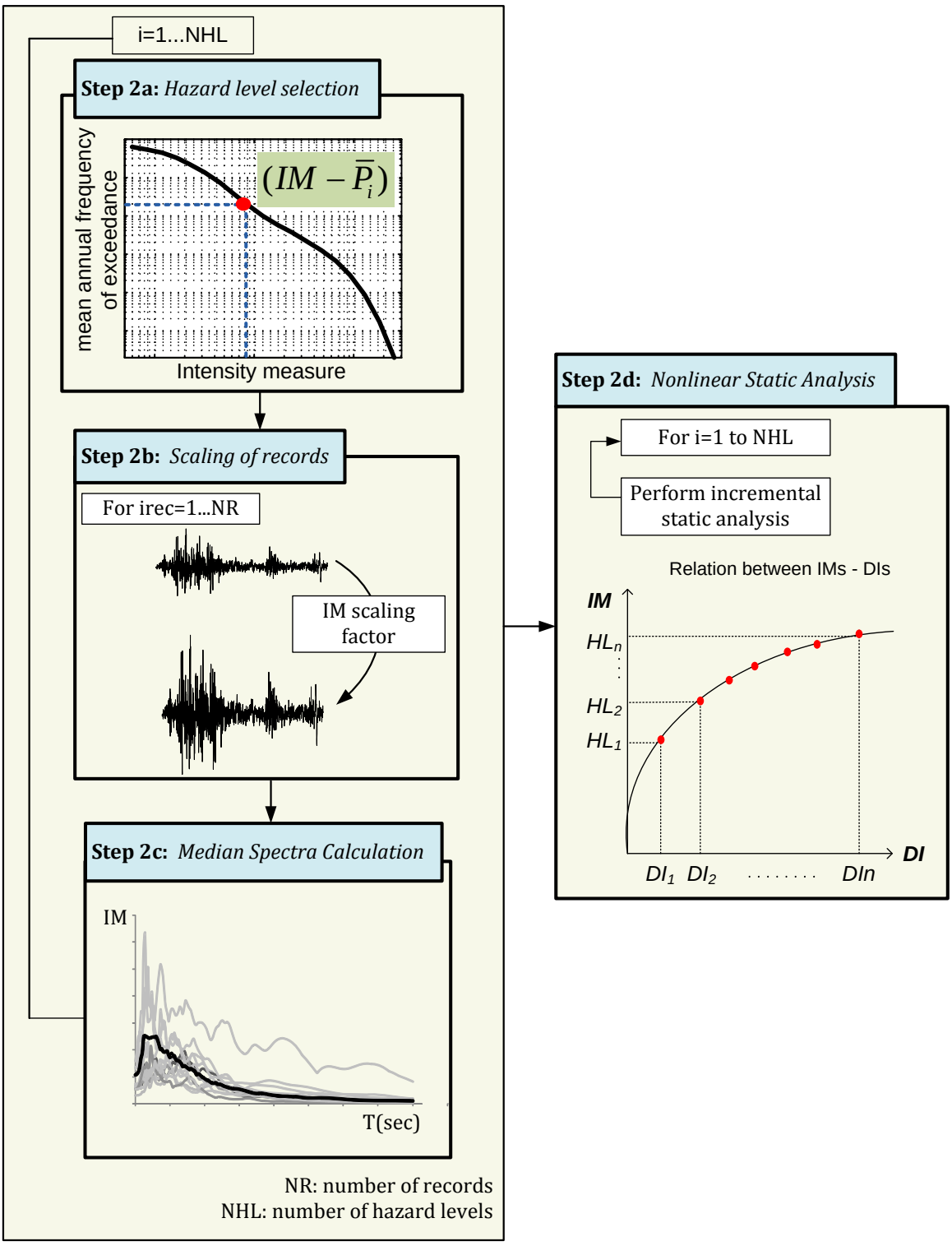

Figure 6.3. Implementation of nonlinear static analysis procedure in LCCA framework.

According to the capacity spectrum method, the capacity of a structural system to resist lateral forces is compared to the demand of an earthquake response spectrum and NSA procedure results with the calculation of the maximum interstorey drift (θ_i). In order to calculate the maximum interstorey drift in multiple hazard levels the corresponding earthquake response spectra are used. These spectra are the median ones of the selected

seismic records when scaled to the corresponding hazard level based on the intensity measure used. Step 2 of the LCCA framework (Figure 6.1) is presented in Figure 6.3 corresponding to the case of NSA. NSA is limited with regard to evaluation of the simultaneous response to ground shaking in different directions. To overcome this deficiency, the recommendation of FEMA-350 (2000) is employed where multidirectional excitation effects are accounted for by combining 100% of the response due to loading in the longitudinal direction with 30% of the response due to loading in the transverse direction, and vice versa. The worst of these two combinations in each hazard level is used in order to assess the structural performance in the corresponding performance levels.

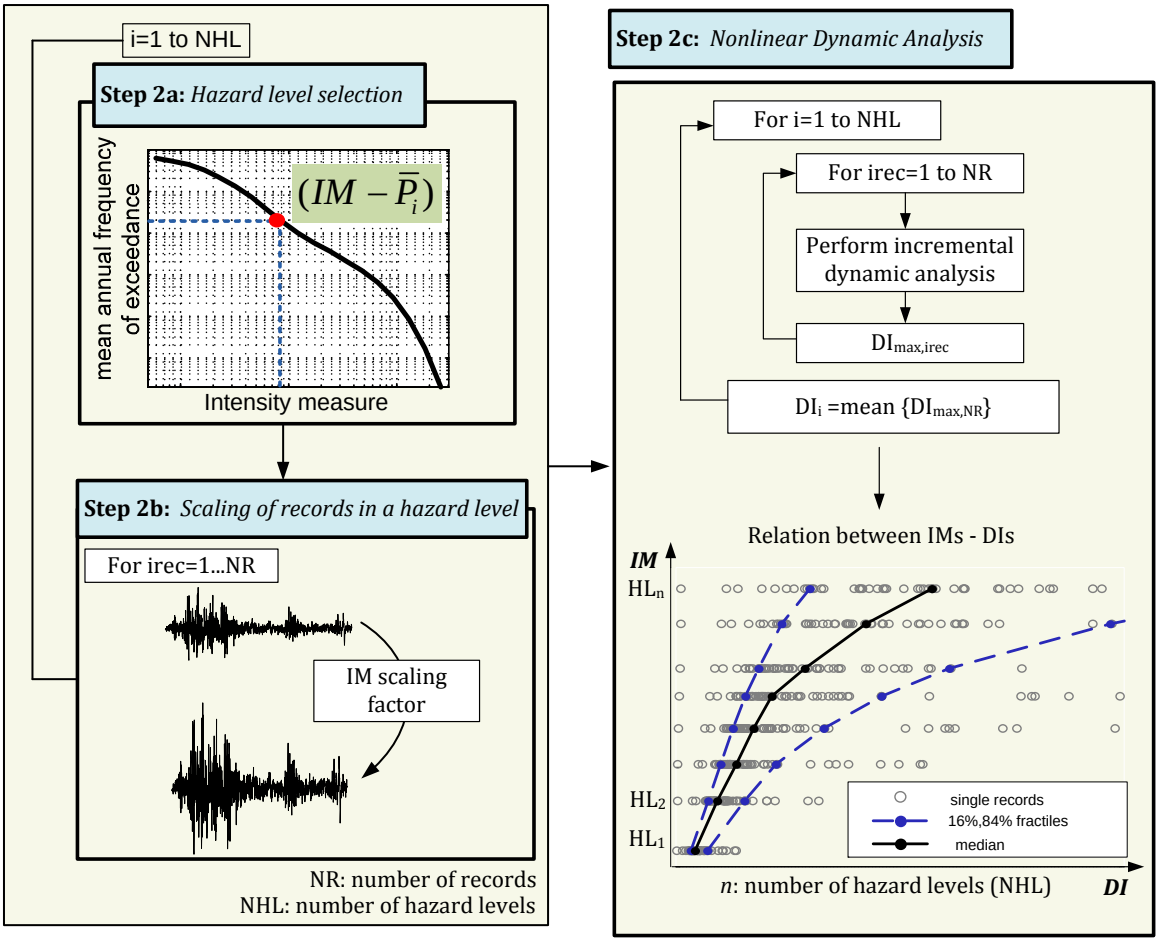

Figure 6.4. Implementation of nonlinear dynamic analysis procedure in LCCA framework.

Nonlinear dynamic analysis procedure

For the implementation of the NDA, multiple nonlinear dynamic analyses have to be performed in order to assess the structural performance in the selected hazard levels. For each hazard level a number of seismic records is selected and the median response among the records is calculated. Therefore, the application of NDA incorporated into LCCA results in a time-consuming and computationally-demanding procedure compared to the

corresponding NSA implementation. From this procedure a scale factor is calculated for each one of the ground motions and for each hazard level. In order to preserve the relative scale of the two components of the records in the longitudinal and transverse directions, the component of the record having the highest intensity measure is scaled first, while a scaling factor that preserves their relative ratio is assigned to the second component (Figure 6.4). More details on the NDA procedures (IDA, MIDA and MSDA) are provided in Chapter 4 of the dissertation.

6.4. Illustrative example

The 3D RC building of Figure 6.5 is considered for the parametric study performed in this part of the chapter. The cross section of all columns is 45×45 cm^2 and 30×60 cm^2 for all beams. The lateral forces were derived from the design response spectrum (5%-damped elastic spectrum divided by the behaviour factor) at the fundamental period of the building. Concrete of class C16/20 (characteristic cylindrical strength of 16MPa) and class S500 steel (characteristic yield stress of 500MPa) are assumed. The base shear is obtained from the response spectrum for soil type A (soil parameter s = 1.0 with characteristic periods T_B = 0.10s, T_C = 0.40s and T_D = 3.00s) and PGA of 0.31 g. Moreover, the importance factor γ_I was taken equal to 1, while the damping correction factor is equal to 1.0, since a damping ratio of 5% has been considered, as it is suggested by EC8 for RC structures, while a behaviour factor equal to 3.0 is considered.

The slab thickness is equal to 15cm and is considered to contribute to the moment of inertia of the beams with an effective flange width according to EC2 (2004). In addition to the self weight of beams and slab, a distributed dead load of 2 kN/m^2 due to floor finishing and partitions is considered, while live load with characteristic value of 1.5 kN/m^2 is also imposed. In the combination of gravity loads ("persistent design situation") nominal dead and live loads are multiplied with load factors of 1.35 and 1.5, respectively. Following EC8, in the seismic design combination, dead loads are considered with their nominal value while live loads with 30% of the nominal value.

The majority of the RC buildings are constructed with masonry infill walls. However, the combination of masonry infill walls with the framed structure is most often neglected during the design procedure, assuming that the structural performance is not influenced. Such an assumption may lead to substantial inaccuracy in predicting the lateral stiffness, strength and ductility of the structure. In the past a number of studies have been devoted on the seismic behaviour of RC frames with masonry infill walls (details can be found in Appendix B) and a number of analytical models for masonry infill walls have been

developed. The model employed in this study for simulating the masonry infill panels is described in Appendix B. According to this model the contribution of a masonry infill wall is modelled by a system of two diagonal masonry compression struts. The two struts are considered ineffective in tension since the tensile strength of masonry is negligible. The combination of both diagonal struts provides the lateral load resisting mechanism for the opposite lateral directions of loading. Each strut element is modelled as a simple longitudinal inelastic spring loaded axially.

Table 6.4. Damage state drift ratio limits for ductile RC moment resisting frames with infills.

Limit State	Damage State	Interstorey Drift (%) (Ghobarah, 2004)
1	None	Δ<0.05
2	Slight	0.05<Δ<0.1
3	Light	0.1<Δ<0.2
4	Moderate	0.2<Δ<0.4
5	Heavy	0.4<Δ<0.7
6	Major	0.7<Δ<0.8
7	Destroyed	0.8<Δ

Table 6.5. Limit state dependent cost calculations for the fully infilled design (in 1,000 MU).

Limit State	C_{dam}	C_{con}	C_{ren}	C_{inc}	$C_{inj,m}$	$C_{inj,s}$	C_{fat}	C_{LS}^{i} (Eq.6.3a)
1	0.00	0.00	0.00	0.00	0.00	0.00	0.00	0.00
2	3.51	1.17	0.52	2.88	0.00	0.00	0.00	8.08
3	35.10	11.70	1.87	10.38	0.00	0.00	0.19	59.05
4	140.40	46.80	6.95	38.63	0.00	0.06	2.32	232.78
5	315.90	105.30	19.56	108.68	0.48	0.66	23.54	549.44
6	561.60	187.20	36.74	204.09	5.06	6.68	235.66	989.63
7	702.00	234.00	56.16	312.00	6.68	67.29	4713.76	1304.16

In this example the calculation of the life-cycle cost of a fully infilled RC structure is described. The life-cycle cost is computed for the seven limit states depicted in Table 6.4 for RC moment frames with infills. The calculation of each limit state cost is based on the calculation formulas described in Table 6.2. The results of the cost calculations for the fully infilled design, given in MU (corresponding to Dollars or Euros), for each limit state are depicted in Table 6.5. This costs calculation dependents on the basic cost values given in Table 6.2. It can be seen in Table 6.5 that, up to the 5th limit state, the costs of damage and

income loss were the prevailing components of the limit state cost, but in 6th and 7th limit states the cost of the human fatality dominates every other component.

In order to calculate the present value of the limit state dependent cost for the code conforming fully infilled design (Figure 6.5) three pairs of annual probability of exceedance and maximum interstorey drift $(\bar{P}_i - DI_i) \Rightarrow (\bar{P}_i - \theta_{max,i})$ were obtained.

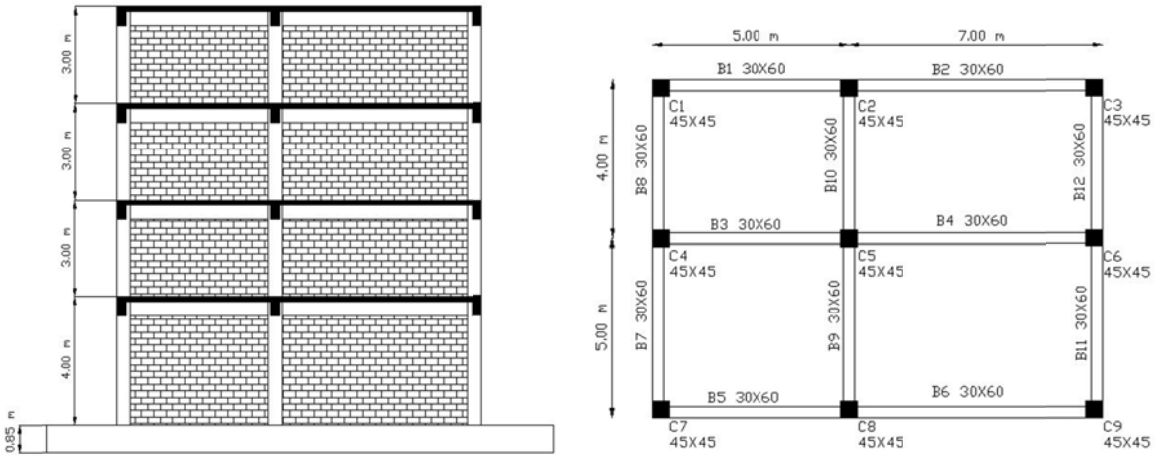

(a) (b)

Figure 6.5. The model for the C7-B5-C8-B6-C9 (a) fully infilled frame and (b) layout.

The abscissa of the $(\bar{P}_i - \theta_{max,i})$ pairs, corresponding to the median value of the maximum interstorey drifts, are obtained through 10 nonlinear time-history analyses performed for each of the three hazard levels (50/50, 10/50 and 2/50) considered (see Figure 6.3, Step 2c). On the other hand the $\bar{P}_i$ values are calculated through the Eq. (6.8) considering $p_{2\%}$ =0.02, $p_{10\%}$ =0.10 and $p_{50\%}$ = 0.50 for the $\bar{P}_{2\%}, \bar{P}_{10\%}, \bar{P}_{50\%}$ respectively. The three pairs obtained from the nonlinear dynamic analyses are given in the following expressions.

$$(\bar{P}_{50\%} = 1.39\% - \theta_{max,50\%} = 1.7 \times 10^{-1}\%) \tag{6.9a}$$

$$(\bar{P}_{10\%} = 2.10 \times 10^{-1}\% - \theta_{max,10\%} = 3.31 \times 10^{-1}\%) \tag{6.9b}$$

$$(\bar{P}_{2\%} = 4.04 \times 10^{-2}\% - \theta_{max,2\%} = 8.93 \times 10^{-1}\%) \tag{6.9c}$$

The ordinates corresponding to the annual probabilities of exceedance are calculated using Eq. (6.6). Subsequently, an exponential function as in Eq. (6.7) is fitted (see Figure 6.6). The best fitted curves for the fully infilled ($\gamma=1.65\times10^{-2}$, k=4.35) and the weak ground storey ($\gamma=6.16\times10^{-2}$, k=1.24) designs are shown in Figure 6.7, where it can be seen that different interstorey drifts correspond to the same annual probability of exceedance for different design concept.

Once the function of the best fitted curve is known the annual probabilities of exceedance $\bar{P}_i$ for each of the seven damage states of Table 6.4 are easily calculated. Finally $\bar{P}_i$ is

substituted to Eq. (6.4b), Eq. (6.5) and Eq. (6.6) in order to calculate the limit state dependent cost value, as a function of the initial volume, as it is described in Table 6.6 for the fully infilled design.

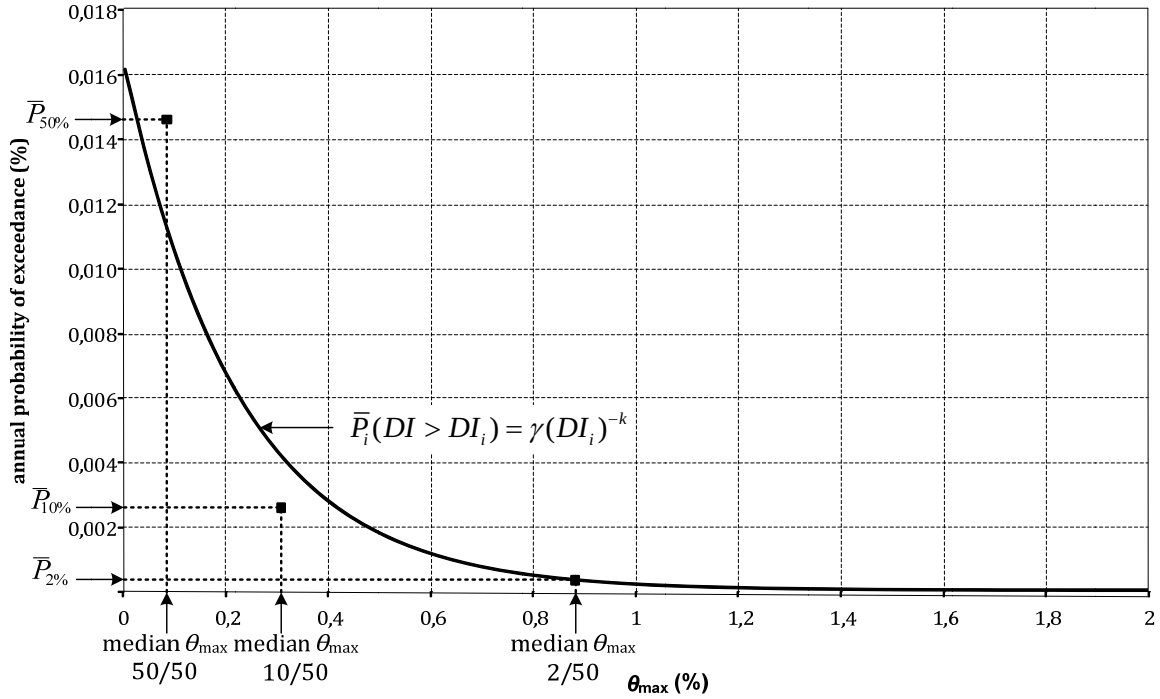

Figure 6.6. $(\overline{P}_i - \theta_{max,i})$ pairs and fitted curve.

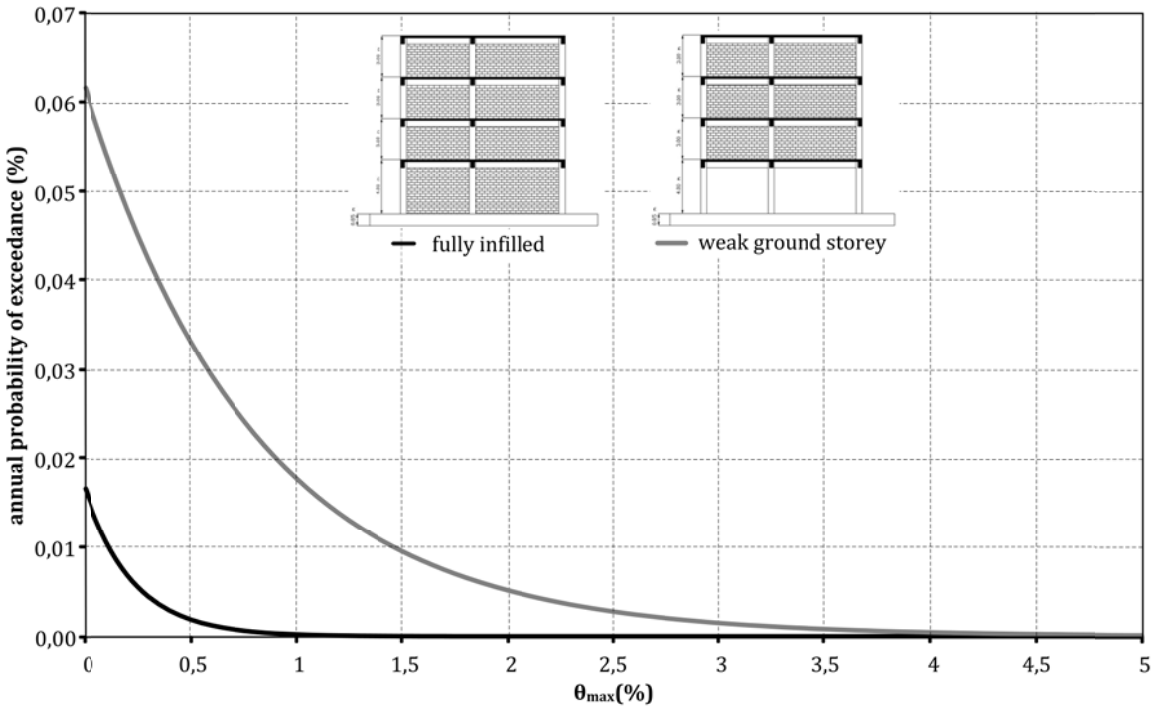

Figure 6.7. Examples of fitted curves.

Table 6.6. Calculation of the limit state dependent cost for the fully infilled design.

Limit States	P_i **(%)** Eq. (6.5)	$C_{LS}^i P_i$ **(MU 1,000)**
1	0.00	0.00
2	$3.8\ 10^{-1}$	2.17
3	$4.0\ 10^{-1}$	14.64
4	$2.7\ 10^{-1}$	38.15
5	$2.1\ 10^{-2}$	7.12
6	$6.5\ 10^{-4}$	0.41
7	$3.6\ 10^{-6}$	0.003
$\sum_{i=1}^{N} C_{LS}^i P_i$		62.48
$\frac{\nu}{\lambda}\left(1-e^{-\lambda t}\right)$		18.36
C^i_{LS} Eq. (6.4b)		1147.18
C_{IN}		388.86

Table 6.7. Five storey test example - Limit state cost components (1,000 MU).

Limit State	C_{dam}^i	C_{con}^i	C_{ren}^i	C_{inc}^i	C_{inj}^i		C_{fat}^i	$C_{LS}^i(I)$	$C_{LS}^i(II)$
					Minor	**Serious**			
1	0.00	0.00	0.00	0.00	0.00	0.00	0.00	0.00	0.00
2	9.38	3.13	1.35	22.50	0.00	0.00	0.07	36.35	36.42
3	93.75	31.25	5.00	83.25	0.02	0.02	0.70	213.25	213.98
4	375.00	125.00	18.60	310.00	0.15	0.20	7.00	828.60	835.95
5	843.75	281.25	52.20	870.00	1.50	2.00	70.00	2047.20	2120.70
6	1500.00	500.00	98.10	1635.00	15.00	20.00	700.00	3733.10	4468.10
7	1875.00	625.00	150.00	2500.00	20.00	200.00	14000.00	5150.00	19370.00

6.5. LCCA of buildings designed based on energy dissipation

In this part of the chapter, two 3D RC MRF buildings have been considered in order to study the influence of the behaviour factor *q* on the design of RC buildings. The first test example is a five storey RC building with non-symmetrical plan view while the second one is an eight storey RC building having symmetrical plan view. Details on the two test examples can be found in Chapter 4 while Appendix B provides all details regarding modelling.

6.5.1. Five storey non-symmetrical test example

The plan and front views of the five storey non-symmetrical test example are shown in Figure 6.8. Table 6.3 provides the ATC-13 (1985) and FEMA-227 (1992) limit state

dependent parameters required for the calculation of the following costs: damage repair, loss of contents, loss of rental, income loss, cost of injuries and that of human fatality. The computed components of the limit states, for the five storey RC building, are listed in Table 6.7. As it can be seen in Table 6.7 two limit state dependent cost values are presented, those corresponding to Sum I and Sum II, as follows:

$$C^i_{LS,Sum\,I} = C^i_{dam} + C^i_{con} + C^i_{ren} + C^i_{inc} \tag{6.10a}$$

$$C^i_{LS,Sum\,II} = C^i_{dam} + C^i_{con} + C^i_{ren} + C^i_{inc} + C^i_{inj} + C^i_{fat} \tag{6.10b}$$

where the limit state cost with and without considering injury and death cost is calculated. From Table 6.7 it can be seen that damage and income loss costs are the dominating cost components for the limit states I through VI representing, by average, the 83% of C^i_{LS}, while the cost of human fatality is the dominant cost (73%) at the highest limit state VII.

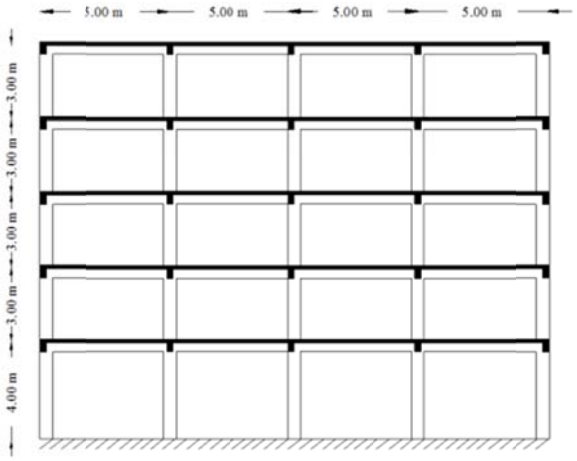

Figure 6.8. Five storey test example - front view.

Below it is explained the calculation procedure of the limit state cost taking as an example the design corresponding to $D_{q=3}$ for the two DIs considered in this study of this Chapter. Similar to the procedure described in section 6.4 of this Chapter, in the first step three $(\overline{P}_i - \theta_i)$ and three $(\overline{P}_i - \alpha_{floor,i})$ pairs are defined corresponding to the three hazard levels:

$$\begin{array}{lll} \overline{P}_{50\%} = 1.39\% & \theta_{50\%} = 0.14\,\% & \alpha_{floor,50\%} = 0.36\,\mathrm{g} \\ \overline{P}_{10\%} = 2.10\times10^{-1}\% & \theta_{10\%} = 0.42\,\% & \alpha_{floor,10\%} = 0.96\,\mathrm{g} \\ \overline{P}_{2\%} = 4.04\times10^{-2}\% & \theta_{2\%} = 1.24\,\% & \alpha_{floor,2\%} = 2.18\,\mathrm{g} \end{array} \tag{6.11}$$

The *abscissa* values for both $(\overline{P}_i - \theta_i)$ and $(\overline{P}_i - \alpha_{floor,i})$ pairs, corresponding to the median values of the maximum interstorey drifts and maximum floor accelerations for the three hazard levels in question, are obtained through 20 Nonlinear time history analyses performed for each hazard level 50/50, 10/50 and 2/50. The median values of the four

designs are shown in Figures 6.9(a) and 6.9(b). The *ordinate* values, corresponding to the annual probabilities of exceedance, are calculated using Eq. (6.8). Subsequently, exponential functions for the two *DIs*, as the one described in Eq. (6.7), is fitted to the pairs of Eq. (6.11), similar to those presented in Figures 6.6 and 6.7. Once the two functions of the best fitted curves are defined the annual probabilities of exceedance $\overline{P}_i$ for each of the seven limit states of Table 6.1 are calculated. Substituting $\overline{P}_i$ into Eq. (6.6) the exceedance probabilities of the limit state given occurrence are computed and the probabilities P_i are then evaluated from Eq. (6.5). This procedure is performed for each one of the DIs, i.e. interstorey drifts and floor accelerations. The limit state cost of Eq. (6.4a) is calculated adding the two components of Eqs. (6.4b) and (6.4c), while these two components are defined combining the numerical values of the cost components of Table 6.7 and the corresponding probabilities P_i.

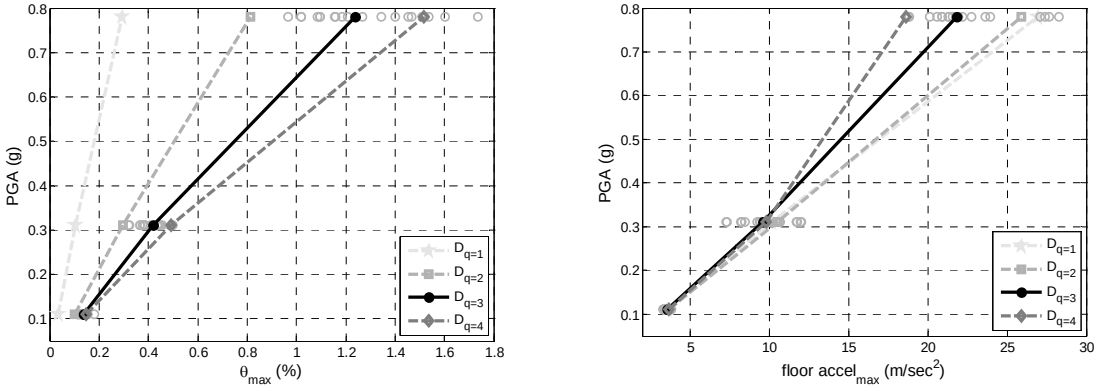

Figure 6.9. Five storey test example – 50% median values of the maximum (a) interstorey drift values and (b) floor accelerations for the four designs.

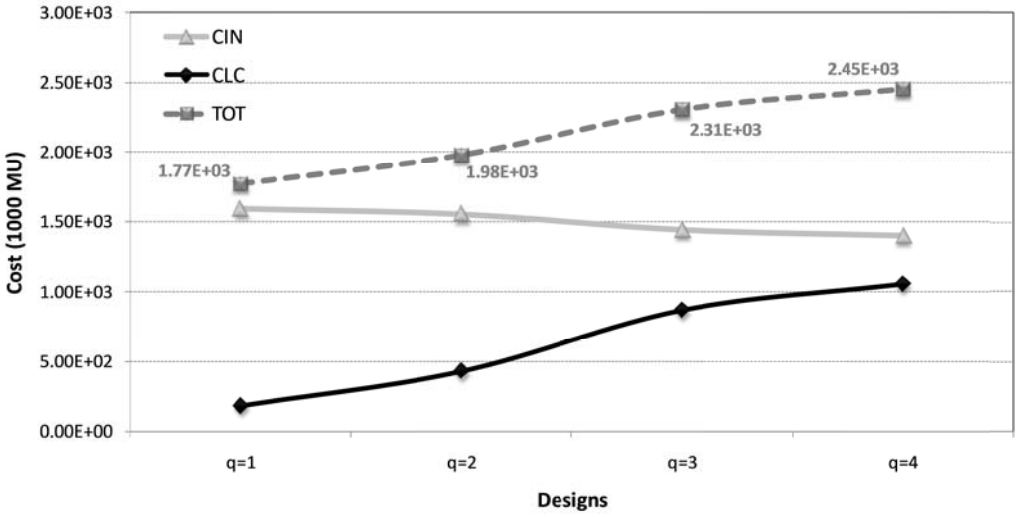

Figure 6.10. Five storey test example - Initial (CIN), expected (CLC) and total expected (TOT) life-cycle costs for different values of the behaviour factor q (t=50 years, λ=5%).

Figure 6.10 depicts the optimum designs obtained with reference to the behaviour factor, along with the initial construction, limit state and total life-cycle costs. The formulation of the optimization problem is presented in section 4.5 of Chapter 4 of this dissertation. From this figure it can be observed that although design $D_{q=1}$ is worst, compared to the other three designs with reference to C_{IN}, design $D_{q=4}$ is the most expensive with respect to C_{TOT}. Comparing design $D_{q=3}$, obtained for the behaviour factor suggested by the Eurocodes for RC buildings, with reference to C_{TOT}, it can be seen that it is 50% and 20% more expensive compared to $D_{q=1}$ and $D_{q=2}$, respectively; while it is 10% less expensive compared to $D_{q=4}$.

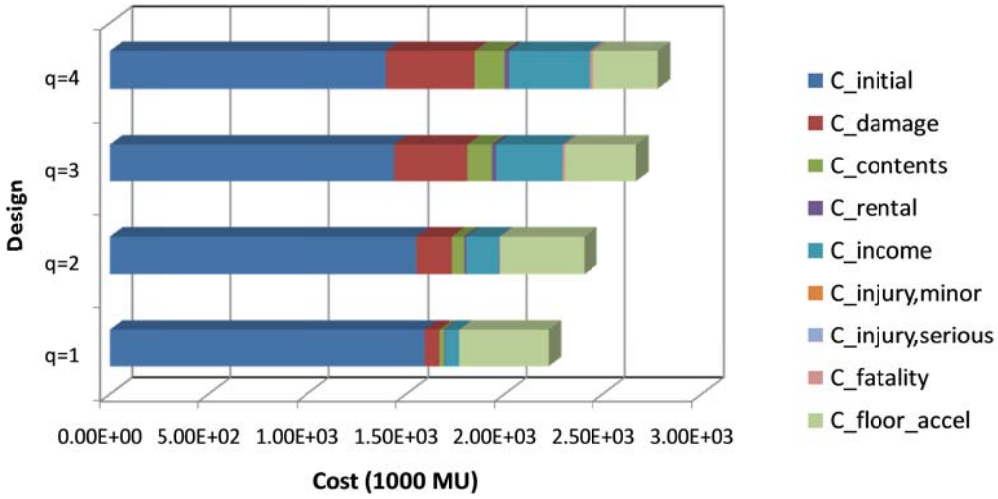

Figure 6.11. Five storey test example - Contribution of the initial cost and limit state cost components to the total expected life-cycle cost for different values of the behaviour factor q.

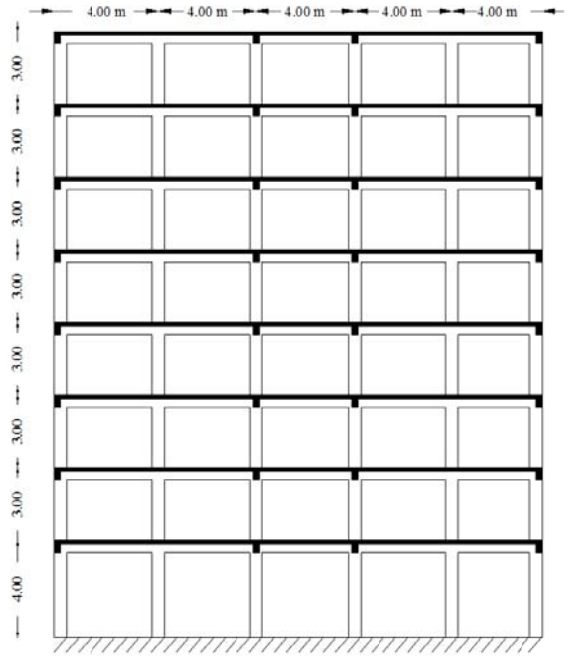

Figure 6.12. Eight storey test example - front view.

The contribution of the initial and limit state cost components to the total life-cycle cost are shown in Figure 6.11. C_{IN} represents the 75% of the total life-cycle cost for design $D_{q=1}$ while for designs $D_{q=2}$, $D_{q=3}$ and $D_{q=4}$ represents the 59%, 50% and 45%, respectively. Although the initial cost is the dominant contributor for all optimum design; for design $D_{q=1}$ the second dominant contributor is the cost of contents due to floor acceleration while for designs $D_{q=2}$, $D_{q=3}$ and $D_{q=4}$ damage and income costs are almost equivalent representing the second dominant contributors. It is worth mentioning, that the contribution of the cost of contents due to floor acceleration on the limit-state cost is only 20% for design $D_{q=4}$ while it is almost 85% for design $D_{q=1}$. This is due to the fact that the latter design is much stiffer and thus increased floor accelerations inflict significant damages on the contents. It has also to be noticed that although the four designs differ significantly, injury and fatality costs represent only a small quantity of the total cost: 0.015% for design $D_{q=1}$, while for designs $D_{q=2}$, $D_{q=3}$ and $D_{q=4}$ represents the 0.25%, 1.0% and 2.3% of the total cost, respectively.

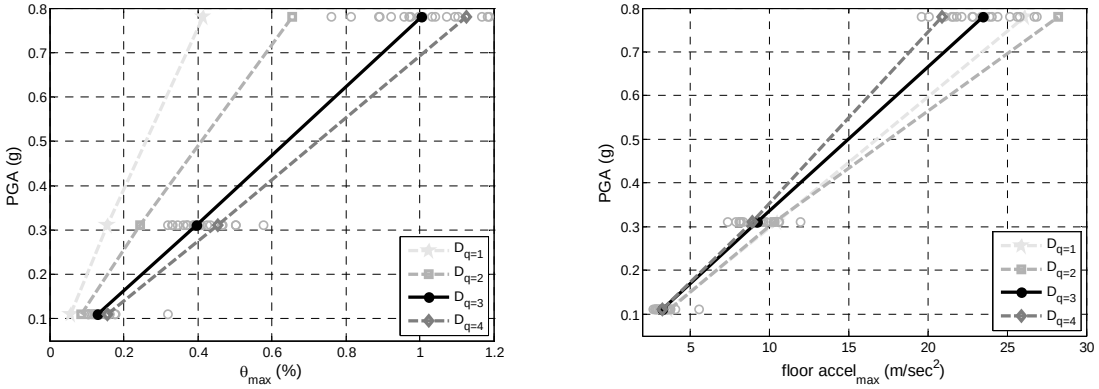

Figure 6.13. Eight storey test example – 50% median values of the maximum (a) interstorey drift values and (b) floor accelerations for the four designs.

6.5.2. Eight storey symmetrical test example

The plan and front views of the eight storey symmetrical test example are shown in Figure 6.12. The median values of the four cases employed for defining the *abscissa* values of both $(\overline{P}_i - \theta_i)$ and $(\overline{P}_i - \alpha_{floor,i})$ pairs, are shown in Figures 6.13(a) and 6.13(b), while they have been obtained through 20 Nonlinear time history analyses performed for each of the three hazard levels (50/50, 10/50 and 2/50). Figure 6.14 depicts the optimum designs (see formulation in section 4.5 of Chapter 4) obtained with reference to the four behaviour factors, along with the initial construction, limit state and total life-cycle costs, calculated for the Ghobarah (2004) drift limits. In accordance to the previous test example, a general observation can be obtained from this figure that design $D_{q=4}$ is worst compared to the other three designs with respect to C_{TOT}. Comparing design $D_{q=3}$, obtained for the behaviour factor

suggested by the Eurocodes for RC buildings, it can be seen that it is 30% and 17% more expensive compared to $D_{q=1}$ and $D_{q=2}$, respectively; while it is 6%, less expensive with reference to C_{TOT}, compared to $D_{q=4}$.

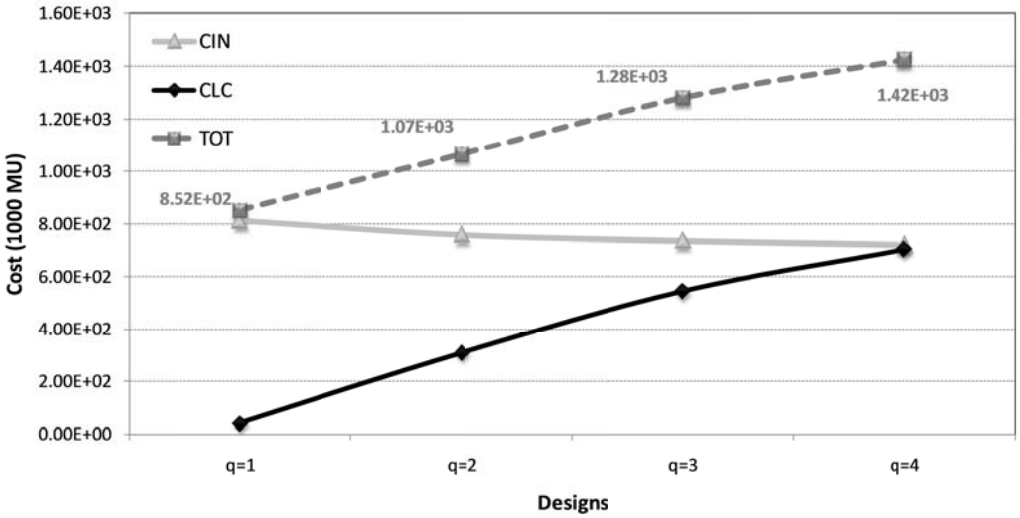

Figure 6.14. Eight storey test example - Initial (CIN), expected (CLC) and total expected (TOT) life-cycle costs for different values of the behaviour factor q (t=50 years, λ=5%).

The contribution of the initial and limit state cost components to the total life-cycle cost are shown in Figure 6.15. C_{IN} represents the 72% of the total life-cycle cost for design $D_{q=1}$ while for designs $D_{q=2}$, $D_{q=3}$ and $D_{q=4}$ represents the 65%, 54% and 50%, respectively. Although the initial cost is the dominant contributor for all optimum design; for designs $D_{q=1}$ and $D_{q=2}$ the second dominant contributor is the cost of contents due to floor acceleration while for designs $D_{q=3}$ and $D_{q=4}$ damage and income costs are almost equivalent representing the second dominant contributors. It is worth mentioning that, as in the previous example, the contribution of the cost of contents due to floor acceleration on the limit-state cost is only 29% for design $D_{q=4}$ while it is almost 76% for design $D_{q=1}$. Furthermore, although the four designs differ significantly, injury and fatality costs represent only a small quantity of the total cost: 0.041% for design $D_{q=1}$, while for designs $D_{q=2}$, $D_{q=3}$ and $D_{q=4}$ represent the 0.14%, 0.46% and 0.68% of the total cost, respectively.

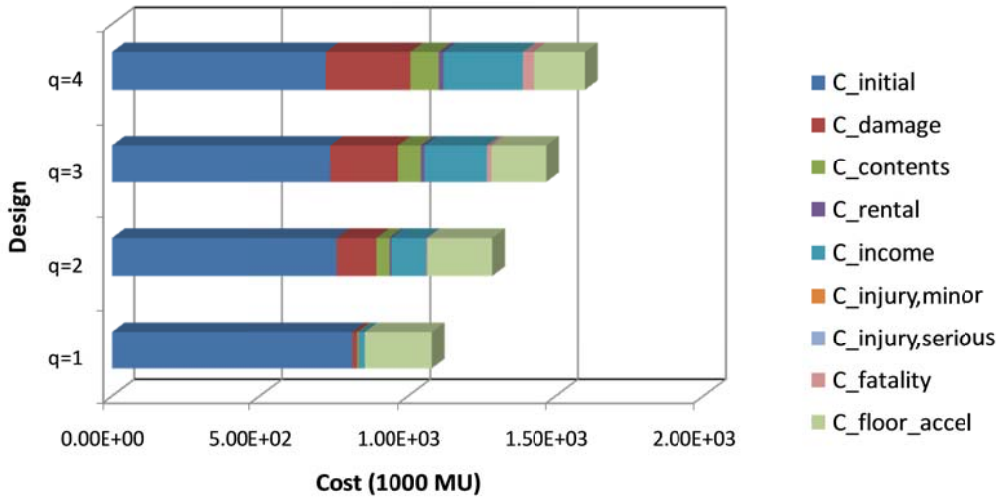

Figure 6.15. Eight storey test example - Contribution of the initial cost and limit state cost components to the total expected life-cycle cost for different values of the behaviour factor *q*.

6.6. Factors affecting the life-cycle cost analysis of reinforced concrete buildings

As it was presented in the first sections of this chapter, LCCA is an assessment tool for the performance of systems; and has been used in many fields of science and engineering. In earthquake engineering LCCA demands the calculation of the cost components that are related to the performance of the structure in multiple earthquake hazard levels. As it was described in detail in subsection 6.3.2 in this Chapter, nonlinear static and dynamic analyses are two procedures that can be used for estimating the seismic capacity of a structural system and can therefore be incorporated into the LCCA methodology. In this part of the Chapter, the influence of the analysis procedure, the number of seismic records imposed, the performance criterion used and the structural type (regular or irregular) on the life-cycle cost analysis procedure is investigated applied to 3D RC structures. In particular the nonlinear static and the multiple stripe incremental dynamic analysis (see Chapter 4) are applied while the maximum interstorey drift and the maximum floor acceleration are adopted as the performance criteria (damage index *DI*) calculated in multiple hazard levels that are required for the life-cycle cost analysis. In both test examples, the life-cycle cost was calculated taking into consideration the damage repair cost, the loss of contents cost due to structural damage that is quantified by the maximum interstorey drift and the floor acceleration, the loss of rental cost, the income loss cost, the cost of injuries and the cost of human fatality.

Two 3D RC buildings have been considered in order to perform LCCA and study the influence of four factors on the LCCA procedure. NSA and MSDA were performed in the two

RC buildings for four groups of seismic events each composed by 10, 20, 40 and 60 records, respectively. In order to study the influence of the damage index considered, for the case of MSDA, the performance of the two buildings was assessed with reference to the maximum interstorey drift and floor acceleration induced by eight hazard levels for each group of ground motions. The final part of this study deals with the evaluation of the influence of four factors: the type of analysis (NSA, MSDA), the number of seismic records (10, 20, 40, 60), the type of the *DI* (maximum interstorey drift-θ_{max} and combination of maximum interstorey drift-θ_{max} and maximum floor acceleration-a_{max}) and the type of the structure (regular or irregular in plan), into the life-cycle cost assessment procedure of 3D RC buildings.

Table 6.8. Eight storey test example – Cross sections of the beams and the columns.

		Storeys 1-3	Storeys 4-6	Storeys 7-8
Columns	**h1×b1**	0.80×0.60, LR: 24Ø28, TR: (4)Ø10/20cm	0.65×0.55,LR:8Ø24+4Ø26, TR: (2)Ø10/20cm	0.55×0.55, LR:8Ø18+ 4Ø22, TR: (2)Ø10/20cm
	h2×b2	0.65×0.60, LR: 26Ø28, TR: (4)Ø10/20cm	0.55×0.55, LR:8Ø24+ 12Ø28, TR: (2)Ø10/20cm	0.55×0.50, LR:6Ø20+ 12Ø28, TR: (2)Ø10/20cm
	h3×b3	0.75×0.65, LR: 28Ø28, TR: (4)Ø10/20cm	0.75×0.50, LR: 24Ø28, TR: (2)Ø10/20cm	0.50×0.50, LR:4Ø22+ 12Ø26, TR: (2)Ø10/20cm
	h4×b4	0.75×0.65, LR: 30Ø28, TR: (4)Ø10/15cm	0.55×0.60, LR: 22Ø28, TR: (2)Ø10/20cm	0.55×0.55, LR:8Ø22+ 12Ø26, TR: (2)Ø10/20cm
Beams	**hl×bl**	0.55×0.55, LR:11Ø18+ 10Ø20, TR: (2)Ø8/15cm		
	ht×bt	0.55×0.50, LR:9Ø18+ 10Ø20, TR: (2)Ø8/15cm		
$C_{IN,\ RC\ Frame}$ (10^3MU)		2.40E+02		
C_{IN} (10^3MU)		1.44E+03		

6.6.1. Structural Models and Numerical Simulation

The two multi-storey 3D RC buildings are shown in Figures 6.8 and 6.12 have been designed for minimum initial cost following an optimization strategy proposed by Mitropoulou et al. (2010) and the formulation of the problem is given in section 4.5 of Chapter 4. The cross-sections of the beams and the columns of the two test examples are provided in Tables 6.8 and 6.9, where hl×bl and ht×bt correspond to the cross sectional dimensions of horizontal and vertical beams. Concrete of class C20/25 (nominal cylindrical strength of 20 MPa) and steel of class S500 (nominal yield stress of 500 MPa) are assumed. The slab thickness is equal to 15 cm for both test examples. In addition to the self weight of beams and slabs, a

distributed permanent load of 2 kN/m^2 due to floor finishing-partitions and an imposed load with nominal value of 1.5 kN/m^2, are considered.

Table 6.9. Five storey test example - Cross sections of the beams and the columns.

		Storeys 1-3	**Storeys 4-5**
Columns	**h1×b1**	0.55×0.55, LR:8Ø20+ 12Ø24, TR: (2)Ø10/20cm	0.55×0.55, LR:8Ø24+ 4Ø28, TR: (2)Ø10/20cm
	h2×b2	0.55×0.55, LR:8Ø22+ 12Ø26, TR: (2)Ø10/20cm	0.45×0.45, LR:4Ø24+ 4Ø28, TR: (2)Ø10/20cm
	h3×b3	0.50×0.50, LR:4Ø22+ 12Ø26, TR: (2)Ø10/20cm	0.35×0.55, LR:7Ø16+ 5Ø20, TR: (2)Ø10/20cm
	h4×b4	0.55×0.55, LR:8Ø18+ 4Ø22, TR: (2)Ø10/20cm	0.35×0.55, LR:8Ø18+ 5Ø20, TR: (2)Ø10/20cm
Beams	**hl×bl**	0.30×0.55, LR:3Ø20+ 4Ø14, TR: (2)Ø10/20cm	
	ht×bt	0.30×0.55, LR:6Ø20, TR: (2)Ø8/15cm	
$C_{IN,\ RC\ Frame}$ (10^3MU)		1.11E+02	
C_{IN} (10^3MU)		7.36E+02	

All structural analyses were performed using the OpenSEES platform (McKenna & Fenves, 2001). Each member is modelled with a single force-based, fibre beam-column element. This element provides a good balance between accuracy and computational cost. The modified Kent-Park model (Kent & Park, 1971) is employed for the simulation of the concrete fibres. This model was chosen because it allows for an accurate prediction of the demand for flexure-dominated RC members despite its relatively simple formulation. The transient behaviour of the reinforcing bars was simulated with the Menegotto-Pinto model (Menegotto & Pinto, 1973), while a nonlinear shear force-shear distortion (V-γ) law is adopted to account for shear failure, based on the work of Marini and Spacone (2006). The effect of gravity loads and second-order effects are considered using geometric stiffness matrix. More details on the two test examples can be found in Chapter 4 while Appendix B provides all details regarding modelling.

6.6.2. Ground motion selection

The selection of the proper external loading for performing life-cycle cost assessment is not an easy task due to the uncertainties involved in the seismic characteristics (see Chapter 5). For this reason a rigorous treatment of the seismic loading is to assume that the structure is subjected to a set of records that are more likely to occur in the region where the structure

is located. In this work a series of 10, 20, 40 and 60 seismic records per hazard level are implemented for both analysis procedures employed (NSA and MSDA). The records were randomly selected from the three lists of records given in Tables A.1 to A.3 (Appendix A). These records have been selected from the PEER strong-motion database (PEER, 2010) according to the following features: (i) Events occurred in specific area (longitude -124^o to -115^o, latitude 32^o to 41^o). (ii) Moment magnitude (M) is equal to or greater than 5. (iii) Epicentral distance (R) is smaller than 150 km. To make sure that the randomly selected number of records *no_recs* (where *no_recs* = 10, 20 or 40) are not dominated by a few events, for both *NSA* and *MSDA* implementations, an equal number of records from the each earthquake was kept. This was performed by means of Latin hypercube sampling (LHS) selecting one, two or more records from the same earthquake depending on the number of records used. Since the records of Tables A.1 to A.3 belong to 12 earthquakes. LHS is a strategy for generating random sample points ensuring that every part of the random space is represented. Latin hypercube samples are generated by dividing each random variable into N non-overlapping segments of equal probability. Thus, if M random variables are considered the random variable space is partitioned into N^M cells. For each random variable, a single value is randomly selected from each segment, producing a set of N values. The values of each random variable are randomly matched with each other to create N samples.

In the implementation of LCCA, in both cases eight pairs are considered corresponding to eight hazard levels (100/50, 83.95/50, 59.47/50, 38.28/50, 24.82/50, 16.35/50, 10.19/50, 5.90/50). The hazard levels are defined in accordance to the hazard curve (Figure 6.2) of the city of San Diego, California (Latitude (N) 32.7^o, Longitude (W) -117.2^o). Based on the flowchart for the NSA implementation in LCCA (Figure 6.3), 10, 20, 40 and 60 records, when scaled to the corresponding hazard level based on the $S_A(T_1,5\%)$, result to four implementations: NSA(i), i=10,20,40,60. In Figure 6.16 the spectra corresponding to the longitudinal and translational components of the records scaled to the 10/50 hazard level are shown. In the case of the MSDA, 60 records were used with $S_A(T_1,5\%)$ as the corresponding IM, while the corresponding implemented procedure is described in Figure 6.4.

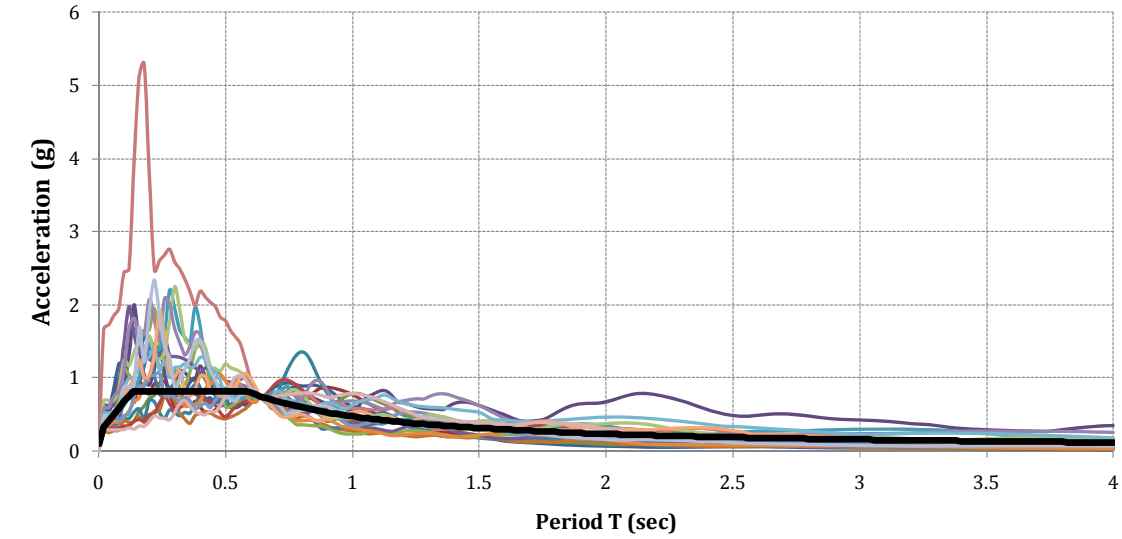

(a)

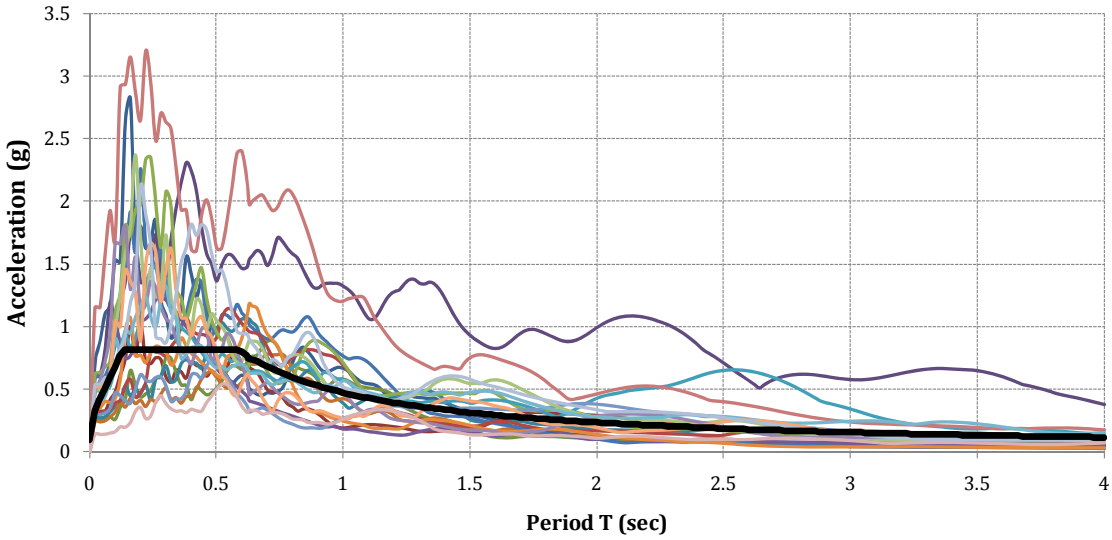

(b)

Figure 6.16. Response spectra of the group of 60 records scaled to the 10/50 hazard level, of the city of San Diego, according to the $S_A(T_1,5\%)$ (a) longitudinal and (b) transverse direction.

6.6.3. Multiple Stripe Analysis Results

Figures 6.17 to 6.20 present four groups of MSDA curves that depict the relation of the maximum interstorey drift and the floor acceleration with reference to eight hazard levels. In particular, the MSDA curves present the first mode spectral acceleration $S_A(T_1,5\%)$ against the maximum interstorey drift in Figures 6.17 and 6.19 and the maximum floor acceleration in Figures 6.18 and 6.20. In these graphs the medians along with the 16% and 84% fractile curves are shown.

As it can be seen in Figures 6.17 the four median curves almost coincide in the lower and the higher hazard levels. The curves corresponding to MSDA(20), MSDA(40) and MSDA(60) are almost identical with respect to the maximum interstorey drift. On the contrary,

deviation in the values of the upper hazard levels is observed for the curves of MSDA(10) with reference to the MSDA(20), MSDA(40) and MSDA(60). More significant variation is noticed with reference to the 16% and 84% fractile curves. In Figures 6.18 the three out of four MSDA median curves differ significantly in for all hazard levels. On the other hand, the curves corresponding to MSDA(20) and MSDA(40) almost coincide while they overestimate the capacity of the structure in comparison with the other two curves. The MSDA curve of the 60 records differs significantly from the other three curves showing greater deviation with higher hazard levels. In Figures 6.20 the three curves of MSDA(20), MSDA(40) and MSDA(60) are close to each other while the MSDA(10) curve(s) presents a more intensive exponential trend and differs in the 3rd to the 6th and in the 8th hazard levels by underestimating the first four levels and overestimating the level related to the capacity of the structure.

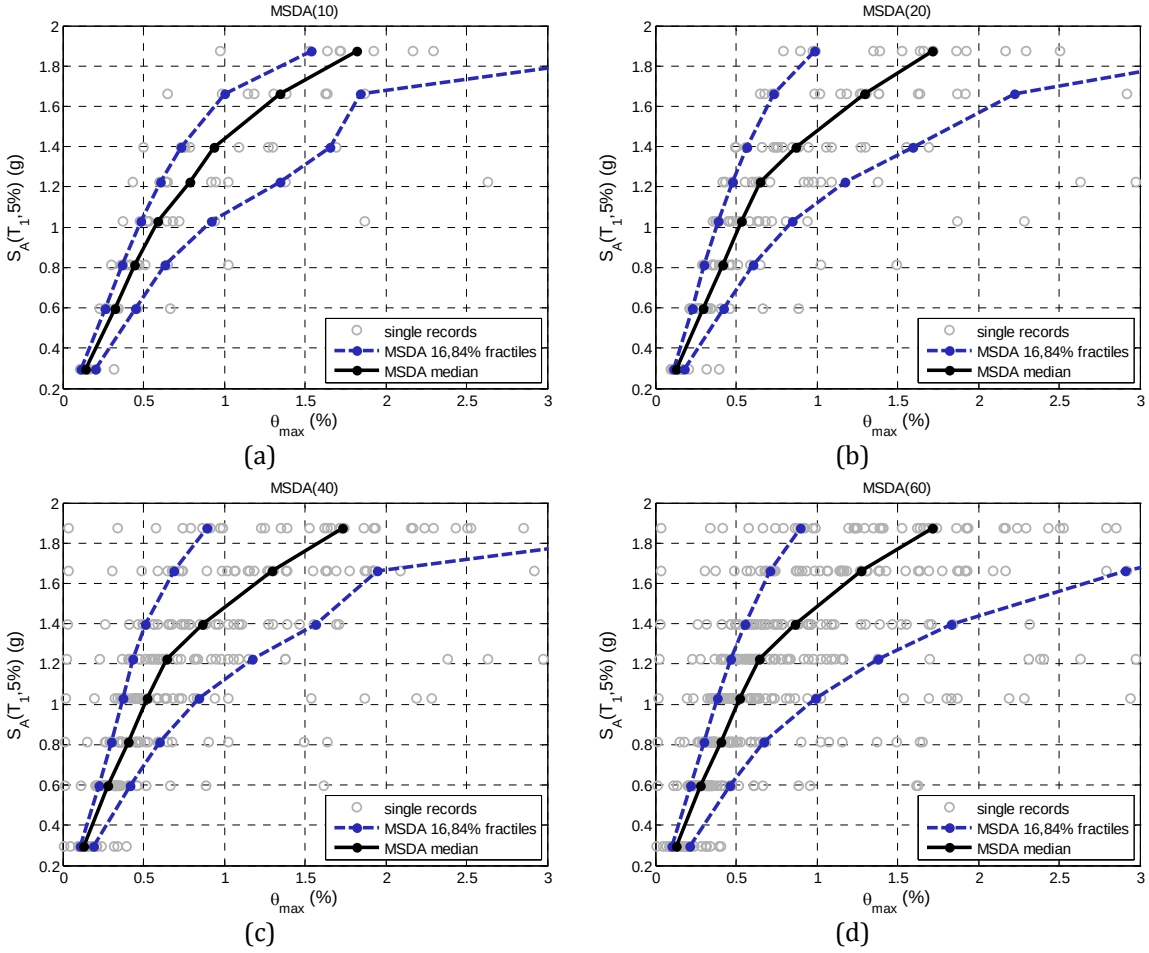

Figure 6.17. Eight storey test example: Medians and 16,84% fractiles of maximum drifts for (a) MSDA(10), (b) MSDA(20), (c) MSDA(40) and (d) MSDA(40).

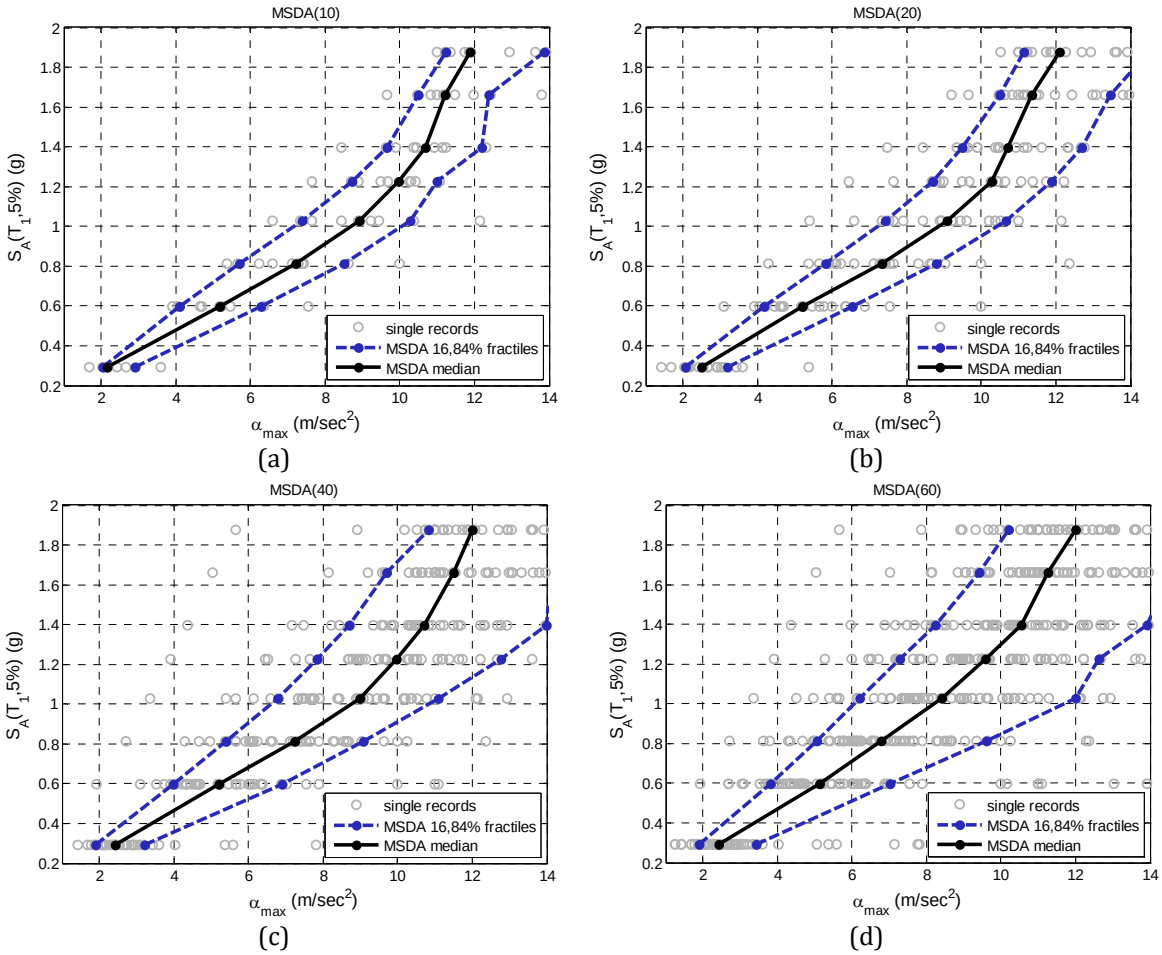

Figure 6.18. Eight storey test example: Medians and 16,84% fractiles of maximum floor acceleration for (a) MSDA(10), (b) MSDA(20), (c) MSDA(40) and (d) MSDA(40).

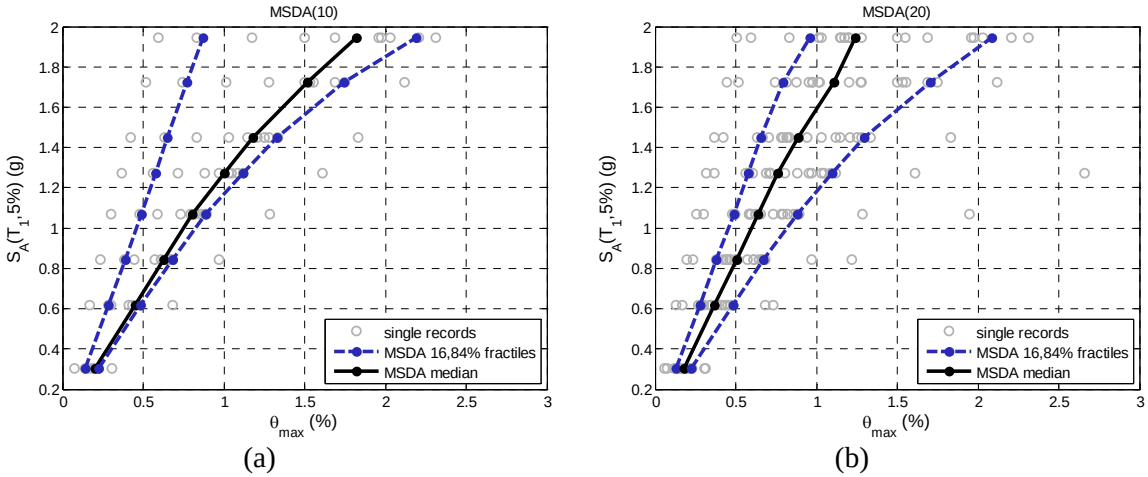

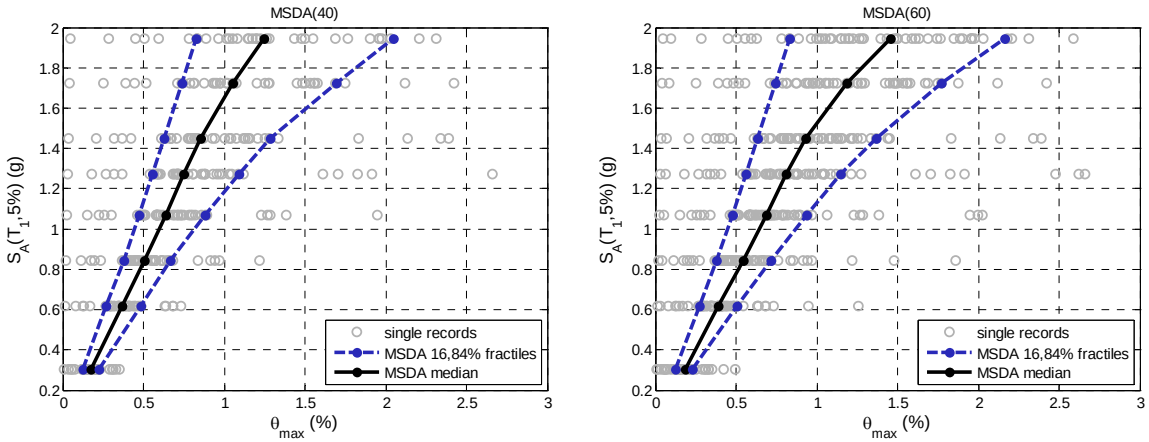

Figure 6.19. Five storey test example: Medians and 16,84% fractiles of maximum drifts for (a) MSDA(10), (b) MSDA(20), (c) MSDA(40) and (d) MSDA(40).

Comparing the MSDA curves of the two test examples it can be noticed that in all graphs the curves of MSDA(10) underestimate the capacity of the structure compared to those of MSDA(60). Furthermore, the curves with respect to the maximum floor acceleration (Figures 6.18 and 6.20) increase exponentially and almost coincide with all hazard levels. On the other hand, the curves with respect to the maximum interstorey drift differ significantly for the five storey test example with irregular plan while they almost coincide for the eight storey test example with symmetrical plan, and only the MSDA(10) curves appear to be different than the curves corresponding to the other 3 hazard levels.

6.6.4. Sensitivity Analysis of LCCA

In the second group of figures (Figure 6.21 and 6.22) the variability of the life-cycle cost with respect to the number of the seismic records is demonstrated. In particular the histograms of Figure 6.21 and 6.22 present the probabilistic distribution of the life-cycle cost values due to the number of seismic records implemented in the MSDA for the two test examples, respectively, along with the 90% confidence bounds for each group of seismic records. The frequency of C_{LS} value occurrence is defined as the ratio of the number of simulations (N_{suc}), corresponding to limit state cost values in a specific range, over the total number of simulations (N_{tot}), where N_{tot} is equal to 10, 20, 40 and 60 related to the 10, 20, 40 and 60 groups of seismic records, respectively.

Comparing the histograms of Figure 6.21 it can be noticed that in Figures 6.21(b) to 6.21(d) histograms the width of the confidence bounds is almost the same. On the other hand, the width of the 90% confidence bounds of the life-cycle cost values when 10 records are implemented for the MSDA is 20% narrower compared to the other three confidence bounds (Figures 6.21(b) to 6.21(d)). Furthermore, the mean value of the life-cycle cost is

almost the same for the MSDA with 20, 40 and 60 records and 15% higher for the MSDA with 10 records. In the histograms of Figure 6.22 the width of the confidence bounds is similar for the MSDA with 10, 20 and 40 records but 40% wider for the 60 seismic records MSDA. When it comes to the mean value of the life-cycle cost, the MSDA 20 and 40 records simulation present almost the same mean life-cycle cost value, while the MSDA 60 and 10 records reached a 23% and 47% higher value, respectively, compared to the other two.

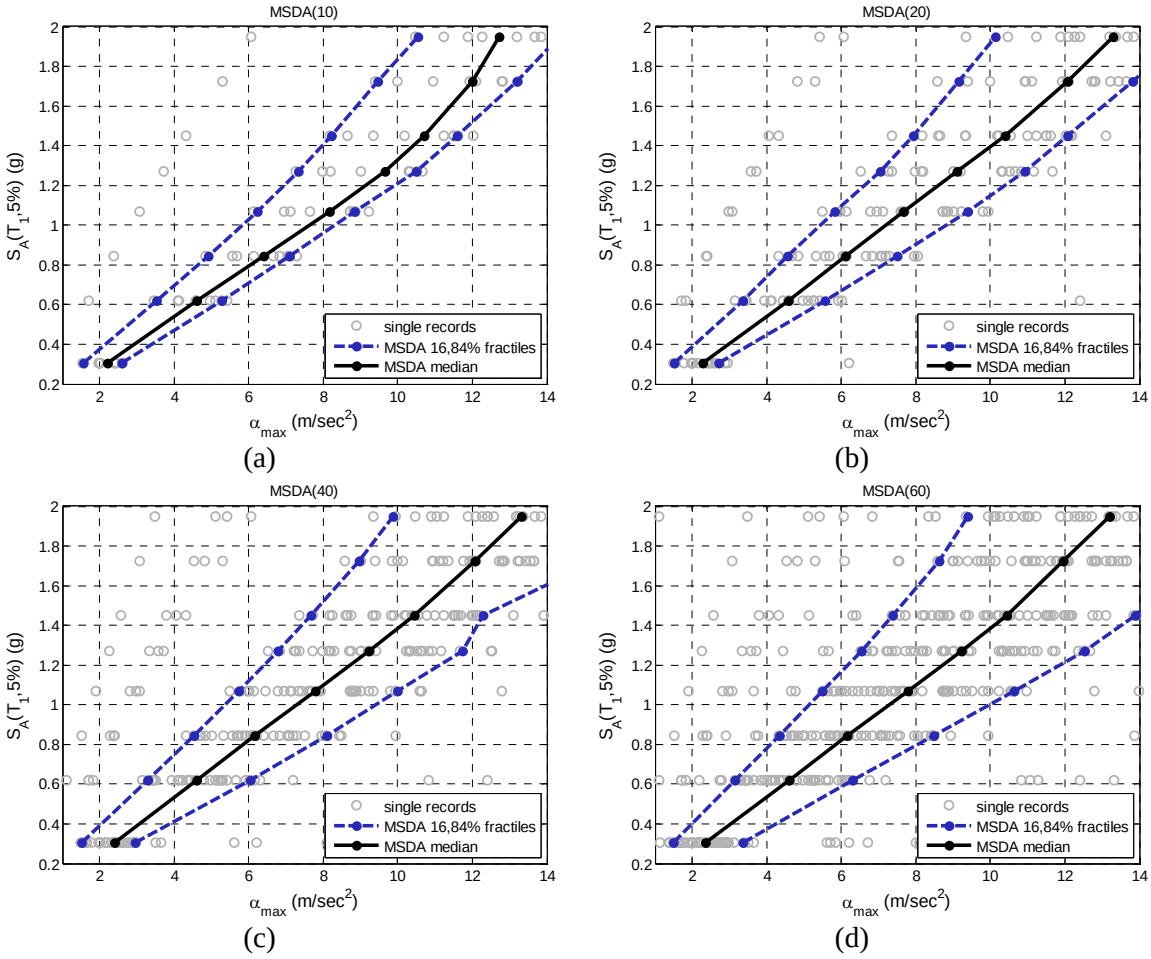

Figure 6.20. Five storey test example: Medians and 16,84% fractiles of maximum floor acceleration for (a) MSDA(10), (b) MSDA(20), (c) MSDA(40) and (d) MSDA(40).

Comparing the histograms of the two test examples, the confidence bounds for the symmetrical test case are much wider that the confidence bounds of the irregular one with respect to the four groups of records (10, 20, 40, 60). On the other hand, the life-cycle cost mean value of the symmetrical test is much lower than the respective value of the irregular test example. The conclusion that can be derived from the histograms of the probabilistic distribution of C_{LS} values are similar to those observing the MSDA curves with respect to the maximum interstorey drift. In fact the performance of the two test examples defined by the value of the interstorey drift at each hazard level has a direct effect on the value of the life-

cycle cost. Thus the maximum interstorey drift plays a more important role in the calculation of the life-cycle cost than the maximum floor acceleration.

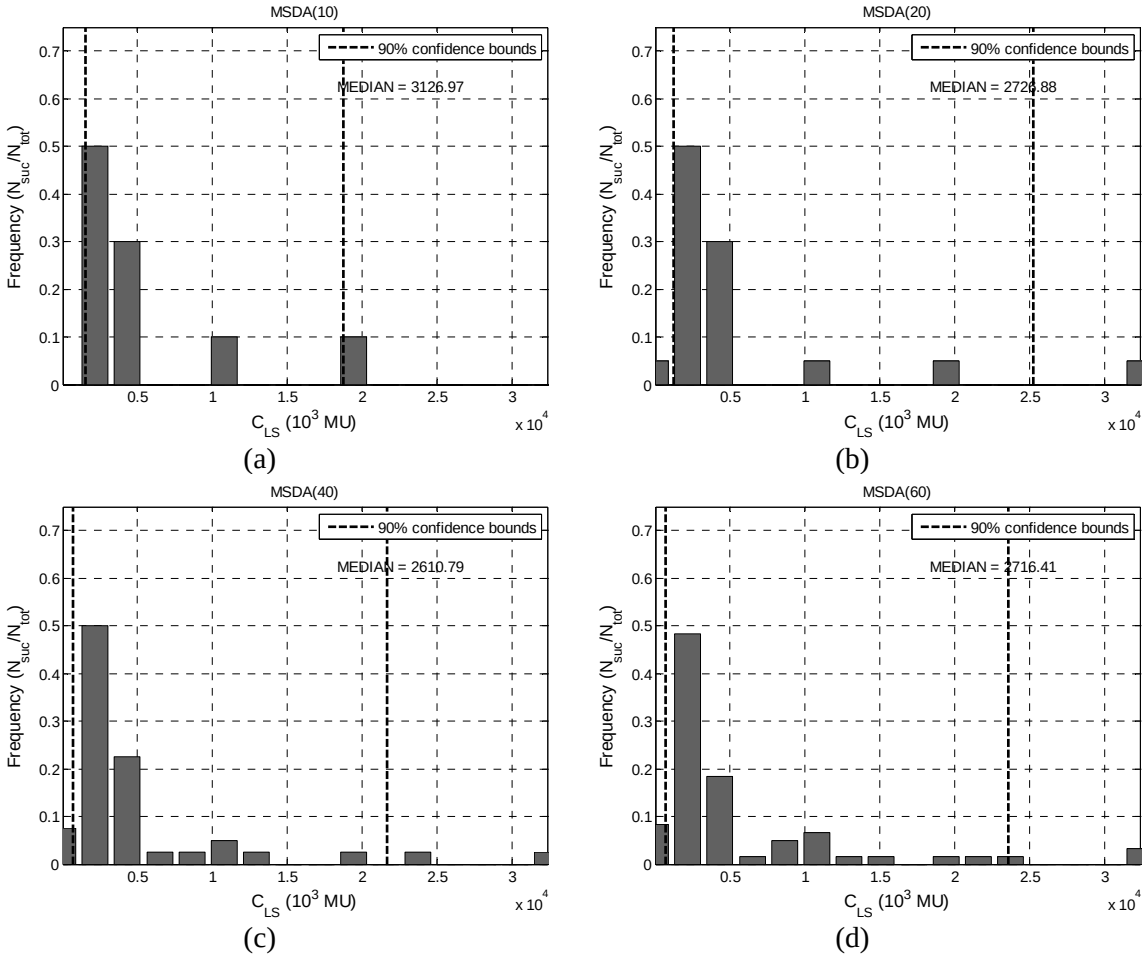

Figure 6.21. Eight storey test case: Frequency of occurrence for the case of (a) MSDA(10), (b) MSDA(20), (c) MSDA(40), (d) MSDA(60).

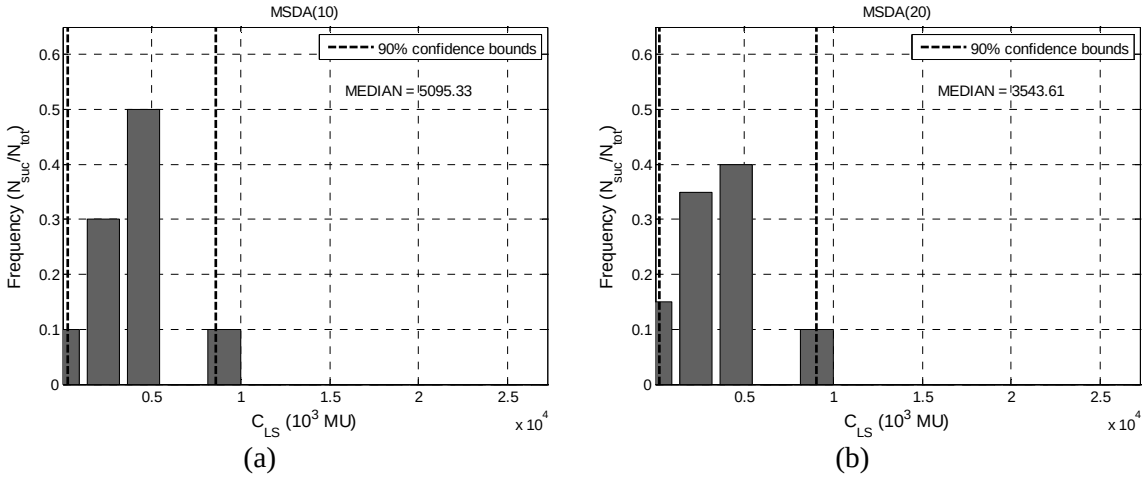

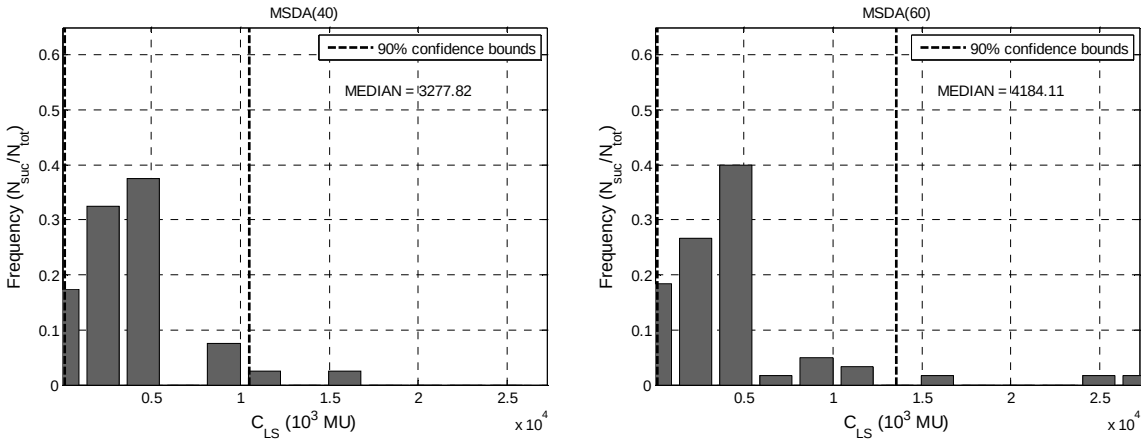

Figure 6.22. Five storey test example: Frequency of occurrence for the case of (a) MSDA(10), (b) MSDA(20), (c) MSDA(40), (d) MSDA(60).

The CDF curves, corresponding to the 10, 20, 40 and 60 groups of records for the symmetrical and irregular test example, are depicted in Figures 6.23 and 6.24. In Figures 6.23(a) and 6.23(b) the CDF for groups of 10, 20, 40 and 60 records coincide significantly up to 5.0 million MU (corresponding to Dollars or Euros) where a sharp slope is exhibited up to the 80% cumulative probability. In this range small increase of C_{LS} causes large increase of probability of occurrence.

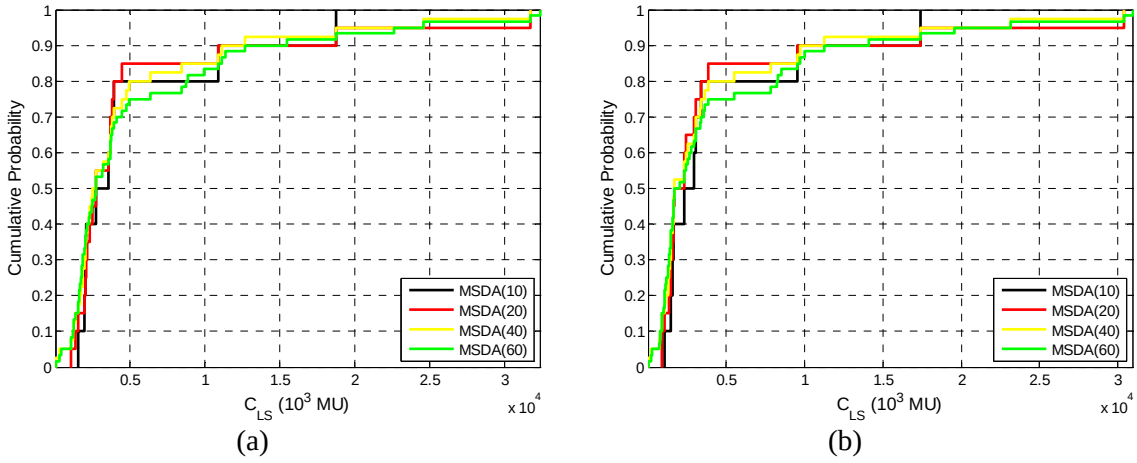

Figure 6.23. Eight storey test example – Cumulative Density Function: (a) drift plus floor acceleration, (b) drift.

On the other hand, in the range 5.0 to 15.0 million MU there is a markedly variation, while a smooth slope is encountered. Finally, for greater values of C_{LS} the three CDF curves for the groups of 20, 40, 60 records reaches asymptotically the 100% cumulative probability, while the CDF curves of 10 group of records has already reached the 100% cumulative probability. In Figure 6.24 the CDF curves for the groups of 20 and 40 records are similar for all the full range of C_{LS}, while the CDF curve for the group of 60 records coincides with the two other CDF curves for the groups of 20 and 40 records until the C_{LS} of

12.5 millions MU. Finally, the CDF curve for the group of 10 records exhibits a significant variation with respect to the other three CDF curves up to the point where the C_{LS} value reaches the higher cumulative probability. It can also be seen that Figures 6.23(a) and 6.24(a) are slightly shifted compared to the corresponding Figures 6.23(b) and 6.24(b). This is because in the first ones the loss of contents due to floor acceleration was taken into account.

6.6.5. Nonlinear Static Analysis vs Nonlinear Dynamic Analysis

In addition to the MSDA a NSA procedure is also implemented for both test examples. In Figure 6.25 and 6.16 the life-cycle cost values for the two test examples are presented following MSDA and NSA procedures imposing 10, 20, 40 and 60 number of seismic records.

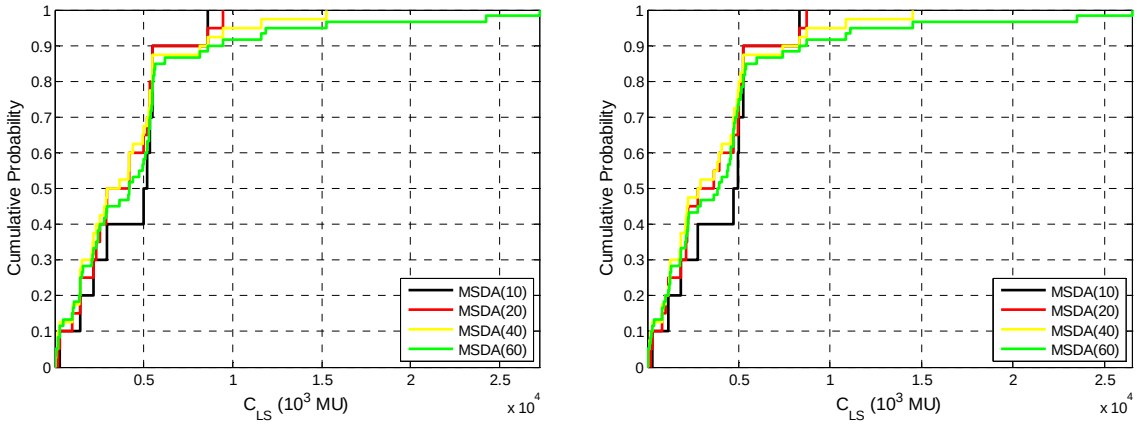

Figure 6.24. Five storey test example - Cumulative Density Function: (a) drift plus floor acceleration, (b) drift.

In the case of MSDA both DIs of maximum interstorey drift (θ) and the combination of θ and maximum floor acceleration ($\theta+\alpha$) are considered. In Figure 6.25 it can be seen that MSDA(θ) gives a more favourable life-cycle cost value compared to the MSDA($\theta+\alpha$). For both MSDA(θ) and MSDA($\theta+\alpha$) the value of life-cycle cost increases as the number of the records increases except of the case of MSDA(40) of Figure 6.26. The NSA case gives much lower values when records 10 and 20 are used and an almost double life-cycle cost value in the case of 60 records compared to the values of the MSDA(θ) and MSDA($\theta+\alpha$) cases.

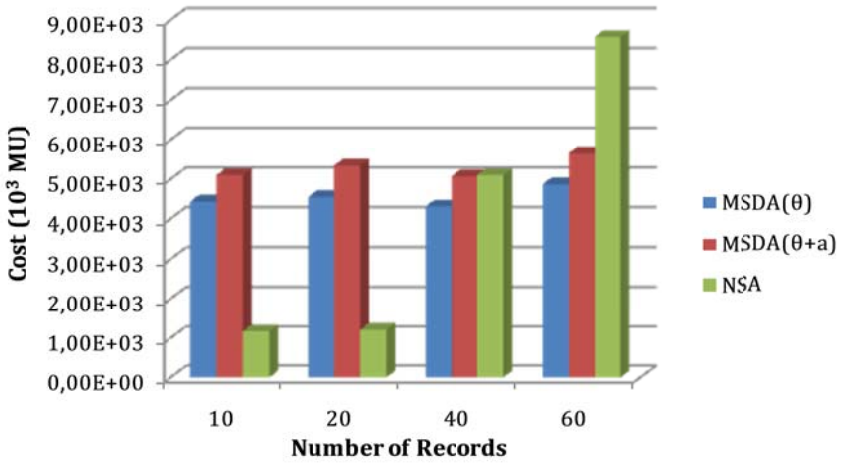

Procedure	Number of records			
	10	20	40	60
MSDA$_{(\theta)}$	4.43E+03	4.55E+03	4.31E+03	4.87E+03
MSDA$_{(\theta+a)}$	5.10E+03	5.34E+03	5.07E+03	5.65E+03
NSA	1.17E+03	1.21E+03	5.10E+03	8.57E+03

Figure 6.25. Eight storey test example: Total life-cycle cost (10³ MU).

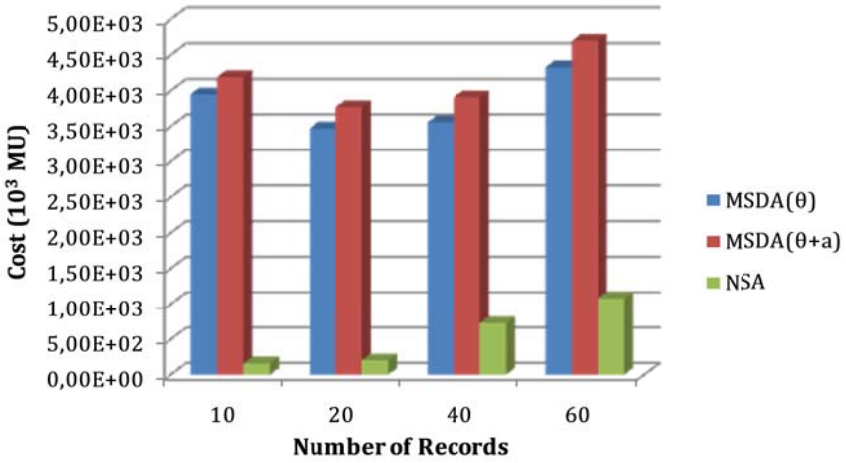

Procedure	Number of records			
	10	20	40	60
MSDA$_{(\theta)}$	3.95E+03	3.47E+03	3.56E+03	4.33E+03
MSDA$_{(\theta+a)}$	4.19E+03	3.77E+03	3.91E+03	4.70E+03
NSA	1.59E+02	2.04E+02	7.31E+02	1.08E+03

Figure 6.26. Five storey test example: Total life-cycle cost (10³ MU).

Comparing the values obtained for the MSDA(θ) and MSDA(θ+α) cases, it can be observed that the life-cycle cost values of MSDA analysis appear to have similar trend for both examples considered. The comparison between the MSDA(θ), MSDA(θ+α) and NSA leads to the same conclusions as in Figure 6.26 with two important exceptions: the life-cycle

cost value of 60 records with NSA is two times higher than the corresponding values of MSDA(θ) and MSDA(θ+α), while the life-cycle cost value of 40 records with NSA test case is one order of magnitude less than the corresponding of MSDA(θ) and MSDA(θ+α) value obtained for the symmetrical test case.

6.7. Discussion

In this chapter the calculation framework of the life-cycle cost of reinforced concrete buildings subjected to seismic actions is presented. The numerical study was performed on 3D RC building structures with regular and irregular plan views. The life-cycle cost estimation is examined with respect to the effect of the behaviour factor q in the final design of reinforced concrete buildings under earthquake loading in terms of safety and economy, the adopted analysis procedure, the number of seismic records imposed, the performance criterion used and the type of the building structure. Multiple stripe dynamic analysis, a variant of the incremental dynamic analysis, and the nonlinear static (pushover) analysis were applied to compute the performance criteria such as maximum interstorey drift and floor acceleration. The initial cost is related to the material and the labour cost for the construction of the building that includes both structural and non-structural component cost. The life-cycle cost refers to the potential damage cost from earthquakes that may occur during the life of the structure. In construction industry decision making for structural systems situated in seismically active regions, requires consideration of the damage and other losses costs resulting from earthquakes occurring during the lifespan of the structure. Thus, the life-cycle cost assessment becomes an essential component of the design process in order to control the initial and the future cost of building ownership. The life-cycle cost was calculated on the basis of the damage repair cost and loss of contents cost, due to structural damage that is correlated to the maximum interstorey drift, the loss of rental cost, the income loss cost, the cost of injuries as well as the cost of human fatality and the loss of contents cost due to floor acceleration.

The most important findings can be summarized as follows:

- The results obtained from the capacity curves and the corresponding life-cycle cost values, as well as from their variation between MSDA(θ) and MSDA(θ+α) cases, lead to the conclusion that the use of 40 records is a sufficient number of seismic records for a reliable performance assessment.
- The use of the maximum interstorey drift as performance criterion, instead of using the combination of both maximum interstorey drift and maximum floor acceleration, leads to an underestimation of the life-cycle cost of the structure. The effect of

interstorey drift appears to be more critical in the calculation of the life-cycle cost than the maximum floor acceleration.

- The nonlinear static analysis procedure is not recommended as a performance estimation tool compared to the nonlinear dynamic analysis. Especially, the life-cycle cost values in the irregular test example based on NSA produced unrealistic predictions of the structural performance.
- The structural type of the building affects its structural performance. It has been verified that a symmetrical structure sustains less damage and therefore less repair cost during its life compared to a non symmetric structure.
- Comparing, the contributing parts of the total life-cycle cost, it can be said that the initial cost, in both test examples, is the first dominant contributor for all designs obtained. The cost of contents due to floor acceleration is the second dominant contributor for stiffer design ($D_{q=1}$ and $D_{q=2}$), while for designs $D_{q=3}$ and $D_{q=4}$ damage and income costs are almost equivalent representing the second dominant contributors. It is also worth mentioning that, although the four designs differ significantly, injury and fatality costs represent only a small percentage of the total cost.
- The contribution of the cost of contents due to floor acceleration on the limit-state cost was in the range 20% to 29% for design $D_{q=4}$ while it was found in the range 76% to 85% for design $D_{q=1}$. This is due to the fact that the latter design is much stiffer compared to the other ones and thus increased floor accelerations inflict significant damages on the contents.

6.8. References

Arditi DA, Messiha HM. Life-cycle costing in municipal construction projects, Journal of Infrastructure Systems 1996; 2(1):5-14.

Asiedu Y, Gu P. Product Life-cycle cost analysis: state of the art review, Int. J. Prod. Res. 1998; 36: 883-908.

ATC-13. Earthquake Damage Evaluation Data for California. Applied Technology Council: Redwood City, CA, 1985.

Beck JL, Porter KA, Shaikhutdinov RV. Simplified estimation of seismic life-cycle costs, In life-cycle Performance of Deteriorating Structures: Assessment, Design, and Management, Frangopol DM, Bruhwiler E, Faber MH, Adey B. (Eds.), 229-236, 2003.

Chopra AK, Goel RK. A modal pushover analysis procedure for estimating seismic demands for buildings, Earthquake Engng Struct. Dyn. 2002; 31(3): 561-582.

EC2. Eurocode 2. Design of Concrete Structures—Part 1: General Rules and Rules for Buildings. European Committee for Standardisation: Brussels, Belgium, The European Standard EN 1992-1-1: 2004.

Elenas A, Meskouris K. Correlation study between seismic acceleration parameters and damage indices of structures, Engineering Structures 2001; 23: 698-704.

Ellingwood BR, Wen Y-K. Risk-benefit-based design decisions for low-probability/high consequence earthquake events in mid-America. Progress in Structural Engineering and Materials 2005; 7(2): 56–70.

Fajfar P. A nonlinear analysis method for performance-based seismic design, Earthquake Spectra 2000; 16(3): 573-592.

FEMA 227. A Benefit–Cost Model for the Seismic Rehabilitation of Buildings. Federal Emergency Management Agency, Building Seismic Safety Council: Washington, DC, 1992.

FEMA-350: Recommended Seismic Design Criteria for New Steel Moment-Frame Buildings. Federal Emergency Management Agency, Washington DC, 2000.

FEMA-356: Prestandard and commentary for the seismic rehabilitation of buildings. Federal Emergency Management Agency, Washington DC, SAC Joint Venture, 2000

Frangopol DM, Lin K-Y, Estes A (1997) Life-cycle cost design of deteriorating structures. Journal of Structural Engineering 123(10): 1390-1401.

Frangopol DM, Liu M. Maintenance and management of civil infrastructure based on condition, safety, optimization, and life-cycle cost, Struct. Infr. Engng. 2007; 3(1): 29-41.

Ghobarah A, Abou-Elfath H, Biddah A. Response-based damage assessment of structures, Earthquake Engng Struct. Dyn. 1999; 28(1): 79-104.

Ghobarah A, Saatcioglu M, Nistor I (2006) The impact of the 26 December 2004 earthquake and tsunami on structures and infrastructure. Engineering Structures 28(2): 312-326.

Ghobarah A. On drift limits associated with different damage levels. International Workshop on Performance- Based Seismic Design, June 28 - July 1, 2004.

http://earthquake.usgs.gov/hazards/designmaps/ US Geological Survey (USGS).

http://peer.berkeley.edu/smcat/search.html/ Pacific Earthquake Engineering Research (PEER). (last accessed February 2010).

Kappos AJ, Dimitrakopoulos EG. Feasibility of pre-earthquake strengthening of buildings based on cost-benefit and life-cycle cost analysis, with the aid of fragility curves. Natural Hazards 2008; 45(1): 33-54.

Kent DC, Park R. Flexural members with confined concrete. Journal of Structural Division 1971; 97(7): 1969-1990.

Khajehpour S, Grierson DE (2003) Profitability versus safety of high-rise office buildings. Structural and Multidisciplinary Optimization 25(4): 279-293.

Lagaros ND, Fotis AD, Krikos SA (2006) Assessment of seismic design procedures based on the total cost. Earthquake Engineering and Structural Dynamics 58(9): 1347-1380.

Lagaros, ND. Life-cycle cost analysis of construction practices, Bulletin of Earthquake Engineering 2007; 5, 425-442.

Liu M, Burns SA, Wen YK (2005) Multiobjective optimization for performance-based seismic design of steel moment frame structures. Earthquake Engineering and Structural Dynamics 34(3): 289-306.

Liu M, Burns SA, Wen YK. Optimal seismic design of steel frame buildings based on life-cycle cost considerations, Earthquake Engineering and Structural Dynamics 2003; 32: 1313-1332.

Marini A, Spacone E. Analysis of reinforced concrete elements including shear effects. ACI Structural Journal 2006; 103(5): 645-655.

McKenna F, Fenves GL. The OpenSees Command Language Manual - Version 1.2, Pacific Earthquake Engineering Research Centre, University of California, Berkeley, 2001.

Menegotto M, Pinto PE. Method of analysis for cyclically loaded reinforced concrete plane frames including changes in geometry and non-elastic behaviour of elements under combined normal

force and bending. Proceedings, IABSE Symposium on Resistance and Ultimate Deformability of Structures Acted on by Well Defined Repeated Loads: 15-22, 1973.

Mitropoulou ChCh, Lagaros ND, Papadrakakis M. Economic building design based on energy dissipation: a critical assessment, Bulletin of Earthquake Engineering Journal, 8(6): 1375-1396, 2010.

Pei S, Van De Lindt JW. Methodology for earthquake-induced loss estimation: An application to woodframe buildings, Structural Safety 2009; 31(1): 31-42.

Rackwitz R, Lentz A, Faber M. Socio-economically sustainable civil engineering infrastructures by optimization. Structural Safety 2005; 27(3): 187-229.

Rackwitz R. The effect of discounting, different mortality reduction schemes and predictive cohort life tables on risk acceptability criteria, Reliability Engineering and System Safety 2006; 91(4): 469-484.

Sanchez-Silva M, Rackwitz R. Socioeconomic implications of life quality index in design of optimum structures to withstand earthquakes, Journal of Structural Engineering 2004; 130(6): 969-977.

Sarma KC, Adeli H (2002) Life-cycle cost optimization of steel structures. International Journal for Numerical Methods in Engineering 55(12): 1451-1462.

Takahashi Y, Der Kiureghian A, Ang AH-S, Life-cycle cost analysis based on a renewal model of earthquake occurrences, Earthquake Engineering and Structural Dynamics 2004; 33: 859-880.

Vamvatsikos D, Cornell CA. Incremental dynamic analysis, Earthquake Engineering and Structural Dynamics, 2002; 31(3): 491-514.

Wen YK, Kang YJ (2001a) Minimum building life-cycle cost design criteria. I: Methodology. Journal of Structural Engineering 127(3): 330-337.

Wen YK, Kang YJ (2001b) Minimum building life-cycle cost design criteria. II: Applications. Journal of Structural Engineering 127(3): 338-346.

Chapter 7

Fragility Assessment of Structural Systems

7.1. Introduction

Over the last decades risk assessment and risk management have earned the attention of various economic and technical decision centres in the modern society. The optimal allocation of the public resources, usually limited, for a sustainable economy entails the need for rational tools for evaluating the consequences of natural and man-made hazardous events on the built environment. The risk management addresses and satisfies this claim indicating the best way for optimal choices. The main purpose of the risk management process is to choose among different options relying on technical and economic considerations. The process of the risk management can be divided in two main steps: the risk assessment step and the decision analysis one. In this context, Civil Engineering provides the technical knowledge to evaluate the probability of damage and failure of facilities or in general the probability of losses due to natural and man-made hazards. In what follows the definition of risk is presented.

A lot of research work has been published in an effort to establish a reliable procedure for assessing the seismic risk of structural systems. Seismic fragility analysis, which provides a measure of the safety margin for the structural system, is considered as the main ingredient of the risk assessment procedure. Kennedy et al. (1980) presented a methodology for determining the probability of radioactive releases due to earthquake. Kircher et al. (1980) described building damage functions that were developed for the FEMA/NIBS earthquake loss estimation methodology. Shinozuka et al. (1997) presented a statistical analysis procedure of structural fragility curves. The significance of inherent randomness and modelling uncertainty in forecasting the building performance was examined by Ellingwood (2001) through the fragility assessment of a steel frame. In the

work by Shinozuka et al. (2003) fragility curves were developed in order to determine the effect of earthquakes on the performance of transportation network systems. The importance of fragility analysis in various stages of consequence-based engineering was indicated by Wen and Ellingwood (2005). A procedure to account for the uncertainty in the characteristics of future ground motions during seismic response assessment was presented in the work by Aslani and Miranda (2005). Fragility functions were developed by Pagni and Lowes (2006) to identify the method to repair older reinforced concrete beam-column joints damaged due to earthquake loading. A methodology for the risk assessment of reinforced concrete and unreinforced masonry structures was presented by Kappos et al. (2006), while Jeong and Elnashai (2007) presented an approach where a set of fragility relationships with known reliability is derived based on the fundamental response quantities of stiffness, strength and ductility. A set of procedures for creating fragility functions from various kinds of data was introduced by Porter et al. (2007). Lagaros (2008) performed fragility analysis in order to assess a group of reinforced concrete structures implementing three design practices.

In this Chapter a general overview of the risk assessment and risk management is illustrated along with some recent approaches to these issues. In particular, the concept of structural reliability theory as a general tool to accomplish the objective of fragility analysis of reinforced concrete buildings is presented along with a new robust and efficient procedure based on neural networks and metaheuristics methodology. In particular, in this chapter the general description of the fragility analysis framework is presented along with methods for dealing with the problem of reliability analysis. Furthermore, SC techniques, like neural networks and metaheuristics, for reducing the computational effort are introduced. In particular, as it is well known (Papadrakakis et al., 1996) one of most successful applications of SC methods, is the incorporation of SC-based approximations into reliability analysis and structural optimization for predicting systems response (Papadrakakis et al., 1996; Papadrakakis & Lagaros, 2002). Fragility analysis of 3D RC buildings is performed following the HAZUS (2003) approach. This approach relies on the assumption that the demand values follow the lognormal distribution, thus the fragility curves are expressed in the form of a two-parameter lognormal distribution where an optimization algorithm is implemented for calculating these two parameters for each limit state considered. In particular the harmony search algorithm, which is an efficient optimization algorithm (Lee & Geem, 2005) belonging to the class of metaheuristics, is employed for solving the optimization problem at hand. Moreover, in order to develop fragility curves structural response estimates are required obtained either by means of

nonlinear static or nonlinear dynamic procedures. In this Chapter the IDA method (Vamvatsikos & Cornell, 2002) is implemented, where 100 natural records in the area under consideration are used, requiring an excessive computational effort. Furthermore, a neural network approximation of the structural response is proposed resulting into one order of magnitude reduction of the computational effort. In the proposed NN-based methodology, uncertainty in demand is treated in a straightforward manner where large bins of records can be considered with insignificant additional computational effort.

7.2. Risk Definition

The exact meaning of the word risk is often difficult and tricky to explain in a simple way. Therefore, first of all, it is worth trying to answer to the following question: "What the risk is exactly?" In broad sense, risk is related to an unwanted event that can be seen as a dangerous one. According to this general definition, any event or activity may or may not be risky. However, this simple definition cannot be applied to actual situations because a dangerous event cannot be excluded altogether. There is always a margin of uncertainty and then the definition of risk must be formulated in probabilistic terms. In the last decades some definitions of risk have been given by several researchers. Together with the risk definition, one must provide the definition of other terms usually involved in risk analysis. Namely: the vulnerability, the natural hazard, the exposure. Following the definitions of UNESCO / UNDRO (1982) (Alexander, 2003) it can be said that:

- *Natural hazard (H)* is the probability of occurrence within a specified period of time and within a given area of a potentially damaging phenomenon;
- *Vulnerability (V)* is the degree of loss to a given element or a group of elements at risk resulting from the occurrence of a hazardous phenomenon of a given magnitude. It is expressed on a scale from 0 (no damage) to 1 (total loss);
- *Specific Risk (R_s)* is the expected degree of loss due to a hazardous phenomenon. It may be expressed by the convolution of *Natural Hazard* times *Vulnerability* ;
- *Elements at risk (E)* (Exposure or Exposition) is the population, properties, economic activities, including public services, etc., at risk in a given area;
- *Total risk (R_t)* is the expected number of lives lost and persons injured, and amount of damage to property, or disruption of the economic activity caused by a particular hazardous phenomenon. In other words is the convolution of specific risk (R_s) and elements at risk (E).

Other broad definitions of risk have been proposed, such as the definition quoted by Rackwitz et al. (2005): "The risk is the chance of an adverse outcome to human health, the

quality of life, or the quality of the environment". The definitions reported above can be specified and modified in order to fit them to a specific field, such as Civil Engineering. In this field the risk is usually associated with physical damage of structures or facilities. Following this concept, the risk could be defined as the "absolute probability of a negative consequence (e.g. damage or collapse) due to a potentially dangerous event" (Augusti et al., 2001). This probability is the "convolution integral" of three terms, namely vulnerability, exposure and site hazard.

The reliability R is defined as the complement of risk (R = 1− *risk*). The *site hazard* is usually identified through an intensity measure (see Chapter 5 for a detailed description). A probability of occurrence in a given time span is associated with each intensity measure. This relation is known as the hazard curve and depends on the site under investigation or simply on the place where the structure has been built. In a specific site there will be different hazard curves, one (or more than one) for each natural event (e.g. earthquake, wind storm, flood, fire, etc.). The *exposure* is defined as the probability of the presence of vulnerable facilities in the site. Typically, the increase of population and economic activities in some areas usually causes an increase of exposition. The *vulnerability* is the probability of attaining or exceeding a damage level conditioned to an event of given intensity measure. Consequences of damage (e.g. losses) are usually measured either in economic term (direct or indirect) or in term of casualties that is losses of human life and injuries. Then the risk can be seen as a probabilistic measure of economic and/or human life losses and injured. This aspect of risk estimation, namely its economic interpretation, is usually used in connection to both decision making theory and insurance.

7.3. Risk Assessment

From the point of view of the reliability theory and structural engineering (Melchers, 1987), the risk is defined as the probability of "structural failure" (the unwanted event) both from violation of predefined limit states (e.g. collapse, damage or serviceability) and from other causes. At this point a question arises: "How the probability of structural failure may be assessed?" Generally, the process of probabilistic assessment of structural failure involves many random variables, such as resistance, action, material behaviour, structural response, dimensions of structural elements, etc. These variables are required for characterizing the behaviour of a structure, while they are called as "basic" variables or random variables. The basic variables are usually defined by the mean of their probability distribution and are assumed to be known or given by experimental test or observations. If $\mathbf{x}$ is the vector of the random variables of the problem, $g(\mathbf{x})$ represents the limit state equation and $f_x(\mathbf{x})$ is the

joint probability density function of the random variables, the probability of exceeding a specified limit state can be evaluated by using the convolution integral of $f_x(\mathbf{x})$ over the failure domain represented by the condition $g(\mathbf{x})<0$ (Melchers, 1987):

$$P_f = P[G(\mathbf{x}) \geq 0] = \int \dots \int_{G(X)\geq 0} f_x(\mathbf{x}) d\mathbf{x} \tag{7.1}$$

In general, the random variables $\mathbf{x}$ are not independent. Conversely, if they are independent the joint probability density function can be expressed as the product of each probability density function for the random variable x_i i=1,2,...,m, where m is the number of random variables (Elishakoff, 1999). Besides the numerical difficulty in carrying out the convolution integral, some other problems arise when one wants to derive the probability of structural failure. In particular, the aspects related to human factor, negligence, poor workmanship, neglected load, lack of knowledge about the structural behaviour etc. should be taken into account during the risk assessment process. Furthermore, some causes of failure cannot be foreseen as being "unimaginable" (for instance an event of big magnitude never recorded before); this increases the level of uncertainty in estimating the risk. As far as the computational aspects are concerned, it can be said that many techniques for evaluating the integral of Eq. (7.1) have been proposed (Melchers, 1987). These techniques are usually based on simplification either for the statistical distributions of each random variable or for the expression of the limit state equation. A typical simplification is to assume that the probability distribution of each random variable is represented by its mean and standard deviation. This corresponds to assume a normal distribution for each random variable involved in the convolution integral. The second simplification is to assume that the limit state function can be approximated by a linear half-space. These are the ingredients for the so-called first-order reliability-method, while second-order reliability-method represents an improvement to FORM, in which the hypothesis of variables normally distributed still holds, but the limit state function is approximated by a hyper-paraboloid in the random variables space. So far the probability of failure of a structure has been tackled disregarding both type of action and structural typology. Considering the seismic action only, it may be said that recently a great deal of effort has been devoted in order to provide a tool of structural design based on the reliability theory. PBEE (Cornell and Krawinkler, 1999) represents one of these tools. Details on this framework can be found in Chapter 4 of this dissertation.

This modern approach to seismic design is also adopted by some design codes such as Vision 2000, FEMA 237, FEMA 356, ATC-32, ATC-40 and is based on the accomplishment, in probabilistic terms, of a generic performance (e.g. no collapse, life safety, operational, fully operational) at various levels of the seismic action. A review of the performance definitions

can be found in ATC-58-2 (2003). In other words, the foundation of PBEE consists of assessing the adequacy of a structure or its design by evaluating, in probabilistic way, a decision variable (DV) (in general a vector of variables) (Cornell and Krawinkler, 2000). The decision variable can assume different meanings, such as the earthquake loss, the exceeding of one or more limit states (e.g. collapse, serviceability). Following the PBEE method, in order to assess the probability of exceeding of DV (λ(DV)) some intermediate variables must be introduced; namely EDP and IM. The methodology of PBEE is illustrated in Figure 7.1, where D represents the location and design features of the structure. In Figure 7.1 *p(x|y)* refers to the probability density of *x* conditioned to *y*, and g(*x*) refers to the occurrence rate of *x* (that is the negative first derivative of the frequency with which *x* is exceeded).

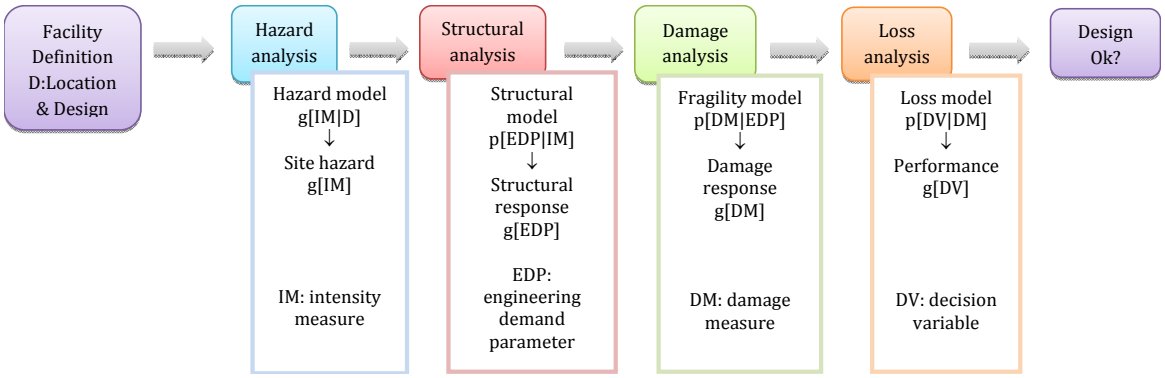

Figure 7.1. PEER analysis framework. Adapted from Porter (2003).

The mathematical meaning of Figure 7.1 is reported in the following expression, that stems from the application of the total probability theorem (Porter, 2003).

$$\nu(\mathrm{DV}\,|\,\mathrm{D}) = \int\int\int \mathrm{p}[\mathrm{DV}\,|\,\mathrm{DM},\mathrm{D}]\cdot\mathrm{p}[\mathrm{DV}\,|\,\mathrm{EDP},\mathrm{D}] \cdot\mathrm{p}[\mathrm{EDP}\,|\,\mathrm{IM},\mathrm{D}]\cdot\mathrm{g}[\mathrm{IM}\,|\,\mathrm{D}]\cdot\mathrm{dDM}\cdot\mathrm{dEDP}\cdot\mathrm{dIM} \tag{7.2}$$

As can be seen in Figure 7.1, the assessment of λ(DV|D) can be accomplished through four analysis steps:

- *Hazard analysis*. It is performed considering the seismic site (nearby faults, their magnitude-frequency recurrence rates, mechanism, site distance, site conditions etc.) and evaluating the seismic hazard at the facility location taking into account all structural features (denoted by the design D). More details can be found in Chapter 5 of this dissertation. This analysis yields a hazard curve which gives the annual frequency with which the seismic action, described by the IM is exceeded. Various IMs have been studied (Giovenale, 2003) with the aim of selecting one of them (or more than one) as more representative of the site hazard. Summarizing, the Hazard

analysis provides an answer to the following question: How likely is an event of intensity IM to happen, for this location?

- *Structural Analysis*. Structural analysis is needed for estimating the uncertain structural response, measured as a vector of EDP conditioned on a seismic IM and design (D), p[EDP|IM,D]. A review of the most important EDP, for both structural framing system and non-structural components, can be found in ATC-58-2 (task 2.2) (2004) and ATC-58-2 (task 2.3) (2004). EDP can contain indices related to hysteretic response of structural elements, local or global deformations, maximum floor accelerations and so on. Detailed description of DIs and EDPs is provided in Chapter 2 of this dissertation. Therefore the structural analysis is usually a nonlinear time-history analysis carried out by using either deterministic finite element models or finite element models with uncertain properties. In short, the question which summarizes the structural analysis step is: What will be the engineering demands (force, deformation, etc.) to which this facility will be subjected?
- *Damage Analysis*. It is also known as fragility analysis. In this step the results of structural analysis (EDP) are used as input for computing the probability of different levels of physical damage conditioned on structural response and design, p[DM|EDP,D]. Thus fragility functions give the probability of various levels of damage for individual beams, columns, nonstructural components as functions of various EDP. In other words, what will be the physical damage this facility will experience?
- *Loss Analysis*. It is the last step and consists of determining the performance, represented by the decision variable *DV*, conditioned on damage and design terms p[*DV*|DM,D]. Decision variables measure the seismic performance of the facility in terms of the main interest of stakeholders. This latter can be both a private owner and a public administrator, so the performance can be measured in terms of money, death, down time, etc. The final step provides an answer to the following question: What will be the loss (economic, casualty, etc.) this facility will experience?

7.4. Fragility Analysis

As it was mentioned in the previous section of this Chapter, earthquake risk assessment of building structures requires the calculation of limit state probabilities for a series of limit-states of monotonically increasing severity. The target is to obtain the limit state probabilities of exceedance that serve as a hazard curve for structural damage. The mean annual frequency of a damage index occurrence exceeding a value *y* is obtained as:

$$v(\mathrm{DI}_{max} \geq \mathrm{y}) = \int P\left(DI_{max} \geq y / IM = x\right)\left|d\lambda_{IM}\left(x\right)\right| \tag{7.3}$$

where $v(DI_{max} \geq y)$ is the rate of *DI*, exceeding the value *y* and $\lambda_{IM}(x)$ is the mean annual frequency of the chosen intensity measure exceeding *x*. In other words, $\lambda_{IM}(x)$ is the hazard curve and $d\lambda_{IM}(x)$ is its slope. The absolute value is used for the slope because it has a negative value.

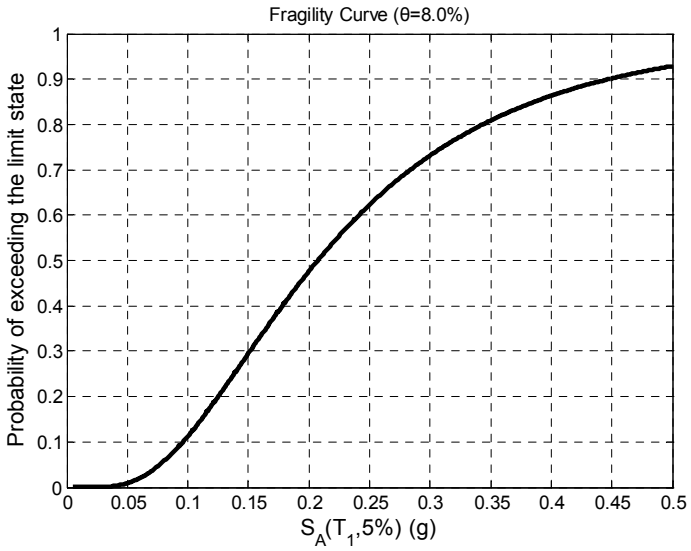

Figure 7.2. Typical fragility curves versus the intensity of the seismic ground motion (F_R)

Fragilities were first introduced in the probabilistic analysis of nuclear power plants (Cornell, 1960), with the purpose of distinguishing the task of structural engineers from that of seismologists. Fragility curves are functions that represent the conditional probability that a given structure's response to various seismic excitations exceeds given performance limit states. Theoretically, seismic fragility F_R represents the probability that the response represented by damage index DI of a specific structure (or family of structures) exceeds a given threshold y_{lim}, associated with a given limit state, conditional on earthquake intensity parameter *I*. In mathematical form, this is a conditional probability (Barron-Corvera, 2000; Reinhorn et al, 2001) (Eq. 7.4). The measure of seismic intensity *IM* may be expressed as peak ground acceleration, spectral acceleration, spectral velocity, or any other control variable that is consistent with the specification of seismic hazard.

$$F_R = P\left[DI_{max} \geq y_{lim} / IM = x\right] \tag{7.4}$$

In general it can be said that developing a fragility curve can be considered as equivalent with solving multiple reliability analysis problems. A typical fragility curve is depicted in Figure 7.2. A large number of records scaled in a number of hazard levels with increased intensity are required for accurate calculation of the probabilities. Therefore a large number

of nonlinear response history analyses are required for every intensity level. The probability F_R is calculated as the number of the nonlinear responses exceeding the limit state threshold for a specific intensity level divided by the total number of the nonlinear responses implemented. In the case that a very small probability is to be calculated the required number of nonlinear responses can become enormous therefore the computational cost is also increased drastically (see Figure 7.3).

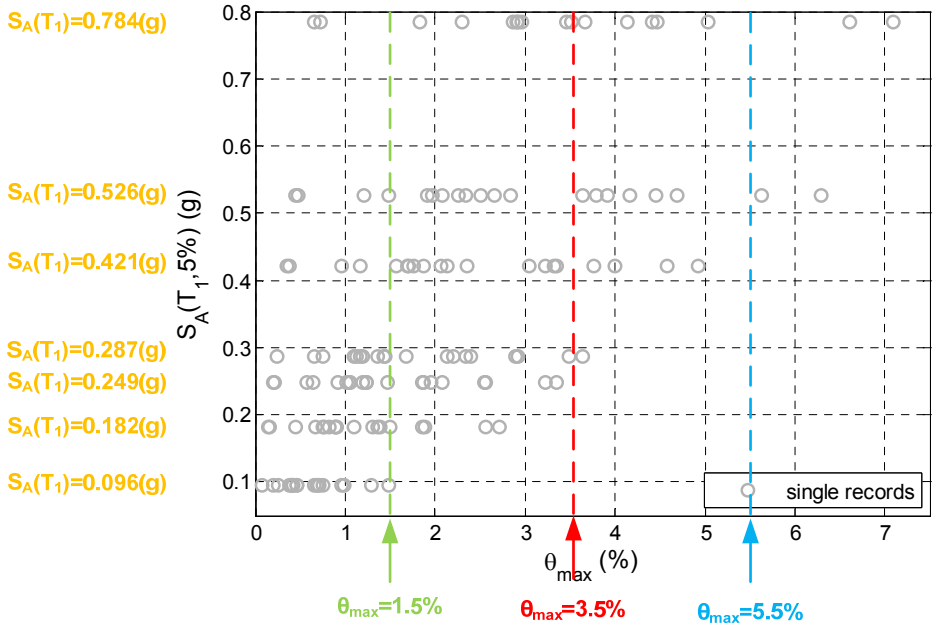

Figure 7.3 Multi-stripe analysis for calculating the probability of exceedance of a limit state.

On the other hand, in order to reduce the computational effort the assumption that seismic data are lognormally distributed (Benjamin and Cornell 1970) is adopted for the analytical calculation of F_R. The curves F_R can be expressed in the form of two-parameter (median-μ and log-standard deviation-β) lognormal distribution functions. Therefore, F_R takes the following form

$$F_R(IM) = \Phi\left[\frac{ln(IM/\mu_k)}{\beta_k}\right] \tag{7.5}$$

in which Φ is the standardized normal distribution function. According to HAZUS the parameter μ_k (k=1, 2,..., n and n is the number of the limit states considered) is calculated by means of nonlinear static analysis, while β_k is calculated according to equation (7.6) and takes discrete values (HAZUS, 2003).

$$\beta_{ds} = \sqrt{(CONV[\beta_c, \beta_D])^2 + (\beta_{T,ds})^2} \tag{7.6}$$

where, β_{ds} is the lognormal standard deviation parameter that describes the total variability of the damage limit state, β_c is the lognormal standard deviation parameter that describes the variability of the capacity curve and β_D is the lognormal standard deviation parameter that describes the variability of the demand spectrum. According to Shinozuka *et al.* (2000) the probability F_R is expressed by equation (7.5) but the estimation of the two parameters is based on nonlinear dynamic analysis and is performed by means of the maximum likelihood method. The likelihood function for the present purpose is expressed as follows:

$$L(\mu_1,\mu_2,\ldots,\mu_n,\beta_1,\beta_2,\ldots,\beta_n)=\prod_{i=1}^{N}\prod_{k=1}^{n}F_R(IM_i,y_k)^{x_{ik}} \tag{7.7}$$

where F_R represents the fragility curve for a specific state of damage; IM_i is the intensity measure value to which the i-th realization of the structure is subjected; x_{ik} is equal to 1 or 0 depending on whether or not the i-th realization of the structure sustains the state of damage under IM_i , N is the total number of structural realizations after the earthquake and n is the total number of the limit states considered. Therefore, F_R takes the following form in which Φ is the standardized normal distribution function. As suggested in Shinozuka *et al.* (2000) the two parameters μ_k and β_k of Eq. (7.7), where k=1, 2,..., n, are computed as the values that maximize ln(L) by implementing an optimization algorithm.

7.4.1. Damage Limit States

The choice of damage scale and measure is fundamental to the fragility curve development. In the case of empirical curves it is essential that the damage scale used is clearly defined in terms of the damage expected in the structural and the non-structural elements of buildings with different lateral load resisting systems. Also, in order to use the fragility curves in a performance-based framework, it is desirable that they provide predictions for at least three damage limit states, corresponding to serviceability, damage control and collapse prevention. In order to define a limit state, different types of parameters are used; most of them, though, with lack of reliability. It has been also proved that limit states have been defined more effectively in terms of deformation exceedance rather than load exceedance. For instance, Onose (1982) proposed a parameter based on structural ductility, but it was deemed unsuitable due to its inability to account for failures caused by damage concentration at the storey level. Mosalam et al (1997), provided analytical fragility curves for four damage states using interstorey drift as the damage index.

Table 7.1. The HRC-Scale: Typical damage expected in ductile, non-ductile and infilled RC moment resisting frames and in RC shear-wall structures (Rossetto & Elnasai, 2003).

DI_{HRC}	Damage State	Ductile MRF	Non-Ductile MRF	Infilled MRF	Frame-Wall
0	**None**	No damage	No damage	No damage	No damage
10	**Slight**	Fine cracks in plaster partitions/infills	Fine cracks in plaster partitions/infills	Fine cracks in plaster partitions/infills	Fine cracks in plaster partitions/infills
20	**Light**	Start of structural damage	Start of structural damage	Cracking at wall-frame interfaces	Start of structural damage
30		Hairline cracking in beams and columns near joints (<1mm)	Hairline cracking in beams and columns near joints (<1mm)	Cracking initiates from corners of openings	Hairline cracking on shear-wall surfaces & coupling beams
40				Diagonal cracking of walls. Limited crushing of bricks at b/c connections	Onset of concrete spalling at a few locations
50	**Moderate**	Cracking in most beams & columns	Flexural & shear cracking in most beams & columns	Increased brick crushing at b/c connections	Most shear walls exhibit cracks
60		Some yielding in a limited number	Some yielding in a limited number	Start of structural damage	Some walls reach yield capacity
70		Larger flexural cracks & start of concrete spalling	Shear cracking & spalling is limited	Some diagonal shear cracking in members especially for exterior frames	Increased diagonal cracking & spalling at wall corners
80	**Extensive**	Ultimate capacity reached in some elements – large flexural cracking, concrete spalling & re-bar buckling	Loss of bond at lap-splices, bar pull-out, broken ties	Extensive cracking of infills, falling bricks, out-of-plane bulging	Most shear walls have exceeded yield, some reach ultimate capacity, boundary element distress seen.
90		Short column failure	Main re-bar may buckle or elements fail in shear	Partial failure of many infills, heavier damage in frame members, some fail in shear	Re-bar buckling, extensive cracking & through-wall cracks. Shear failure of some frame members
100	**Partial Collapse**	Collapse of a few columns, a building wing or single upper floor	Shear failure of many columns or impending soft-storey failure	Beams &/or columns fail in shear causing partial collapse. Near total infill failure	Coupling beams shattered and some shear walls fail
	Collapse	Complete or impending building collapse	Complete or isoft-storey failure at ground floor	Complete or impending building collapse	Complete or impending building collapse

Apart from these two researchers many other research teams (HRC, HAZUS99, VISION2000, FEMA273, EMS98, MSK, AIJ, ATC-13, ATC-20, EPPO(Gr.)) have already

proposed individual limit states, which are given in Table 7.1 under a unique damage index (DI_{HRC}) for comparative reasons. The effectiveness of a damage index which is based on its linear and simple relationship to the damage was presented by Rossetto and Elnashai (2003) compared to complicated ones involving other parameters like cost. That means that performance states defined by economic criteria (e.g. Algermissen et al 1978, Miyakoshi et al. 1997) can preclude the curve application to locations other than those considered. There is no simple relationship that can be drawn between damage and monetary loss, and the latter definition of performance may introduce a time dependency if the limit state values used are linked to the financial situation at the location and the time of the curve derivation (Rossetto & Elnasai, 2003).

Table 7.2 An approximate equivalence between existing damage scales and the HRC-Scale (Rossetto & Elnasai, 2003).

DI_{HRC}	HRC	HAZUS 99	VISION 2000	FEMA 273	EMS98	MSK	AIJ	ATC-13	ATC-20	EPPO (Gr.)
0	**None**	No damage limit state								
10	**Slight**	Slight damage	Fully operational	Immediate occupancy	Grade 1	D1	Slight	Slight	Green Tag	Green Tag
20	**Light**				Grade 2	D2	Minor	Light		
30				Damage control						
40			Operational					Moderate		
50					Grade 3	D3	Moderate		Yellow Tag	Yellow Tag
60	**Moderate**	Moderate damage		Life safe						
70			Life safe	Limited safety				Heavy		
80	**Extensive**	Extensive damage			Grade 4	D4	Severe			
90			Near collapse	Collapse prevention				Major	Red Tag	Red Tag
100	**Partial collapse**		Partial collapse				Collapse			
	Collapse	Collapse limit state								

The maximum interstorey drift ratio was found to provide the optimum parameter for describing the global damage observed in reinforced concrete buildings in reviews of existing local and global energy, force and deformation-based structural response parameters. This is due to its ability to detect both soft-storey and ductile modes of failure, and due to its simplicity of evaluation from experimental tests. It is a fact that the roof drift is a useful measure of the overall structural deformation, but it does not reflect the

distribution of damage along the height of the structure, and it does not identify weak elements or soft stories. Instead, interstorey drift can be directly correlated with damage at a given story level. For existing non-ductile structures and poorly designed frames such as those with soft story, the maximum interstorey drift of the soft story may indicate collapse while the roof drift may still correspond to a lower damage level (see Chapter 2 of the dissertation).

Damage to elements and components of the structural system should be tabulated as a function of the lateral displacement of the building, quantified by the average interstorey drift ratio (i.e., roof displacement divided by building height). Of course, individual stories of multi-story building would not all be expected to have the same drift, nor would interstorey drift be the same at all locations on a given floor if there is diaphragm flexibility or a rotational component to the mode shape. However, average interstorey drift provides a convenient measure of building response that may be compared against default values of average interstorey drift that define damage states for generic building types of HAZUS (2003), (see Table 7.1 and 7.2). From a range of different limit states, it is obvious that there is a need for determining each limit states through either analysis or experiment. Without such calibration, the fragility limit states may not accurately reflect the performance of a building and may lead to incorrect decisions (Rossetto & Elnasai, 2003).

7.4.2. Calculation of Damage-State Probability

The fragility curves distribute damage among different damage states (for example slight, moderate, extensive and complete recommendation of HAZUS, 2003). For any given value of the response, discrete damage-state probabilities are calculated as the difference of the cumulative probabilities of reaching, or exceeding, successive damage states. The probabilities of a building reaching or exceeding the various damage levels at a given response level sum to 100%.

Fragility curves define boundaries between damage limit states. Therefore, the median value of the limit state of interest defines the threshold of damage, and this state of damage is assumed to exist up to next state of damage. This description is illustrated in Figures 7.4, which includes an example of the fragility curves for slight, moderate, extensive and complete structural damage. In this illustration, a region between the green and the yellow curves illustrates the probability-response space associated with slight damage. The boundary on the left of this region is defined by the fragility curve for slight (or greater) structural damage, and the boundary on the right is defined by the fragility curve for moderate (or greater) damage. The probability of slight damage at a given level of demand

is calculated as the difference of the probability of slight (or greater) damage less the probability of moderate (or greater) damage – a probability of 0.50 at 3.0 m/sec² of peak ground acceleration in the example shown in Figure 7.4.

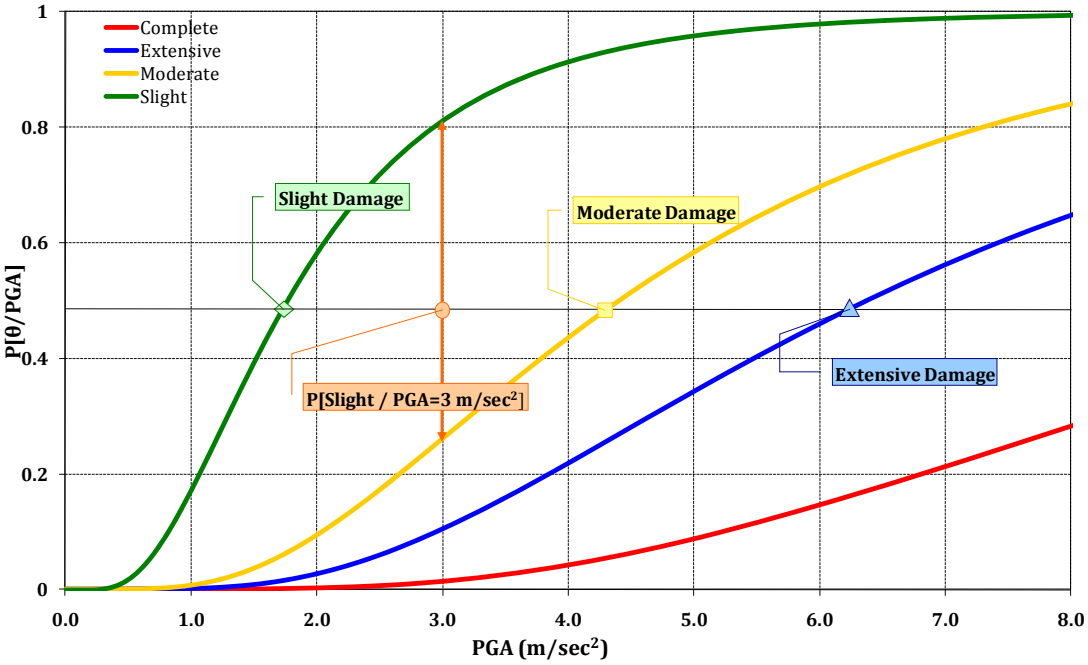

Figure 7.4. Example of fragility curves - Calculation of damage-state probability

7.4.3. Factors influence the shape of fragility curves

Fragility curves are sensitive to several parameters concerning their shape. These parameters can be the damage models and their thresholds are considered (both as random and multidimensional), the analysis methods, input ground motion, structural modelling and the structural parameters (damping ratio, stiffness etc.), (Cimellaro et al., 2006). These parameters have been seen to cause significant discrepancies in the derivation of empirical fragility curves by different authorities for the same location, even in cases where the same structure and seismicity are considered, (Priestley, 1998).

It is widely known that the development of the fragility curves for a class of buildings or for an individual building is always related to the choice of the structural model, and the structural parameters involved in the modelling of the structure which are inherently uncertain. The uncertainty is both in the mechanical properties, such as yield strength and stiffness, and geometric properties, such the modelling of the beam-column connections and others. The damage models shown in Table 7.1, influence the form of a fragility curve, according to the structural model and the seismic response system. The structural model is related to the height of a building that can change considerably the shape of a fragility curve. The difference in curve shape for building to building can be explained by the fact that

structures of different heights tend to be built according to different building regulations and hence exhibit markedly different seismic resistance. The different building regulations established by the seismic codes become an additional influential factor affecting the shape of the fragility curves. In buildings which are designed according to the pre-seismic codes (HAZUS, 2003), the shape of the fragility curves is affected by the absence of capacity design in structures, which results in their failure via predominantly soft storey modes under earthquake excitation. Failures of this type are associated with a rapid transition between low-levels of damage and the collapse limit state that is reflected in the vulnerability plot by a closer proximity of the curves.

The fragility curves are also affected by the lognormal standard deviation value (β) referring to its slope. The smaller the value of β is, the less variable the damage state, and the steeper the fragility curve. The larger the value of beta (β) is, the more variable the damage state, and the better the fragility curve. Beta values usually ranging from 0.4 to 1.2 (Rossetto & Elnasai, 2003).

7.5. Artificial neural networks

ANN are biologically inspired, since they are composed by elements that perform in a manner analogous to the elementary functions of a biological neuron. These elements are known as artificial neurons. They are composed of a large number of fully or partially interconnected processing elements (called neurons) working in union to solve specific problems. A typical fully connected ANN is shown in Figure 7.5. As in biological systems, learning involves adjustments to the synaptic connections that exist between the neurons. ANNs, with their remarkable ability to derive meaning from complicated or imprecise data, can be used to extract patterns and detect trends that are too complex to be noticed by either humans or conventional computational techniques. ANN are organized in a way that is related to the anatomy of the brain and they exhibit a surprising number of the brain's characteristics such as: learning from experience, generalizing from previous examples and abstracting essential characteristics from sets of inputs containing irrelevant data.

An ANN is configured for a specific application, such as pattern recognition or data classification, through a learning process. ANNs, like human beings, learn by example. A trained ANN provides a rapid mapping of a given input into the desired output quantities, thereby enhancing the efficiency of the analysis process. This major advantage of a trained ANN over a conventional procedure, under the provision that the predicted results fall within acceptable tolerances, is that it leads to results that can be produced in a few clock

cycles, representing orders of magnitude less computational effort than the conventional procedure (Papadrakakis et al., 1998).

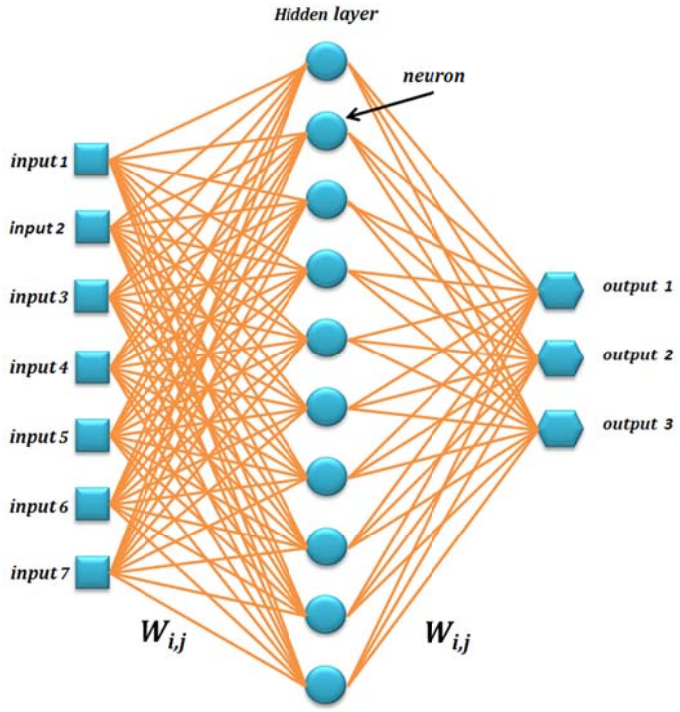

Figure 7.5. A typical artificial neural network

The ANN learning process progresses iteratively, through a number of epochs. On each epoch the training patterns are submitted in turn to the network and target and actual outputs are compared and the error is calculated. This error, together with the error surface gradient, is used to adjust the weights, and then the process is repeated. Training stops when a given number of epochs elapses, or when the error reaches an acceptable level, or when the error ceases to decrease (user-defined convergence criteria). The ANN training comprises the following tasks: (i) select the proper training set, (ii) find the suitable network architecture and (iii) determine the appropriate values of characteristic parameters; two user defined parameters that affects the learning procedure.

A feed-forward NN attempts to create a desired mapping between the inputs and the targets of a training set. The training set is composed of *m* input-target pairs $\mathbf{D}=[\mathbf{x}^m, \mathbf{t}^m]$. A Neural Network architecture A consists of a specific number of layers, a number of units in each layer and a type of activation function. The use of hidden layers and nonlinear activation functions enhance the ability of the ANN to "learn" the complicated relationship between a set of input and a set of output data. If a set of weight parameters $\mathbf{w}$ is assigned to the connections of the network, a mapping $\mathbf{y}(\mathbf{x}^m; \mathbf{w}, A)$ is defined between the input vector

$\mathbf{x}^m$ and the output vector $\mathbf{y}$. The quality of this mapping is measured using the following error function:

$$E_D(\mathbf{D}|\mathbf{w},A) = \sum_m \frac{1}{2}\left(\mathbf{y}(\mathbf{x}^m;\mathbf{w},A) - \mathbf{t}^m\right)^2 \tag{7.8}$$

A learning algorithm tries to determine the weight parameters $\mathbf{w}$ in order to minimize the error function E_D. Iterative minimization algorithms are therefore used to obtain the optimum values of the weight parameters $\mathbf{w}$. For the solution of the minimization problem, an operator O is applied, resulting to the following iterative formula:

$$\mathbf{w}^{(t+1)} = O(\mathbf{w}^{(t)}) = \mathbf{w}^{(t)} + \Delta\mathbf{w}^{(t)} \tag{7.9}$$

Most of the numerical minimization methods are based on the above expression, while to initiate the algorithm a starting vector of weight parameters $\mathbf{w}^{(0)}$ is necessary. The initial weight parameters usually are selected randomly. The changing part of the algorithm $\Delta\mathbf{w}^{(t)}$ can be further decomposed in:

$$\Delta\mathbf{w}^{(t)} = a_t \cdot \mathbf{d}^{(t)} + \eta \cdot \Delta\mathbf{w}^{(t-1)} \tag{7.10}$$

where $\mathbf{d}^{(t)}$ specifies the direction of search and a_t is the corresponding step size while η is the momentum term defined in [0,1).

7.5.1. Regularization

In the error function E_D various modifications have been applied, like the addition of the momentum term and the inclusion of noise in the learning process. In this dissertation an extra regularizing term $E_W(w)$ is added to the E_D, which penalizes the large values of the weights in order to achieve a smoother mapping:

$$E_W(\mathbf{w},A) = \sum_i \sum_j \frac{1}{2} w_{ij}^2 \tag{7.11}$$

the E_W is called weight energy term, and the error function to be minimized becomes:

$$E = \alpha E_W(\mathbf{w},A) + \beta E_D(D|\mathbf{w},A) \tag{7.12}$$

The constant α is called regularizing constant and should not be confused with the momentum term. The two constant α and β are determined using the following two rules (MacKay, 1992):

$$\begin{aligned} 2\alpha E_W &= \mu \\ 2\beta E_D &= N - \mu \end{aligned} \tag{7.13}$$

with

$$\mu = \sum_{i}^{k} \frac{\lambda_i}{\lambda_i + i} \tag{7.14}$$

where λ_i are the eigenvalues of the quadratic form βE_D, N is the number of output nodes times the number of the training pairs and k is the total number of the weight parameters.

7.5.2. Learning Algorithms

Learning algorithms are classified into local or global algorithms. Global algorithms make use of the knowledge about the state of the entire network, such as the direction of the overall weight update vector. In the widely used back-propagation usually global learning algorithms, like the gradient descent algorithm are used. In contrast, local adaptation strategies are based on specific information of the weight values such as the temporal behaviour of the partial derivative of the weights. The local approach is more closely related to the NN concept of distributed processing in which computations can be made independent to each other. Furthermore, it appears that for many applications local strategies achieve faster and reliable prediction than global techniques despite the fact that they use less information (Riedmiller, 1994). The Resilient backpropagation learning algorithm, abbreviated as Rprop (Riedmiller and Braun, 1993), is adopted in this study. Rprop is a local algorithm, based on an adaptive version of the Manhattan-learning rule that has been proved very efficient in the past (Riedmiller, 1994).

Global Adaptive Techniques

The algorithms most frequently used in the NN training are the steepest descent, the conjugate gradient and the Newton's methods with the following direction vectors:

Steepest descent method: $d^{(t)} = -\nabla E(w^{(t)})$

Conjugate gradient method: $d^{(t)} = -\nabla E(w^{(t)}) + \beta_{t-1} d^{(t-1)}$ where β_t is defined:

$$\beta_{t-1} = \nabla E_t \cdot \nabla E_t / \nabla E_{t-1} \cdot \nabla E_{t-1} \text{ Fletcher-Reeves} \tag{7.15}$$

Newton's method: $d^{(t)} = -\left[H(w^{(t)}) \right]^{-1} \nabla E(w^{(t)})$

The convergence properties of optimization algorithms for differentiable functions depend on the properties of the first and/or second derivatives of the functions to be optimized. When optimization algorithms converge slowly in their implementation for NN problems, this suggests that the corresponding derivative matrices are numerically ill-conditioned. It has been shown that these algorithms converge slowly when rank-deficiencies appear in the Jacobian matrix of the NN, making the problem numerically ill-conditioned (Lagaros and Papadrakakis, 2004).

Local Adaptive Techniques

To improve the performance of weight updating, two completely different approaches have been proposed, namely Quickprop (Fahlman, 1988) and Rprop (Riedmiller and Braun, 1993).

The Quickprop method. This method is based on a heuristic learning algorithm for a multi-layer perceptron, developed by Fahlman (1988), which is partially based on the Newton's method. Quickprop is one of most frequently used adaptive learning paradigms. The weight updates are based on estimates of the position of the minimum for each weight, obtained by solving the following equation for the two following partial derivatives:

$$\frac{\partial E_{t-1}}{\partial w_{ij}} \tag{7.16a}$$

and

$$\frac{\partial E_{t}}{\partial w_{ij}} \tag{7.16b}$$

and the weight update is implemented as follows:

$$\Delta w_{ij}^{(t)} = \frac{\dfrac{\partial E_t}{\partial w_{ij}}}{\dfrac{\partial E_{t-1}}{\partial w_{ij}} - \dfrac{\partial E_t}{\partial w_{ij}}} \Delta w_{ij}^{(t-1)} \tag{7.17}$$

The learning time can be remarkably improved compared to the global adaptive techniques.

The Rprop method. Another heuristic learning algorithm with locally adaptive learning rates based on an adaptive version of the Manhattan-learning rule and developed by Riedmiller and Braun (1993) is the **R**esilient back**prop**agation abbreviated as **Rprop**. The weight updates can be written:

$$\Delta w_{ij}^{(t)} = -\eta_{ij}^{(t)} \cdot \operatorname{sgn}\left(\frac{\partial E_t}{\partial w_{ij}} \right) \tag{7.18}$$

where

$$\eta_{ij}^{(t)} = \begin{cases} \min(\alpha \cdot \eta_{ij}^{(t-1)}, \eta_{max}), \text{ if } \dfrac{\partial E_t}{\partial w_{ij}} \cdot \dfrac{\partial E_{t-1}}{\partial w_{ij}} > 0 \\ \max(b \cdot \eta_{ij}^{(t-1)}, \eta_{min}), \text{ if } \dfrac{\partial E_t}{\partial w_{ij}} \cdot \dfrac{\partial E_{t-1}}{\partial w_{ij}} < 0 \\ \eta_{ij}^{(t-1)}, \text{otherwise} \end{cases} \tag{7.19}$$

where α=1.2, b= 0.5, η_{max}=50 and η_{min}=0.1 (Riedmiller, 1994). The learning rates are

bounded by upper and lower limits in order to avoid oscillations and arithmetic underflow. It is interesting to note that, in contrast to other algorithms, Rprop employs information about the sign and not the magnitude of the gradient components. In the present investigation a fully connected network with two hidden layer is used. The ANN training has been performed using the **Rprop** algorithm.

7.6. Calculating the Probabilities - Solving the Reliability Analysis Problem

As it was mentioned earlier in Section 7.3, the advancements in structural reliability theory during the last twenty years and the attainment of more accurate quantification of the uncertainties associated with structural loads and resistances have stimulated the interest in the probabilistic treatment of structural systems (Schuëller, 2006). The reliability of a structure or its probability of failure is an important factor in the design procedure since it investigates the probability of the structure to successfully accomplish its design requirements. Reliability analysis leads to safety measures that a design engineer has to take into account due to the aforementioned uncertainties. Although from a theoretical point of view the field has reached a stage where the developed methodologies are becoming widespread, from a computational point of view serious obstacles have been encountered in practical implementations. FORM and SORM, that have been developed to perform structural reliability, although they lead to elegant formulations, they require prior knowledge of the means and variances of the component random variables and the definition of a differentiable limit-state function. On the other hand the MCS method is not restricted by the form and the knowledge of the limit-state function but is characterized by the high computational cost.

7.6.1. Monte Carlo simulation

The MCS method is applied in stochastic mechanics when an analytical expression of the limit-state function is not attainable. This is mainly the case in problems of complex nature with a large number of random variables, where all other stochastic analysis methods are not applicable. In structural stochastic analysis problems, the probability of exceedance of the limit state (as a simplification of Eq. (7.1)) can be written as:

$$p_{viol} = \int_{g(\boldsymbol{x})\geq 0} f_x(\boldsymbol{x}) d\boldsymbol{x} \tag{7.20}$$

where $f_x(\boldsymbol{x})$ denotes the joint probability density function of the random variables, the limit-state function $g(\boldsymbol{x})<0$ defines the safe region and $\boldsymbol{x}$ is the vector of the m random variables.

Considering that MCS is based on the theory of large numbers (N_∞) an unbiased estimator of the probability of violation is given by:

$$p_{viol} = \frac{1}{N_\infty} \sum_{j=1}^{N_\infty} I(\boldsymbol{x}_j) \tag{7.21}$$

where $\boldsymbol{x}_j$ is the j-th vector of the random structural parameters, and $I(\boldsymbol{x}_j)$ is an indicator for successful and unsuccessful simulations defined as:

$$I(\boldsymbol{x}_j) = \begin{cases} 1 & \text{if } g(\boldsymbol{x}_j) \geq 0 \\ 0 & \text{if } g(\boldsymbol{x}_j) < 0 \end{cases} \tag{7.22}$$

In order to estimate p_{viol} an adequate number of N_{sim} independent random samples is produced using a specific, uniform probability density function of the vector $\boldsymbol{x}_j$. The value of the violation function is computed for each random sample $\boldsymbol{x}_j$ and the Monte Carlo estimation of p_{viol} is given in terms of sample mean by:

$$p_{viol} \cong \frac{\mathrm{N_H}}{\mathrm{N_{sim}}} \tag{7.23}$$

where N_H is the number of successful simulations and N_{sim} the total number of simulations.

The basic MCS is simple to use and has the capability of handling practically every possible case regardless of its complexity. However, for typical structural reliability problems the computational effort involved becomes excessive due to the enormous sample size required. To reduce the computational effort more elaborate simulation methods, called variance reduction techniques, have been developed, their efficiency though is limited for larger probability values. Moreover, despite the improvements achieved on the efficiency of computational methods for treating structural analysis problems of large scale structures, they still require disproportional computational effort for reliability analysis of realistic problems. This is the reason why very few successful numerical investigations are known in estimating the probability of failure and are mainly restricted to simple elastic frames and trusses (Jiang et al., 2007).

In a previous work (Papadrakakis & Lagaros, 2002) two methodologies have been proposed where neural networks have been incorporated into a reliability problem or a RBO problem in order to reduce the computational cost of MCS. Both methodologies take advantage of the global approximation capabilities of the neural networks. The first one exploits the global approximation capabilities over the design variables space while the second operates on the space of the random variables. In the first methodology the NN is trained once outside the RBO phase, while in the second one a new NN is trained for every new candidate design inside the RBO procedure. As it can be seen from Figure 7.6(a), three

steps are required for the first implementation. The first step corresponds to the construction of the training set, where N design vectors are generated using the LHS technique (Olson et al., 2003) and their feasibility with respect to both deterministic and probabilistic constraints is evaluated. The training phase of the ANN is performed in step 2. This phase consists of the selection of a suitable NN architecture and the training/testing procedures. The trained NN is used to predict the feasibility of new design vectors both in terms of deterministic and probabilistic constraint checks. The RBO procedure is performed using a metaheuristic optimization algorithm in the last step of the methodology where the trained NN is used to assess the feasibility and the quality of every new candidate design selected by the metaheuristics algorithm (like those described in Chapter 3).

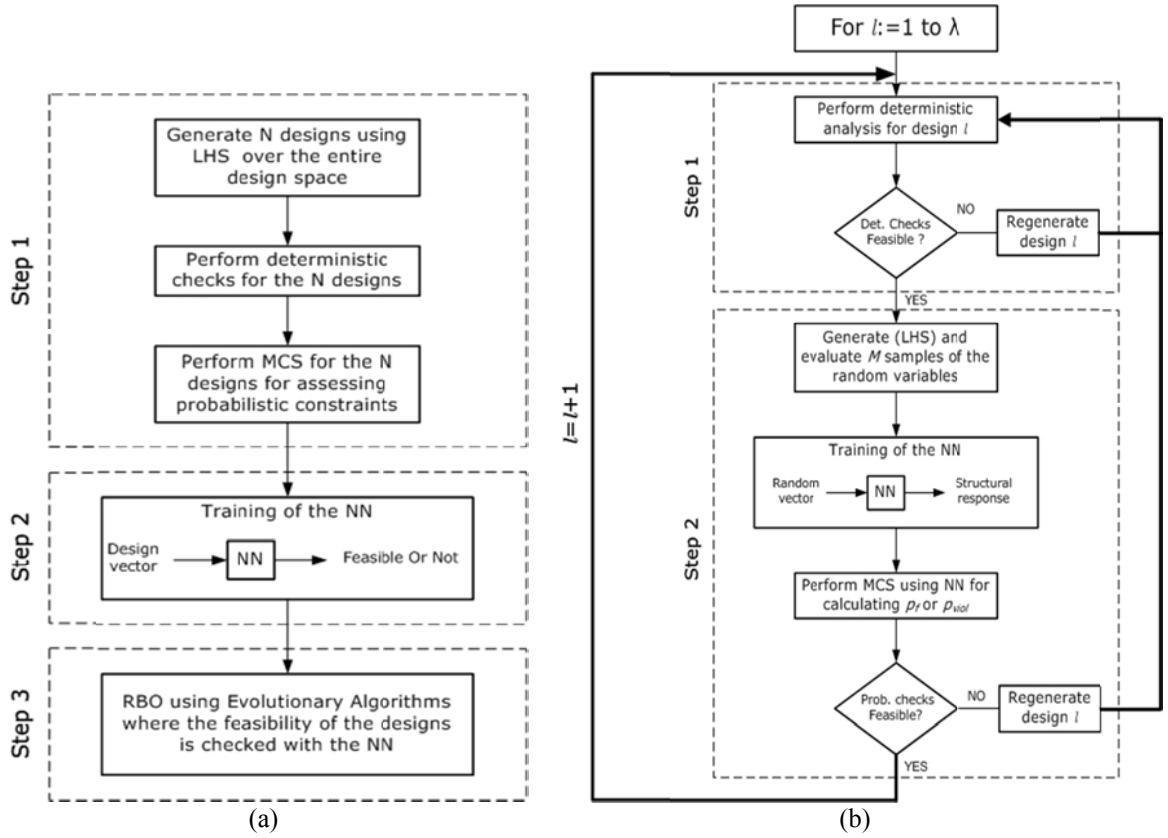

Figure 7.6. MCS-NN - (a) Methodology 1, (b) Methodology 2.

In the second methodology, shown schematically in the flowchart of Figure 7.6(b), for every new candidate design inside the optimization procedure, a new NN is trained in order to replace the analyses required during the MCS. Figure 7.6(b) describes the procedure for assessing the λ offsprings of an optimization cycle (generation) of the metaheuristic algorithm. As soon as the NN is trained over a sample of M random vectors generated using LHS, the trained NN is applied to predict the structural performance for every new vector of random variables encountered during the MCS. The second methodology has been proved more efficient (Papadrakakis & Lagaros, 2002) in terms of robustness and computational

effort. Special care has been taken in this implementation to alleviate this extrapolation drawback of NN by generating the training sample using the Latin hypercube sampling method in the range of $\mu_i \pm 6\ \sigma_i$ for, where μ_i and σ_i are the mean value and standard deviation of the i-th random variable.

7.6.2. First-Order Reliability method

In the general case of a nonlinear limit state function the main objective of the FORM is to calculate the reliability index *β*. The Hasofer-Lind reliability index *β* (Der Kureghian, 2005) is calculated by a process of minimization, and the probability of violation is approximated by:

$$p_{viol} = \Phi(-\beta) \tag{7.24}$$

where Φ is the standard normal cumulative distribution function. This equation is exact when the failure criterion is linear and all random variables have normal distributions. Given a vector of basic variables $\mathbf{x}$, a failure surface $\partial\omega$ on which the failure criterion $g(\mathbf{x})=0$ is satisfied and a safe region denoted by $g(\mathbf{x})>0$, the vector of the reduced variables $\mathbf{z}$ is defined as follows:

$$\mathbf{z} \equiv \mathbf{S}_x^{-1} \cdot (\mathbf{x} - \boldsymbol{\mu}_x) \tag{7.25}$$

where $\mathbf{S}_x$, is a diagonal matrix of the standard deviations and $\boldsymbol{\mu}_x$ is the vector of mean values. Then the Hasofer-Lind reliability index β is defined as:

$$\beta \equiv \min_{z \in \partial\omega} \sqrt{\mathbf{z}^T \mathbf{z}} \tag{7.26}$$

The point on the failure surface $g(\mathbf{x})=0$, where its transformation to the $\mathbf{z}$ space satisfies equation (7.25), is called *design* or *most probable point* and will be denoted as $\mathbf{z}_D$. The design point $\mathbf{z}_D$ is located on the limit-state surface, $g(\mathbf{x})=0$ and has minimum distance from the origin in the standard normal space. For the application of either first or second-order methods to complex structural models it is necessary to have an explicit expression or an approximation of either the entire limit-state function $g(\mathbf{x})$ or of its limit-state surface $g(\mathbf{x})=0$ in the space of the random variables $\mathbf{x}$. This is because these methods require not only knowledge of the function but also of its gradient in the vicinity of its limit-state surface. In the case of unknown expression, the limit-state function is usually approximated by the response surface method.

The Response Surface (RS) method

The RS method was originally proposed by Box (1954) as a statistical tool, to find the

operating conditions of a chemical process at which some response was optimized. In order to reduce the computational effort while maintaining an acceptable accuracy, two important issues should be considered when applying the RS method to the failure probability: (i) The definition of experimental points for defining the approximation of the limit-state function, (ii) The analytical expression of the RS function (Rajashekhar, 1993). Usually, a quadratic RS function is assumed:

$$\bar{g}(\mathbf{x}) = a + \sum_{i=1}^{m} b_i x_i + \sum_{i=1}^{m} c_i x_i^2 \tag{7.27}$$

defined in an m-dimensional random variable space where the constants a, b_i and c_i are determined by evaluating $g(\mathbf{x})$ at certain specified experimental points, while x_i, i=1, …,m are the random variables. Higher order functions are not generally used for conceptual as well as for computational reasons.

Bucher and Bourgund (1990) proposed an interpolation scheme for the solution of structural reliability problems, where the quadratic RS function of Eq. (7.27) is defined with $2m+1$ experimental points. It was suggested the experimental points x_i, to be taken as $x_i = \mu_i \pm f\,\sigma_i$, where μ_i and σ_i are the mean value and standard deviation of the i-th random variable and f is an arbitrary factor taken equal to 3. Figures 7.7(a) and 7.7(b) depict the sampling method for defining the $2m+1$ experimental points where $x_{i,low} = \mu_i - 6\,\sigma_i$ and $x_{i,up} = \mu_i + 6\,\sigma_i$. In order to avoid the undesirable case of Figure 7.7(a), where unrealistic values of the random variables are generated (i.e. a negative value of the modulus of elasticity), a correction of the experimental points is performed by moving all trial points to an acceptable region as shown in Figure 7.7(b). It was later shown (Rajashekhar, 1993, Guan & Melchers, 2001) that using a constant value of f = 3 may not always yield good solutions, particularly when $g(\mathbf{x})$ is highly nonlinear. A better fit of the RS function was obtained by updating the centre point:

$$x_{i,M} = \mu_i + \frac{(x_{i,D} - \boldsymbol{\mu}_i)\cdot g(\boldsymbol{\mu})}{g(\boldsymbol{\mu}) - g(\mathbf{x}_D)} \tag{7.28}$$

which helps to locate the new centre point closer to the actual $g(\mathbf{x})$=0, and by decreasing the value of the parameter f in subsequent cycles of updating. Then the interpolation scheme of Eq. (7.27) is repeated using $\mathbf{x}_M$ as a new center point. A number of modifications for better estimating the RS through the generation of the experimental points have been proposed (Liu and Moses, 1994; Kim and Na, 1997; Kaymaz and McMahon, 2005; Breitung and Faravelli, 1996; Der Kiureghian and Dakessian, 1998; Rackwitz and Fiessler, 1978; Mahadevan and Shi, 2001; Gupta and Manohar, 2004; Lu et al., 2007) in order to alleviate

the shortcomings of the method.

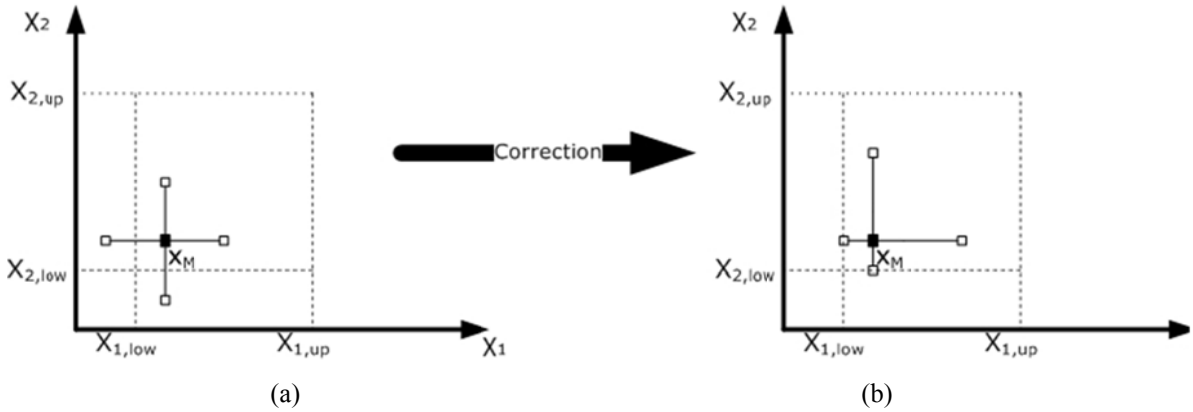

Figure 7.7. Standard sampling method (Bucher and Bourgund, 1990) (a) before and (b) after correction.

Neural network approximation of the limit-state function

In the previously mentioned implementations of the RS method, it was found that the performance of the method is significantly influence by the polynomial representation and the way the experimental points are generated. In an effort to improve the robustness of the approximation procedure the polynomial representation of RS was replaced by an approximation produced by neural networks. Based on this implementation the local approximation capabilities of the neural networks in the vicinity of the centre point $\mathbf{x}_M$ are implemented with the intention to reduce the number of the training patterns required by the global NN approximator.

Hurtado (2004) confirmed with statistical learning concepts the sensitivity of the RS approximation via polynomial expressions compared to the neural network approximations. The global capabilities of the neural network approximator were examined (Gui et al., 2004, Gomes & Awruch, 2005) in the framework of FORM for simple analytic limit-state functions or academic structural reliability problems. The local approximation capabilities of the neural networks in conjunction with reliability analysis methods are examined in a simple portal frame by Deng et al. (2005). In this methodology neural networks, denoted as FORM-NN, are implemented as a local approximator in the vicinity of the centre point $\mathbf{x}_M$ in a similar way that the RS based FORM is used. More specifically a neural network approximation of the limit-state function replaces the polynomial expression of RS. The steps of the FORM-NN methodology are given in Figure 7.8. In the first step of the proposed implementation a number of experimental points are generated through the LHS technique. Figures 7.9(a) and 7.9(b) demonstrate schematically the LHS technique with a correction procedure.

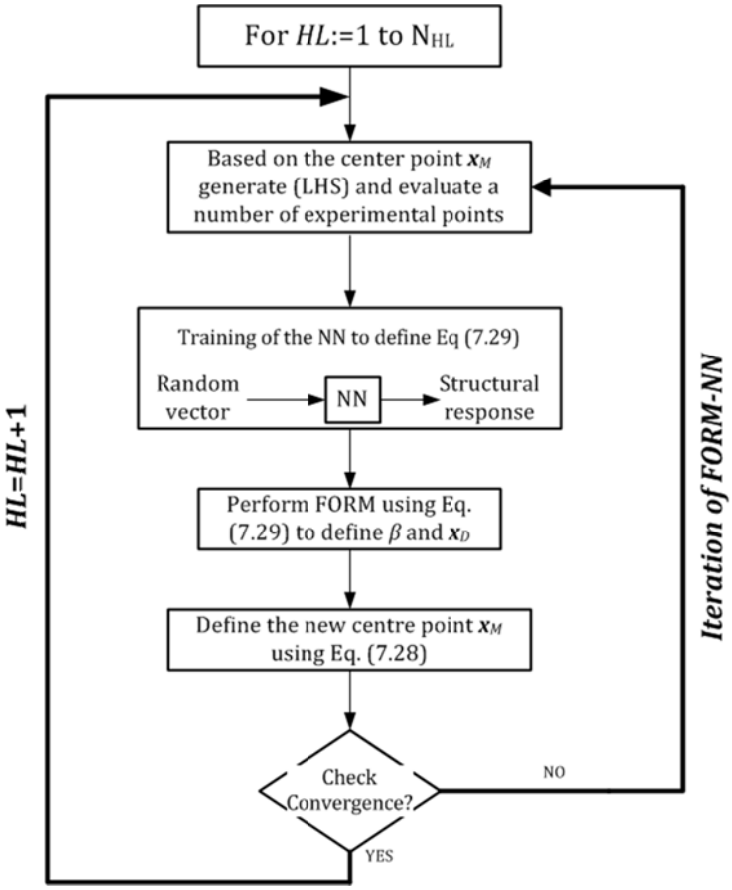

Figure 7.8. The FORM-NN methodology.

This sampling method can generate a variable number of samples well distributed over the entire range of interest. On the other hand, the number of samples generated with the standard sampling procedure (Bucher & Bourgund, 1990), (Figure 7.7) is fixed to $2m+1$ experimental points. According to LHS the distribution function of each random variable is divided into a number of stratums of equal marginal probability. These stratums are randomly selected for each random variable and randomly shuffled among different variables to define the experimental points. The main advantage of the LHS technique is that it produces well distributed samples of almost any sample size of experimental points. This characteristic feature of LHS is demonstrated in the framework of FORM-NN in the numerical studies where it is shown that a reduced number of experimental points are required for adequately defining the NN approximation. It has to be emphasized that FORM-NN does not suffer from the extrapolation drawback since any point outside the range of interest is corrected as it demonstrated in Figures 7.9.

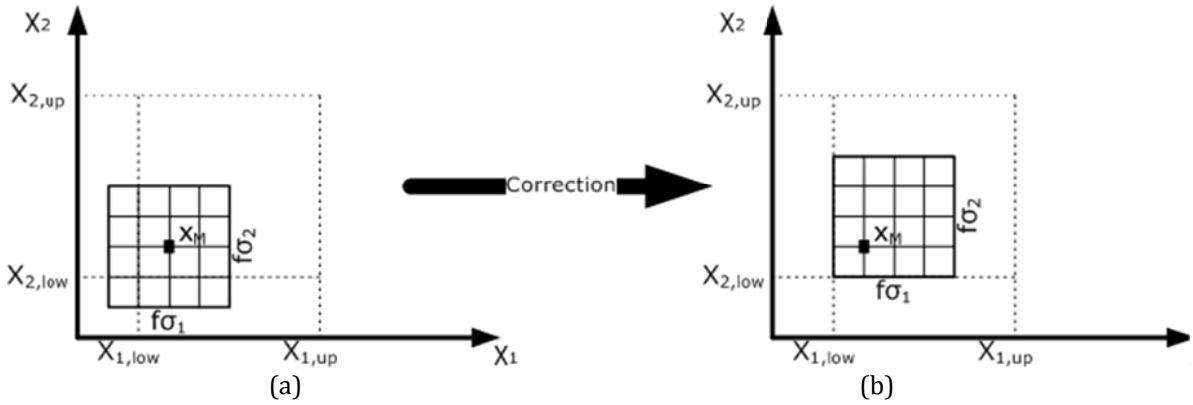

Figure 7.9. LHS technique (a) before and (b) after correction.

In the next step the experimental points are used to define the NN approximation of the limit state function according to the following equation:

$$\overline{g}(x) = f\left(\sum_{i=1}^{k} w_{H,ij} \times f\left(\sum_{i=1}^{m} w_{0,ij} \times x_k\right)\right) \tag{7.29}$$

where k is the number of the hidden layer neurons, $\mathbf{w}_H$ and $\mathbf{w}_0$ are the weight parameters of the hidden and output layers, respectively, and f(x) is the sigmoid transfer function:

$$f(y) = \frac{1}{1 + \exp(-\gamma y)} \tag{7.30}$$

The coefficient γ defines the slope of the sigmoid function. By the time the NN is trained and the weight parameters are defined, FORM is performed in order to define the reliability index β and the corresponding design point $\mathbf{x}_D$. Hereafter, the new centre point $\mathbf{x}_M$ is defined according to Eq. (7.28). If there is no convergence with respect to the reliability index β and the corresponding design point $\mathbf{x}_D$, new experimental points are generated with LHS for the new centre point $\mathbf{x}_M$, in order to define the new approximation of limit-state function (Eq. (7.29)). The advantages of the proposed NN approximation scheme are demonstrated in the numerical test section, where it is shown, that contrary to the quadratic polynomial approximation of RS, this methodology is not affected by the number of the interpolation points and the area from which the points are generated as defined by the coefficient *f*.

7.7. Vertical & Horizontal Statistics - Incremental Dynamic Analysis

As it was described in detail in Chapter 4 of this dissertation, the main objective of an IDA study is to define a curve through the relation of the intensity level with the maximum seismic response of the structural system. The intensity level and the seismic response are described through an IM and an EDP, respectively. The IDA concept is implemented with the following steps: (i) simulate the structure with a FE model capable of predicting the

nonlinear dynamic structural response; (ii) select a suit of natural records; (iii) select a proper intensity measure and an engineering demand parameter; (iv) employ an appropriate algorithm for selecting the record scaling factor in order to obtain the IDA curve by performing the least required nonlinear dynamic analyses and (v) employ a summarization technique for exploiting the results of multiple records.

The fragility analysis based on the IDA procedure, requires dynamic analyses for different intensity levels to be carried out for a sufficiently large number of ground motions in order to perform a statistical evaluation of the results. Statistical information necessary to understand and quantify the behaviour of structural systems can be presented in different formats depending upon the objective. For instance, if the issue is the loss assessment, for which it is important to evaluate the distribution, mean value and/or dispersion of a DI given the IM, the "horizontal" statistics format is considered as the most appropriate to be implemented (see Figure 7.10). However, if the issue is conceptual design or fragility analysis, where the designer wants to find the global strength required to limit the value of a DI to a certain quality, then "vertical" statistics are the most suitable (see Figure 7.10). "Vertical" statistics are also used to quantify the ground motion intensity at which a system approaches a certain limit state. The terms "horizontal" and "vertical" described above presuppose that DIs are plotted on the horizontal axis and IMs on the vertical axis. Since the work involved in this chapter is concerned with fragility analysis, the focus is on "vertical" statistics in order to calculate, via an optimization algorithm, the two parameters μ and β of Eq. (7.7) that maximize ln(L).

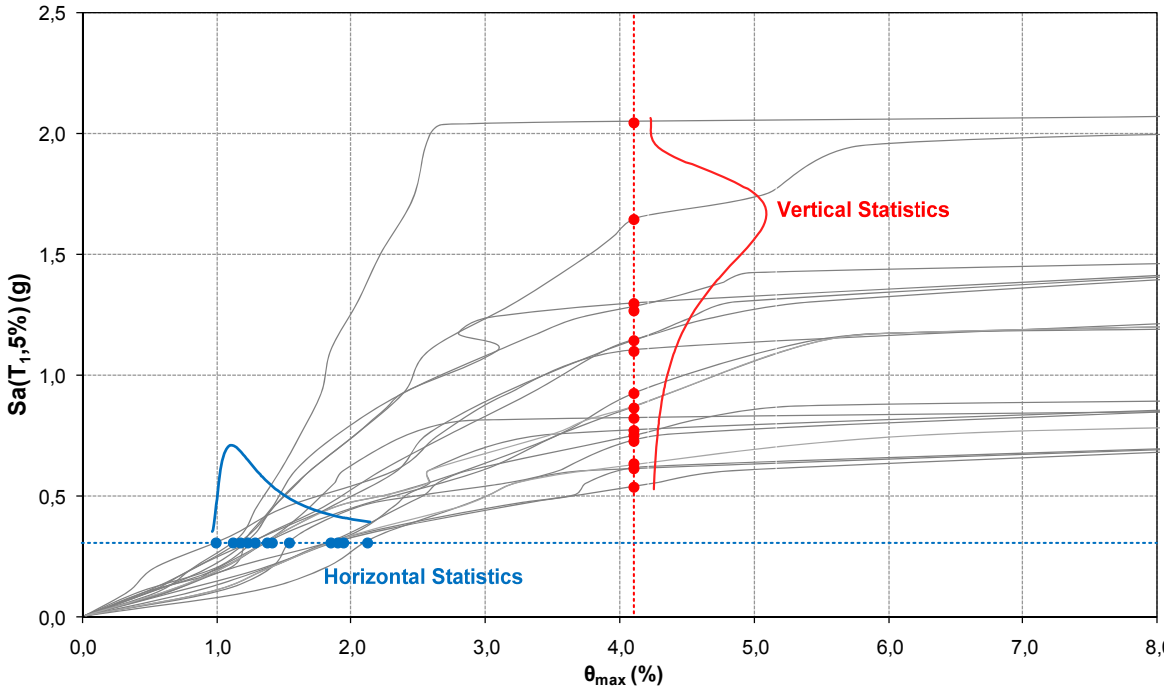

Figure 7.10. IDA curve-"vertical" and "horizontal" statistics.

7.8. Seismic demand evaluations using neural networks

The main objective of the study described in this section of this Chapter is to perform computationally efficient fragility analysis studies of 3D RC structures. In particular, the two parameters μ_k and β_k of Eq. (7.15) need to be computed for each limit state under consideration with a computational efficient manner. The quality of the fragility analysis depends on the estimation of these two parameters which is influenced by the size of the set of natural records. For this purpose a trained NN is used to obtain the level of seismic demand corresponding to a DI, expressed in terms of the $S_A(T_1,5\%)$. The DI under consideration is the maximum interstorey drift (θ_{max}). The seismic records, which represent the uncertainty in demand, are identified by the NN with the help of a vector of IMs. More specifically IMs are representative parameters for each seismic record therefore they are used as input to the NN.

7.8.1. Selection of intensity measures

Strong ground motions are extremely complicated and it is required a lot of data for their full description. The definition of a number of ground motion parameters, named intensity measures, simplifies the description of a strong ground motion and links the seismic hazard with the structural data required for the solution of earthquake engineering problems. The most significant characteristics of a ground motion from an earthquake engineering point of view are the *amplitude*, the *frequency content* and the *motion duration*. Some of the IMs are related to one or more of the three essential ground motion characteristics. The IMs that are related to the effect of more than one ground motion characteristics are considered more reliable for the description of a ground motion and are more suitable to reflect the potential damage that a ground motion can induce into a structural system.

The most commonly used *amplitude* IMs derived from an accelerogram are the peak ground acceleration (high frequency component), peak velocity (intermediate frequency component), peak displacement (low frequency component), sustained maximum acceleration and velocity and the effective design acceleration. Amplitude IMs are used for the derivation of empirical attenuation relationships used in probabilistic hazard analysis, because their generation is based on IMs' dependence, on the magnitude of the earthquake and on the site-to-source distance. *Frequency content* IMs describe through different types of spectra, the distribution of the amplitude of a ground motion among different frequencies. IMs related to frequency content are Fourier spectra and power spectra that correspond to the frequency content of the ground motion itself, and the response spectra, that correspond to the influence of the ground motion on structures with different

fundamental eigenperiods. Among this type of IMs are spectral parameters, like the predominant period, bandwidth, central frequency, shape factor, Kanai-Tajimi parameters and the ratio v_{max}/a_{max} which describes the frequency content of a ground motion. The most commonly used *duration* IM is the bracketed duration which is defined as the time between the first and the last exceedance of a threshold acceleration, usually equal to 0.05g. *Arias Intensity* (I_A), *Characteristic intensity* (I_C) and *Cumulative Absolute Velocity* (CAV) IMs reflect the amplitude, the frequency content and the duration of a strong ground motion respectively and they correlate well with structural damage. More details on the IMs used in this dissertation can be found in Chapter 5.

7.8.2. Prediction scheme

As it was mentioned previously the main objective of the IDA methodology is to define a curve described with an intensity measure and the maximum seismic response of the structural system described by means of an EDP. The objective of the proposed prediction scheme is to train a NN in order to predict the seismic demand, which is expressed in terms of the $S_A(T_1,5\%)$ for a given value of the represented by the maximum interstorey drift limit state. Thus, the NN should be able to correctly predict $S_A(T_1,5\%)$ from a triad of I_A, I_C and CAV of the ground motion record in consideration. The intensity measures for a given intensity should correlate well with the seismic demand in order to be used as input to the NN reflecting the properties of the record.

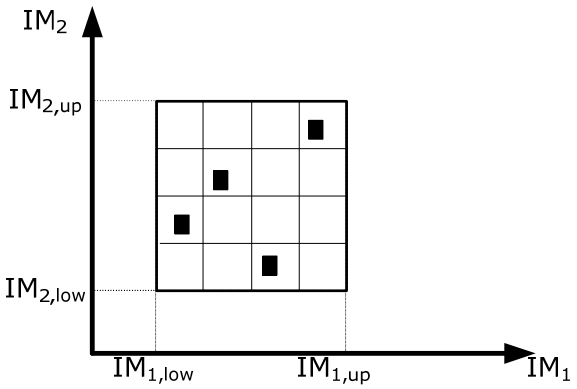

Figure 7.11. Latin hypercube sampling in the two-dimensional space.

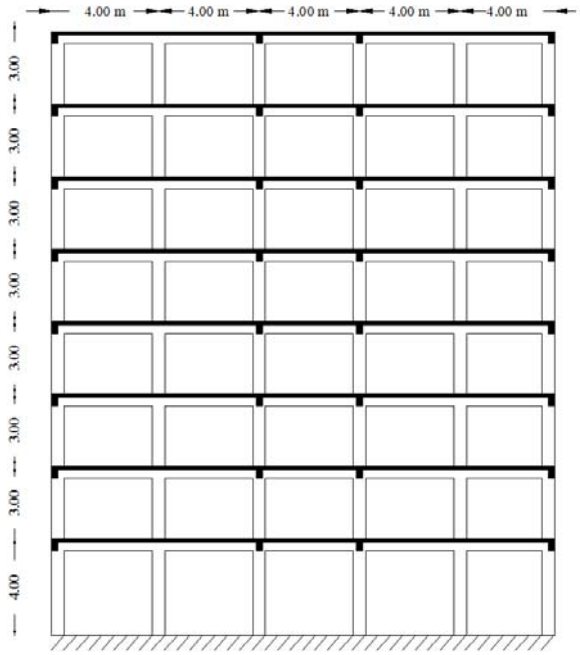

Figure 7.12. Eight storey test example-front view.

In this part of the dissertation a prediction scheme of the structural response by properly trained NN is implemented in the framework of fragility analysis of structures. The first step of the prediction scheme corresponds to the definition of the training set, where *N* vectors of IMs are generated using the LHS technique (Olson, 2003) while the structural response in the limit states considered are obtained over the set of ground motions (see Tables A.4 to A.7 in Appendix A). The *N* realizations are assessed by means of a nonlinear dynamic finite element analysis with reference to their structural performance. LHS initially was employed in an effort to reduce the required computational effort of random sampling methodologies. In the context of statistical sampling, a square grid containing sample positions is a Latin square if there is only one sample in each row and each column. Figure 7.11 depicts an example of four samples in the two-dimensional space. As soon as the training and testing procedures are performed successfully the trained NN is then able to predict the seismic demand of all limit states considered without performing any computationally demanding nonlinear dynamic finite element analyses.

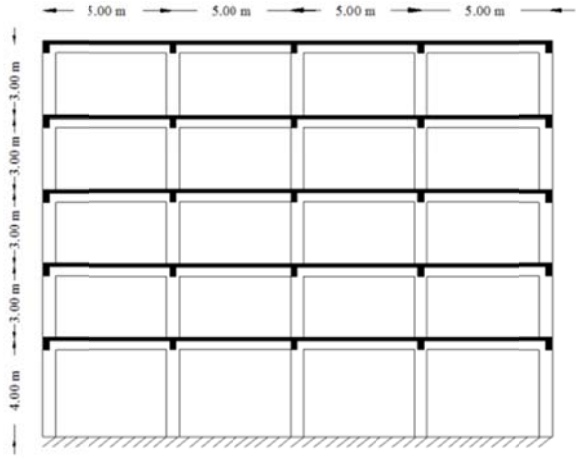

Figure 7.13. Five storey test example-front view.

Table 7.3. Eight storey test example – Cross sections of the beams and the columns.

		Storeys 1-3	Storeys 4-6	Storeys 7-8
Columns	**h1×b1**	0.80×0.60, LR: 24Ø28, TR: (4)Ø10/20cm	0.65×0.55,LR:8Ø24+4Ø26, TR: (2)Ø10/20cm	0.55×0.55, LR:8Ø18+ 4Ø22, TR: (2)Ø10/20cm
	h2×b2	0.65×0.60, LR: 26Ø28, TR: (4)Ø10/20cm	0.55×0.55, LR:8Ø24+ 12Ø28, TR: (2)Ø10/20cm	0.55×0.50, LR:6Ø20+ 12Ø28, TR: (2)Ø10/20cm
	h3×b3	0.75×0.65, LR: 28Ø28, TR: (4)Ø10/20cm	0.75×0.50, LR: 24Ø28, TR: (2)Ø10/20cm	0.50×0.50, LR:4Ø22+ 12Ø26, TR: (2)Ø10/20cm
	h4×b4	0.75×0.65, LR: 30Ø28, TR: (4)Ø10/15cm	0.55×0.60, LR: 22Ø28, TR: (2)Ø10/20cm	0.55×0.55, LR:8Ø22+ 12Ø26, TR: (2)Ø10/20cm
Beams	**hl×bl**	0.55×0.55, LR:11Ø18+ 10Ø20, TR: (2)Ø8/15cm		
	ht×bt	0.55×0.50, LR:9Ø18+ 10Ø20, TR: (2)Ø8/15cm		
$C_{IN,\ RC\ Frame}$ (10^3MU)		2.40E+02		
C_{IN} (10^3MU)		1.44E+03		

7.9. Structural models and Numerical simulation

The two multi-storey 3D RC buildings shown in Figures 7.12 and 7.13 are considered for the numerical tests performed in this study. The first test example is an eight storey RC building having symmetrical plan view, while the second one is a five storey RC building with non-symmetrical plan view. Both buildings have been designed according to Eurocodes for minimum initial cost, following an optimization strategy proposed by Mitropoulou *et al.* (2010). The cross-sections of the beams and the columns of the two test examples are hl×bl and ht×bt which correspond to the cross sectional dimensions of horizontal and vertical beams, respectively. The cross section for the eight storey test example is provided in Table

7.3 while those for the five storey in Table 7.4. Concrete of class C20/25 (characteristic cylindrical strength of 20 MPa) and steel of class S500 (characteristic yield stress of 500 MPa) are assumed. The slab thickness is equal to 15 cm for both test examples. In addition to the self weight of beams and slabs, a distributed permanent load of 2 kN/m^2 due to floor finishing-partitions and an imposed load with nominal value of 1.5 kN/m^2, are considered. More details for the two test example uses in this investigation can be found in Chapter 4.

Table 7.4. Five storey test example - Cross sections of the beams and the columns.

		Storeys 1-3	**Storeys 4-5**
Columns	**h1×b1**	0.55×0.55, LR:8Ø20+ 12Ø24, TR: (2)Ø10/20cm	0.55×0.55, LR:8Ø24+ 4Ø28, TR: (2)Ø10/20cm
	h2×b2	0.55×0.55, LR:8Ø22+ 12Ø26, TR: (2)Ø10/20cm	0.45×0.45, LR:4Ø24+ 4Ø28, TR: (2)Ø10/20cm
	h3×b3	0.50×0.50, LR:4Ø22+ 12Ø26, TR: (2)Ø10/20cm	0.35×0.55, LR:7Ø16+ 5Ø20, TR: (2)Ø10/20cm
	h4×b4	0.55×0.55, LR:8Ø18+ 4Ø22, TR: (2)Ø10/20cm	0.35×0.55, LR:8Ø18+ 5Ø20, TR: (2)Ø10/20cm
Beams	**hl×bl**	0.30×0.55, LR:3Ø20+ 4Ø14, TR: (2)Ø10/20cm	
	ht×bt	0.30×0.55, LR:6Ø20, TR: (2)Ø8/15cm	
$C_{IN,\ RC\ Frame}$ (10^3MU)		1.11E+02	
C_{IN} (10^3MU)		7.36E+02	

All structural analyses were performed using the OpenSEES platform (McKenna & Fenves, 2001). Each member is modelled with a single force-based, fibre beam-column element. This element provides a good balance between accuracy and computational cost (Fragiadakis & Papadrakakis, 2008). The modified Kent-Park model (Kent & Park, 1971) is employed for the simulation of the concrete fibres. This model was chosen because it allows for an accurate prediction of the structural demand for flexure-dominated RC members despite its relatively simple formulation. The inelastic behaviour of the reinforcing bars was simulated with the Menegotto-Pinto model (Menegotto & Pinto, 1973), while a nonlinear shear force-shear distortion (V-γ) law is adopted to account for shear failure, based on the work of Marini and Spacone (2006). More details on the material laws and modelling characteristics employed in this study can be found in Appendix B. The effect of gravity loads and second-order effects are considered through the consideration of geometric nonlinearities.

7.10. Numerical tests

As it was mentioned earlier, the numerical investigation performed in this study comprises the ANN prediction-capabilities, the development of the fragility curves, the calculation of the mean annual frequency of exceedance of the limit states and the required computing cost. For the purposed of this study 100 natural records have been used, these records are selected randomly from the lists of records given in Tables A.4 to A.7 of Appendix A. These records have been chosen from the PEER strong-motion database (PEER, 2010) according to the following features: (i) events occurred in specific area (longitude -124° to -115°, latitude 32° to 41°); (ii) moment magnitude (M) is equal to or greater than 5; (iii) epicentral distance (R) is smaller than 150 km.

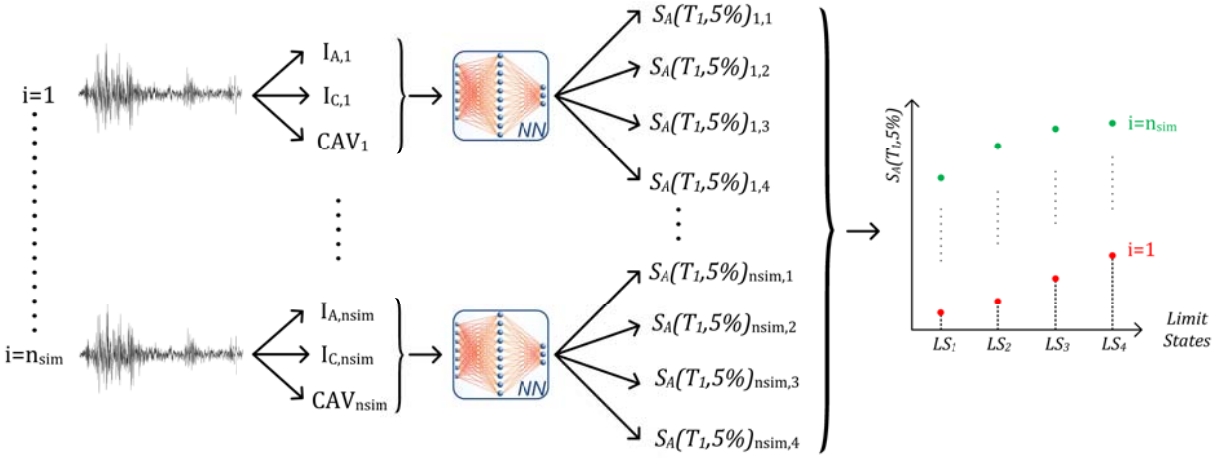

Figure 7.14. ANN-based incremental dynamic analysis.

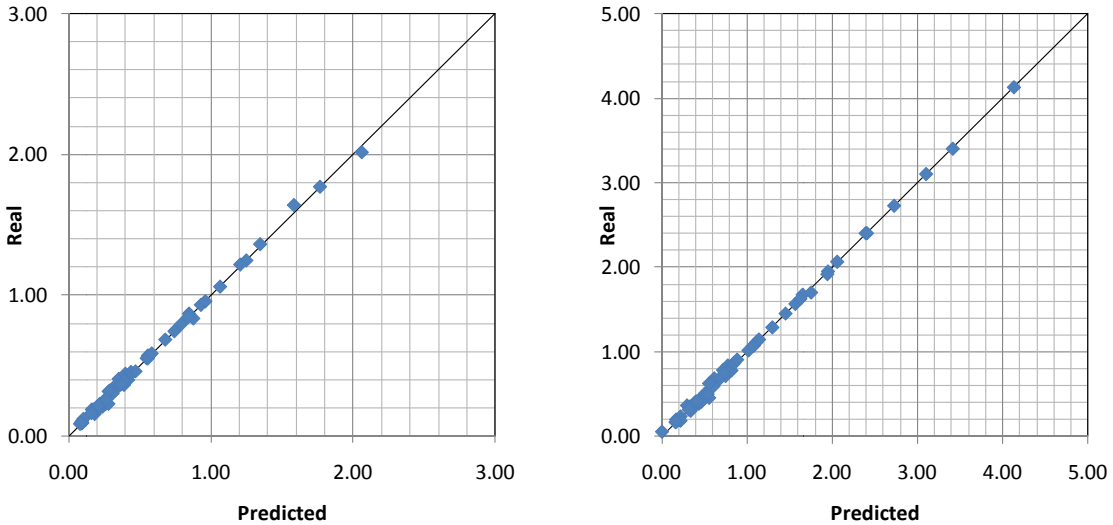

(a) (b)

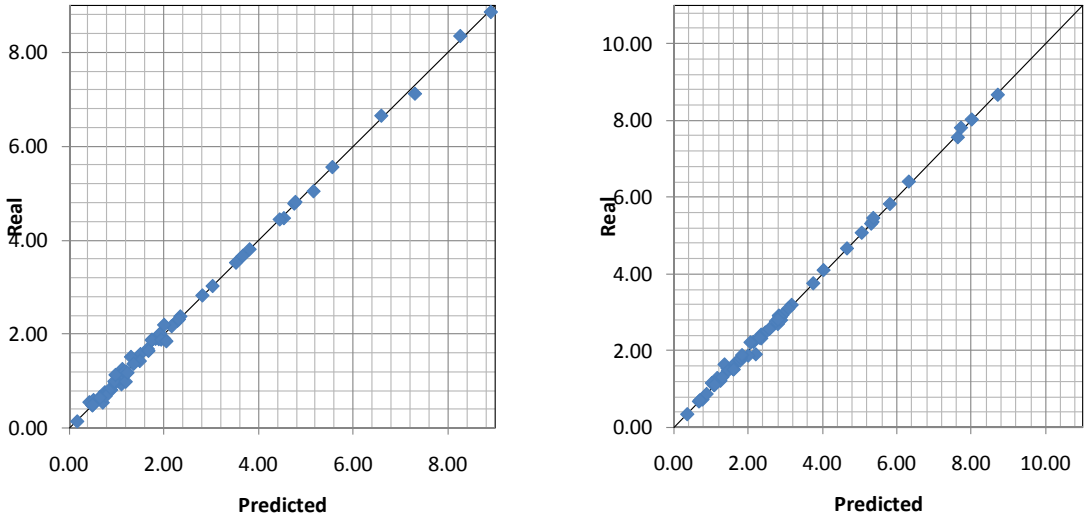

Figure 7.15. Eight storey test example-ANN prediction capability over the testing set: (a) Slight damage limit state (0.25%), (b) Moderate damage limit state (0.50%), (c) Extensive damage limit state (1.50%) and (b) Collapse limit state (4.00%).

7.10.1. ANN predictions

In the first part of this numerical investigation the prediction capabilities of the trained ANN are reported for the two test examples considered. The objective of the ANN prediction scheme is to predict the demand given the limit state value for various combinations of the three IMs that are considered more reliable for the description of the ground motion. Therefore the number of input nodes of the ANN is 3 for both test examples, while the two hidden layers contain 45 nodes each, as it was found, by a trial and error procedure, that this number of hidden nodes provides a compromise between accurate predictions and computationally efficient calculations during the training and testing procedures. The output layer has 4 nodes corresponding to the fundamental period spectral acceleration $S_A(T_1,5\%)$ for the limit state in question. Thus, a 3-45-45-4 ANN configuration is used for both test examples (Figure 7.14).

As it was mentioned in section 7.5 of this Chapter, there are typically two types of networks, namely fully and partially connected networks. In a fully connected network each unit in a layer is connected to all the units of the previous and the next layer. This type of network architecture is widely used. Alternatively, some local associativity between the units may be created or the number of connections may be reduced producing a patterned connected network. The number of neurons to be used in the hidden layers is not known in advance and usually is estimated by a trial and error approach. At the first phase of learning it is convenient to gradually increase the number of hidden units and next, after achieving the desired convergence to try to remove some of them in order to find the minimal size of the network which performs the desired task. After the selection of the suitable ANN

architecture and the training procedure, the network is then used to provide inexpensive predictions of the seismic demand given the limit state corresponding to different values of the input IMs.

The extrapolation capabilities of ANN are problematic despite the fact that special types of ANN have been proposed for this reason. This is due to the property of ANN to virtually map any function by adjusting its parameters according to the presented training data. Hence it is important to have sufficient and properly distributed, over the range of interest, training data to avoid ANN performing extrapolation instead of interpolation. This drawback is alleviated by generating the training sample using the Latin Hypercube Sampling method in the range of the bounds of the IMs, thus ANN will always predict interpolated values.

The performance of the ANN is demonstrated in Figures 7.15 and 7.16, where the ANN predicted values are plotted versus the results obtained by a full IDA. Two different training sets, of size 20 and 40 records, have been examined. It was found that both performed equally well, hence the first one was selected since it requires less computing time for preparing the training set. The sets of records have been selected using the LHS method while 40 patterns corresponding to 40 natural records have been used for testing the prediction capabilities of the trained ANN. As it can be seen in Figures 7.15 and 7.16 and 20 training patterns are adequate for training efficiently the ANN in order to predict the fundamental period spectral acceleration $S_A(T_1,5\%)$ for the four limit states under consideration.

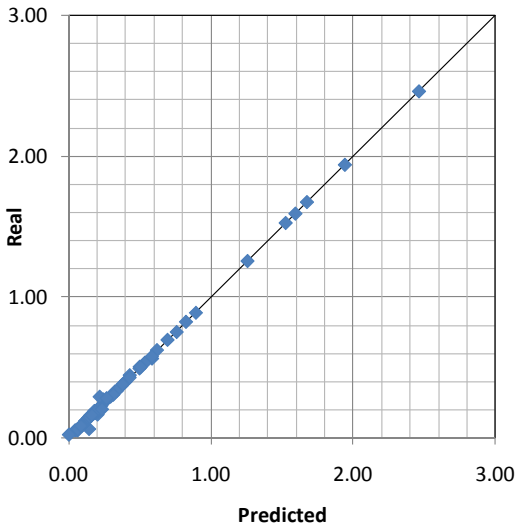

(a)

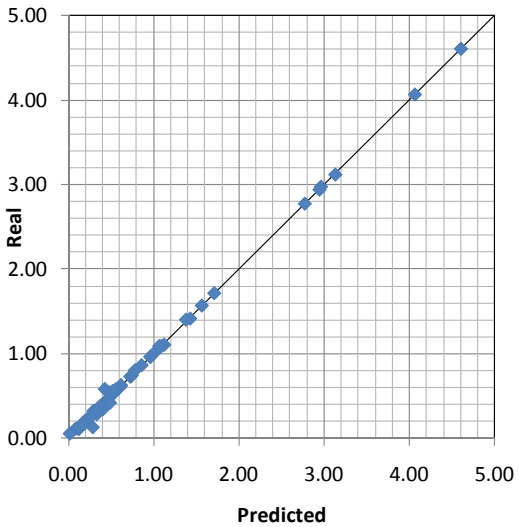

(b)

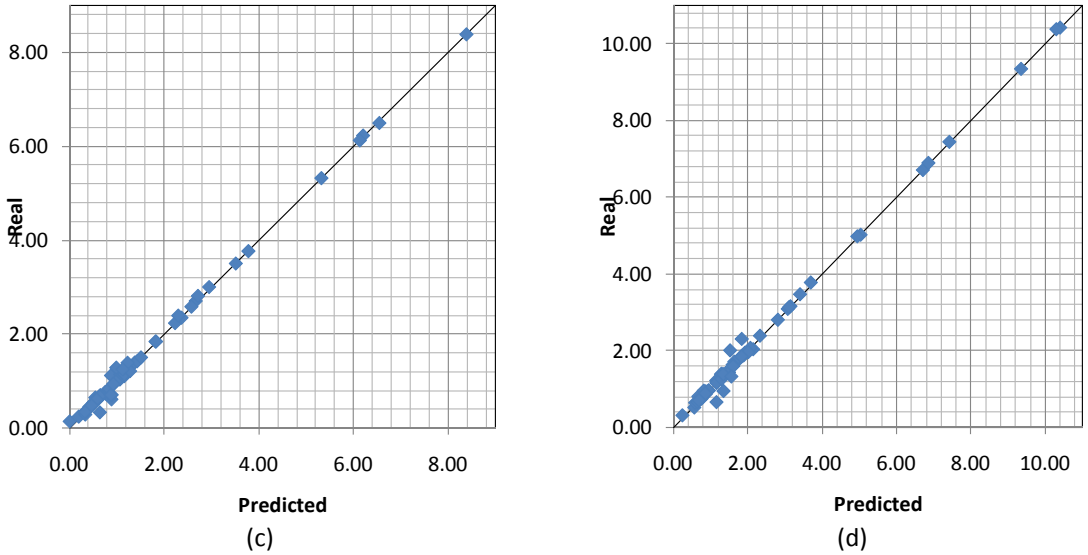

Figure 7.16. Five storey test example-ANN prediction capability over the testing set: (a) Slight damage limit state (0.30%), (b) Moderate damage limit state (0.70%), (c) Extensive damage limit state (2.00%) and (b) Collapse limit state (5.33%).

7.10.2. Fragility analysis

In the second part of this numerical investigation four limit-state fragility curves are obtained for each one of the two buildings of Figures 7.12 and 7.13. The limit states considered are defined by means of maximum interstorey drift values and cover the whole range of structural damage from serviceability, to life safety and finally to the onset of collapse. The following $\theta_{\max}$ values are chosen, according to HAZUS (2003), for each of the four limit states: 0.25%, 0.50%, 1.50% and 4.0% for the eight storey symmetric RC building while 0.30%, 0.70%, 2.00% and 5.33% for the five storey non-symmetric RC building. For each limit state the IDA and "vertical" statistics are implemented for computing the two parameters μ and β of Eq. (7.5) that maximize ln(L) by implementing the harmony search algorithm, a metaheuristic optimization algorithm (Geem et *al*., 2001), where no gradient evaluations are required. The first mode spectral acceleration $S_A(T_1,5\%)$ is used to represent the intensity of the seismic ground motion. Thus the seismic fragility curves are defined as

$$F_R = P\left[\theta_{max} \geq y_{lim} / S_A(T_1,5\%) = x\right] \tag{7.31}$$

The parameters used for the HS algorithm are based on the recommended parameters in (Mahdavi, 2007), as follows: the harmony memory size *HMS* = 100, the harmony memory consideration rate *HMCR* = 0.90, while the pitch adjusting rate *PAR* was taken equal to 0.35. A detailed description of the HS can be found in Chapter 3 of this dissertation where various metaheuristic optimization algorithms are presented. The optimization procedure is terminated when the best value of the objective function in the last 20 generations remains unchanged. "Vertical" statistics is performed for all four limit states described above. For the

purposes of the present investigation five cases have been examined for the calculation of the two parameters (μ_k , β_k , k=1,..4) : IDA_{20}, IDA_{40}, IDA_{60}, IDA_{80} and IDA_{100} , where 20 to 100 records are implemented.

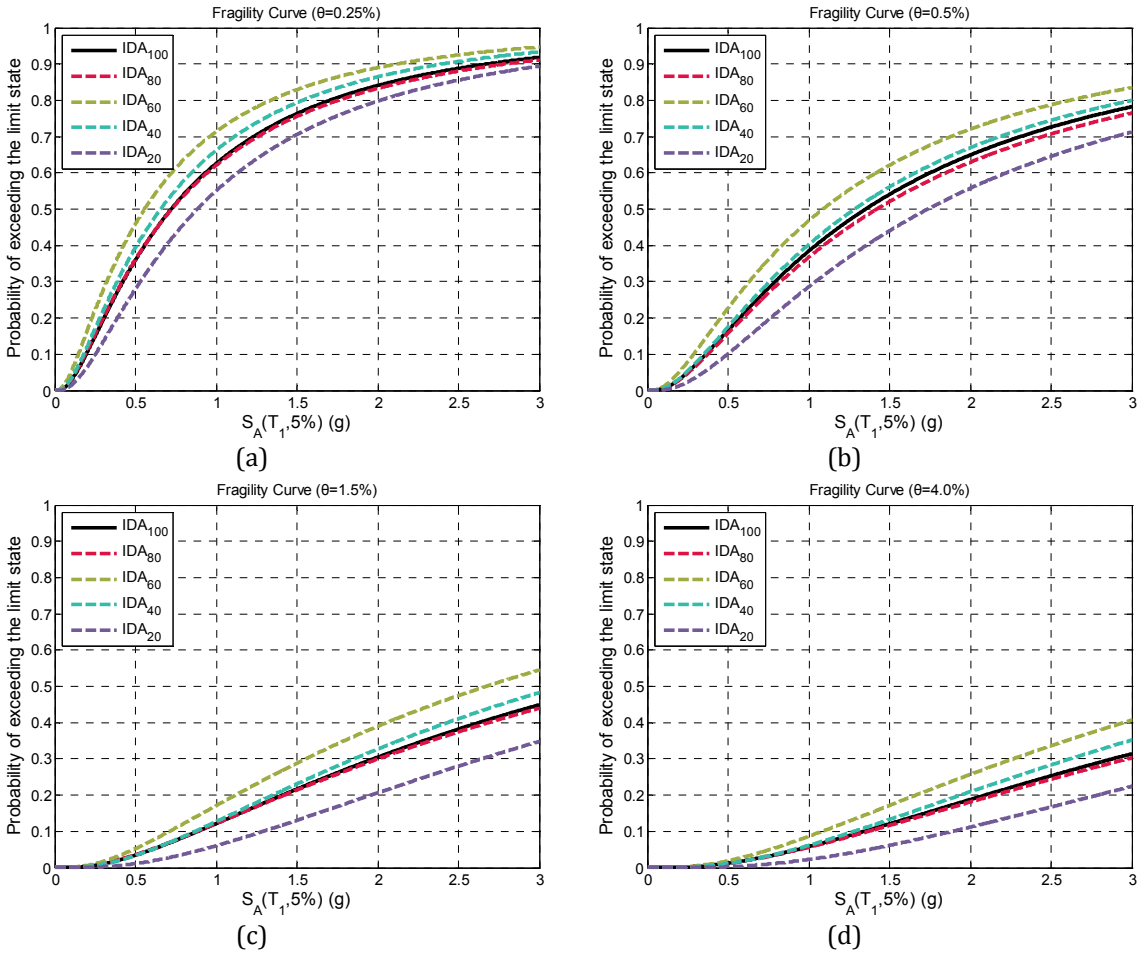

Figure 7.17. Eight storey test example-Fragility curves for four limit-states using alternative number of records.

Figures 7.17 and 7.18 depict the fragility curves corresponding to limit states that cover the whole range of structural damage developed for two buildings considered. For both test examples the fragility curves corresponding to IDA_{100} are considered as the "correct" ones. For the case of the eight storey symmetric building, it can be seen that for all limit states IDA_{20} overestimates the structural capacity while in the cases of IDA_{40} and IDA_{60} the structural capacity is underestimated. Furthermore, it can be seen that 80 records provide a good estimate of the two parameters μ_k and β_k, since the fragility curves of IDA_{80} almost coincide with those of IDA_{100} case. Therefore, it can be said that IDA_{80} case is a good compromise between robustness and efficiency. Similar observations are obtained for the five storey non-symmetric test example, since the fragility curves corresponding to IDA_{20}, IDA_{40} and IDA_{60} cases exhibit similar performance, while IDA_{80} case differs with reference to IDA_{100}. Therefore, it can be said that for the second test example more natural records are

required for a robust and efficient calculation of the two parameters μ_k and β_k and consequently for the calculation of the limit state fragility curves.

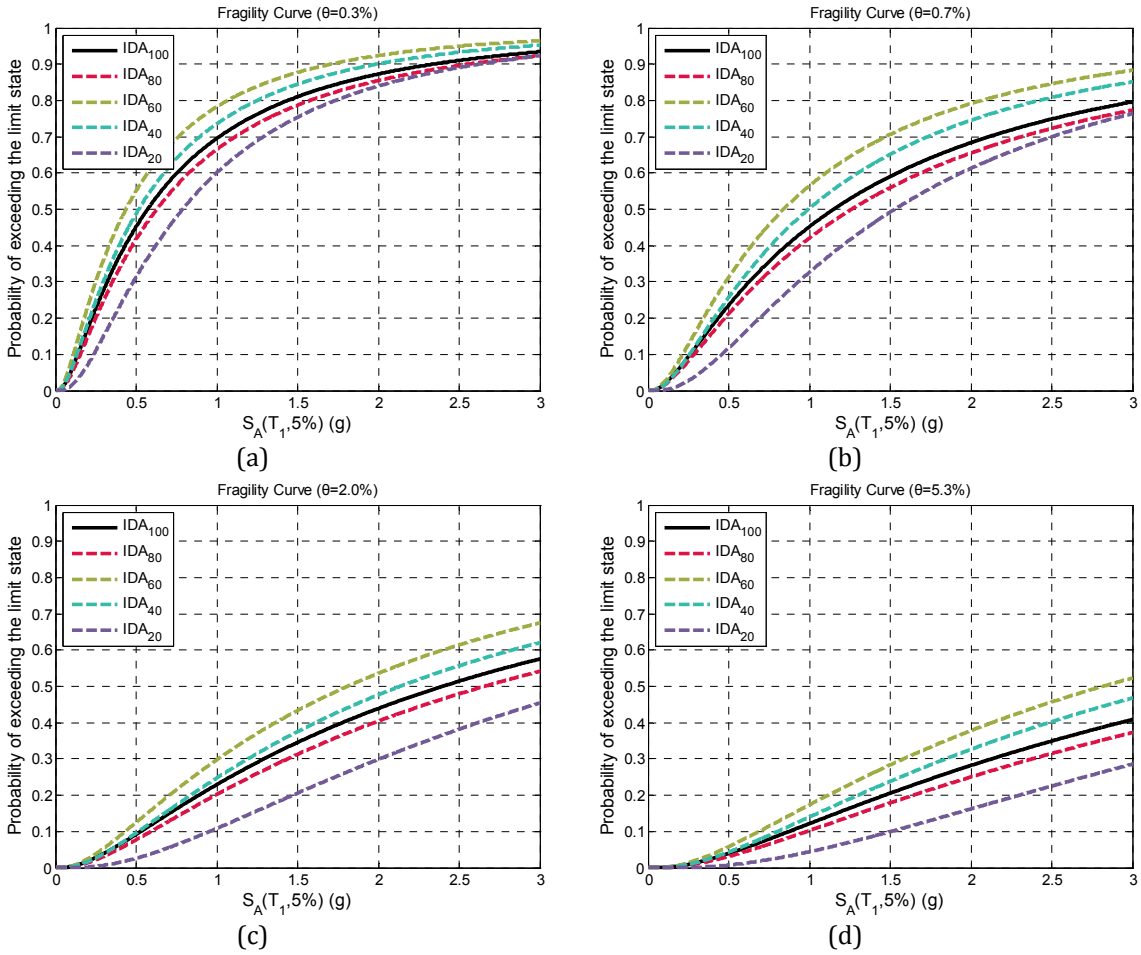

Figure 7.18. Five storey test example-Fragility curves for four limit-states using alternative number of records.

Table 7.5. Eight storey test example-Mean annual frequencies of limit-state exceedance.

	$\theta_{max} \geq 0.25\%$	$\theta_{max} \geq 0.5\%$	$\theta_{max} \geq 1.5\%$	$\theta_{max} \geq 4.0\%$
IDA_{100}	4.15E-03	1.13E-03	1.48E-04	3.95E-05
IDA_{80}	4.53E-03	1.08E-03	1.61E-04	4.00E-05
IDA_{60}	4.83E-03	1.20E-03	1.31E-04	3.44E-05
IDA_{40}	7.23E-03	1.95E-03	2.41E-04	6.42E-05
IDA_{20}	2.35E-03	5.06E-04	3.38E-05	6.76E-06

Since the end product of fragility analysis would be to compute the long-term probability that a certain drift is exceeded in a building located at a certain site, it is essential to evaluate the influence of the sources of uncertainty in terms of the MAFs of limit-state exceedance. Tables 7.5 and 7.6 show the mean annual frequencies obtained after convolving the fragilities of Figures 7.17 and 7.18 with the hazard curve of Figure 7.19, as described in

equation (7.3). For the eight storey symmetric building compared to IDA_{100} , the differences between MAF of IDA_{80} are negligible for all limit-states. The estimation of MAF for cases IDA_{20} and IDA_{40} varies from 45% to 85%, while IDA_{60} varies up to 20%. For the five storey nonsymmetric building the estimation of MAF for cases IDA_{20} and IDA_{40} varies from 35% to 90%, while IDA_{60} and IDA_{80} varies from 5% to 25%.

Table 7.6. Five storey test example-Mean annual frequencies of limit-state exceedance.

	$\theta_{max} \geq 0.3\%$	$\theta_{max} \geq 0.7\%$	$\theta_{max} \geq 2.0\%$	$\theta_{max} \geq 5.3\%$
IDA_{100}	8.21E-03	2.75E-03	6.82E-04	2.19E-04
IDA_{80}	6.83E-03	2.30E-03	5.24E-04	1.61E-04
IDA_{60}	8.55E-03	2.50E-03	6.22E-04	2.13E-04
IDA_{40}	1.17E-02	3.61E-03	9.17E-04	3.12E-04
IDA_{20}	2.56E-03	5.76E-04	9.42E-05	2.29E-05

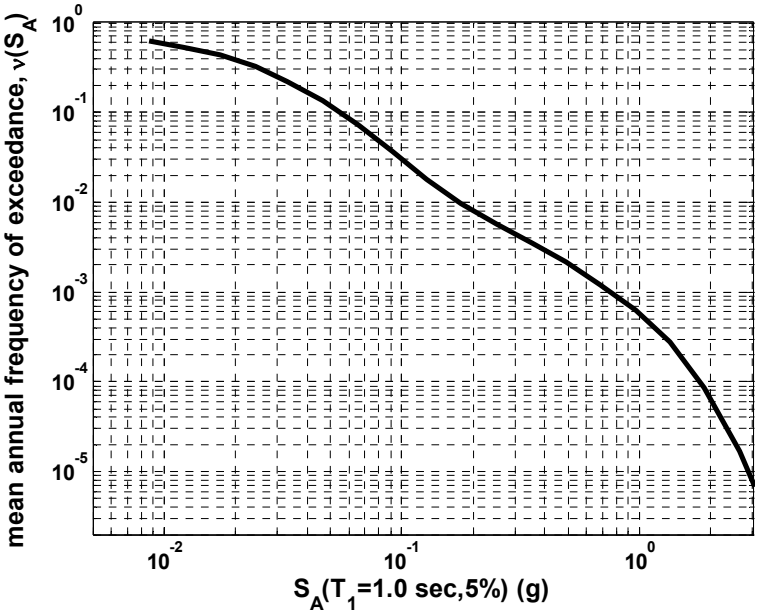

Figure 7.19. Hazard curve for $S_A(T_1=1.0\ sec,5\%)$.

7.10.3. Computational cost

In the last part of this numerical investigation the computational cost of the five cases considered is examined. In this work, the implementation of IDA requires 20 nonlinear dynamic analyses for defining the complete IDA curve, i.e. one record is scaled up to collapse in 20 hazard levels of increased intensity. For developing the fragility curves a number of complete IDA curves are required. Therefore, the total number of analyses for the fragility curves are equal to the number of records times 20. For example in case that 10 records are considered, 200 nonlinear dynamic FE analyses are carried out (10 IDA curves × 20 dynamic

analyses). In Tables 7.7 and 7.8 the computational cost required (in days) along with the nonlinear dynamic FE analysis (in brackets) is provided.

Table 7.7. Eight storey test example-Computational time in days.

Method	HAZUS(no FEA)	ANN scheme (No FEA)
IDA_{20}	21.72(400)	21.73(400)
IDA_{40}	43.44(800)	21.73(400)
IDA_{60}	65.17(1200)	21.73(400)
IDA_{80}	86.89(2400)*	21.73(400)
IDA_{100}	108.61(2000)*	21.73(400)

*Estimation

The computational cost corresponding to the ANN scheme is composed of: (a) the computational cost for assessing, by means of FE analysis, the structural response and define the training sets, (b) the time required for performing training and testing of the ANN and (c) the computational cost required for the prediction of the response. As it can be seen in Tables 7.7 and 7.8 for both test examples the reduction of the computational effort achieved with the ANN prediction is one order of magnitude.

Table 7.8. Five storey test example-Computational time in days.

Method	HAZUS(No FEA)	ANN scheme (No FEA)
IDA_{20}	5.34(400)	5.35(400)
IDA_{40}	10.69(800)	5.35(400)
IDA_{60}	16.03(1200)	5.35(400)
IDA_{80}	21.38(2400)*	5.35(400)
IDA_{100}	26.72(2000)*	5.35(400)

*Estimation

7.11. Discussion

In this chapter a general description of the risk assessment procedure and the methodologies used for developing fragility curves is provided, while a short description of the theory of neural networks is also presented. A computationally efficient procedure for developing fragility curves associated with different limit-states of 3D reinforced concrete buildings is proposed. The fragility curves are defined by means of maximum drift values and cover the whole range of structural damage from serviceability, to life safety and finally to the onset of collapse. In order to perform fragility analysis based on the incremental dynamic analysis methodology, dynamic analyses for different intensity levels need to be

carried out for a number of ground motions sufficiently large to perform statistical evaluation of the results. Statistical information necessary to understand and quantify the behaviour of structural systems can be presented in different formats (horizontal or vertical statistics) depending upon the objective. In the case of fragility analysis where the designer looks for the seismic demand given the structural capacity represented by the value of an engineering demand parameter, "vertical" statistics are required. For the calculation of the optimum values of the two characteristic parameters of the fragility curve function the harmony search optimization algorithm is implemented

A Neural network-based, procedure is proposed for obtaining inexpensive estimates of the seismic demand given the structural capacity which is then used for the fragility assessment of 3D reinforced concrete buildings. In particular, the capability of a neurocomputing prediction scheme when incorporated into the incremental dynamic analysis framework is presented. The main objective is to propose a procedure able to provide accurate enough seismic demand estimates of structural systems at an affordable computational time, in order to be incorporated into the computationally demanding fragility analysis procedure. The time requirements of repeated analyses involved in the incremental dynamic analysis methodology, motivated the use of neural networks. Neural networks are trained using a set of intensity measures that can be easily extracted from a bin of natural ground motion records. The computational effort involved in a "vertical" statistics based methodology for limit-state fragilities, becomes excessive because of the required sample size. The use of ANN can practically eliminate any limitation on the sample size and lead to more accurate development of the fragilities. The results obtained once combined with regional hazard curves can be directly applied for risk assessment of structures.

For the purpose of demonstrating the efficiency of the proposed implementation an eight storey symmetric and a five storey non-symmetric reinforced concrete 3D buildings has been considered. The numerical investigation is performed in three parts. In the first part the prediction capabilities of the trained neural networks are examined. As it was shown 20 training patterns (vectors of IMs – seismic demand) are adequate for training efficiently the ANN in order to predict the seismic demand represented by the fundamental period spectral acceleration for the four limit states. In the second part four limit state fragility curves are developed based on the predictions of the trained ANN. In the last part of this numerical investigation the computational cost of the proposed neurocomputing scheme is examined where it was shown that the reduction of the computational effort achieved with the ANN

prediction is in the range of more than one order of magnitude compared to the conventional procedure.

7.12. References

Alexander, D. (2003) Vulnerability estimation. Lecture held for the Socrate project, Villa Vigoni, Italy.

Algermissen ST, Steinbrugge KV. Earthquake losses to buildings in the San Francisco Bay area. In: Proceedings of the Second National Conference on Microzonation for Safer Construction-Research and Application, National Science Foundation, San Francisco, vol. 1. 1978. p. 291–302.

Aslani H, and Miranda E 2005. Probability-based Seismic Response Analysis, Engineering Structures, 27(8): 1151-1163.

ATC-58-2 (2003) Preliminary evaluation of methods for defining performance. Technical Report.

ATC-58-2 (task 2.2) (2004) Engineering Demand Parameters for Structural Framing Systems. Technical Report.

ATC-58-2 (task 2.3) (2004) Engineering Demand Parameters for Nonstructural Components. Technical Report

Augusti, G., Borri, C. and Niemann H-J. (2001) Is Aeolian risk as significant as other environmental riks? Reliability Engineering and System Safety, Vol. 74, pp 227-237.

Barron-Corverra, R. (2000). "Spectral Evaluation of Seismic Fragility in Structures." PhD Dissertation, Department of Civil, Structural & Environmental Engineering, University at Buffalo, The State University of New York, Buffalo, N.Y.

Benjamin JR, and Cornell CA., 1970. Probability, Statistics, and Decision for Civil Engineers. McGraw-Hill: New York.

Box GEP. The exploration and exploitation of response surfaces: some general considerations and examples. Biometrics; 10: 16–60, (1954)

Breitung K, Faravelli L. Response surface methods and asymptotic approximations, in: Casciati F, Roberts JB (Eds.), Mathematical Models for Structural Reliability, ch. 5, CRC. Press, Boca Raton, FL, pp. 227-286, (1996).

Bucher CG, Bourgund U. A fast and efficient response surface approach for structural reliability problems. Structural Safety; 7(1): 57-66, (1990).

Cimellaro GP., Reinhorn AM., Bruneau M. and Rutenberg A. 2006. Multi-Dimensional Fragility of Structures: Formulation and Evaluation, Technical Report MCEER-06-0002, March 2006

Cornell, C.A. and Krawinkler, H. (1999) Advancing Performance-Based Earthquake Engineering, PEER Center News 2(1), January 1999 pp 1-3.

Deng J, Gu D, Li X, Yue ZQ. Structural reliability analysis for implicit performance functions using artificial neural network. Structural Safety; 27(1): 25-48, (2005).

Der Kiureghian A, Dakessian T. Multiple design points in first and second-order reliability. Structural Safety; 20(1): 37-49, (1998).

Der Kiureghian A. First- and second-order reliability methods. Chapter 14 in Engineering design reliability handbook, Nikolaidis E, Ghiocel DM, Singhal S. (Eds.), CRC Press, Boca Raton, FL, (2005).

Elishakoff, I. Probabilistic Theory of Structures, Dover, New York, 1999.

Ellingwood BR 2001. Earthquake Risk Assessment of Building Structures, Reliability Engineer-ing and System Safety, 74(3): 251-262.

Fahlman, S., An Empirical Study of Learning Speed in Back-Propagation Networks, Carnegie Mellon: CMU-CS-88-162 (1988).

FEMA 273. NEHRP Guidelines for seismic rehabilitation of buildings. Federal Emergency Management Agency, Washington, DC, 1997.

FEMA-National Institute of Building Sciences. HAZUS-MH MR1, Multi-hazard Loss Estima-tion Methodology Earthquake Model, Washington, DC, 2003.

Fragiadakis M, Papadrakakis M. 2008. Modeling, analysis and reliability of seismically excited structures: Computational issues. International Journal of Computational Methods, 5(4): 483–511.

Ghobarah A, Abou-Elfath H, Biddah A. 1999. Response-based damage assessment of structures, Earthquake Engineering and Structural Dynamics, 28(1): 79-104.

Giovenale P, Cornell CA, Esteva L. 2004. Comparing the adequacy of alternative ground motion intensity measures for the estimation of structural responses, Earthquake Engineering and Structural Dynamics, 33(8): 951-979.

Giovenale, P., (2003) Valutazione del rischio sismico di strutture: caratterizzazione dell'azione e tecniche di analisi. PhD Thesis, Univerisity of Rome, December 2002. (in Italian).

Gomes HM, Awruch AM. Reliability analysis of concrete structures with neural networks and response surfaces. Engineering Computations; 22(1), 110-128, (2005).

Guan XL, Melchers RE. Effect of response surface parameter variation on structural reliability estimates. Structural Safety; 23(4): 429-444, (2001).

Gui J, Sun H, Kang H. Structural reliability analysis via global response surface method of BP neural network. Advances in Neural Networks-ISNN 2004: 799-804.

Gupta S, Manohar CS. An improved response surface method for the determination of failure probability and importance measures. Structural Safety; 26(2): 123-139, (2004).

Hosni Elhewy A, Mesbahi E, Pu Y. Reliability analysis of structures using neural network method. Probabilistic Engineering Mechanics; 21(1), 44-53, (2006).

http://peer.berkeley.edu/smcat/search.html/ Pacific Earthquake Engineering Research (PEER). (last accessed November 2010).

Hurtado JE. An examination of methods for approximating implicit limit state functions from the viewpoint of statistical learning theory. Structural Safety; 26(3): 271-293, (2004).

Jeong SH, and Elnashai AS 2007. Probabilistic fragility analysis parameterized by fundamental response quantities, Engineering Structures, 29(6):1238-1251.

Jiang C, Han X, Liu GR. Optimization of structures with uncertain constraints based on convex model and satisfaction degree of interval, Computer Methods in Applied Mechanics and Engineering; 196(49-52): 4791-4800 (2007).

Kappos AJ, Panagopoulos G, Panagiotopoulos C and Penelis G 2006. A hybrid method for the vulnerability assessment of R/C and URM buildings, Bulletin of Earthquake Engineering, 4(4): 391-413.

Kaymaz I, McMahon CA. A response surface method based on weighted regression for structural reliability analysis. Probabilistic Engineering Mechanics; 20(1): 11-17, (2005).

Kennedy RP, Cornell CA, Campbell RD, Kaplan S and Perla HF 1980. Probabilistic Seismic Safety Study of an Existing Nuclear Power Plant, Nuclear Engineering and Design, 59(2): 315-338.

Kent DC, Park R. 1971. Flexural members with confined concrete. Journal of Structural Divi-sion, 97(7):1969-1990.

Kim S-H, Na S-W. Response surface method using vector projected sampling points. Structural Safety; 19(1): 3-19, (1997).

Kircher CA, Nassar AA, Kustu O and Holmes WT 1997. Development of building damage functions for earthquake loss estimation, Earthquake Spectra, 13(4): 663-682.

Kramer SL. Geotechnical Earthquake Engineering, Prentice Hall, 1996.

Lagaros ND 2008. Probabilistic fragility analysis of RC buildings designed with different rules, Earthquake Engineering and Engineering Vibration, 7(1), 45-56.

Lagaros, N.D., Papadrakakis, M. Learning improvement of neural networks used in structural optimization, Advances in Engineering Software, 35 (2004) 9-25.

Lee KS, Geem ZW. 2005. A new meta-heuristic algorithm for continuous engineering optimization: Harmony search theory and practice. Comput Methods Appl Mech Eng, 194(36-38):3902-3933

Liu YW, Moses F. A sequential response surface method and its application in the reliability analysis of aircraft structural systems. Structural Safety; 16(1): 39-46, (1994).

Lu Z-Z, Zhao J, Yue Z-F. Advanced response surface method for mechanical reliability analysis. Applied Mathematics and Mechanics; 28(1): 19-26, (2007).

MacKay DJC. A practical Bayesian framework for backprop networks. Neural Computation 1992; 4: 448-472.

Mahadevan S, Shi P. Multiple linearization method for nonlinear reliability analysis. J Engineering Mechanics; 127(11): 1165-1173, (2001).

Mahdavi M, Fesanghary M, Damangir E. 2007. An improved harmony search algorithm for solving optimization problems, Applied Mathematics and Computation, 188(2): 1567-1579.

Marini A, Spacone E. 2006. Analysis of reinforced concrete elements including shear effects. ACI Structural Journal, 103(5): 645-655.

McKenna F, Fenves GL. 2001. The OpenSees Command Language Manual - Version 1.2. Pacific Earthquake Engineering Research Centre, University of California, Berkeley.

Melchers, R.E., (1987) Structural Reliability Analysis and Prediction, Wiley, New York.

Menegotto M, Pinto PE. Method of analysis for cyclically loaded reinforced concrete plane frames including changes in geometry and non-elastic behaviour of elements under combined normal force and bending. Proceedings, IABSE Symposium on Resistance and Ultimate Deformability of Structures Acted on by Well Defined Repeated Loads: 15-22, 1973.

Mitropoulou ChCh, Lagaros ND, Papadrakakis M. 2010. Economic building design based on energy dissipation: a critical assessment, Bulletin of Earthquake Engineering, 8(6): 1375-1396.

Mitropoulou ChCh, Lagaros ND, Papadrakakis M. 2010. Life-cycle cost assessment of reinforced concrete buildings subjected to seismic actions, (submitted for publication).

Miyakoshi J., Hayashi Y., Tamura K., Fukuwa N. Damage ratio functions of buildings using damage data of the 1995 Hyogoken-Nanbu Earthquake. ICOSSAR 1997.

Mosalam KM, Ayala G, White RN, Roth C. Seismic fragility of LRC frames with and without masonry infill walls. Journal of Earthquake Engineering 1997;1(4):693–719.

Olsson A, Sandberg G. Dahlblom O. 2003. On Latin hypercube sampling for structural reliability analysis. Structural Safety, 25(1): 47-68.

Onose J-I. Prediction of damage ratio of reinforced concrete buildings due to earthquakes and comparison with actual damage ratio. In: Proceedings of the 6th Japan Earthquake Engineering Symposium: Japan Society of Civil Engineers, Tokyo. 1982. p.2081–2088.

Pagni CA and Lowes LN 2006. Fragility Functions for Older Reinforced Concrete Beam-column Joints, Earthquake Spectra, 22(1):215-238.

Papadrakakis M, Lagaros ND, Tsompanakis Y. Structural optimization using evolution strategies and neural networks. Comput. Methods Appl. Mech. Engrg. 1998; 156: 309-333.

Papadrakakis M, Papadopoulos V, Lagaros ND. 1996. Structural Reliability analysis of elastic-plastic structures using neural networks and Monte Carlo simulation, Computer Methods in Ap-plied Mechanics and Engineering, 136, 145-163.

Papadrakakis M. Lagaros ND. 2002. Reliability-based structural optimization using neural net-works and Monte Carlo simulation, Computer Methods in Applied Mechanics and Engineering, 191(32): 3491-3507.

Porter K, Kennedy R and Bachman R 2007. Creating Fragility Functions for Performance-based Earthquake Engineering, Earthquake Spectra, 23(2): 471-489.

Porter, K.A. (2003) An Overview of PEER's Performance-Based Earthquake Engineering Methodology. ICASP9, July 6-9, 2003, San Francisco, CA.

Priestley MJN. Displacement-based approaches to rational limit states design of new structures. In: Proceedings of the 11th European Conference on Earthquake Engineering. Rotterdam: AA Balkema; 1998.

Rackwitz R, Fiessler B. Structural reliability under combined random load sequences. Computers & Structures; 9: 489-494, (1978).

Rackwitz, R., Lentz, A. and Faber, M. (2005) Socio-economically Sustainable Civil Engineering Infrastructue by Optimization. Structural Safety, Vol. 27, pp 187-229.

Rajashekhar MR, Ellingwood BR. A new look at the response surface approach for reliability analysis. Structural Safety; 12(3): 205-220, (1993).

Reinhorn, A. M., Barron-Corverra, R., and Ayala, A. G. (2001). "Spectral Evaluation of Seismic Fragility of Structures." Proceedings ICOSSAR 2001, Newport Beach CA, June 2001.

Riedmiller M, Braun H. A direct adaptive method for faster back-propagation learning: the RPROP algorithm. Proceedings of the IEEE International Conference on Neural Networks (ICNN), San Francisco, pp. 586–591, 1993.

Riedmiller M. Advanced supervised learning in multi-layer perceptrons - from backpropagation to adaptive learning algorithms. Int. Journal of Computer Standards and Interfaces - Special Issue on Neural Networks 1994; 16: 265 - 278.

Rossetto T., Elnasai A., Derivation of vulnerability functions for European-type RC structures based on observational data, Engineering Structures 25 (2003) 1241–1263.

Schuëller GI. Developments in stochastic structural mechanics. Archive of Applied Mechanics; 75(10-12): 755-773, (2006).

Schueremans L, Van Gemert D. Benefit of splines and neural networks in simulation based structural reliability analysis. Structural Safety; 27 (3): 246-261, (2005).

Shinozuka M, Feng MQ, Lee J and Naganuma T 2000. Statistical Analysis of Fragility Curves, Journal of Engineering Mechanics, 126(12): 1224-1231.

Shinozuka M, Murachi Y, Dong X, Zhou Y and Orlikowski MJ 2003. Effect of Seismic Retrofit of Bridges on Transportation Networks, Earthquake Engineering and Engineering Vibration, 2(2): 169-179.

Vamvatsikos D, Cornell CA. 2002. Incremental dynamic analysis, Earthquake Engineering and Structural Dynamics, 31(3): 491-514.

Wen YK and Ellingwood BR 2005. The Role of Fragility Assessment in Consequence-based Engineering, Earthquake Spectra, 21(3): 861-877.

Chapter 8

Conclusions & Recommendations for Further Study

8.1. Contributions of the Study

The contribution achieved in the context of this dissertation can be summarized as follows: i) Calibration of the damage indices, ii) Antiseismic design procedures, iii) Life cycle cost analysis and iv) Fragility analysis.

8.1.1. Calibration of the damage indices

The first contribution of this work is the objective calibration of some of the most important damage indices that have been used by many researchers to identify the state of damage of reinforced concrete structures based on the flexural crack width. In particular the Park and Ang local damage index; its modified variant proposed by Kunnath, Reinhorn and Lobo; the Chung, Meyer and Shinozuka local damage index. Together with the maximum softening and final softening damage indices proposed by DiPasquale and Çakmak, maximum interstorey drift and maximum floor acceleration, these indices have been calibrated with reference to the level of damage and consequently the repair cost that corresponds to this damage state.

8.1.2. Antiseismic design procedures

Antiseismic Design for Energy Dissipation

In the context of this dissertation an analytical investigation was performed in order to identify the effect of the behaviour factor q in the final design of reinforced concrete buildings in terms of safety and economy. The numerical tests were performed on two multi-storey reinforced concrete buildings having symmetrical and non symmetrical plan views, which were optimally designed according to the Eurocodes EC2 and EC8. The most important findings of this investigation can be summarized as follows:

- The initial cost of reinforced concrete structures, taking into account the cost of both structural and non-structural elements, designed on the basis of elastic response $D_{q=1}$ is not excessive since it varies, for the two representative test cases considered, from 3% to 15% compared to the initial cost of the conventionally performed designs $D_{q=2}$ to $D_{q=4}$, respectively. In fact, the designs $D_{q=1}$ were only 10% more expensive compared to the cost of the designs obtained for the value of the behaviour factor suggested by the Eurocode (and Greek Norms). In the case, though, that these four designs are compared with reference to the cost of the RC framing members alone, design $D_{q=1}$ is up to 95% more expensive compared to D_q (q=2,3,4). This is attributed to the invariant contribution of the concrete slabs, and will change with frame geometry and vertical loading.
- Comparing the contributing parts of the total life-cycle cost, it can be said that the initial cost, in both test examples, is the most important component for all designs obtained. The cost of building content damage due to floor acceleration is the second dominant contributor for stiffer design ($D_{q=1}$ and $D_{q=2}$), while for designs $D_{q=3}$ and $D_{q=4}$ damage and income costs are almost equivalent representing the second most dominant contributors.
- Considering the total cost in the design lifetime of a building, and for the test examples considered it has been shown that designing with the behaviour factor adopted herei, by the 2000 Greek National Seismic Design code the resulting design will be more vulnerable to future earthquakes, thereby leading to a much higher total cost compared to the design obtained with the performance-based procedure or the design obtained according to the Greek national seismic design code but using a behaviour factor between 1 to 1.5.
- It has also been demonstrated how the concept of PBD can be integrated in a structural design procedure in order to obtain a design that fulfils the provisions of contemporary design codes such as the three performance objectives employed in this study. Even though these conclusions cannot be generalized, it is an indication about the performance of the designs according to a prescriptive design code and to a performance-based design procedure.

Performance-Based Design

The contribution of this work in the context of performance-based design is that based on the calibration of the damage indices it was possible to incorporate all DIs examined in this dissertation into a performance-based design framework and to identify the DI that provide

reliable information on damage level and depicts less dispersion for different hazard levels. This was achieved by means of lower bound performance-based design. The ultimate objective of this task was to compare lower-bound designs satisfying the code requirements in the most cost-effective way, i.e. those with minimum cross section and reinforcement dimensions. For this reason, a structural optimization problem was formulated and the designs obtained were then assessed in the framework proposed. In this context it was found that maximum interstorey drift cannot be considered as the sole representative of damage for the global behaviour of a reinforced concrete structure.

8.1.3. Life cycle cost analysis procedure

In the context of this dissertation a new procedure was proposed to calculate the life-cycle cost of reinforced concrete buildings subjected to seismic actions. The life-cycle cost estimation was examined with respect to the adopted analysis procedure, the number of seismic records imposed, the performance criterion used and the type of the building structure. Multiple stripe dynamic analysis, a variant of the incremental dynamic analysis, and the nonlinear static (pushover) analysis were applied to compute the performance criteria such as maximum inter-storey drift and floor acceleration. The most important findings of this part of this dissertation study can be summarized as follows:

- From the examination of the multiple-stripe dynamic analysis curves, it can be concluded that 20 records are not enough to obtain reliable estimates of the structural life-cycle cost.
- The results obtained from the capacity curves and the corresponding life-cycle costs, as well as from the variation of these between $MSDA_{(\theta)}$ and $MSDA_{(\theta+\alpha)}$ cases, it was demonstrated that the use of 40 seismic records is a sufficient number of seismic records for a reliable performance assessment.
- The use of the maximum inter-storey drift as performance criterion, instead of using the combination of both maximum inter-storey drift and maximum floor acceleration, leads to an underestimation of the life-cycle cost of the structures. Based on this work it was shown that the effect of inter-storey drift appears to be more critical in the calculation of the life-cycle cost than the maximum floor acceleration.
- The nonlinear static analysis procedure is not recommended as a performance estimation tool compared to the IDA. Especially, the life-cycle cost values in the irregular test example based on *NSA* produced unrealistic predictions of structural performance.

- The structural type of the building affects its structural performance. It exhibits been verified that a symmetrical structure sustains less damage and therefore less repair cost during its lifetime compared to a non symmetric structure.
- Last but not least, the most important outcome of this investigation is the development of a computational tool for a quantitative assessment of the structural performance of any type of RC building.

8.1.4. Fragility analysis procedure

In the framework of fragility analysis a computationally efficient procedure for developing fragility curves associated with different limit-states of 3D reinforced concrete buildings was proposed. In particular a neural network-based procedure is proposed for obtaining inexpensive estimates of the seismic demand given the structural capacity which is subsequently used for the fragility assessment of 3D reinforced concrete buildings. The objective of this investigation is to propose a procedure able to provide accurate seismic demand estimates of structural systems at an affordable computational time, which is then incorporated into the computationally demanding fragility analysis. The CPU time requirements of repeated analyses involved in the IDA procedure, motivated the use of neural networks. In the two test examples considered it was observed that fragility analysis and mean annual frequency estimates are highly dependent on the bin of records used, the more records used, the better estimates being obtained. The computational effort involved in a "vertical" statistics based methodology for limit-state fragilities, becomes excessive because of the large sample size required. The use of neural networks managed to practically eliminate any limitation on the sample size and lead to more accurate development of the fragilities.

8.2. Software development

In the framework of this dissertation various source codes have been developed in Fortran and Matlab:

- IDA & MSDA (Fortran): Source code for performing incremental dynamic analysis written in Fortran.
- Life-cycle cost analysis of structures (Matlab and Fortran). Source code was developed for the calculation of the probabilities of exceedance, definition of the best fitted curve through pairs of annual probability of exceedance and maximum response quantity, etc following the procedure described in Chapter 6.

- EC8 (Fortran): Source code was developed for the definition of the earthquake loads and the implementation of the checks imposed by the code.
- EC2 (Fortran): Source code was developed for the implementation of the checks imposed by the code, serviceability and ultimate limit state checks, capacity design, etc.
- UART (Fortran): Source code was developed for the generation of artificial accelerograms taking into account various sources of randomness, as described in Chapter 5.
- The software used for the nonlinear static and nonlinear dynamic analyses are the OpenSEES (2008) for the case of the beam simulation and the ATENA (2009) for the 3D simulation, while the software for the design based on the Greek National Codes is the STRAD (2006) and the Eurocodes 2 and 8 is the SCADA Pro (2009).

8.3. General Conclusions

This dissertation is a step towards a comprehensive quantification of the limit states with reference to some damage indices along with the improvement of performance-based design procedure and life cycle cost and fragility assessment frameworks. The conclusions drawn from this study are limited by the scope and assumptions made throughout this work. In particular, the research work carried out for the purposes of this dissertation led to the following overall conclusions:

- It has been demonstrated how the concept of performance-based design can be integrated in a structural design procedure in order to obtain designs that fulfil the provisions of contemporary design codes, like the performance objectives employed in this study. Even though these conclusions cannot be generalized, it provides a tool for achieving designs according to a prescriptive design code and to a performance-based design procedure.
- The initial cost for a RC structure, designed to permit elastic behaviour for the response spectrum of the antiseismic design code and seismic zone considered, is not excessive compared to designs with q>1.
- The nonlinear static analysis procedure when used as a performance estimation tool, especially for the life-cycle cost estimation of irregular buildings produced unrealistic predictions of the structural performance, compared to the nonlinear dynamic analysis.
- A valuable contribution of this work is the development of a robust and efficient methodology for both life cycle cost analysis and fragility assessment of reinforced

concrete structures. For further reduction of the computational cost, NN metamodels can be applied as proposed in the thesis, providing acceptable numerical results at very low computational cost.

The research goal of this investigation is to show the potential of these advanced design methodologies hoping that they will be used in engineering practice in the near future.

8.4. Recommendation for Further Research

Areas for future research on the evaluation of collapse potential of structures in earthquakes include the following:

- Implementation of this new design framework into special type of structures like bridges, nuclear facilities, etc.
- Extension of the assessment methodology to allow for the evaluation of existing structures, monuments, etc.
- Development of simplified procedures, software tools and design methodologies for the direct use by practitioning engineers, which will be based on the findings of this study.
- Use advanced solution techniques implemented in parallel computing environment in order to use more refined models of structures into the design and assessment frameworks presented in this study.

8.5. Publications

In total the published research work prepared by Ch.Ch. Mitropoulou in the framework of the current dissertation can be summarized as follows: (i) four publications in contributed international books (Mitropoulou et al., 2008; Mitropoulou et al., 2010a; Mitropoulou et al., 2010b; Mitropoulou et al., 2011), (ii) six publications in refereed journals (Mitropoulou et al., 2010; Mitropoulou and Papadrakakis, 2010; Mitropoulou et al., 2011; Mitropoulou and Papadrakakis, 2011a; Mitropoulou and Papadrakakis, 2011b; Mitropoulou and Papadrakakis, 2011c), (iii) one publication in journal without referees (Mitropoulou et al., 2010) and (iv) six papers in international conference proceedings (Mitropoulou et al., 2006; Mitropoulou et al., 2007; Mitropoulou et al., 2008; Mitropoulou et al., 2009; Mitropoulou et al., 2010a; Mitropoulou et al., 2010b).

Chapters in contributed international books

Mitropoulou Ch.Ch., Bakas N.P., Lagaros N.D., M. Papadrakakis, Advances in design optimization of reinforced concrete structural systems, in Computational Structural Dynamics and Earthquake

Engineering, M. Papadrakakis, D.C. Charmpis, N.D. Lagaros and Y. Tsompanakis (Eds.), Taylor & Francis, (November 2008).

Mitropoulou Ch.Ch., Krikos S.A., Fotis A.D., Lagaros N.D., Papadrakakis M., Economic Seismic Design of Buildings, in Developing trends in seismic design of structures, N.D. Lagaros, Y. Tsompanakis & M. Papadrakakis (Eds.), Saxe-Coburg publisher, (2010a).

Mitropoulou Ch.Ch., Lagaros N.D., Papadrakakis M., Advances in structural life cycle cost analysis, in Computational Methods in Earthquake Engineering, M. Papadrakakis, M. Fragiadakis, N.D. Lagaros (Eds.), Springer publisher, (2010b).

Mitropoulou Ch.Ch., Lagaros N.D., Papadrakakis M., Structural Optimization: An assessment approach of design procedures against earthquake hazard, in Protection of build environment against earthquakes, Matjaž Dolšek (Ed.), Springer publisher, 2011.

Papers in refereed journals

Mitropoulou Ch.Ch., Lagaros N.D., Papadrakakis M., "Economic building design based on energy dissipation: a critical assessment", Bulletin of Earthquake Engineering, 8(6): 1375-1396, 2010.

Mitropoulou Ch.Ch., Lagaros N.D., Papadrakakis M., "Life-cycle cost assessment of reinforced concrete buildings subject to seismic actions", Reliability Engineering and System Safety (accepted for publication), 2010.

Mitropoulou Ch.Ch., Papadrakakis M., "Selection of the seismic excitations for the assessment of life-cycle cost of structures", (under review), 2010.

Mitropoulou Ch.Ch., Papadrakakis M., "Fragility Analysis of Structures: A computationally efficient approach with Neural Network predictions", Engineering Structures (accepted for publication), 2011a.

Mitropoulou Ch.Ch., Papadrakakis M., Calibration of damage indices with reference to repair cost, (under review), 2011b.

Mitropoulou Ch.Ch., Papadrakakis M., New performance-based antiseismic design framework based on various damage indices, (under review), 2011c.

Papers in non refereed journals

Μητροπούλου Χ.Χ., Φώτης Α.Δ., Κρίκος Σ.Α., Λαγαρός Ν.Δ., "Αξιολόγηση μεθοδολογιών αντισεισμικού σχεδιασμού κατασκευών με βάση το κόστος κύκλου ζωής", Περιοδικό Συλλόγου Πολιτικών Μηχανικών Ελλάδος (ΣΠΜΕ), Νο 385, 2010.

Papers in international conference proceedings

Mitropoulou Ch.Ch., Lagaros N.D., Papadrakakis M., "Structural optimization based on assessment of seismic design codes for RC buildings", The First South-East European Conference on Computational Mechanics, Kragujevac, Serbia, June 28-30, 2006.

Mitropoulou Ch.Ch., Lagaros N.D., Papadrakakis M., Life cycle cost assessment of EC8 based optimum design, COMPDYN 2007, June 13-16, 2007, Rethymno, Crete, Greece.

Mitropoulou Ch.Ch., Lagaros N.D., Papadrakakis M., Fragility based critical assessment of design codes, CST2008, The 9th International Conference on Computational Structures Technology, Athens, Greece, 2-5 September 2008.

Mitropoulou Ch.Ch., Lagaros N.D., Papadrakakis M., Optimum Building Design Based on Energy Dissipation, COMPDYN 2009, June 22-24, 2009, Island of Rhodes, Greece.

Mitropoulou Ch.Ch., Lagaros N.D., Papadrakakis M., Soft computing methodologies in computational earthquake engineering, IV European Congress on Computational Mechanics (ECCM IV): Solids, Structures and Coupled Problems in Engineering, Paris, France, 16-21 May, 2010a.

Mitropoulou Ch.Ch., Fragiadakis M., Lagaros N.D., Papadrakakis M., Structural Optimization: An assessment approach of design procedures against the earthquake hazard, International Workshop on Protection of build environment against earthquakes, Ljubljana, 27-28. August 2010b.

Appendix A

Seismic Records

A.1. Introduction

In this appendix the list of recorded excitations that have been used in the framework of this dissertation are provided. These records have been selected from the PEER strong-motion database (PEER, 2010) according to the following selection criteria: (i) Events occurred in a specific area (longitude -124^{o} to -115^{o}, latitude 32^{o} to 41^{o}). (ii) Moment magnitude (M) is equal to or greater than 5. (iii) Epicentral distance (R) is smaller than 150 km.

A.2. Seismic Records

In the following seven Tables (A.1 to A.7), the following information, among others, is provided:

[1]Campbell's R Distance

[2]Distance from the recording site to epicentre

[3]Campbell's site classification: A (Firm Soil), B (Very Firm Soil), C (Soft Rock), D (Firm Rock), E (Shallow Soils)

[4]Fault rupture mechanism: SS (Strike Slip), N (Normal), RN (Reverse-Normal), RO (Reverse-Oblique), NO (Normal- Oblique)

Table A.1. Characteristics of the first group of 20 records

Earthquake Station	R[1] (km)	EpiD[2] (km)	Recording Angle log/tran (°)	Duration (sec)	PGA_{log} (g)	PGA_{tran} (g)	Campbell's GEOCODE[3]	Fault rupture[4]
Superstition Hills 1987 (B) (M=6.7)								
El Centro Imp. Co Cent	18.5	35.83	000/090	40.00	0.36	0.26	A	SS
Wildlife Liquefaction Array	24.1	29.41	090/360	44.00	0.18	0.21	A	SS
Imperial Valley 1979 [23:16]. (M=6.5)								
Chihuahua	8.4	18.88	012/282	40.00	0.27	0.25	A	SS
Compuertas	15.3	24.43	015/285	36.00	0.19	0.15	A	SS
Plaster City	31.1	54.26	045/135	18.75	0.042	0.057	A	SS
El Centro Array #12	18.85	31.99	140/230	39.00	0.143	0.116	A	SS
El Centro Array #13	22.83	35.95	140/230	39.50	0.117	0.139	A	SS
San Fernando 1971 (M=6.6)								
LA, Hollywood Stor. Lot	25.9	39.49	090/180	28.00	0.21	0.17	A	RN
Northridge 1994 (M=6.7)								
Leona Valley #2	37.2	51.88	000/090	32.00	0.09	0.06	A	RN
LA, Baldwin Hills	29.9	28.20	090/360	40.00	0.24	0.17	C	RN
Lake Hughes #1	89.67	93.22	000/090	32.00	0.087	0.077	A	RN
LA, Hollywood Stor FF	114.62	118.26	090/360	40.00	0.231	0.358	A	RN
LA, Centinela St.	31.53	32.72	155/245	30.00	0.465	0.322	A	RN
Loma Prieta 1989 (M=6.9)								
Hollister Diff Array	24.8	45.10	165/255	39.64	0.27	0.28	A	RO
WAHO	17.5	12.56	000/090	24.96	0.37	0.64	C	RO
Halls Valley	30.5	36.31	000/090	39.95	0.13	0.10	B	RO
Agnews State Hospital	24.6	40.12	000/090	40.00	0.17	0.16	A	RO
Anderson Dam (Downstream)	4.4	16.67	270/360	39.61	0.244	0.240	B	RO
Coyote Lake Dam (Downstream)	20.8	30.89	195/285	39.95	0.160	0.179	B	RO
Hollister - South & Pine	27.93	48.24	000/090	60.00	0.371	0.177	A	RO

Table A.2. Characteristics of the second group of 20 records

Earthquake Station	R[1] (km)	EpiD[2] (km)	Recording Angle log/tran (°)	Duration (sec)	PGA_{log} (g)	PGA_{tran} (g)	Campbell's GEOCODE[3]	Fault rupture[4]
Whittier Narrows 1987/10/01 (M=6.0)								
Pasadena - CIT Athenaeum	17.24	10.64	180/270	32.00	0.174	0.101	B	RO
Alhambra - Fremont School	14.66	6.77	180/270	40.00	0.333	0.414	B	RO
LA - Hollywood Stor FF	24.08	24.21	000/090	40.00	0.221	0.124	A	RO
Altadena - Eaton Canyon	19.52	14.28	000/090	40.00	0.299	0.151	A	RO
Beverly Hills - 12520 Mulhol	29.90	31.09	032/122	32.22	0.089	0.138	C	RO
Brea Dam (Downstream)	23.99	22.72	040/130	30.00	0.163	0.313	A	RO
Glendale - Las Palmas	22.82	21.73	177/267	31.50	0.296	0.166	A	RO
Chalfant Valley 1986/07/20 (M=5.9)								
Benton	21.92	31.25	270/360	32.00	0.061	0.052	A	SS
Bishop - Paradise Lodge	18.31	15.42	070/160	39.95	0.046	0.095	C	SS
Bishop - LADWP South St	17.17	20.27	180/270	39.93	0.129	0.094	A	SS
Lake Crowley - Shehorn Res.	22.08	16.59	009/099	40.00	0.051	0.031	A	SS
Zack Brothers Ranch	7.58	14.33	270/360	39.87	0.285	0.207	A	
Coalinga 1983/05/02 [23:42] (M=6.4)								
Cantua Creek School	24.02	30.06	270/360	40.00	0.227	0.281	A	RN
Parkfield - Cholame 2WA	44.72	55.67	000/090	40.00	0.109	0.114	A	RN
Parkfield - Cholame 5W	48.70	59.67	270/360	40.00	0.147	0.131	A	RN
Parkfield - Fault Zone 1	41.99	52.86	000/090	40.00	0.194	0.111	A	RN
Parkfield - Fault Zone 14	29.48	38.54	000/090	40.00	0.282	0.274	A	RN
Parkfield - Gold Hill 3W	39.12	49.47	000/090	40.00	0.137	0.122	B	RN
Parkfield - Stone Corral 3E	34.00	44.66	000/090	24.00	0.151	0.106	C	RN
Pleasant Valley P.P. - yard	8.41	9.98	045/135	39.97	0.592	0.551	A	RN

Table A.3. Characteristics of the third group of 20 records

Earthquake Station	R[1] (km)	EpiD[2] (km)	Recording Angle log/tran (°)	Duration (sec)	PGA_{log} (g)	PGA_{tran} (g)	Campbell's GEOCODE[3]	Fault rupture[4]
Cape Mendocino 1992 (M=7.1)								
Cape Mendocino	6.96	10.36	000/090	30.00	1.497	1.039	D	RN
Eureka - Myrtle & West	41.97	53.34	000/090	44.00	0.154	0.178	B	RN
Fortuna - Fortuna Blvd	19.95	29.55	000/090	44.00	0.116	0.114	A	RN
Petrolia	8.18	4.51	000/090	36.00	0.590	0.662	A	RN
Rio Dell Overpass - FF	14.33	22.64	270/360	36.00	0.385	0.549	A	RN
Shelter Cove Airport	28.78	36.28	000/090	36.00	0.229	0.189	E	RN
Coyote Lake 1979 (M=5.7)								
Gilroy Array #1	10.67	12.56	230/320	26.84	0.103	0.132	D	SS
Coyote Lake Dam (SW Abut)	6.13	7.95	160/250	28.82	0.157	0.279	D	SS
Gilroy Array #2	9.02	10.94	050/140	26.86	0.211	.339	A	SS
Gilroy Array #6	3.11	4.37	230/320	27.10	0.434	0.316	C	SS
San Juan Bautista	19.70	23.24	213/303	28.46	0.108	0.107	B	SS
Westmorland 1981 (M=5.8)								
Brawley Airport	15.57	15.71	225/315	28.41	0.169	0.171	A	SS
Niland Fire Station	15.45	18.45	000/090	40.00	0.105	0.176	A	SS
Parachute Test Site	16.81	20.47	225/315	40.00	0.242	0.155	A	SS
Superstition Mtn Camera	19.50	25.02	045/135	28.36	0.071	0.116	D	SS
Westmorland Fire Sta	6.87	7.02	090/180	40.00	0.368	0.496	A	SS
Salton Sea Wildlife Ref	8.15	8.62	225/315	28.75	0.199	0.176	A	SS
Landers 1992 (M=7.3)								
Desert Hot Springs	21.98	27.33	000/090	50.00	0.171	0.154	A	SS
Amboy	69.17	75.20	000/090	50.00	0.115	0.146	E	SS
Lucerne	3.71	44.02	000/090	48.13	0.721	0.785	D	SS

Table A.4. Characteristics of the fourth set of 22 natural records

Earthquake Station	R[1] (km)	EpiD[2] (km)	Recording Angle log/tran (°)	Duration (sec)	PGA_{log} (g)	PGA_{tran} (g)	Campbell's GEOCODE[3]	Fault rupture[4]
Northridge 1994 (M=6.7)								
Leona Valley #2	37.2	51.88	000/090	32.00	0.09	0.06	A	RN
LA, Baldwin Hills	29.9	28.20	090/360	40.00	0.24	0.17	C	RN
Lake Hughes #1	89.67	93.22	000/090	32.00	0.087	0.077	A	RN
LA, Hollywood Stor FF	114.62	118.26	090/360	40.00	0.231	0.358	A	RN
LA, Centinela St.	31.53	32.72	155/245	30.00	0.465	0.322	A	RN
Anaheim - W Ball Rd	68.62	70.45	220/310	34.99	0.066	0.072	A	RN
Bell Gardens - Jaboneria	44.11	45.26	000/090	34.99	0.049	0.068	A	RN
Loma Prieta 1989 (M=6.9)								
Hollister Diff Array	24.8	45.10	165/255	39.64	0.27	0.28	A	RO
WAHO	17.5	12.56	000/090	24.96	0.37	0.64	C	RO
Halls Valley	30.5	36.31	000/090	39.95	0.13	0.10	B	RO
Agnews State Hospital	24.6	40.12	000/090	40.00	0.17	0.16	A	RO
Anderson Dam (Downstream)	4.4	16.67	270/360	39.61	0.244	0.240	B	RO
Coyote Lake Dam (Downstream)	20.8	30.89	195/285	39.95	0.160	0.179	B	RO
Hollister - South & Pine	27.93	48.24	000/090	60.00	0.371	0.177	A	RO
Imperial Valley 1979 [23:16], (M=6.5)								
Chihuahua	8.4	18.88	012/282	40.00	0.27	0.25	A	SS
Compuertas	15.3	24.43	015/285	36.00	0.19	0.15	A	SS
Plaster City	31.1	54.26	045/135	18.75	0.042	0.057	A	SS
El Centro Array #12	18.85	31.99	140/230	39.00	0.143	0.116	A	SS
El Centro Array #13	22.83	35.95	140/230	39.50	0.117	0.139	A	SS
Bonds Corner	4.01	6.20	140/230	37.60	0.42	0.59	A	SS
Brawley Airport	10.57	43.15	225/315	37.82	0.15	0.16	A	SS
Calexico Fire Station	11.56	17.65	225/315	37.80	0.19	0.27	A	SS

Table A.5. Characteristics of the fifth set of 30 natural records

Earthquake Station	R[1] (km)	EpiD[2] (km)	Recording Angle log/tran (°)	Duration (sec)	PGA_{log} (g)	PGA_{tran} (g)	Campbell's GEOCODE[3]	Fault rupture[4]
Superstition Hills 1987 (B) (M=6.7)								
El Centro Imp. Co Cent	18.5	35.83	000/090	40.00	0.36	0.26	A	SS
Wildlife Liquefaction Array	24.1	29.41	090/360	44.00	0.18	0.21	A	SS
Parachute Test Site	3.53	15.99	225/315	22.31	0.46	0.38	A	SS
Plaster City	22.50	25.98	045/135	22.14	0.19	0.12	A	SS
Brawley Airport	17.37	29.91	225/315	21.97	0.16	0.12	A	SS
Calipatria Fire Station	27.21	31.62	225/315	22.11	0.25	0.18	A	SS
Kornbloom Road	18.79	19.28	270/360	21.98	0.12	0.14	A	SS
Poe Road	11.67	11.20	270/360	22.30	0.30	0.45	A	SS
Salton Sea Wildlife Refuge	26.11	26.48	225/315	21.89	0.17	0.12	A	SS
Superstition Mtn Camera	6.56	7.50	045/135	22.21	0.68	0.89	D	SS
Westmorland Fire Sta	13.47	19.51	090/180	40.00	0.17	0.21	A	SS
San Fernando 1971 (M=6.6)								
LA, Hollywood Stor. Lot	25.9	39.49	090/180	28.00	0.21	0.17	A	RN
Pasadena - CIT Athenaeum	27.16	42.75	000/090	28.49	0.11	0.09	B	RN
LB - Terminal Island	61.82	76.38	249/339	79.98	0.013	0.011	A	RN
San Onofre - So Cal Edison	126.78	142.62	033/303	23.00	0.029	0.029	C	RN
Castaic - Old Ridge Route	22.63	25.36	021/291	30.00	0.17	0.27	C	RN
Cedar Springs, Allen Ranch	89.72	100.39	095/185	14.66	0.009	0.015	D	RN
Lake Hughes #1	27.40	26.10	021/111	30.00	0.098	0.11	A	RN
Santa Anita Dam	31.41	45.86	003/273	29.66	0.062	0.151	D	RN
Coalinga 1983/05/02 [23:42] (M=6.4)								
Cantua Creek School	24.02	30.06	270/360	40.00	0.227	0.281	A	RN
Parkfield - Cholame 2WA	44.72	55.67	000/090	40.00	0.109	0.114	A	RN
Parkfield - Cholame 5W	48.70	59.67	270/360	40.00	0.147	0.131	A	RN
Parkfield - Fault Zone 1	41.99	52.86	000/090	40.00	0.194	0.111	A	RN
Parkfield - Fault Zone 14	29.48	38.54	000/090	40.00	0.282	0.274	A	RN
Parkfield - Gold Hill 3W	39.12	49.47	000/090	40.00	0.137	0.122	B	RN
Parkfield - Stone Corral 3E	34.00	44.66	000/090	24.00	0.151	0.106	C	RN
Pleasant Valley P.P. - yard	8.41	9.98	045/135	39.97	0.592	0.551	A	RN
Parkfield - Fault Zone 4	34.59	44.83	000/090	40.00	0.067	0.12	C	RN
Parkfield - Vineyard Cany 2W	30.35	38.47	000/090	30.00	0.073	0.083	C	RN
Slack Canyon	27.46	33.52	045/315	30.00	0.153	0.166	D	RN

Table A.6. Characteristics of the sixth set of 23 natural records

Earthquake Station	R[1] (km)	EpiD[2] (km)	Recording Angle log/tran (°)	Duration (sec)	PGA_{log} (g)	PGA_{tran} (g)	Campbell's GEOCODE[3]	Fault rupture[4]
Whittier Narrows 1987/10/01 (M=6.0)								
Pasadena - CIT Athenaeum	17.24	10.64	180/270	32.00	0.174	0.101	B	RO
Alhambra - Fremont School	14.66	6.77	180/270	40.00	0.333	0.414	B	RO
LA - Hollywood Stor FF	24.08	24.21	000/090	40.00	0.221	0.124	A	RO
Altadena - Eaton Canyon	19.52	14.28	000/090	40.00	0.299	0.151	A	RO
Beverly Hills - 12520 Mulhol	29.90	31.09	032/122	32.22	0.089	0.138	C	RO
Brea Dam (Downstream)	23.99	22.72	040/130	30.00	0.163	0.313	A	RO
Glendale - Las Palmas	22.82	21.73	177/267	31.50	0.296	0.166	A	RO
Riverside Airport	55.48	59.59	180/270	39.99	0.05	0.047	A	RO
Chalfant Valley 1986/07/20 (M=5.9)								
Benton	21.92	31.25	270/360	32.00	0.061	0.052	A	SS
Bishop - Paradise Lodge	18.31	15.42	070/160	39.95	0.046	0.095	C	SS
Bishop - LADWP South St	17.17	20.27	180/270	39.93	0.129	0.094	A	SS
Lake Crowley - Shehorn Res.	22.08	16.59	009/099	40.00	0.051	0.031	A	SS
Zack Brothers Ranch	7.58	14.33	270/360	39.87	0.285	0.207	A	
Coyote Lake 1979 (M=5.7)								
Gilroy Array #1	10.67	12.56	230/320	26.84	0.103	0.132	D	SS
Coyote Lake Dam (SW Abut)	6.13	7.95	160/250	28.82	0.157	0.279	D	SS
Gilroy Array #2	9.02	10.94	050/140	26.86	0.211	.339	A	SS
Gilroy Array #6	3.11	4.37	230/320	27.10	0.434	0.316	C	SS
San Juan Bautista	19.70	23.24	213/303	28.46	0.108	0.107	B	SS
Halls Valley	33.83	36.29	150/240	40.00	0.039	0.050	B	SS
SJB Overpass, Bent 3 g.l.	20.67	23.91	067/337	26.83	0.124	0.097	D	SS
Overpass, Bent 5 g.l.	20.67	23.91	067/337	26.83	0.114	0.073	D	SS
Gilroy Array #3	7.42	9.59	050/140	26.80	0.228	0.272	A	SS
Gilroy Array #4	5.70	7.67	270/360	27.18	0.271	0.248	A	SS

Table A.7. Characteristics of the seventh set of 25 natural records

Earthquake Station	R[1] (km)	EpiD[2] (km)	Recording Angle log/tran (°)	Duration (sec)	PGA_{log} (g)	PGA_{tran} (g)	Campbell's GEOCODE[3]	Fault rupture[4]
Cape Mendocino 1992 (M=7.1)								
Cape Mendocino	6.96	10.36	000/090	30.00	1.497	1.039	D	RN
Eureka - Myrtle & West	41.97	53.34	000/090	44.00	0.154	0.178	B	RN
Fortuna - Fortuna Blvd	19.95	29.55	000/090	44.00	0.116	0.114	A	RN
Petrolia	8.18	4.51	000/090	36.00	0.590	0.662	A	RN
Rio Dell Overpass - FF	14.33	22.64	270/360	36.00	0.385	0.549	A	RN
Shelter Cove Airport	28.78	36.28	000/090	36.00	0.229	0.189	E	RN
Westmorland 1981 (M=5.8)								
Brawley Airport	15.57	15.71	225/315	28.41	0.169	0.171	A	SS
Niland Fire Station	15.45	18.45	000/090	40.00	0.105	0.176	A	SS
Parachute Test Site	16.81	20.47	225/315	40.00	0.242	0.155	A	SS
Superstition Mtn Camera	19.50	25.02	045/135	28.36	0.071	0.116	D	SS
Westmorland Fire Sta	6.87	7.02	090/180	40.00	0.368	0.496	A	SS
Salton Sea Wildlife Ref	8.15	8.62	225/315	28.75	0.199	0.176	A	SS
Landers 1992 (M=7.3)								
Desert Hot Springs	21.98	27.33	000/090	50.00	0.171	0.154	A	SS
Amboy	69.17	75.20	000/090	50.00	0.115	0.146	E	SS
Lucerne	3.71	44.02	000/090	48.13	0.721	0.785	D	SS
Hemet Fire Station	68.72	72.51	000/090	56.00	0.081	0.097	A	SS
Indio - Coachella Canal	54.34	59.68	000/090	60.00	0.104	0.109	A	SS
Joshua Tree	11.43	13.67	000/090	44.00	0.274	0.284	A	SS
Morongo Valley	17.58	21.29	000/090	70.00	0.14	0.188	A	SS
North Palm Springs	27.01	32.26	000/090	70.00	0.134	0.136	A	SS
Palm Springs Airport	36.27	41.87	000/090	60.00	0.089	0.076	A	SS
Puerta La Cruz	94.53	100.12	000/090	65.00	0.044	0.047	E	SS
Riverside Airport	96.05	97.13	180/270	50.00	0.041	0.043	A	SS
Arcadia - Campus Dr	135.26	147.53	009/279	59.08	0.051	0.046	A	SS

A.3. References

http://peer.berkeley.edu/smcat/search.html/ Pacific Earthquake Engineering Research (PEER). (last accessed February 2010).

Appendix B

Modelling & Constitutive Laws

B.1. Introduction

In this appendix the modelling and material laws used in the framework of this dissertation are described. Since this is not part of the scope of the research study these subjects are not presented in detail.

B.2. Numerical Modelling

B.2.1. Three-Dimensional Finite Element - Embedded Reinforcement Simulation

There are three methods available for the simulation of reinforcement in three-dimensional (3D) nonlinear finite-element (FE) analysis of reinforced concrete (RC) structures: *smeared*, *discrete* and *embedded* (ASCE, 1982). The smeared formulation is more suitable to surface-type structures, where the distributed-reinforcing mesh permits modelling of each reinforcement layer with a membrane layer of equal cross-sectional area. For sparsely located (nonuniformly spaced) reinforcing bars, either the discrete or embedded formulation is more appropriate. In the discrete formulation, the bars are often modelled with axial elements located at the boundaries of concrete elements. An obvious restriction is then imposed by having to use a concrete element mesh based on the locations of the reinforcement, rather than the need to simulate the flow of stresses. Especially in 3D applications, this can lead to prohibitive computational costs due to the use of many unnecessarily small elements or inaccuracies caused by elements with undesirable-aspect ratios. To alleviate these problems, some investigators have altered the actual arrangement

of reinforcement during FE modelling (Abdel-Halim and Abu-Lebdeh, 1989; Gonzalez Vidosa et al., 1990).

In order to deal with these shortcomings, embedded formulation is more preferable, which is also implemented in the software (ATENA, 2009) used for performing the 3D simulations required in the framework of the present research study. This method, however, has mainly been used in two-dimensional (2D) FE analyses. The original formulation presented by Phillips and Zienkiewicz (1976) was modified to allow for a straight reinforcing bars segment to be placed at any angle with respect to the local axes of the isoparametric concrete elements. Balakrishnan and Murray (1986) introduced an embedded formulation with bond-slip capability between reinforcement and concrete. Further improvements by Elwi and Hrudey (1989) allowed for a more general embedded curved reinforcement formulation. EI-Mezaini and Citipitioglu (1991) introduced isoparametric elements with movable nodes to define a more efficient formulation when bond-slip is modelled.

The inherent requirement in the embedded formulations is that the global coordinates of the intersection points of individual reinforcement and concrete elements should be provided. Although such data in the case of 2D models may be manageable, the task of identifying such points, their correspondence with each concrete element, and the manual definition of the coordinates for many such points in 3D applications is formidable. These problems, and difficulties associated with calculation of the stiffness for arbitrary location of bar elements embedded in 3D meshes, have led to simplifications in the case of 3D FE analyses. Isenberg and Levine (1985) restricted the embedded bars to pass through the centres of hexahedral concrete elements, Cervera et al. (1996) smeared a group of bars at a given location and used them as embedded layers inside the concrete-solid elements, while Zienkiewicz et al. (1972) and Bhatt et al. (1989) restricted the embedded bars to being parallel to the local-isoparametric coordinates.

B.2.2. Formulation of Beam-Column Element

In order to consider the inelastic behaviour either the plastic-hinge or the fibre approach can be adopted. Given that the plastic hinge approach has limitations in terms of accuracy fibre beam-column elements are preferable (Fragiadakis and Papadrakakis, 2008). According to the fibre approach each structural element is discretized into a number of integration sections, and each section is divided into a number of fibres (Figure B.1) with specific material properties (A_{fib}, E_{fib}), which are restrained to beam kinematics. Each fibre in the section can be assigned concrete, structural steel, or reinforcing bar material

properties. The sections are located either at the centre of the structural element or at its Gaussian integration points.

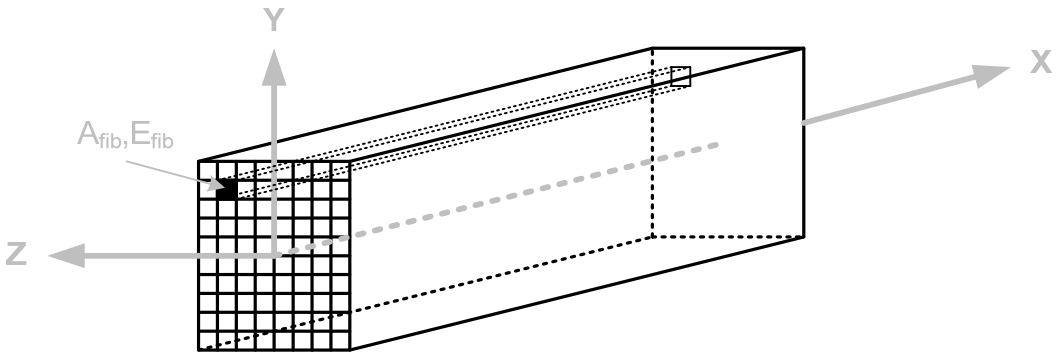

Figure B.1. Modelling of the inelastic behaviour-the fibre approach

The main advantage of the fibre approach is that every fibre has a simple uniaxial material model allowing an easy and efficient implementation of the inelastic behaviour. This approach is considered to be suitable for inelastic beam-column elements under dynamic loading and provides a reliable solution compared to other formulations. However, it results to higher computational demands in terms of memory storage and CPU time. When a displacement-based formulation is adopted the discretization should be adaptive with a dense mesh at the joints and a single elastic element for the remaining part of the member. On the other hand, force-based fibre elements allow modelling a member with a single beam-column element. Therefore, in this work each structural member is modelled with a single force-based, fibre beam-column element.

B.2.3. Modelling of Infill Walls

Many reinforced concrete (RC) buildings are skeletal structures infilled with masonry walls. Although these are primarily intended to serve as partitions, their structural contribution in increasing the lateral stiffness of the frame is long recognized. Many of the contemporary design procedures neglect the interaction of masonry infills with the framed structure on the assumption that the influence of the infill walls on the structural performance is always positive. Such an assumption may lead to inaccurate prediction of the lateral stiffness, strength and ductility of the structure, and thus obtain unacceptable designs. Moreover, a wide range of structural damages observed during past earthquakes across the world, has been very educative in identifying construction features related to the shape, size and geometry of the structure that must be avoided. For instance, buildings that have fewer columns, or are fully infilled in some of the storeys, or have partially infilled storeys tend to be more vulnerable to earthquake loading. Buildings with columns that hang or float on

beams at an intermediate storey and do not extend up to the foundation also show poor structural performance against earthquake. The influence of various construction practices in the structural performance of RC buildings was examined in a recent study (Lagaros, 2007). Furthermore, as it was reported in a number of studies (Dolšek and Fajfar, 2001; Ghobarah et al., 2006; Watanabe, 1997; Mitchell et al., 1996), a large number of multi-storey RC buildings collapsed during earthquakes due to construction features like weak stories, short columns, combination of strong beams-weak columns, large and heavy overhangs, among others. In the past, a number of studies have been performed on the seismic behaviour of RC buildings with masonry infill walls and there are several numerical models for the masonry infills available in the literature (Saneinejad and Hobbs, 1995; Madan et al., 1997; Perera et al., 2004; Dolšek and Fajfar, 2005; Sullivan et al., 2005; Kakaletsis and Karayannis, 2008). In some of them, the numerical models are verified with reference to experimental results, while all numerical models are aimed at contributing to a rational design of RC framed structures.

In the work by Calvi et al. (1996) a detailed parametric study is performed with respect to the parameters that affect the modelling of the infill walls. In this work the masonry infill walls are modelled by replacing their structural behaviour with a system of two equivalent diagonal compression struts (Saneinejad and Hobbs, 1995; Madan et al., 1997).

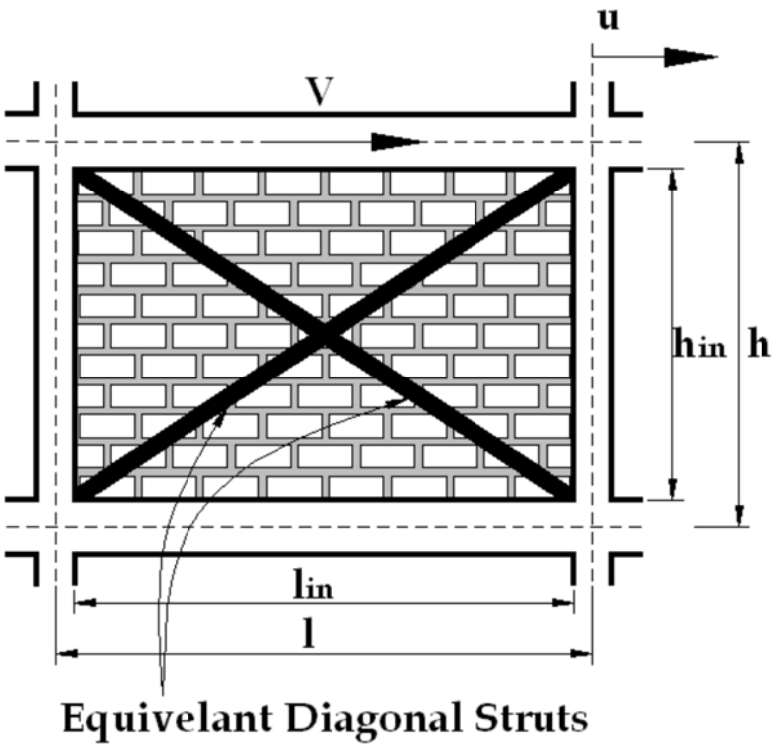

Figure B.2. The equivalent diagonal struts.

Figures B.2 and B.3 depict the model and the strength envelope for masonry infill walls. The user defined parameters of the strength envelope model, described in Figure B.3, are the cracking shear V_y, the maximum strength V_m and the post-peak residual shear strength V_p together with the corresponding lateral displacement values, u_y, u_m and u_p. The coefficient α, is the ratio of stiffness after yielding to the initial stiffness. In order to define the parameters of the envelope curve, the maximum strength V_m is first estimated considering the two critical failure modes, i.e. sliding shear and compression failures (Madan et al., 1997), while the remaining of the parameters are defined through the following expressions.

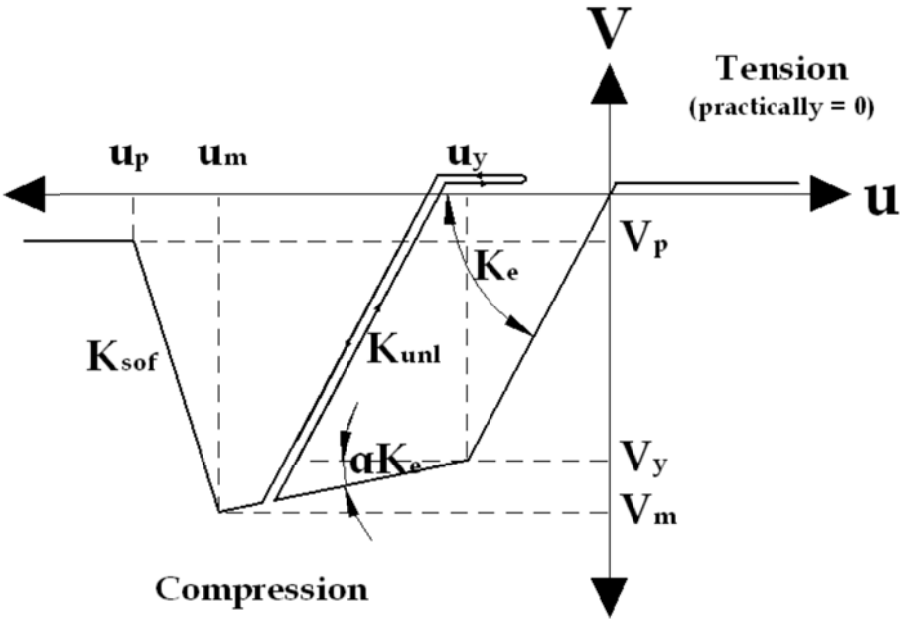

Figure B.3. Strength envelope for conventional masonry infill walls.

The maximum strength is calculated based on the formula given in the work by Dolšek and Fajfar (2002):

$$V_m = 0.818 \frac{l_{in} t_w f_{tp}}{C_l}\left(1+\sqrt{C_l^2+1}\right)$$
$$C_l = 1.925 \frac{l_{in}}{h_{in}} \qquad \text{(B.1)}$$

where f_{tp} is the cracking strength of the infill (taken equal to 0.38 MPa according to Dolšek and Fajfar, 2002), t_w is the infill wall thickness, l_{in} and h_{in} are the length and the height of the infill. The maximum displacement u_m, corresponding to the maximum lateral force, is estimated according to Madan et al. (1997) as follows:

$$u_m = \frac{\varepsilon_m' d_{in}}{\cos\theta} \qquad \text{(B.2)}$$

where $\varepsilon_m^{'}$ is the maximum masonry compression strain taken equal to 0.0015 (Saneinejad and Hobbs, 1995), d_{in} is the diagonal strut length while θ is the inclination of the diagonal strut with respect to the horizontal axis. The initial stiffness K_e can be estimated by:

$$K_e = 2(V_m / u_m) \tag{B.3}$$

The lateral yielding force V_y, and corresponding displacement u_y are calculated from the envelope geometry:

$$V_y = \frac{V_m - \alpha K_e u_m}{1 - \alpha} \tag{B.4}$$

$$u_y = \frac{V_y}{K_e} \tag{B.5}$$

The coefficient α is assumed to be equal to 0.2, while the post-peak residual shear strength V_p is considered as a function of the cracking shear (Repapis et al., 2006):

$$V_p = \tfrac{1}{3} V_y \tag{B.6}$$

The corresponding displacement value u_p is calculated based on the assumption that the stiffness of the softening K_{sof} branch is taken equal to 10% of the initial stiffness (Calvi et al., 1996). For the dynamic analyses performed in this study, the unloading stiffness K_{unl} is assumed equal to the initial elastic stiffness.

B.2.4. Modelling of shear reinforcement

The constitutive model adopted for the shear reinforcement is a nonlinear shear force-shear distortion (V-γ) law based on the work of Marini and Spacone (2006). The shear law (see Figure B.4.) has an initial parabolic branch and peaks at V_{Rd}, γ_y, which represents the section shear capacity. A linear branch follows, whose initial and final points are V_{Rd}, γ_y (γ_y=0.25%) and V_u, γ_u (γ_u=2.5%), respectively. The last point represents the residual shear capacity (V_{max}, γ_{max}), where γ_{max}=3.0%. For $\gamma > \gamma_u$, $V = V_u$. The definition of V_{Rd} is a fundamental step in the description of the shear response. According to Park and Paulay (1975) and to several design codes (see for example Eurocode 2, 2004), the section shear capacity V_{Rd} is the sum of the shear force which can be sustained by the yielding shear reinforcement V_{Rds}, and the shear resistance of the member without shear reinforcement V_{Rdc}:

$$V_{Rd} = V_{Rds} + V_{Rdc} \tag{B.7}$$

More details on the calculation formulas of V_{Rds} and V_{Rdc} can be found in Eurocode 2 (2004).

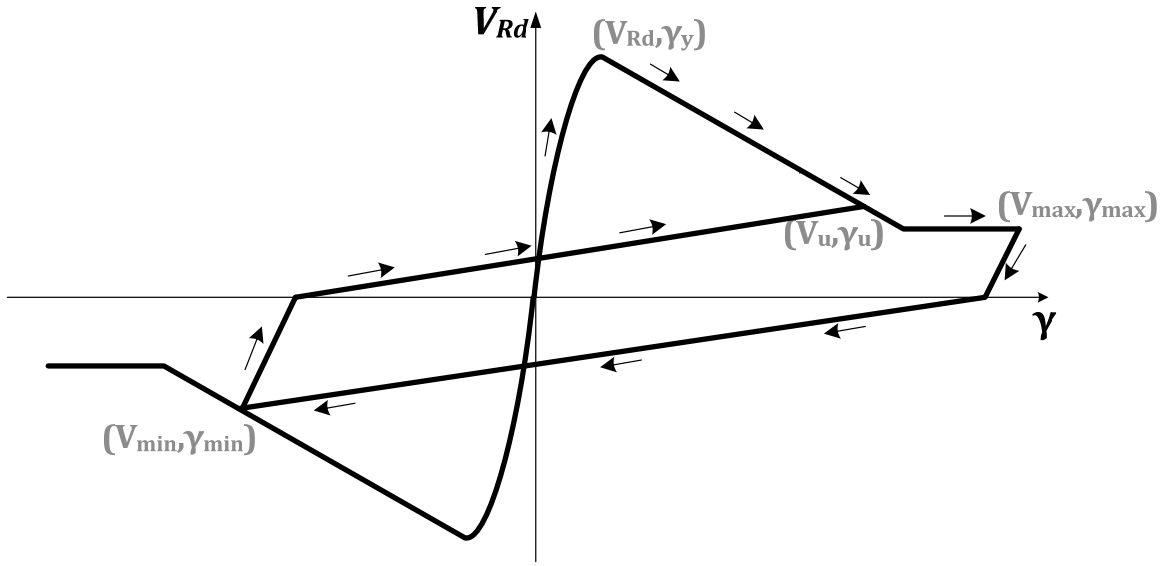

Figure B.4. Shear law.

B.3. Constitutive Models

B.3.1. Constitutive law for 3D solid elements

Fracture-plastic model combines constitutive models for tensile (fracturing) and compressive (plastic) behaviour. The fracture model is based on the classical orthotropic smeared crack formulation and crack band model. It employs Rankine failure criterion, exponential softening, and it can be used as rotated or fixed crack model. The hardening/softening plasticity model is based on Menetrey-Willam failure surface. The model uses return mapping algorithm for the integration of constitutive equations. Special attention is given to the development of an algorithm for the combination of the two models. The combined algorithm is based on a recursive substitution, and it allows for the two models to be developed and formulated separately. The algorithm can handle cases when failure surfaces of both models are active, but also when physical changes such as crack closure occur. The model can be used to simulate concrete cracking, crushing under high confinement, and crack closure due to crushing in other material directions.

Although many papers have been published on plasticity models for concrete (for instance Pramono and Willam, 1989; Menetrey et al., 1997; Feenstra, 1993; Feenstra et al., 1998; Etse 1992) or smeared crack models (Rashid, 1968; Cervenka and Gerstle, 1971; Bazant and Oh, 1983; De Borst, 1986; Rots and Blaauwendraad, 1989), there are not many descriptions of their successful combination in the literature. Owen et al. (1983) presented a combination of cracking and visco-plasticity. Comprehensive treatise of the problem was provided also by de Borst (1986), and recently several works have been published on the combination of damage and plasticity (Simo and Ju, 1987). The model used in this

dissertation (ATENA, 2009) differs from the above formulations by the ability to handle also physical changes like for instance crack closure, and it is not restricted to any particular shape of hardening/softening laws. Also within the proposed approach it is possible to formulate the two models (i.e. plastic and fracture) entirely separately, and their combination can be provided in a different algorithm or model. From programming point of view such approach is well suited for object oriented programming.

The method of strain decomposition, as introduced by de Borst (1986), is used to combine fracture and plasticity models together. Both models are developed within the framework of return mapping algorithm by Wilkins (1964). This approach guarantees the solution for all magnitudes of strain increment. From an algorithmic point of view the problem is then transformed into finding an optimal return point on the failure surface. The combined algorithm must determine the separation of strains into plastic and fracturing components, while it must preserve the stress equivalence in both models. The proposed algorithm is based on a recursive iterative scheme. It can be shown that such a recursive algorithm cannot reach convergence in certain cases such as, for instance, softening and dilating materials. For this reason the recursive algorithm is extended by a variation of the relaxation method to stabilize convergence. In this work the material model formulation is based on the strain decomposition into elastic ε_{ij}^{e}, plastic ε_{ij}^{p} and fracturing ε_{ij}^{f} components (de Borst, 1986), while Rankine criterion is used for concrete cracking.

B.3.2 Constitutive law for fibre beam-column elements

In the numerical test examples, all analyses have been performed using the OpenSEES (McKenna and Fenves, 2001) platform. A bilinear material model with pure kinematic hardening is adopted for the steel fibres, while geometric nonlinearity is explicitly taken into consideration. For the simulation of the concrete fibres the modified Kent-Park model, where the monotonic envelope of concrete in compression follows the model of Kent and Park (1971) as extended by Scott et al. (1982), is employed for the simulation of the concrete fibres. This model was chosen because it allows for an accurate prediction of the demand for flexure-dominated RC members despite its relatively simple formulation. The transient behaviour of the reinforcing bars was simulated with the Menegotto-Pinto model 1973, while the effects of shear and bond-slip are neglected. The effect of gravity loads and second-order effects are considered using the geometric stiffness matrix.

Concrete Stress-Strain Relation

In order to compute the concrete stress in each layer, a material law describing the concrete stress-strain relation under arbitrary cyclic strain histories is needed. There is some

uncertainty as to the influence of the concrete model on the overall behaviour of RC members subjected to bending and small values of axial force. Some investigators have concluded that a crude concrete model suffices to accurately predict experimental results. This might be true in the case of monotonic loading and cyclic loading that is restricted to small excitations. It is not true, however, in the case of severe cyclic loading. The results of the study by Scott et al. (1982) indicated that the strength deterioration of RC members under large cyclic excitations depends largely on the capacity of confined concrete to sustain stresses in the strain range beyond the maximum strength. This requires the use of a refined concrete model.

The monotonic envelope curve of concrete in compression follows the model of Kent and Park (1971) that was later extended by Scott et al. (1982). Even though more accurate and complete models have been published, the modified Kent and Park model offers a good balance between simplicity and accuracy. In the modified Kent and Park model the monotonic concrete stress-strain relation incompression is described by three regions:

$$\sigma_c = Kf_c'\left[\frac{2\varepsilon_c}{\varepsilon_0} - \left(\frac{\varepsilon_c}{\varepsilon_0}\right)^2\right] \text{for } \varepsilon_c \le \varepsilon_0 \tag{B.8a}$$

$$\sigma_c = Kf_c'\left[1 - Z(\varepsilon_c - \varepsilon_0)\right] \ge 0.2Kf_c' \text{ for } \varepsilon_0 \le \varepsilon_c \le \varepsilon_u \tag{B.8b}$$

$$\sigma_c = 0.2Kf_c' \text{ for } \varepsilon_c \ge \varepsilon_u \tag{B.8c}$$

where ε_0=0.002K while

$$K = 1 + \frac{\rho_s f_{yh}}{f_c'}$$

and

$$Z = \frac{0.5}{\frac{3 + 0.29f_c'}{145f_c' - 1000} + 0.75\rho_s\sqrt{\frac{h'}{s_h}} - 0.002K} \tag{B.9}$$

where ε_0 is the concrete strain at maximum stress, *K* is a factor which accounts for the strength increase due to confinement, *Z* is the strain softening slope, f_c' is the concrete compressive cylinder strength in MPa, f_{yh} is the yield strength of stirrups in MPa, ρ_s is the ratio of the volume of hoop reinforcement to the volume of concrete core measured to outside of stirrups, h' is the width of concrete core measured to outside of stirrups, and s_h is the center to center spacing of stirrups or hoop sets.

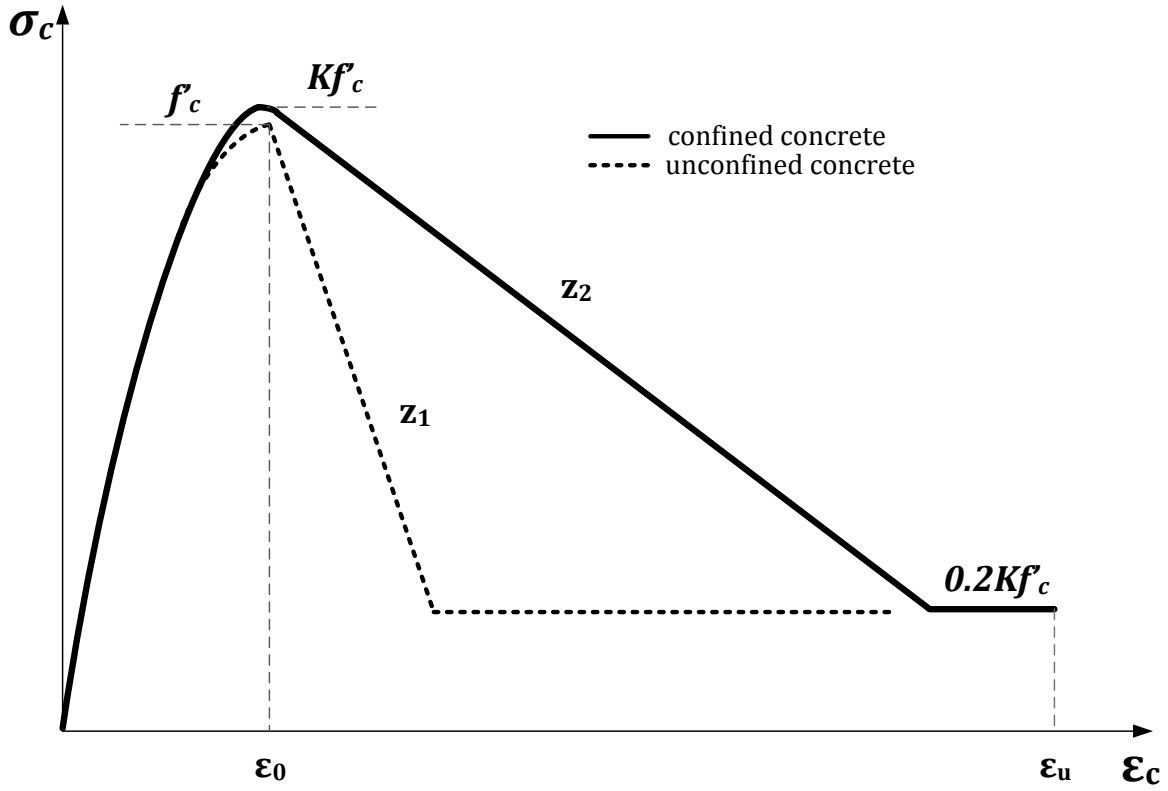

Figure B.5. Modified Kent-Park model, stress-strain relation for confined and unconfined concrete

In the case of *concrete confined by stirrup-ties*, Scott et al. (1982) suggest that ε_u is determined from the following expression:

$$\varepsilon_u = 0.004 + 0.9\rho_s \frac{f_{yh}}{300} \tag{B.10}$$

To account for crushing of the concrete cover the strength in the cover layer is reduced to $0.2f_c'$ once the compressive strain exceeds the value of ε_u, which in this study is set equal to 0.005. The following rules govern the hysteretic behaviour of the concrete stress-strain relation (Figure B.5.):

1. Unloading from a point on the envelope curve takes place along a straight line connecting the point ε_r at which unloading starts to a point ε_ρ on the strain axis given by the expressions

$$\varepsilon_u = 0.145\left(\frac{\varepsilon_r}{\varepsilon_0}\right)^2 + 0.13\left(\frac{\varepsilon_r}{\varepsilon_0}\right), \text{for } \frac{\varepsilon_r}{\varepsilon_0} < 2.0 \tag{B.11a}$$

$$\varepsilon_u = 0.707\left(\frac{\varepsilon_r}{\varepsilon_0} - 2.0\right) + 0.834, \text{for } \frac{\varepsilon_r}{\varepsilon_0} \geq 2.0 \tag{B.11b}$$

where ε_o is the strain level corresponding to the maximum stress in compression.

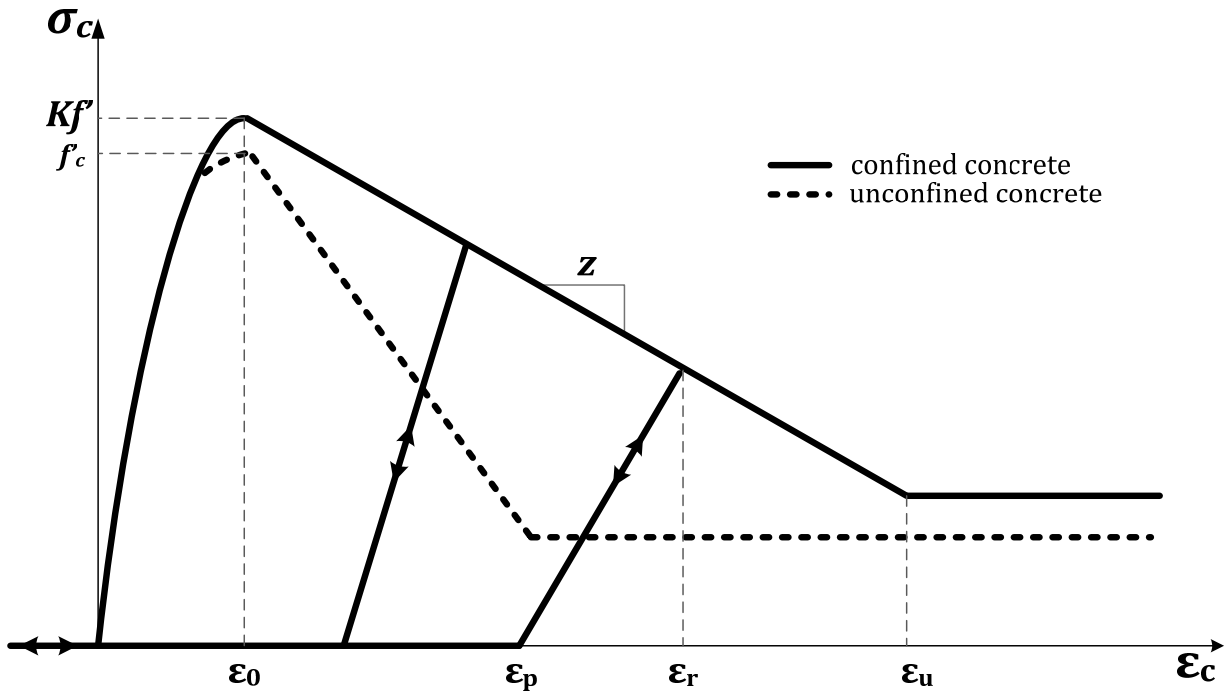

Figure B.6. Hysteric concrete stress-strain relation

The first part of the expression (Eq. (B.11a)) was proposed by Karsan and Jirsa (1969) and relates the normalized strain on the envelope with the strains at the completion of unloading through a quadratic formula. Eq. (B.11b) was added to the model since Eq. (B.11a) exhibits unreasonable behaviour under high compressive strain conditions.

2. The concrete stress is equal to zero for strains smaller than the strain at complete unloading since the tensile resistance is neglected.
3. On reloading in compression the stress is zero as long as the strain is smaller than the strain at complete unloading. Once the concrete strain becomes larger than that value, reloading continues along the previous unloading path (Figure B.6.).

Reinforcement Stress-Strain Laws

The steel reinforcement was modelled using a bilinear constitutive law. In a bilinear material model (Figure B.7.) the elastic behaviour of the material is determined by the Hooke law, having the initial modulus of elasticity equal to E and yield point, determined by the yield stress σ_y. The behaviour of the material after the yield point is determined by a second inclined line whose slope is determined by the tangent modulus of elasticity E_T. The tangent modulus of elasticity E_T is determined by means of the initial modulus of elasticity through the hardening coefficient b by the relationship:

$$E_T = b \cdot E \tag{B.12}$$

For a perfectly plastic material the hardening coefficient *b* is equal to zero. Apart from the coefficient *b*, the hardening parameter H is often used, which connects the stress σ with the plastic strain ε_{PL} through the relation:

$$\sigma = \mathrm{H} \cdot \varepsilon_{pl} \tag{B.13}$$

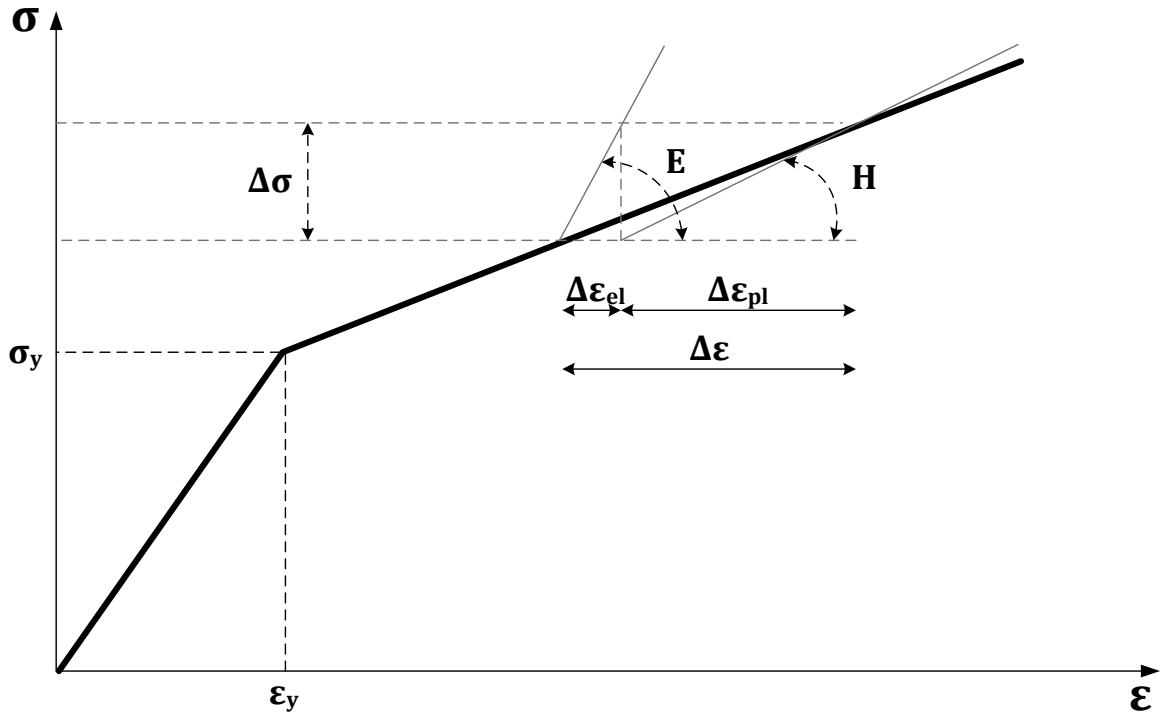

Figure B.7. The multi-linear stress-strain law for reinforcement

The hardening parameter H, the tangent modulus of elasticity E_T and the hardening coefficient b are related through the following expression:

$$\mathrm{H} = \frac{\mathrm{E_T}}{1 - \mathrm{b}}$$

or

$$\mathrm{E_T} = \mathrm{E} \cdot \left(1 - \frac{\mathrm{E}}{\mathrm{E} - \mathrm{H}}\right) \tag{B.14}$$

In the case of steel structures, where the yield strength in tension exceeds the yield stress in compression, the yield strength at the next load loop will be different. This phenomenon is known as the Bauschinger. The Bauschinger effect refers to a material property, where the characteristics of stress - strain of the material changed as a result of microscopic stress distribution in the material.

B.4. References

Abdel-Halim, M.A.H., Abu-Lebdeh. T.M., Analytical Study for Concrete Confinement in Tied Columns, J. Structural Engineering Div., ASCE, No.11, 115(1989) 2810-2828.

ASCE Task Committee on Finite Element Analysis of Reinforced Concrete Structures. (1982). State-of-the-Art Report on Finite Element Analysis of Reinforced Concrete, ASCE Special Publications.

Balakrishnan S. Murray D.W. (1988), Concrete Constitutive model for NLFE analysis of structures, J. Structural Engineering Div., ASCE, 114(7) 1449-1466.

Bazant, Z.P, Oh, B.H (1983) Crack Band Theory for Fracture of Concrete, Materials and Structures, RILEM, Vol. 16, 155-177.

Bhatt, P., M.S. Barj, G.F. Elnounu and M. Memon, Non-linear finite element analysis of shear wall-floor slab junction. In: D.R. Owen, E. Hinton and E. Oñate, Editors, Proc Second Int. Conf. on Computational Plasticity, Pineridge Press, Swansea, Wales (1989), pp. 1319–1330.

Calvi GM, Via G, Vintzileou E. Reinforced concrete infilled frames, In: RC frames under earth-quake loading, CEB Bulletin 231, Thomas Telford, 1996, 231-284.

Červenka V, Jendele L, Červenka J, ATENA Theory Manual. Cervenka Consulting; 2009.

Cervera M., Oliver J., Manzoli O. A rate-dependent isotropic damage model for the seismic analysis of concrete dams. Earthquake Engineering and Structural Dynamics 25 (1996), pp. 987–1010.

de Borst, R. (1986), Non-linear analysis of frictional materials, Ph.D. Thesis, Delft University of Technology, 1986.

Dolšek M, Fajfar P. Simplified non-linear seismic analysis of infilled reinforced concrete frames. Earthquake Engineering and Structural Dynamics 2005; 34: 49-66.

Dolšek M, Fajfar P. Soft storey effects in uniformly infilled reinforced concrete frames. Journal of Earthquake Engineering 2001; 5(1): 1-12.

Dolšek M, Fajfar, P. Mathematical modelling of an infilled RC frame structure based on the results of pseudo-dynamic tests, Earthquake Engineering Structural Dynamics 2002; 31: 1215-1230.

EC8. Eurocode 8: Design of Structures for Earthquake Resistance. European Committee for Standardisation: Brussels, Belgium, The European Standard EN 1998-1: 2004.

El-Mezaini, N., and Citipitioglu, E. (1991). Finite element analysis of prestressed and reinforced concrete structures. Journal of Structural Engineering, 117(10), 2851–2864.

Elwi, A.E., Hrudey,T.M., Finite element model for curved embedded reinforcement. J. Eng. Mech. Div. 115 4 (1989), pp. 740–745.

Etse, G., Theoretische und numerische Untersuchung zum diffusen und lokalisierten Versagen in Beton, Ph.D. Thesis, University of Karlsruhe 1992.

Feenstra, P.H., Computational Aspects of Bi-axial Stress in Plain and Reinforced Concrete. Ph.D. Thesis, Delft University of Technology, 1993.

Feenstra, P.H., Rots, J.G., Amesen, A., Teigen, J.G., Hoiseth, K.V., A 3D Constitutive Model for Concrete Based on Co-rotational concept. Proc. EURO-C 1998, 1, pp. 13-22.

Fragiadakis, M., Papadrakakis, M. Modelling, analysis and reliability of seismically excited structures: Computational issues. International Journal of Computational Methods, 5(4): 483–511, 2008.

Ghobarah A, Saatcioglu M, Nistor I. The impact of the 26 December 2004 earthquake and tsunami on structures and infrastructure. Engineering Structures 2006; 28(2): 312-326.

González Vidosa, F., Kotsovos, M.D. Pavlović, M.N. Three-dimensional finite element analysis of structural concrete. In: N. Bicanic and H. Mang, Editors, Computer Aided Analysis and Design of Concrete Structures Vol. 2, Pineridge Press, Swansea (1990), pp. 1029–1040.

Isenberg J, Levine HS. Analysis of reinforced concrete under shock loading. Finite Element Analysis of Reinforced Concrete Structures, ASCE Task Committee on Concrete and Masonry Structures, ASCE, 1985. pp. 444–464.

Kakaletsis DJ, Karayannis CG. Influence of masonry strength and openings on infilled RC frames under cycling loading. Journal of Earthquake Engineering 2008; 12(2): 197-221.

Kent, D.C., Park, R. Flexural members with confined concrete. Journal of Structural Division; 97(7): 1969-1990, 1971.

Lagaros ND. Life-cycle cost analysis of construction practices, Bulletin of Earthquake Engineering 2007; 5: 425-442.

Madan, A., Reinhorn, A.M., Mander, J.B., Valles, R.E., Modelling of masonry infill panels for structural analysis. Journal of Structural Engineering 1997; 123(10): 1295-1302.

Marini A, Spacone E. Analysis of reinforced concrete elements including shear effects. ACI Structural Journal 2006; 103(5): 645-655.

McKenna F, Fenves GL. The OpenSees Command Language Manual (1.2. edn). PEER, 2001

Menegotto, M., Pinto, P.E. Method of analysis for cyclically loaded reinforced concrete plane frames including changes in geometry and non-elastic behaviour of elements under combined normal force and bending. Proceedings, IABSE Symposium on Resistance and Ultimate De-formability of Structures Acted on by Well Defined Repeated Loads: 15-22, 1973.

Menetrey, Ph., Walther, R., Zimmerman, Th., Willam, K.J., Regan, P.E. Simulation of punching failure in reinforced concrete structures. Journal of Structural Engineering, 1997, 123(5), pp 652-659.

Mitchell D, DeVall RH. Kobayashi K, Tinawi R, Tso WK. Damage to concrete structures due to the January 17, 1995, Hyogo-ken Nanbu (Kobe) earthquake, Canadian Journal of Civil Engineering 1996; 23(3): 757-770.

Owen, J.M., Figueiras, J.A., Damjanic, F., Finite Element Analysis of Reinforced and Pre-stressed concrete structures including thermal loading, Comp. Meth. Appl. Mech. Eng., 1983, 41, pp 323-366.

Park, R., and Paulay, T., 1975, Reinforced Concrete Structures, John Wiley & Sons, Inc., 1975, 800 pp.

Perera, R., Gomez, S., Alarcon E., Experimental and analytical study of masonry infill reinforced concrete frames retrofitted with steel braces. Journal of Structural Engineering 2004; 130(12): 2032-2039.

Phillips, D.V., Zienkiewicz, O.C. (1976) Finite Element Analysis of Concrete Structures, Proc. Instn. Civ. Eng., Part 2, 61, 59-88.

Pramono, E, Willam, K.J., Fracture Energy-Based Plasticity Formulation of Plain Concrete, ASCE-JEM, 1989, 115, pp 1183-1204.

Rashid, Y.R. (1968), Ultimate Strength Analysis of Pre-stressed Concrete Pressure Vessels, Nuclear Engineering and Design,1968, 7, pp 334-344.

Repapis C, Zeris C, Vintzileou E. Evaluation of the seismic performance of existing RC buildings: I. Suggested methodology, Journal of Earthquake Engineering 2006; 10(2): 265-287.

Rots, J.G., Blaauwendraad, J., Crack models for concrete: discrete or smeared? Fixed, multi-directional or rotating? HERON 1989, 34 (1).

Saneinejad A, Hobbs B. Inelastic design of infilled frames. Journal of Structural Engineering 1995; 121(4): 634-650.

Scott, B.D., Park, R., Priestley, M.J.N. Stress–strain behaviour of concrete confined by overlap-ping hoops at low and high strain rates. ACI Journal; 79: 13-27, 1982.

Simo, J.C., Ju, J.W., Strain and Stress-based Continuum Damage Models-I. Formulations, II Computational Aspects, Int. J. Solids Structures, 1987, 23(7), pp 821-869.

Sullivan TJ, Priestley MJN, Calvi GM. Development of an innovative seismic design procedure for frame-wall structures. Journal of Earthquake Engineering 2005; 9(2): 279-307.

Watanabe F. Behaviour of reinforced concrete buildings during the Hyougoken-Nanbu earth-quake. Cement and Concrete Composites 1997; 19(3): 203-211.

Wilkins, M.L., Calculation of Elastic-Plastic Flow, Methods of Computational Physics, 3, Academic Press, New York, 1964.

Zienkiewickz, O.C., Owen, D.R.J., Phillips, D.V., Nayak, G.C., Finite element methods in the analysis of reactor vessels. Nuclear Engineering Design 20 (1972), pp. 507–541.